Assessing the Spatial and Temporal Controls on Plant Function Using Ground Based Remote Sensing

A Dissertation

Presented in Partial Fulfillment of the Requirements for the

Degree of Doctorate of Philosophy

with a

Major in Natural Resources

in the

College of Graduate Studies

University of Idaho

by

Troy S. Magney

Major Professors: Lee A. Vierling, Ph.D.; Jan U.H. Eitel, Ph.D.

Committee Members: David R. Huggins, Ph.D.; Kevin L. Griffin, Ph.D.

Department Administrator: Anthony S. Davis, Ph.D.

May 2015

Authorization to Submit Dissertation

This dissertation of Troy S. Magney, submitted for the degree of Doctorate of Philosophy with a Major in Natural Resources and titled "Assessing the Spatial and Temporal Controls on Plant Function Using Ground Based Remote Sensing," has been reviewed in final form. Permission, as indicated by the signatures and dates below, is now granted to submit final copies to the College of Graduate Studies for approval.

Major Professor: _____ Date:_____
Lee A. Vierling, Ph.D.

Co-Major Professor: _____ Date:_____
Jan U.H. Eitel, Ph.D.

Committee Members: _____ Date:_____
David R. Huggins, Ph.D.

_____ Date:_____
Kevin L. Griffin, Ph.D.

Department Administrator: _____ Date:_____
Anthony S. Davis, Ph.D.

Abstract

The global terrestrial carbon cycle is driven by the photosynthetic process, whereby chemical energy is created from a variable stream of solar photons that ultimately provide energy for life on Earth. Improved temporal and spatial monitoring of plant function for terrestrial biosphere modelling and management purposes rely heavily and increasingly on remote sensing systems; however, the interpretation of these data at leaf, canopy, and ecosystem scales require a nuanced understanding of vegetation structure and physiology. In this work, I seek to develop new and validate existing remote sensing techniques to map plant function in both space and time in the Palouse region of Eastern Washington, and the arctic tundra of Northern Alaska. From both an applied and theoretical framework, this work uses a variety of ground-based remote sensing tools to better understand how plants respond to their environment; and further, how aboveground biomass responds to environmental stressors via spectral reflectance measurements of the photochemical reflectance index (PRI) and the normalized difference vegetation index (NDVI). High resolution NDVI and PRI data were used to predict crop yield, biomass, protein concentration and nitrogen uptake in wheat, as well as track crop response to environmental conditions throughout the growing season. In the Arctic tundra, a 3-D plant canopy model derived from terrestrial light detection and ranging (LiDAR) measurements was coupled with a ray tracing model – demonstrating a new technique that reveals photosynthetic partitioning according to light availability within a small, Arctic shrub. In addition, a meta-analysis of xanthophyll cycle pool size (photoprotective pigments) on a global scale reveals patterns of xanthophyll accumulation coincident with extreme temperatures and water deficits, particularly in the Arctic tundra. This finding provides suggestions for how remote sensing techniques sensitive to xanthophyll cycle pool size may enable the eventual mapping of plant physiological status using spectral reflectance. To this end, it is my hope that this work provides techniques to enable an improved understanding of plant function across space and time, towards advancing the global mapping of photosynthesis - ultimately reducing uncertainties in not only the *when* and *where*, but also the *why* and *how* of land-atmosphere CO_2 exchange.

Acknowledgements

I am forever indebted to the many mentors, collaborators, teachers, students, friends, and family members that have facilitated and supported me throughout my academic career. Drs. Lee Vierling and Jan Eitel deserve more thanks than can be confined to the word limit designated by the formatting handbook. Jan first pitched the opportunity to me as I was leading a group of eager sixth graders into the field to learn about science, the idea was later embraced with full support from Lee, and by some stroke of a miracle I was lucky enough to learn more than I had envisioned about science, life, lasers, and everything in between from both of these fine mentors. I admire Jan and Lee for their patience, passion, and dedication to their field, and I can only hope to follow in their path as I build my own career. The many whiteboards we filled up during idea generating meetings, the troubleshooting of instruments in the field, the rescuing of trucks immobile in wet soil, and the mosquitos that relentlessly attacked us in the tundra will be memories I cherish forever. Additional gratitude goes out to my committee: Dr. David Huggins, for always challenging me to think about the application of the tools, for berating me about the differences between nitrogen concentration and nitrogen content, and for helping me design rigorous and reproducible studies; and Dr. Kevin Griffin, for his contagious passion for plant physiology, incredible support, and discussions spanning science, baseball, beer, and music. Lastly, the support of Dr. Barry Logan has been crucial to my development as a 'plant sunscreen investigator' and interdisciplinary scientist.

Additional thanks go out to 'Team Laser' – Heather Greaves, Dr. Natalie Boelman, Moyo Ajayi, Case Prager, Rebecca Gibson, Libby Fortin, and Ruth Oliver, and all the support staff at the Toolik Lake research station for field, equipment, and data processing assistance, idea generation, and great times. The Site-Specific Climate Friendly Farming team including Sam Finch, Nicole Ward, Matt Yourek, Dr. Erin Brooks, Dr. Dave Brown, Leanna Dann, Jyoti Jennowoin, Dr. Caley Gasch, and Tabitha Brown, played an integral role in facilitating not only meaningful science, but helping and orchestrating Palouse field work. Lastly, it is not without the encouragement of friends and colleagues at the McCall Outdoor Science School, where my journey at the University of Idaho began, that I have ended up on this road.

This work was supported by a NASA Idaho Space Grant Fellowship NNX10AM75H, NASA Terrestrial Ecology award number NNX12AK83G, and US Department of Agriculture - National Institute of Food and Agriculture award number 2011-637003-3034.

Dedication

Because it seems to me a bit of a self-aggrandizing endeavor to dedicate this body of work to any number of people, I am approaching this 'dedication' section as a continuation of my acknowledgements - after all, maybe these people don't want to be associated with it anyway? (← joke). The love and support of my family and friends have enabled an outlet for endless adventures and laughs that I will take with me forever. The friends I have made during my time in Idaho have provided me with some of the richest memories I could have imagined. My time here has been filled with what seemed like a never-ending whirlwind of the true essence of a 'work-hard, play-hard' lifestyle, where most Fridays entailed a frantic packing of vehicles with skiing, rafting, mountain biking, fishing, backpacking, or general adventuring equipment, before venturing off into some previously unexplored region of the Pacific or Inland Northwest. In addition to these trips, time spent in the Palouse attending barbeques and potlucks; attempting to garden, build furniture, and mildly repair vehicles; playing softball, hockey, soccer, basketball, and frisbee, have helped me maintain sanity and take a fresh, clear approach to my work. This work is dedicated to all of the friends responsible for organizing and advocating these activities. Thank you so much. Most of all, none of this work would be possible without the relentless support of my parents, Mark and Tammy, who have forever inspired me with their innovation and creativity. They have taught me that a genuine, inventive, hard-working, and positive approach to life will open up opportunities and empower change and goodwill. It is with them that I have shared the many ups and the occasional downs that are hidden between the lines of these papers, and without their support – in addition to my Grandma Zana and Grandpa Art, aunts, uncles, and cousins – this work would not have been possible. My sister Mya has supported me as a best friend with an unwavering smile that persists through long discussions concerning our fears and hopes for the future. Lastly, and perhaps most importantly, I am forever indebted to the love, support, laughs, adventures, patience, and moments of understanding that I have shared with Dr. Becky Rittenburg throughout this dissertation journey. She has provided unwavering support and endured more discussions regarding my interpretation of the PRI signal than I'm sure she cared to. She has inspired me with her holistic, creative, and optimistic approach to life, and I cannot thank her enough. I consider myself extremely lucky to be surrounded by you all.

Table of Contents

List of Tables

List of Figures

Chapter 1: Response of High Frequency Photochemical Reflectance Index (PRI) Measurements to Environmental Conditions in Wheat

Magney, T.S., Vierling, L.A., Eitel, J.U.H., Huggins, D.R., Garrity, S.R.

Remote Sensing of Environment, under consideration

Abstract: Remotely sensed data that are sensitive to rapidly changing plant physiology can provide real-time information about crop responses to abiotic stressors. The photochemical reflectance index (PRI) has shown promise when measured at short timesteps to remotely estimate dynamics in xanthophyll pigment interconversion - a plant photoprotective mechanism that results in lowered photosynthetic efficiency. To gain a better understanding of this dynamic spectral response to environmental conditions, we investigated PRI over two seasons (2013 and 2014) in rainfed soft white spring wheat (Triticum aestivum L.). Highly temporally resolved (measurement frequency = five minutes) in-situ radiometric measurements of PRI were collected at field plots of varying nitrogen (N) and soil water conditions (n = 16). We calculated a corrected PRI (PRI_c, as midday PRI - early morning PRI) to represent the diurnal magnitude of xanthophyll pigment interconversion. The advantage of using PRI_c is that it can empirically deconvolve the diurnally changing (facultative) from the seasonally changing (constitutive) component of the PRI signal. PRI_c was correlated with continuous, unattended crop responses associated with vapor pressure deficit ($0.50 > R^2 > 0.42$), stomatal conductance ($R^2 = 0.40$), and air temperature ($0.45 > R^2 > 32$). Further, the sensitivity with which PRI_c responded to solar radiation under varying N treatments and periods of soil water availability (surplus, depletion, and deficit) suggests that crop growth may be inhibited by a xanthophyll cycle mediated stress response, detectable by PRI_c. A major implication of these findings is that highly temporally and spatially resolved PRI_c data could be used to track plant stress. In this study, a ~15 day earlier PRI_c response was observed prior to the onset of senescence as compared to NDVI.

1.1. Introduction

Better understanding of crop response to environmental stress conditions may be possible using near-surface remote sensing platforms (Zhang & Kovacs, 2012). By collecting, processing, and communicating data in real-time, such technology could lead to more rapid and efficient methods for targeting site-specific management practices such as irrigation, fertilization or cultivar selection. Ground-based remote sensing is well established as a tool for assessing crop eco-physiological variables and has garnered wide interest from agricultural practitioners as a tool to track crop performance with higher temporal and spatial resolution than airborne or satellite data (Mulla, 2013). Further, ground based remote sensing techniques can provide valuable information towards scaling daily crop photosynthesis from the plot to the landscape scale via airborne and satellite sensors (Cheng et al., 2013; Zarco-Tejada et al., 2013a,b; Drolet et al., 2005). Of particular interest for bridging this gap is the photochemical reflectance index (PRI, Gamon et al., 1992; Garbulsky et al., 2011), due to its differing sensitivity to plant function at different timescales (Gamon and Berry, 2012).

Research from a wide range of disciplines has highlighted the potential of the PRI to remotely detect a photoprotective response of green plants to excess light (Penuelas et al., 1995; Gamon et al., 1997; Gamon & Surfus, 1999). At short (e.g. diurnal) timescales, the functional basis of the PRI is related to its sensitivity to rapid changes in carotenoids through the de-eopoxidation of the xanthophyll pigments (Gamon et al., 1992). De-epoxidation of the xanthophyll cycle results in a decrease in leaf optical reflectance between ~ 510 nm and ~550 nm centered at 531 nm (Gamon et al., 1990; Gamon et al., 1992; Peñuelas et al., 1995, Gamon & Surfus, 1999). This decrease in reflectance can be detected using remote sensing devices capable of measuring narrowband (~1-10 nm bandwidth) spectral reflectance. Typically, the reflectance at 531 nm is used in conjunction with a reference band at 570 nm that is insensitive to changes in xanthophyll cycle de-epoxidation to calculate the PRI (Eq.1) (Gamon et al., 1992):

$$PRI = (\rho 531 - \rho 570) / (\rho 531 + \rho 570) \quad \text{(Eq.1)}$$

The xanthophyll cycle can be triggered at differing light intensities based on the photosynthetic potential of a plant (Demmig-Adams & Adams, 1992). Numerous abiotic environmental conditions – nutrient availability (Shrestha et al., 2012), air temperature (Dobrowski et al., 2005; Sims et al., 2006), and water availability (Suárez et al., 2008, 2009,

2010) – have been shown to enhance the apparent drop in reflectance at 531 nm, based on the well-established observation that this phenomenon is associated with changes in the concentration of xanthophyll cycle constituents (from violaxanthin to antheraxanthin, and eventually zeaxanthin under increasing irradiance; Demmig-Adams and Adams, 1996; Garbulsky et al., 2011). Thus, the presence of any environmental stress will increase the magnitude of the PRI response to excess light at short time scales (i.e., tens of seconds to minutes, Hartel et al. 1999; Peguero-Pina et al., 2013).

PRI has been shown to be one of the only vegetation indices (VIs) sensitive to rapid changes in plant physiology (Gamon et al., 1992; Gamon et al., 1997; Penuelas et al., 1995). In addition to PRI, reflectance based approaches measuring chlorophyll fluorescence have been used to track plant physiological status, but the overall reflectance signal (<1%) is often muted by confounding signals and difficult to interpret (e.g., Zarco-Tejada et al., 2000; Zarco-Tejada et al., 2003; Shrestha et al. 2012; Porcar-Castell, 2014). While there is strong evidence that PRI is able to capture rapid changes in photosynthetic status in dark-light transition experiments across a wide range of species (e.g., Penuelas et al. 1995; Gamon et al. 1997; Guo & Trotter et al., 2004; Magney et al. 2014), PRI measurements in field settings are generally only taken at infrequent ($\leq$ 1 measurement per day) intervals and thus might not be representative of this rapidly changing plant physiological process throughout a day (e.g., Harris et al., 2014). Some of the first demonstrations of the potential for using highly temporally resolved diurnal PRI canopy reflectance data stemmed from work by Hilker and Hall et al. (Hall et al., 2008; Hilker et al., 2008; Hilker et al., 2009), who reported that the effects of canopy shading caused by sun angle strongly influenced the relationship between PRI and canopy light-use efficiency (LUE). The confounding effects of canopy architecture on high frequency spectral data have been further confirmed in both modelling (Barton & North, 2001) and field based studies, where new PRI reference bands have been explored (Hernández-Clemente et al. 2011). Results from these studies have spurred further research into the mechanistic linkages between the diurnal spectral and physiological behavior of plants.

At longer time scales, studies have used diurnal PRI measurements to track seasonal fluctuations in photosynthetic efficiency (Nichol et al. 2006, 6 times per day) under nutrient (Strachan et al., 2002) and water (Thenot et al., 2002; Hmimina et al., 2015) stress conditions.

Interpreting the PRI across a season can be challenging as chlorophyll (Chl) and carotenoid absorption, which overlap with the spectral bands sensitive to xanthophyll pigments, further confound estimates of photosynthetic performance by the PRI (Stylinski et al., 2002; Sims et al., 2006; Filella et al. 2009; Garrity et al. 2011; Gamon &Berry, 2012; Zarco-Tejada et al. 2013b; Hmimina et al., 2014, 2015). Most of the formative development of the PRI technique, whereby PRI is linked to LUE from CO2 flux observations, has been conducted on canopies that have relatively little variation in their structural (e.g., variations in leaf area index) and foliar pigment concentration over seasonal time scales (Gond et al., 1999). Further research is required to elucidate the temporal and spatial dynamics in photosynthetic status by using PRI measurements in the presence of varying concentrations of xanthophylls, chlorophylls, anthocyanins, and carotenes over a range of canopy structures and crop growth stages (Filella et al., 2009; Penuelas et al., 2011; Gamon & Bond, 2013).

We hypothesize that diurnal PRI measurements can be used in a similar way as the widely used field-portable pulse amplitude modulated (PAM) fluorimeter technique to assess plant stress (Bilger et al., 1995; Logan et al., 2007). Chlorophyll fluorescence derived from PAM measures the photosynthetic efficiency of photosystem II by comparing a dark-acclimated pre-photosynthetic minimum fluorescence (Fo) to a light saturated maximal fluorescence (Fm; Baker et al., 2004). The difference between Fm and Fo is termed variable fluorescence (Fv), and by normalizing Fm by Fv one can determine how many photosynthetic reaction centers are open under saturating light. The ratio of (Fv/Fm), or the efficiency of photosystem II, will fluctuate on a diurnal time scale depending on the potential for incident irradiation to be used for photosynthesis, re-emitted as fluorescence, or dissipated as heat. All three of these energy pathways will fluctuate depending on light availability and resources available for achieving maximum photosynthesis. Similar to Fv/Fm, extracting information about xanthophyll mediated thermal energy dissipation could be done by subtracting an early morning PRI value (effectively a 'dark-state', prior to xanthophyll cycle de-epoxidation) from PRI measurements throughout the day (Gamon and Berry, 2012; Liu et al., 2013; Hmimina et al., 2014, 2015). A recently developed technique is to subtract a dark-state PRI (PRIo) - which has been quantified as both a true dark-adapted PRI (Gamon and Berry, 2012) or the intercept of incident irradiance and PRI (Hminana et al., 2014) - from the PRI estimate under light, to effectively obtain a change in PRI (ΔPRI). The current study presents a similar technique to

those previously published by using a simple, corrected PRI (PRI_c) - derived from an early morning PRIo - to disentangle the facultative (diurnally changing) and constitutive (seasonally changing) components of the PRI signal.

In this study, we examine the change in the PRI signal at both diurnal and seasonal time-steps, with the ultimate goal of enabling early (pre-visual) detection of crop responses to abiotic conditions. To address questions related to the interpretation of daily and seasonal variations in the PRI signal for crop monitoring, our specific goals were to:
1) Determine the sensitivity of PRI, PRI_o, and PRI_c to diurnal and seasonal changes in solar radiation, VPD, stomatal conductance, air temperature, relative chlorophyll concentration (SPAD) and leaf area index (LAI) in soft white spring wheat (Triticum aestivum L),
2) Compare the magnitude of the response of the PRI_c signal to solar radiation under different applied nitrogen (N) treatments and water availability periods, over two growing seasons, and
3) Assess the potential for PRI_c to be used as an indicator of stress-inhibited crop growth across spring wheat developmental stages.

To accomplish these objectives, measurements of stomatal conductance, solar radiation, VPD, air temperature, soil volumetric water content (SVWC), relative chlorophyll concentration, and LAI were compared at physiologically relevant time scales with continuous and automated spectral reflectance measurements of the PRI and the Normalized Difference Vegetation Index (NDVI) at the canopy scale.

1.2. Materials and Methods

1.2.1. Study Area

Soft white spring wheat (Triticum aestivum L.) was grown following soft white winter wheat (Tritivum aestivum L.) during the 2013 and 2014 growing seasons in eight, 100 m2 (10 m x 10 m) plots with 19 cm row spacing at the Washington State University Cook Agronomy Farm (CAF) near Pullman, Washington, USA (N 46.7805, W 117.0855). In each of the two seasons, the eight research plots were divided into two fields, where four plots were located on a south-facing hilltop slope (field A, historically dry site), and four plots were located on a north-facing draw (field B, historically moist site) to promote a wide range of soil water availability periods (Fig. 1.1). Further, to investigate crop response to varying N conditions, four N application rates were used at each of the two fields (0, 40, 80, and 120 kg

N ha-1) using granular urea (46% N) that was applied via "top-dressing" three days after planting (similar to Eitel et al. 2014) (Fig. 1.1). The amount of residual inorganic N in the soil prior to planting was <30 kg/ha and did not significantly differ across the plots in fields A and B (data not shown). The soil at this site can generally be categorized as Palouse silt loam (fine-silty, mixed, superactive, mesic Pachic Ultic Haploxerolls) formed in loess and some ash (Soil Survey Staff, 2013). Permeability is moderate to high and available water capacity through the entire soil profile is about 29 cm (Soil Survey Staff, 2013). The average annual precipitation ranges from 260 to 610 mm, the average annual air temperature is 8-10 ºC, and the average frost-free period is 130-150 days. No irrigation was applied, as this is a completely snow/rainfed cropping system.

1.2.2. Data Collection

1.2.2.1. Canopy Spectral Reflectance Data

Canopy spectral reflectance measurements began immediately upon crop emergence and continued through harvest. Canopy spectral reflectance measurements were collected in a fixed location throughout the sampling period at each of the treatment plots using low-cost (<$302 as of 2015) Spectral Reflectance Sensors (SRS, Decagon Devices, Pullman, WA). SRS sensors are two-band radiometers that measure either incident or reflected radiation in wavelengths appropriate for calculating the NDVI and PRI (after Garrity et al. 2010). The NDVI sensors used in the current study used LEDs with peak sensitivity centered at 630 and 800 nm, with 50 and 40 nm full width half maximum band widths, respectively. Newer models of SRS NDVI sensors use different detectors with different spectral characteristics. PRI wavebands are centered at 532 and 570 nm, with 10 nm full width half maximum band widths. Both NDVI and PRI sensors can be equipped with hemispherical sensors using Teflon diffusers to make cosine-corrected measurements, and collected measurements of incident irradiation by placing them at a sky-looking view zenith angle of 180º. In addition, down-facing sensors equipped with a field-stop (restricting the field of view to 20º) were placed 1.5 m above the crop canopy at a 20º view zenith angle to measure reflected radiation (similar to Soudani et al., 2014). Field-stop reflected radiation is then divided by incident irradiation measured from the hemispherical sensors to obtain a true canopy reflectance value normalized for incident irradiation (reflectance (ρ)). A test for cross-calibration was done in the field using a 99% reflectance, white Spectralon reference panel (Labsphere Inc., North Sutton, NH)

and no significant differences between sensors was found. Reflectance measurements were logged using Decagon's Em50 datalogger (Decagon Devices, Pullman, WA) for each waveband and recorded at five minute intervals throughout the sampling period. The PRI was calculated according to eq. 1 and the NDVI was calculated according to eq. 2:

$$NDVI = (\rho 800nm - \rho 630nm) / (\rho 800nm + \rho 630nm) \quad \text{(Eq. 2)}$$

NDVI was measured to provide information on actual growth parameters to compare changes in greenness to physiological changes detected by PRI. Due to interactions between sun angle and a fixed sensor location, time of day exerts a strong influence on the apparent spectral reflectance; therefore, NDVI measured at solar noon was used to summarize an entire day into a single value (Gamon et al., 2006; Ryu et al., 2010).

In order to reduce the effects of sun-sensor-surface geometry and bidirectional reflectance effects, all down-facing sensors were mounted facing the same azimuthal direction. We make the assumption that a separation of the physiologically and directionally induced changes in PRI using bidirectional reflectance distribution function (BRDF) models is not necessary (Hilker et al., 2008) because of a) the consistent view zenith, solar zenith and azimuth angles at each of our plots, and b) our study utilizes relative (rather than absolute) differences in the PRI response of different wheat canopies. We used relative differences in PRI because these data are not being employed to predict a physiological function directly, but rather to assess how the magnitude of the PRI signal varies in response to environmental stress caused by different water and nutrient conditions. Further, multiple angle measurements as proposed for tree canopies by Hall, Hilker and others (e.g., Hall et al. 2008; Hilker et al. 2008) may not be necessary to account for self-shading in wheat canopies due to their relatively simple structure that limits self-shading in the upper canopy.

Previous studies have shown that correlations between LUE and PRI are strongest under high direct-to-total radiation ratios (e.g., Soudani et al., 2014). Because of this, days in which the average direct-to-total radiation fraction was less than 0.2 were not used in analysis. This threshold was chosen to retain > 80% of the data, and ensure that a low sunlight day (resulting in little PRI response) didn't misguide interpretation of PRI sensitivity. For visualization purposes (e.g. Figs., 1.5c,d & 1.6c,d), days that were discarded were smoothed using a locally weighted regression with a smoothing parameter (α) of 0.5 (loess, Cleveland, 1979; Cleveland & Devlin, 1988).

1.2.2.2. Biophysical Measurements

Non-destructive, relative leaf chlorophyll measurements (relative units from 0-60) were made using a portable soil plant analysis development (SPAD-502) chlorophyll meter (Konica Minolta Sensing, Inc., Osaka Japan). Relative chlorophyll meter readings were collected on the lower, middle, and upper parts (following Shrestha et al., 2012) of 12 randomly selected, top-of canopy, fully-emerged flag leaves within the ~ 1.5 m2 ground instantaneous field of view (GIFOV) of the SRS sensors (according to Eitel et al., 2008). We refer to these relative chlorophyll concentration values as "SPAD" values. LAI (m2 m-2) was measured using a LI-COR model LAI-2000 plant canopy analyzer (LI-COR, Lincoln, NE). Within each plot and within the sensor field of view, three measurements taken with the plant canopy analyzer were averaged. LAI and SPAD values were collected weekly during the growing season (attempting to acquire data during each of the Feekes developmental stages 1-11) in early morning (low light conditions) at each of the eight plots (10 weeks in 2013 (n=88), and 12 weeks in 2014 (n = 96).

To evaluate the diurnal response of the PRI to changes in photosynthetic capacity regulated by stomatal closure, measurements of stomatal conductance (g_s, mmol m-2 s-1) were made using a leaf porometer (SC-1, Decagon Devices, Pullman, WA, USA) (after Zarco-Tejada et al., 2013b). At four different times throughout the 2014 growing season (DOY 155, 168, 171, 190, at Feekes developmental stages 7, 8, 9, and 10, respectively), g_s measurements were made in early morning, mid-morning, and early afternoon on twelve fully developed leaves exposed to direct solar radiation within the PRI sensor field of view. A time-stamp and location (each of the eight treatment plots) was recorded to be compared directly to spectral reflectance measurements at the time of data collection.

Soil Volumetric Water Content (SVWC, $m^3\ m^{-3}$) measurements were taken within close proximity (5 m) of the plots to represent the general trend in SVWC at each of the plots. The SVWC was measured at soil depths of 5 and 15 cm every 15 minutes using EC-5 SVWC sensors (Decagon Devices, Pullman, WA, USA); however, an average of the soil profile at 5 and 15 cm depths below the ground surface were used for visualization purposes in this study. Because SVWC experienced fluctuations throughout the day, daily averages were calculated for each sensor location. A total of four sensors were used to capture variability in each of the low and high SVWC water positions during two seasons.

1.2.2.3 Meteorological Measurements

Meteorological measurements were collected at 15 minute intervals from instrumentation located on a tower in close proximity (< 30 meters) to the plots following AgWeatherNet system protocols (Pullman NE location, at the Cook Agronomy Farm, Washington State University; http://weather.wsu.edu/awn.php). Solar radiation was measured in units of W/m^2 at wavelengths from 360 to 1,200 nm (CS300-L Pyranometer, Campbell Scientific, Logan, UT, USA). VPD (kPa) was computed using the known relationship between air temperature and saturation vapor pressure (SVP (kPa); Murray et al., 1967) and the current relative humidity (RH (%)) at the time of interest. VPD was then calculated as [(100-RH)/100]*SVP.

1.2.3. Data Analysis

The formulation and rationale for the different PRI variants are noted in Table 1. Due to the large body of evidence suggesting that the relationship between PRI and independent variables (in particular, LUE, Peñuelas et al., 2015; Garbulsky et al., 2011) is weakened due to differences in canopy structure and pigments, the PRI_c attempts to correct for these seasonally changing biochemical and biophysical canopy constituents. While this study does not reveal strong relationships between PRI and canopy structure (LAI, Table 2), the reference PRI measurement (PRI_o) does appear to be significantly related to chlorophyll concentration (SPAD, Table 2).

Data analyses were performed at different time scales throughout the season. For diurnal correlations between vegetation indices and biophysical measurements (solar radiation, air temperature, VPD, g_s), data collected at 15 minute intervals were used. Seasonal correlations were made using PRI_c derived by subtracting the daily minimum PRI value from PRI_o. These analysis were done using simple linear regressions and a coefficient of determination (R^2). Because simple linear models would violate assumptions of independence, individual plots were used as a covariate in the analysis. All data were visually examined for non-linear relationships, which are noted in the correlation matrix if present.

For the second set of analyses, the data were broken into three different water availability periods associated with (1) water surplus, (2) water depletion, and (3) water deficit (see Fig. 1.5 for example). We binned the data into three water availability periods to examine whether the magnitude of the PRI response on a diurnal time-step (to solar radiation)

increased as water became more limiting, thereby suggesting a water stress induced PRI response. Four inflection points in the data were created based on these criteria: a) onset of vegetative growth, as inferred by NDVI data, b) onset of water depletion, as observed by SVWC data, c) end of rapid water depletion, as observed by SVWC data, and d) onset of senescence, as inferred by the NDVI data (see Figs. 1.5 & 1.6 for examples). Data before and after vegetative and reproductive growth were not considered for this step of analysis so as to reduce confusion from soil background (during emergence) and large pigment pool changes (during senescence). To determine the inflection-points used to derive the three water availability periods, piecewise linear regression modeling was applied to the seasonal NDVI and SVWC curves using the "segmented" package (Muggeo, 2008) in R (R Core Team, 2014, similar to Sweet et al., 2015). The piecewise regression outputs include inflection-point locations (day of year) with standard errors. The inflection points with the smallest standard error were used to define the exact bins used in this analysis. The algorithms and conceptual framework used to find inflection (or break) points is outlined in Muggeo (2003, 2008).

The binning of water surplus, depletion, and deficit conditions allowed the response of PRI to solar radiation - which is the primary abiotic driver of xanthophyll de-epoxidation - to be compared among the same treatment plots throughout the season. The regressions between PRI_c and solar radiation at each of the different N treatment plots were compared using analysis of covariance (ANCOVA) to determine whether the slopes were significantly different ($p<0.05$), implying that a steeper slope would be the result of a greater xanthophyll mediated response to stress (similar to Claudio et al., 2006). No statistical analysis was done on the intercepts of the data because the normalization procedure that produces PRI_c corrected for the dark-adapted PRI value, which permits comparisons of the relative magnitude of the PRI response to light. ANCOVA was similarly used to determine whether the slopes of the same treatment plot differed as water became more limiting, and a Tukey's test was done to determine which slopes were different from one another. To meet the assumptions required to perform an ANCOVA, tests for linearity, normality of residuals, homogeneity of error variances, and independence of error terms were tested. In the final step of statistical analysis, the slope of the PRI vs. solar radiation regression lines at each N treatment plot, and during each water availability period, was used as an indicator to investigate the PRI inferred stress impact on biomass accumulation. In these correlations, biomass accumulation is determined

by NDVI and LAI at the end of each of the three water availability conditions and was used as the dependent variable.

1.3. Results & Discussion

1.3.1. Diurnal Patterns of the Photochemical Reflectance Index (PRI)

Fig. 1.2 demonstrates the diurnal response of PRI relative to patterns of solar radiation, vapor pressure deficit, and air temperature using selected days from Field A in 2013. A visual examination of the diurnal PRI data in Fig. 1.2 suggests that under consistent irradiation intensities and varying environmental conditions, wheat canopies with increasingly limited water or nitrogen availability experience the deepest PRI-implied photosystem II (PSII) downregulation during the day. For example, during the early part of the growing season, when water is plentiful, and VPD and air temperature are low, there is a small response of PRI and minimal spread between fertilizer regimes; whereas, when water becomes more depleted, the magnitude of the diurnal PRI signal increases and greater spread occurs between fertilizer regimes. These results support findings by Verhoeven et al., 1997, who found that the rate of xanthophyll cycle interconversion increases as nutrients become more limiting in spinach, all else being equal. Further, the timing of the PRI response is consistent with a wide body of literature suggesting that the modulation of photosynthetic energy conversion efficiency throughout the day parallels irradiance conditions with a slight 'leveling off' during peak irradiance (see Demmig-Adams et al., 2012 for review). PRI data from this experiment generally follow a predicted diurnal pattern, with the lowest PRI implied xanthophyll inter-conversion occurring in latter parts of the day as the season progresses - coinciding with the greatest daily leaf-to-air VPD and air temperature. By using the minimum PRI data point for each day, rather than an approximated time of a xanthophyll induced physiological response, the PRI_c technique should more accurately represent the maximal diurnal stress response of plants representative of xanthophyll cycle de-epoxidation on the seasonal time scale.

1.3.2. Seasonal patterns of NDVI, PRI_c, SVWC, VPD, & Air Temperature

VIs were related with key environmental variables at the seasonal timescale (Figs. 1.3 & 1.4). Seasonal patterns of NDVI and PRI_c reveal several interesting patterns as compared against environmental conditions, with a particularly strong response to SVWC, as would be hypothesized in a rainfed wheat system such as this (Figs. 1.3 & 1.4). Because field locations

were chosen to capture the full range of soil water conditions, there is a substantial difference in the range and duration of seasonal SVWC patterns among all four fields. In 2013, the water surplus time period (as determined from inflection points in the NDVI and SVWC data) was nearly twice as long as in 2014, resulting in more time for vegetative growth – which can be seen in the rapid increase in NDVI data. While the soil moisture conditions (both magnitude and timing) in 2014 are very similar, in 2013 the onset of water depletion occurred nearly 10 days later in field B and dropped at a faster rate and to a greater extent before reaching water deficit conditions. In all fields over both seasons, the water deficit period is coincident with limited (if any) vegetative growth (as indicated by a leveling off of NDVI values) during crop reproductive stages. While Figs. 1.3a,b & 1.4a,b reveal nearly symmetrical growth patterns (NDVI) relative to SVWC prior to the onset of senescence, a response to applied nitrogen also occurs towards the end of vegetative growth; for example, high and medium N addition plots begin to achieve higher maximal growth during rapid vegetative growth as indicated by NDVI data.

Figs. 1.3c,d & 1.4c,d show the seasonal trends in PRI_c and mean daily VPD/air temperature. In both 2013 and 2014, a general increase in VPD and air temperature can be observed, but primarily not until the crop has reached the reproductive stage. The PRI_c data reveals a general trend downward across all treatment plots, coincident with decreasing SVWC and increasing VPD and air temperatures throughout the season. The most drastic drop in PRI_c appears prior to senescence, exhibiting a ~15 day earlier decline as compared with NDVI in 2013. The PRI_c data representative of applied N treatments deviate further from one another as the season progresses, with the control and low N plots experiencing the lowest PRI_c values, while medium and high N addition plots experience the least amount of PRI inferred stress. An explanation of this phenomenon is likely the larger chlorophyll pools (higher SPAD) in the high N addition plots, which are able to theoretically achieve greater rates of photosynthesis under high light (Evans, 1983), limiting the need to for increased photoprotective xanthophyll cycle interconversion.

Interpreting the PRI_c data as a diurnal 'stress signal' (facultative rather than constitutive, Gamon and Berry et al., 2012) here suggests that PRI_c could be used as an early warning sign of a drastic physiological change prior to senescence. There is substantial variability in the PRI_c data as compared with the NDVI data, particularly when NDVI values

are saturated following vegetative growth. During this time, when the crop has begun investing energy into grain production as opposed to vegetative growth, there is little variation in SPAD and LAI readings, implying that limited changes in carotenoid/chlorophyll concentration or vegetation structure are occurring (prior to senescence); meanwhile sudden drops in the PRI_c signal are indicative of the deployment of a xanthophyll driven photoprotective response to low soil water and increasing VPD/air temperatures. Due to the weak relationships between PRI_c /SPAD/LAI (table 2), we make the assumption that the seasonal responses of PRI_c are mainly facilitated by short term changes in the xanthophyll cycle as opposed to longer-term pigment changes, though both are likely playing a complimentary role in driving the PRI_c signal.

While it is difficult to tease apart the relative contributions of each of these environmental parameters on the overall inferred PRI_c stress response, these patterns manifest themselves in a predictable manner (i.e., plants with more N available will have less of a stress response to excess light than those with limited N); this approach could reveal new techniques to further examine how PRI is responding to N availability at the field scale. Due to the high co-linearity between explanatory variables, the differences in sampling time scale, and the multifaceted contributions to spectral reflectance, it was beyond the scope of this study to examine the explanatory power of each dependent variable on the PRI signal (i.e., using a random forest approach, Soudini et al., 2014), though future work should explore questions along these lines. Further elaboration of PRI response to VPD, air temperature, stomatal conductance, N and water availability specifically will be discussed in section 1.3.3 1.3.4 & 1.3.4.

1.3.3. Relationships between Vegetation Indices, Meteorological, Biochemical, and Canopy Properties across the Entire Growing Season

The results presented in Table 2 provide a general overview of vegetation index response to the wide range of environmental conditions experienced throughout the two growing seasons. On a diurnal time scale, air temperature ($Temp_d$), stomatal conductance (g_s), and vapor pressure deficit (VPD_d) are mechanistically related to each other but also empirically related to PRI, and to a greater extent, PRI_c, suggesting that the PRI is sensitive to conditions where high VPD_d and $Temp_d$ limit g_s - similar to findings in Soudani et al., 2014. Conversely, the structural index, NDVI, is not significantly related to $Temp_d$, and VPD_d.

NDVI is also weakly correlated to g_s, whereas PRI variants respond strongly to the variation in g_s.

On a seasonal time scale, the daily mean vapor pressure deficit (VPDs) and air temperature ($Temp_s$) were significantly correlated to PRI variants, with the strongest and most significant correlation to PRI_c (Table 2). These results further confirm the hypothesis that the plant functional response to VPD is linked with a more physiologically sensitive VI (PRI, as opposed to NDVI). The weak relationships between seasonal VPD, LAI, and SPAD, provide further evidence of the PRI responding to environmental variables such as VPD at shorter time scales than pigment and structural changes. Other significant correlations of note are the strong relationships between NDVI/LAI, and PRI_o/SPAD. Both of these empirical relationships support the wide bodies of evidence that NDVI is sensitive to structural changes (LAI) in the canopy and that a single PRI (PRI & PRI_o) value taken during the day is sensitive to pigment changes throughout the season (e.g., Garrity et al., 2011). When PRI is corrected to account for the relative differences in pigment concentrations, the R2 value decreases, though is still significant. Scatterplots of the relationships between the uncorrected PRI, and PRIc and their relation to LAI and relative chlorophyll concentration can be seen in Fig 1.5.

Fig. 1.5 compares the traditional PRI vegetation index with the corrected PRI (PRI_c) designed to account for confounding structural and non-xanthophyll pigment effects on the PRI at the seasonal time scale in order to better understand plant responses to environmental stress. While several studies have corrected for structure and non-xanthophyll pigment effects using modeling approaches and alternative reference bands (e.g. Suárez et al. 2009; Hernández-Clemente et al. 2011), this work is among the first to demonstrate the utility of a corrected PRI using entirely spectrally derived data from low-cost, automated, off the shelf spectral radiometers collecting high temporal resolution data (Garrity et al., 2010; Gamon et al., 2015). Previous studies have demonstrated a response of PRI to xanthophyll cycle de-epoxidation and LUE over short time scales (Gamon et al., 1990, 1992,1997), whereas contrasting results have been reported among studies conducted over longer time scales at the leaf (e.g., Rahimzadeh-Bajgiran et al. 2012) and canopy scales (e.g Porcar-Castell et al. 2012). Fig. 1.5 broadly agrees with previous studies that have found that long term PRI variability is driven by canopy chlorophyll and structure (Stylinski et al., 2002; Nakaji et al., 2006; Garrity et al., 2011; Porcar-Castell et al., 2012). Substantial improvement in

deconvolving the seasonal pigment response of PRI by subtracting a dark-state PRI (PRI_o) was done by creating PRI_c as a novel derivation to isolate the diurnal PRI signal from the background seasonal PRI signal (Fig. 1.5). However, PRI_c made limited improvements decoupling the structural (LAI) effect from the raw PRI signal. This suggests that PRIo was primarily sensitive to variability in pigment concentrations and should not be used in this system to correct for changes in LAI. This is not of major concern considering that, in general, environmental drivers of a PRI inferred stress in a rainfed system will increase as the season progresses coincident with leaf area. Meanwhile, the variability in pigment concentrations, which was primarily affected by applied N at planting, changes little until the crop begins to senesce towards the end of the season. Using NDVI and PRI_c data in conjunction could help scientists or practitioners understand field scale variability in physiological stress (PRI_c) and its effect on crop growth (NDVI).

Due to the limited variation in relative chlorophyll concentration during the growing season in each of the treatment plots, the scatter around SPAD values > 40 in Fig. 1.5 suggests that PRI_c was not responding to constitutive pigment related changes prior to senescence. While the dataset presented here is not robust enough to quantify complete pigment pools or canopy structure complexities, further evidence that PRI_c may be correcting for the confounding effects of seasonally varying biophysical and biochemical canopy components can be explained by the weak relationship between NDVI and PRI_c (Table 2). NDVI is physically based on chlorophyll absorption in the red portion of the spectrum (i.e. pigment related) and total leaf area reflectance in near infrared portion of the spectrum (i.e. structurally related) (Tucker et al., 1979). While NDVI is responding on a seasonal time scale to both of these biophysical and biochemical canopy constituents, PRI_c is not. Rather, PRI_c is isolating the shorter term stress signals of the plants.

Because only NDVI and PRI reflectance data were collected in this study, more advanced correction techniques that could have further de-convolved structural and pigment related PRI variability were not explored. Future work should investigate waveband selection for normalization of PRI variants as they relate to the specific canopy under investigation. Recent work by Hminana et al. (2014) suggests that subtracting a dark-state PRI_o from a "light-exposed" PRI to infer a ΔPRI is more representative of the facultative xanthophyll response PRI was designed to detect (Gamon et al., 2015); but other work by Hminana et al.

(2015) and Zarco-Tejada et al. (2013) make use of the red-edge band (because of the strong link to chlorophyll concentration) which shows to have a similar normalization effect by accounting for the variability of the "light-exposed" PRI that is not caused by variations in structure and non-xanthophyll pigments. Gamon and Bond (2013) note that the use of a dark-state PRI_o as a reference value (described in table 1 of this work), and the normalization of PRI by solar radiation, is somewhat analogous to recent methods that consider a sunlit fraction of stand-level PRI measurements (Hall et al., 2008; Hilker et al., 2008), which could help to reduce the errors due to variation in constitutive pigment levels (Gamon and Berry 2012). While our PRI_c estimate showed moderate insensitivity to chlorophyll and LAI throughout the sampling period for this particular canopy (Table 2 & Fig. 1.5), this relationship may lose power if used over a time frame where changes over a wide range of pigment concentrations are experienced or a given canopy is more complex (e.g. Barton and North, 2001; Hall et al., 2008, Hilker et al., 2008). In addition, though no strong empirical relationship was determined between LAI and PRI_c, it makes physiological sense that the range in PRI values observed throughout the day would increase as leaf area increased, assuming that that total xanthophyll pool of the canopy increases with leaf area. To account for this, our data show that PRI_o and PRI_c decreases as leaf area increases, and thus when it is subtracted by the greater range of PRI values, it should account for this phenomenon - though further research along these lines is needed.

Lastly, by using an empirically derived PRI_c to investigate plant physiological responses to abiotic conditions, this work seeks to estimate a parameter that cannot be tested using radiative transfer models. Current modelling methods lack a proper assessment of this rapid conversion of xanthophyll pigments as a function of stress; rather, they rely on simulating the 531 and 570 nm bands as a function of structure variation and pigment concentration. Radiative transfer models often require a demanding parameterization of leaf and canopy variables, long development time and extensive computational costs (Malenovsky et al., 2009), hampering their current operational use. Due to the promising capability of PRI_c found in this study, the remaining results will only show data using PRI_c.

Fig. 1.6 shows the statistically significant and strong inverse relationship observed in PRI_c as VPD increases at both seasonal (Fig. 1.6a, against the daily mean VPD value) and diurnal (Fig. 1.6b, against 15 minute data throughout the entire two growing seasons) time

steps. The patterns observed in Fig. 1.6 highlight the sensitivity of PRI_c to environmental conditions that affect plant physiology, as compared to the poor relationships between NDVI and VPD in Table 2. Because PRI_c is a relative value and SRS calibration, viewing angle, and conditions are not identical across all plots, the statistical model results include individual plot (n=16) as a covariate; however, data are plotted without a covariate for visualization purposes (2-D, opposed to 3-D). Due to the collinearity of VPD and air temperature ($R^2 = 0.71$), a similar response of PRI_c to each meteorological variable was observed (Fig. 1.7). Increasing air temperature appears to induce a xanthophyll driven PRI response at both seasonal (mean daily air temp) and diurnal (15 minute) time scales.

Figs. 1.6 and 1.7 demonstrate that wheat canopies under increasing temperatures and leaf-to-air VPD may be experiencing the deepest PRI-implied photosystem II (PSII) downregulation during the day. This is confirmed both quantitatively (Figs. 1.6 & 1.7) but also qualitatively in Fig. 1.2, when the daily timing of maximum photosynthetic depression in the diurnal PRI signal also appears to occur following the greatest expected leaf-to-air VPD and air temperature during the day, and Figs. 1.3 & 1.4 when seasonal fluctuations in VPD and air temperatures generally coincide with PRI_c sensitivity. To quantify the diurnal response of PRI_c to physiological mechanisms changing on a diurnal time step, gs was measured on leaves within the SRS field of view (Fig. 1.8).

Because gs measurements were collected on days when air temperature, VPD, and solar radiation were high, a midday photosynthetic depression was observed, whereby low PRI values during mid-day (peak VPD, solar radiation, and air temperature) coincided with low stomatal conductance. Low midday g_s can be explained by a midday stomatal closure due to environmental conditions (Demmig-Adams et al., 2012). Fig. 1.8 shows that a significant linear relationship was observed between leaf level g_s and canopy level PRI_c. These data suggest that the processes by which stomatal aperture are controlled due to environmental conditions similarly drive sensitivity of the PRI. Similar to findings by Zaro-Tejada et al. (2013b), results from this study found a strong link between g_s and PRI_c ($R2 = 0.40$), regardless of the inherent variability in leaf-level g_s within a plant canopy. The highest PRI_c and g_s values were observed in mid-morning, before light induced stress caused a drop in reflectance at 531 nm, resulting in high stomatal conductance and expected photosynthesis. Table 2 and Figs. 1.6-1.8 confirm that PRI_c is sensitive to meteorological conditions that

control stomatal aperture; however, in the context of agricultural management, growers and practitioners would likely want to use this information to explore the response of crops to environmental variables that are more manageable such as nitrogen and water availability. And further, this method might also be useful for crop researchers trying to find phenotypes that are well suited to grow under harsh environmental conditions.

1.3.4. Sensitivity of PRI_c to Solar Radiation under Water and Nitrogen Availabilities

Because plant photoprotective mechanisms are a response to irradiance levels that exceeds the capacity for photosynthetic electron transport, we used linear regressions of PRI_c and solar radiation to explore the effects of nitrogen and water availability on reductions in crop photosynthetic potential. This analysis was facilitated by the linear response of PRI_c to solar radiation, reaching un-sustained saturation during peak sunlight (as would be expected in a light-response curve; Hminana et al. 2015). The sensitivity of PRI_c to solar radiation under all available nitrogen and water regimes is explored in Fig. 1.9. The results of the ANCOVA, which is a general linear model combining analysis of variance (ANOVA) and regression analysis to examine significant differences between slopes and across categorical independent variables (here, applied N and water availability), are displayed in the Fig. 1.9 legends. We evaluated whether or not a significant difference existed between treatment plots during each water availability period from Figs. 1.3 & 1.4, and the assumptions outlined previously for the conducting an analysis of variance between study plots water availability scenarios were met.

Figs. 1.9a-c show the rate and magnitude of the PRI_c response to solar radiation at field A in 2013 using a least squares best fit line and confidence intervals, suggesting that a highly significant difference exists among treatment plots during each stage of water availability. A Tukey's test suggests that during water surplus and depletion (1.9a&b), no significant difference existed between the control and low N plots or the medium and high N plots; however, during water deficit, a significant difference existed among all four treatment plots. Further, as the season progressed, and water availability became more limiting, PRI_c exhibited a stronger response to incident irradiation across all treatment plots (Fig. 1.9c).

Fig. 1.9d-f represents the PRI_c response to solar radiation at Field B in 2013. The ANCOVA suggests significant differences among all treatment plots at any given time of year. The treatment plots during water surplus deviated least from one another. During water

surplus, there was no significant difference between the low and medium treatment plots; and also no significant difference between the high and medium plots during water depletion. Throughout the season, a significant difference was experienced between water stages at all treatment plots except the low N availability plot, which showed no significant difference in rate of PRI_c to solar radiation between water surplus and depletion. Further, a significant increase in the response of PRI_c to solar radiation was observed between water surplus and depletion in the medium and high N treatment plots, while every other significant difference between water availability periods was due to an increasingly negative slope.

Fig. 1.9g-i demonstrates the rate and magnitude of the PRI_c response to solar radiation at field A in 2014. Results from the ANCOVA show no significant difference between treatment plots during water surplus, while deviation in the rate of response of the PRI_c according to N availability increases as water becomes more limiting. Tukey's test revealed no significant differences between the high and control treatment plots during water depletion and between the low, medium, and high treatment plots during water deficit. Significantly more negative responses of PRI_c were seen at all plots as water became more limiting except at the medium N plot between surplus and depletion, and at the high N plot between depletion and deficit.

Fig. 1.9j-l exemplifies the sensitivity of PRI_c to solar radiation at treatment plots during differing water availability periods in field B during the 2014 growing season, where significant differences among all treatments under each water availability period existed. However, three non-significant differences exist among treatment plots: 1) between low and control during water surplus, 2) between high and medium during depletion, and 3) between low and control during deficit. All treatment plots show a significantly different and more negative response between water surplus and water depletion; whereas during water deficit, all treatment plots show a significantly more negative response of the PRI_c to solar radiation from water surplus, but the slope of the high N plot is significantly greater and the low N plot is not significantly different from the water depletion.

Over all treatment plots during both seasons, a significantly different response of the PRI_c to solar radiation appeared in every water availability period except for water surplus in field A, 2014. This suggests that nitrogen availability is a primary driver of PRI_c sensitivity, and that, in most cases, the response was stronger (greater slope) in plots with less applied N

at planting. In general, the range of differences among treatment plots increased as the season progressed, suggesting that the PRI_c response to N availability was more pronounced as leaf area increased and SVWC decreased. At the individual plot scale, water limitation caused a significant increase in the rate of PRI_c response to solar radiation in 24 out of 32 total transitions between SVWC stages. This suggests that, in addition to a strong sensitivity of PRI_c to N availability, PRI_c is also highly responsive to water availability in this system.

1.3.5. PRI_c Sensitivity to Biomass Accumulation & Implications for Scaling PRI Data

In the final step of analysis, we compared LAI and NDVI values at the end of each water availability period with the slope of the PRI_c vs. solar radiation relationship from Fig. 1.9 to understand the relationship between remotely inferred stress and biomass accumulation. In theory, if PRI_c is tightly coupled to daily and seasonal fluctuations in abiotic stressors, a large PRI_c signal should indicate that the inferred crop stress would inhibit photosynthesis and biomass accumulation. To test this, we compared the magnitude of the daily response of PRI_c to solar radiation (slope of the line) against actual leaf area accumulation at the end of each water availability period. Fig 1.10 shows a statistically insignificant and weak relationship (R^2 = 0.22, 0.23, Fig. 1.10a, 10d) between LAI/NDVI and the PRI_c vs. solar radiation slope during the water surplus period. Significant and strong relationships were observed between the magnitude and rate of the PRI_c response to solar radiation and LAI/NDVI during the water depletion (R^2 = 0.70, 0.55, respectively, Fig. 1.10b, 1.10e), and water deficit periods (R^2 = 0.78, 0.83, respectively, Fig. 1.10c, 1.10f). These results suggest that a larger xanthophyll mediated drop in reflectance at 531 may be contributing to a lower capacity for photosynthesis at high light levels, resulting in stress-inhibited reduction in biomass accumulation. For example, higher N availability plots resulted in a smaller magnitude response of the PRI_c to light, resulting in greater biomass accumulation as measured by LAI and NDVI. The interpretation of this phenomena could be driving the relationships seen in Figs. 1.10a,b,d,&e, where biomass accumulation was occurring; however, during water deficit (Figs. 1.10 c,f), when little change in NDVI and LAI occurred, contrasting conclusions could be drawn suggesting that the less productive canopies actually spurred higher PRI_c response to sunlight.

The results in Fig. 1.10 show compelling evidence that theoretically more stress results in less biomass; however, a different interpretation of these data could assume that

PRI_c is more sensitive to total leaf area than the empirical relationships from this study suggest, and that PRI_c is responding to leaf area (particularly during the water deficit stage when the change in LAI and NDVI is minimal, Fig. 1.10c&f), as opposed to stress-inhibited biomass accumulation. While the predicative and explanatory variables in this relationship could be interchangeable, it can generally be assumed that a less productive wheat crop experiences a greater response of PRI_c to solar radiation. As a result, in this particular system, early detection of crop stress could be done by examining the diurnal deviation of PRI from a dark-state PRI_o. With this understanding, highly temporally and spatially resolved PRI_c data could enable growers and practitioners to monitor decreases in plant physiological condition days to weeks prior than could be detected using traditional remote sensing techniques (such as the NDVI, (Vierling et al., in review)).

PRI derived inferences of canopy photosynthetic performance via a xanthophyll mediated photoprotective response of green plants have been widely applied with varying degrees of success (Garbulsky et al., 2011); however, the interpretation of these data may be limited due to a lack of high temporally and spatially resolved spectral reflectance data over a wide range of plant structure and pigment conditions. Automated, well-calibrated sensors that enable high frequency data collection on the ground will surely help advance our scientific understanding of the PRI (Gamon et al., 2015). The technique proposed by Hall et al. (2012), and Hilker et al., (2012), whereby a physiologically based model (derived from APAR, temperature, and VPD) is combined with a single estimate of a PRI derived LUE from the CHRIS/PROBA satellite imaging spectrometer to down-regulate LUE at 30 minute intervals, could be further validated using ground-based sensors. Results from this study suggest that researchers should use caution when using satellite interpretations of daily photosynthesis via the PRI, as the timing of image acquisition, and the lack of a PRI_o, will play a major role on inferences made using the PRI. PRI scaling techniques could be improved and further validated using ground based (temporally overdetermined) data, as satellite- and airborne-based (spatially overdetermined) PRI measurements that only capture a single daily PRI value, for example, may be limited in their operational capacity.

1.4. Conclusion

We evaluated the utility of highly temporally resolved ground based radiometric measurements of PRI to capture crop response to environmental stress conditions (SVWC, nitrogen availability, VPD, temperature, gs) during two complete seasons in spring wheat. As with many other annual and deciduous canopies, wheat experiences substantial seasonal changes in foliar pigments and LAI, which have been shown to affect PRI. Our assessment evaluated a corrected PRI_c to account for structure and non-xanthophyll pigment variations, and determined that PRI_c adequately accounts for constitutive effects on the PRI signal related to changes in pigment concentration. From this, we determined the PRI_c does indeed respond to diurnal physiological changes resulting from changes in VPD, air temperature, and stomatal conductance. To determine the drivers of the magnitude of seasonal PRI_c patterns, we examined the slope of the relationship between PRI_c and solar radiation for each day in which sufficient sun was available to initiate xanthophyll cycle interconversion. The slope of the PRI_c vs. solar radiation least squares line was then compared using an ANCOVA between N treatments and three binned water availability periods (based on SVWC), and it was concluded that the PRI_c signal is more sensitive to conditions where water and nutrients are more limiting. The predictive capacity of these slopes (magnitude of PRI inferred stress) were then related to biomass accumulation – derived from LAI and NDVI - at the end of each binned soil water period, and it was determined that there is a tight correlation between total biomass accumulation and environmental stress conditions detectable using the PRI; however, the strength of this relationship during differing water availabilities can be interpreted in a number of independent and complimentary ways. Further research is necessary to decouple the relative contributions of different abiotic environmental stressors on the PRI stress response signal, but an examination of the diurnal PRI_c response to solar radiation here implies the magnitude of stress could be used in the future to elucidate the spatial and temporal variation in crop performance at the field scale.

This study has potentially broad implications for the scaling and future interpretation of the PRI as an indicator of plant stress. Further development of these techniques could lead to early stress detection for site-specific irrigation and nutrient management in agricultural systems or to infer future crop breeding endeavors focused on targeting stress during specific plant phenophases. These results support a growing body of evidence that the standard PRI

formulation needs to be corrected for canopy pigment content and seasonal changes in LAI, and that fine temporal resolution measurements might be necessary to completely capture the midday photosynthetic depression response seen in plants.

References:

Baker N. R., Oxborough K., (2004) Chlorophyll fluorescence as a probe of photosynthetic productivity in "Chlorophyll a Fluorescence a Signature of Photosynthesis". eds. George Papaqeorgiou and Govindjee. Springer Dordrecht, The Netherlands

Barton, C. V. M., & North, P. R. J. (2001). Remote sensing of canopy light use efficiency using the photochemical reflectance index Model and sensitivity analysis. *Remote Sensing of Environment*, *78*, 264–273.

Bilger W, Schreiber U, Bock M (1995) Determination of the quantum efficiency of photosystem II and of nonphotochemical quenching of chlorophyll fluorescence in the field. *Oecologia* 102, 425–432. doi: 10.1007/BF00341354

Cheng, Y.-B., Middleton, E., Zhang, Q., Huemmrich, K., Campbell, P., Corp, L., Cook, B., Kustas, W., Daughtry, C. (2013). Integrating Solar Induced Fluorescence and the Photochemical Reflectance Index for Estimating Gross Primary Production in a Cornfield. *Remote Sensing*, *5*(12), 6857–6879. doi:10.3390/rs5126857

Claudio, H., Cheng, Y., Fuentes, D., Gamon, J., Luo, H., Oechel, W., Qiu, J, Rahman, A, Sims, D. (2006). Monitoring drought effects on vegetation water content and fluxes in chaparral with the 970 nm water band index. *Remote Sensing of Environment*, *103*(3), 304–311. doi:10.1016/j.rse.2005.07.015

Cleveland, W.S., (1979). Robust locally weighted regression and smoothing scatter- plots. *J. Am. Stat. Assoc*. 74, 829–836.

Cleveland, W.S., Devlin, S.J., (1988). Locally weighted regression – an approach to regression analysis by local fitting. *J. Am. Stat. Assoc*. 83, 596–610.

Demmig-Adams, B., & Adams, W. W. (1992). Photoprotection and other responses of plants to high light stress. *Annual Review of Plant Physiology*, 599–626.

Demming-Adams, B., & Adams, W. W. (1996). The role of xanthophyll cycle carotenoids in the protection of photosynthesis. *Trends in Plant Science*, *1*(1), 21–26.

Demmig-Adams, B., Cohu, C. M., Muller, O., & Adams, W. W. (2012). Modulation of photosynthetic energy conversion efficiency in nature: from seconds to seasons. *Photosynthesis Research*, *113*(1-3), 75–88. doi:10.1007/s11120-012-9761-6

Dobrowski, S., Pushnik, J., Zarcotejada, P., & Ustin, S. (2005). Simple reflectance indices track heat and water stress-induced changes in steady-state chlorophyll fluorescence at the canopy scale. *Remote Sensing of Environment*, *97*(3), 403–414. doi:10.1016/j.rse.2005.05.006

Drolet, G. G., Huemmrich, K. F., Hall, F. G., Middleton, E. M., Black, T. A., Barr, A. G., & Margolis, H. A. (2005). A MODIS-derived Photochemical Reflectance Index to detect inter-annual variations in the photosynthetic light-use efficiency of a boreal deciduous forest. *Remote Sensing of Environment*, 98,212−224.

Eitel, J. U. H., Long, D. S., Gessler, P. E., & Hunt, E. R. (2008). Combined Spectral Index to Improve Ground-Based Estimates of Nitrogen Status in Dryland Wheat. *Agronomy Journal*. doi:10.2134/agronj2007.0362

Eitel, J. U. H., Magney, T. S., Vierling, L. A., Brown, T. T., & Huggins, D. R. (2014). LiDAR based biomass and crop nitrogen estimates for rapid , non-destructive assessment of wheat nitrogen status. *Field Crops Research*, *159*, 21–32.

Filella, I., Porcar-Castell, A., Munné-Bosch, S., Bäck, J., Garbulsky, M. F., & Peñuelas, J. (2009). PRI assessment of long-term changes in carotenoids/chlorophyll ratio and short-term changes in de-epoxidation state of the xanthophyll cycle. *International Journal of Remote Sensing*, *30*(17), 4443–4455. doi:10.1080/01431160802575661

Gamon, J.A., Field, C.B., Bilger, W., Björkman, O., Fredeen, A.L., Penuelas J. (1990). Remote sensing of the xanthophyll cycle and chloro- phyll fluorescence in sunflower leaves and canopies. *Oecologia*, *85,* 1–7

Gamon, J. A., Penuelas, J., & Field, C. B. (1992). A Narrow-Waveband Spectral Index That Tracks Diurnal Changes in Photosynthetic Efficiancy. *Remote Sensing of Environment*, *41*, 35–44.

Gamon, J. A., Serrano, L., & Surfus, J. S. (1997). The photochemical reflectance index: an optical indicator of photosynthetic radiation use efficiency across species, functional types, and nutrient levels. *Oecologia*, *112*(4), 492–501. doi:10.1007/s004420050337

Gamon, J. A., & Surfus, J. S. (1999). Assessing leaf pigment content and activity with a reflectometer. *New Phytologist*, *143*(1), 105–117. doi:10.1046/j.1469-8137.1999.00424.x

Gamon, J., Cheng, Y., Claudio, H., Mackinney, L., & Sims, D. (2006). A mobile tram system for systematic sampling of ecosystem optical properties. *Remote Sensing of Environment*, *103*(3), 246–254. doi:10.1016/j.rse.2006.04.006

Gamon, J. A., & Berry, J. A. (2012). Facultative and constitutive pigment effects on the Photochemical Reflectance Index (PRI) in sun and shade conifer needles. *Israel Journal of Plant Sciences*, *60*(1), 85–95. doi:10.1560/IJPS.60.1-2.85

Gamon, J. A., & Bond, B. (2013). Effects of irradiance and photosynthetic downregulation on the photochemical reflectance index in Douglas-fir and ponderosa pine. *Remote Sensing of Environment*, *135*, 141–149. doi:10.1016/j.rse.2013.03.032

Gamon, J. A., Kovalchuk, O., Wong, C. Y. S., Harris, A., & Garrity, S. R. (2015). Monitoring seasonal and diurnal changes in photosynthetic pigments with automated PRI and NDVI sensors. *Biogeosciences Discussions*, *12*, 2947–2978. doi:10.5194/bgd-12-2947-2015

Garbulsky, M. F., Peñuelas, J., Gamon, J., Inoue, Y., & Filella, I. (2011). The photochemical reflectance index (PRI) and the remote sensing of leaf, canopy and ecosystem radiation use efficienciesA review and meta-analysis. *Remote Sensing of Environment*, *115*(2), 281–297. doi:10.1016/j.rse.2010.08.023\

Garrity, S. R., Vierling, L. A., & Bickford, K. (2010). A simple filtered photodiode instrument for continuous measurement of narrowband NDVI and PRI over vegetated canopies. *Agricultural and Forest Meteorology*, *150*(3), 489–496. doi:10.1016/j.agrformet.2010.01.004

Garrity, S. R., Eitel, J. U. H., & Vierling, L. A. (2011). Disentangling the relationships between plant pigments and the photochemical reflectance index reveals a new approach for remote estimation of carotenoid content. *Remote Sensing of Environment*, *115*(2), 628–635. doi:10.1016/j.rse.2010.10.007

Gond, V., De Pury, D. G. G., Veroustraete, F., & Ceulemans, R. (1999). Seasonal variations in leaf area index, leaf chlorophyll, and water content; scaling-up to estimate fAPAR and carbon balance in a multilayer, multispecies temperate forest. *Tree Physiology*, *19*(10), 673–679.

Guo, J., & Trotter, C.M. (2004). Estimating photosynthetic light-use efficiency using the Photochemical Reflectance Index: Variations among species. *Functional Plant Biology*, 31, 255−565.

Hall, F. G., Hilker, T., Coops, N. C., Lyapustin, A., Huemmrich, K. F., Middleton, E., Margolis, H., Drolet, G., Black, T. A. (2008). Multi-angle remote sensing of forest light use efficiency by observing PRI variation with canopy shadow fraction. *Remote Sensing of Environment*, *112*(7), 3201–3211. doi:10.1016/j.rse.2008.03.015

Hall, F. G., Hilker, T., & Coops, N. C. (2012). Data assimilation of photosynthetic light-use efficiency using multi-angular satellite data: I. Model formulation. *Remote Sensing of Environment*, *121*, 301–308. doi:10.1016/j.rse.2012.02.007

Harris, a., Gamon, J., Pastorello, G. Z., & Wong, C. (2014). Retrieval of the photochemical reflectance index for assessing xanthophyll cycle activity: a comparison of near-surface optical sensors. *Biogeosciences Discussions*, *11*(8), 11903–11942. doi:10.5194/bgd-11-11903-2014

Hartel, H., Lokstein, H., Grimm, B., & Rank, B. (1999). Kinetic Studies on the Xanthophyll Cycle in Barley Leaves. *Plant Physiology*, *110*, 471–482.

Hernández-Clemente, R., Navarro-Cerrillo, R. M., Suárez, L., Morales, F., & Zarco-Tejada, P. J. (2011). Assessing structural effects on PRI for stress detection in conifer forests. *Remote Sensing of Environment*, *115*(9), 2360–2375. doi:10.1016/j.rse.2011.04.036

Hilker, T., Coops, N. C., Hall, F. G., Black, T. A., Wulder, M. a., Nesic, Z., & Krishnan, P. (2008). Separating physiologically and directionally induced changes in PRI using BRDF models. *Remote Sensing of Environment*, *112*(6), 2777–2788. doi:10.1016/j.rse.2008.01.011

Hilker, T., Coops, N. C., Coggins, S. B., Wulder, M. a., Brown, M., Black, T. A., Nesic, Z., Lessard, D. (2009). Detection of foliage conditions and disturbance from multi-angular high spectral resolution remote sensing. *Remote Sensing of Environment*, *113*(2), 421–434. doi:10.1016/j.rse.2008.10.003

Hilker, T., Hall, F. G., Tucker, C. J., Coops, N. C., Black, T. A., Nichol, C. J., Munger, J. W. (2012). Data assimilation of photosynthetic light-use efficiency using multi-angular satellite data: II Model implementation and validation. *Remote Sensing of Environment*, *121*, 287–300. doi:10.1016/j.rse.2012.02.008

Hmimina, G., Dufrêne, E., & Soudani, K. (2014). Relationship between photochemical reflectance index and leaf ecophysiological and biochemical parameters under two different water statuses: towards a rapid and efficient correction method using real-time measurements. *Plant, Cell & Environment*, *37*(2), 473–87. doi:10.1111/pce.12171

Hmimina, G., Merlier, E., Dufrêne, E., & Soudani, K. (2015). Deconvolution of pigment and physiologically-related PRI variability at the canopy scale over an entire growing season. *Plant, Cell and Environment*. doi:10.1111/pce.12509

Liu, L., Zhang, Y., Jiao, Q., & Peng, D. (2013). Assessing photosynthetic light-use efficiency using a solar-induced chlorophyll fluorescence and photochemical reflectance index. *International Journal of Remote Sensing*, *34*(12), 4264–4280.

Logan, B. a., Adams, W. W., & Demmig-Adams, B. (2007). Viewpoint: Avoiding common pitfalls of chlorophyll fluorescence analysis under field conditions. *Functional Plant Biology*, *34*(9), 853. doi:10.1071/FP07113

Malenovsky, Z., Mishra, K. B., Zemek, F., Rascher, U., & Nedbal, L. (2009). Scientific and technical challenges in remote sensing of plant canopy reflectance and fluorescence. *Journal of Experimental Botany,* 60, 2987−3004.

Magney, T. S., Eusden, S. A., Eitel, J. U. H., Logan, B. A., Jiang, J., & Vierling, L. A. (2014). Assessing leaf photoprotective mechanisms using terrestrial LiDAR: towards mapping canopy photosynthetic performance in three dimensions. *New Phytologist*, *201*, 344-356

Muggeo, V.M.R. (2003). Estimating regression models with unknown break-points. *Statistics in Medicine*, 22, 3055–3071.

Muggeo, V.M.R. (2008). segmented: an R package to fit regression models with broken- line relationships. *R News*, 8/1,20–25. Available at: http://cran.r-project.org/doc/ Rnews/ (accessed 18 September 2014).

Mulla, D. J. (2013). Twenty five years of remote sensing in precision agriculture: Key advances and remaining knowledge gaps. *Biosystems Engineering*, *114*(4), 358–371. doi:10.1016/j.biosystemseng.2012.08.009

Nakaji, T., Oguma, H., & Fujinuma, Y. (2006). Seasonal changes in the relationship between photochemical reflectance index and photosynthetic light use efficiency of Japanese larch needles. *International Journal of Remote Sensing*, *27*(3), 493–509.

Nichol, C. J., Rascher, U., Matsubara, S., & Osmond, B. (2006). Assessing photosynthetic efficiency in an experimental mangrove canopy using remote sensing and chlorophyll fluorescence. *Trees*, *20*(1), 9–15. doi:10.1007/s00468-005-0005-7

Peguero-Pina, J. J., Gil-Pelegrín, E., & Morales, F. (2013). Three pools of zeaxanthin in Quercus coccifera leaves during light transitions with different roles in rapidly reversible photoprotective energy dissipation and photoprotection. *Journal of Experimental Botany*. doi:10.1093/jxb/ert024

Penuelas, J., Filella, I., & Gamon, J. a. (1995). Assessment of photosynthetic radiation-use efficiency with spectral reflectance. *New Phytologist*, *131*(3), 291–296. doi:10.1111/j.1469-8137.1995.tb03064.x

Penuelas, J., Garbulsky, M. F., & Filella, I. (2011). Photochemical reflectance index (PRI) and remote sensing of plant CO 2 uptake. *New Phytologist*, *191*, 596–599.

Porcar-Castell, A., Garcia-Plazaola, J. I., Nichol, C. J., Kolari, P., Olascoaga, B., & Kuus. (2012). Physiology of the seasonal relationship between the photochemical reflectance index and photosynthetic light use efficiency. *Oecologia*, *170*, 313–323. doi:10.1007/s00442-012-2317-9

Rahimzadeh-Bajgiran, P., Munehiro, M., & Omasa, K. (2012). Relationships between the photochemical reflectance index (PRI) and chlorophyll fluorescence parameters and plant pigment indices at different leaf growth stages. *Photosynthesis Research*, *113*(1-3), 261–71. doi:10.1007/s11120-012-9747-4

Ryu, Y., Baldocchi, D. D., Verfaillie, J., Ma, S., Falk, M., Ruiz-Mercado I.,, Hehn, T., Sonnentag, O. (2010). Testing the performance of a novel spectral reflectance sensor, built with light emitting diodes (LEDs), to monitor ecosystem metabolism, structure and function. *Agricultural and Forest Meteorology*, *150*(12), 1597–1606. doi:10.1016/j.agrformet.2010.08.009

Shrestha, S., Brueck, H., & Asch, F. (2012). Chlorophyll index, photochemical reflectance index and chlorophyll fluorescence measurements of rice leaves supplied with different N levels. *Journal of Photochemistry and Photobiology. B, Biology*, *113*, 7–13. doi:10.1016/j.jphotobiol.2012.04.008

Sims, D., Luo, H., Hastings, S., Oechel, W., Rahman, A, & Gamon, J. (2006). Parallel adjustments in vegetation greenness and ecosystem CO2 exchange in response to drought in a Southern California chaparral ecosystem. *Remote Sensing of Environment*, *103*(3), 289–303. doi:10.1016/j.rse.2005.01.020

Soudani, K., Hmimina, G., Dufrêne, E., Berveiller, D., Delpierre, N., Ourcival, J.-M., Rambal, S., Joffre, R. (2014). Relationships between photochemical reflectance index and light-use efficiency in deciduous and evergreen broadleaf forests. *Remote Sensing of Environment*, *144*, 73–84. doi:10.1016/j.rse.2014.01.017

Strachan, I. B., Pattey, E., & Boisvert, J. B. (2002). Impact of nitrogen and environmental conditions on corn as detected by hyperspectral reflectance. *Remote Sensing of Environment*, *80*(2), 213–224. doi:10.1016/S0034-4257(01)00299-1

Stylinski, C., Gamon, J., & Oechel, W. (2002). Seasonal patterns of reflectance indices, carotenoid pigments and photosynthesis of evergreen chaparral species. *Oecologia*, *131*(3), 366–374. doi:10.1007/s00442-002-0905-9

Suárez, L., Zarco-Tejada, P. J., Sepulcre-Cantó, G., Pérez-Priego, O., Miller, J. R., Jiménez-Muñoz, J. C., & Sobrino, J. (2008). Assessing canopy PRI for water stress detection with diurnal airborne imagery. *Remote Sensing of Environment*, *112*(2), 560–575. doi:10.1016/j.rse.2007.05.009

Suárez, L., Zarco-Tejada, P. J., Berni, J. a. J., González-Dugo, V., & Fereres, E. (2009). Modelling PRI for water stress detection using radiative transfer models. *Remote Sensing of Environment*, *113*(4), 730–744. doi:10.1016/j.rse.2008.12.001

Suárez, L., Zarco-Tejada, P. J., González-Dugo, V., Berni, J. a. J., Sagardoy, R., Morales, F., & Fereres, E. (2010). Detecting water stress effects on fruit quality in orchards with time-series PRI airborne imagery. *Remote Sensing of Environment*, *114*(2), 286–298. doi:10.1016/j.rse.2009.09.006

Sweet, S. K., Griffin, K. L., Steltzer, H., Gough, L., & Boelman, N. T. (2015). Greater deciduous shrub abundance extends tundra peak season and increases modeled net CO 2 uptake. *Global Change Biology*, Early view. doi:10.1111/gcb.12852

Thenot, F., Methy, M., & Winkel, T. (2002). The Photochemical Re ectance Index (PRI) as a water-stress index. *International Journal of Remote Sensing*, *23*(23), 5135–5139.

Tucker, C. J. (1979). Red and photographic infrared linear combinations for monitoring vegetation. *Remote Sensing of Environment*, 8,127–150.

Verhoeven, A. S., Demmig-Adams, B., & Adams III, W. W. (1997). Enhanced Employment of the Xanthophyll Cycle and Thermal Energy Dissipation in Spinach Exposed to High Light and N Stress. *Plant Physiology*, *113*(3), 817–824.

Zarco-Tejada, P. J., Catalina, A., González, M. R., & Martín, P. (2013a). Relationships between net photosynthesis and steady-state chlorophyll fluorescence retrieved from airborne hyperspectral imagery. *Remote Sensing of Environment*, *136*, 247–258. doi:10.1016/j.rse.2013.05.011

Zarco-Tejada, P. J., Morales, A., Testi, L., & Villalobos, F. J. (2013b). Spatio-temporal patterns of chlorophyll fluorescence and physiological and structural indices acquired from hyperspectral imagery as compared with carbon fluxes measured with eddy covariance. *Remote Sensing of Environment*, *133*, 102–115. doi:10.1016/j.rse.2013.02.003

Zhang, C., & Kovacs, J. M. (2012). The application of small unmanned aerial systems for precision agriculture: a review. *Precision Agriculture*, *13*(6), 693–712. doi:10.1007/s11119-012-9274-5

Table 1.1. Formulation of vegetation indices used in this study.

Index	Equation	Explanation	References
NDVI	(ρ800-ρ630) /(ρ800+ρ630)	Widely accepted spectral index for changes in vegetation structure.	Tucker et al. (1979)
PRI	(ρ531-ρ570)/(ρ531+ρ570)	PRI at time of sample (i.e., g_s) for diurnal correlations or minimum PRI for given day for seasonal correlations.	Gamon et al. (1992)
PRI_o	(ρ531-ρ570)/(ρ531+ρ570)	Mean PRI value between solar radiation levels between 50 and 150 W/m^2 . In this regard PRI_o serves as a "dark-state" PRI, which is influenced by structural and biochemical components.	Adapted from Hmimani et al., 2014 & Soudani et al., 2014
PRI_c	PRI - PRI_0	Using PRI_0 as a proxy for constitutive (seasonal) PRI dynamics, a ΔPRI in computed to account for changes in pigment composition throughout the season effectively measuring the "departure from steady state/ xanthophyll cycle de-epoxidation". PRI at time of sample (i.e., g_s) is for diurnal correlations or minimum PRI for given day for seasonal correlations.	Adapted from Liu et al., 2013

Table 1.2. Coefficients of determination (R^2) among stomatal conductance (g_s, mmol m^{-2} s^{-1}), diurnal vapor pressure deficit (VPD_d, kPa), average daily vapor pressure deficit (VPDs, kPa, seasonal), diurnal air temperature ($Temp_d$, ºC), average daily air temperature ($Temp_s$ ºC), relative chlorophyll concentration (SPAD), Leaf Area Index (LAI, m^2 m^{-2}), and NDVI, PRI, PRI_o, PRI_c. Relationships are derived from data spanning both the 2013 and 2014 growing seasons over all experimental plots.

	g_s	VPD_d	$Temp_d$	VPD_s	$Temp_s$	SPAD	LAI	NDVI	PRI	PRI_o	PRI_c
g_s	1.00										
VPD_d	0.45*	1.00									
$Temp_d$	0.38*	0.71*	1.00								
VPD_s				1.00							
$Temp_s$				0.74*	1.00						
SPAD				0.40*	0.29*	1.00					
LAI				0.27*	0.15	0.01	1.00				
NDVI	0.17	0.11	0.09	0.10	0.05	0.10	0.64*	1.00			
PRI	0.38*	0.28*	0.21*	0.33*	0.24*	0.44*	0.27*	0.05	1.00		
PRI_o				0.30*	0.22*	0.55*	0.32*	0.16	0.45*	1.00	
PRI_c	0.40*	0.42*	0.32*	0.50*	0.45*	0.27*	0.24*	0.05	0.47*	0.79*	1.00

*correlations significant at the p <.05 level

Sample size (n):

Top performing vegetation index — g_s = 96

Diurnal data available for correlations — VPD & Temp (d) - diurnal = 5,284

Diurnal data not available for correlatations — LAI & SPAD = 176

No color: All other correlations (seasonal) — Seasonal (s) relationships = 1,416

Figures:

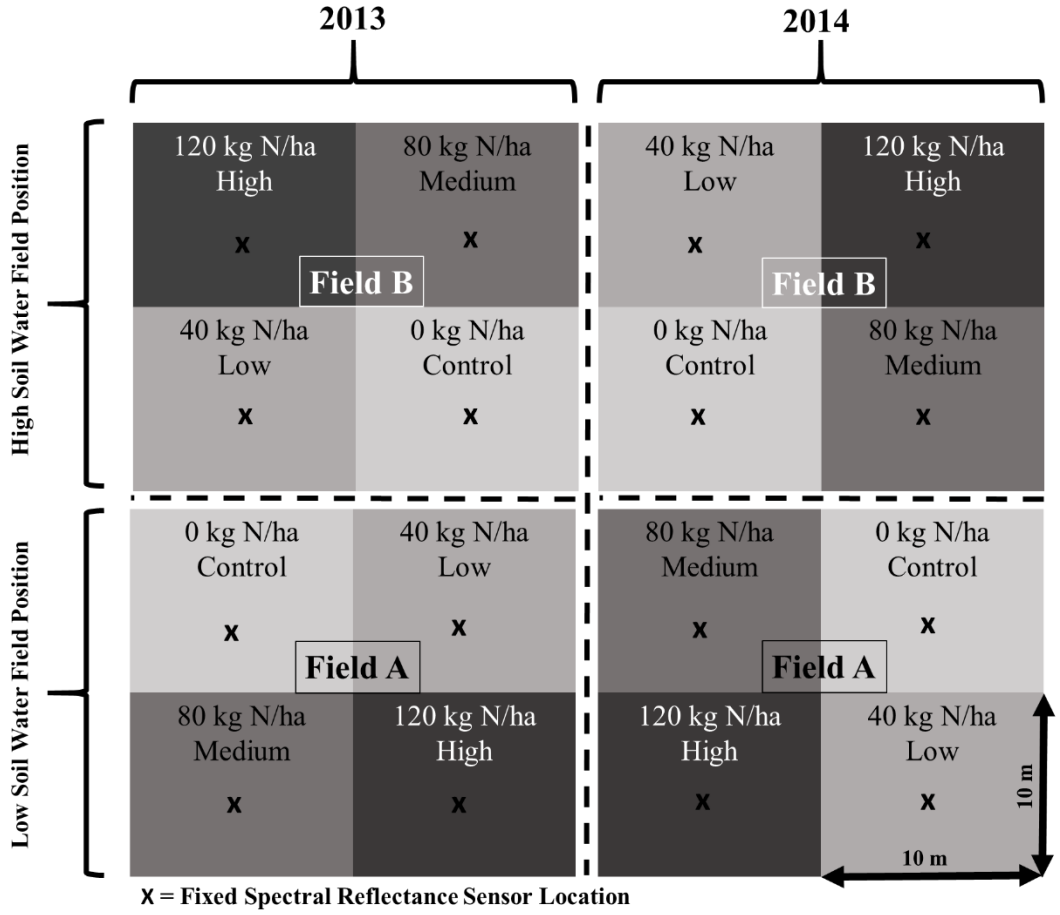

Figure 1.1. Overview of the experimental design of the study. Plots with four applied nitrogen (N) treatments (control, low, medium, and high) placed in historically low (south facing)and high (north facing) soil water field positions during the 2013 and 2014 growing seasons. Note that between years the relative positions of the two plot locations are not to scale.

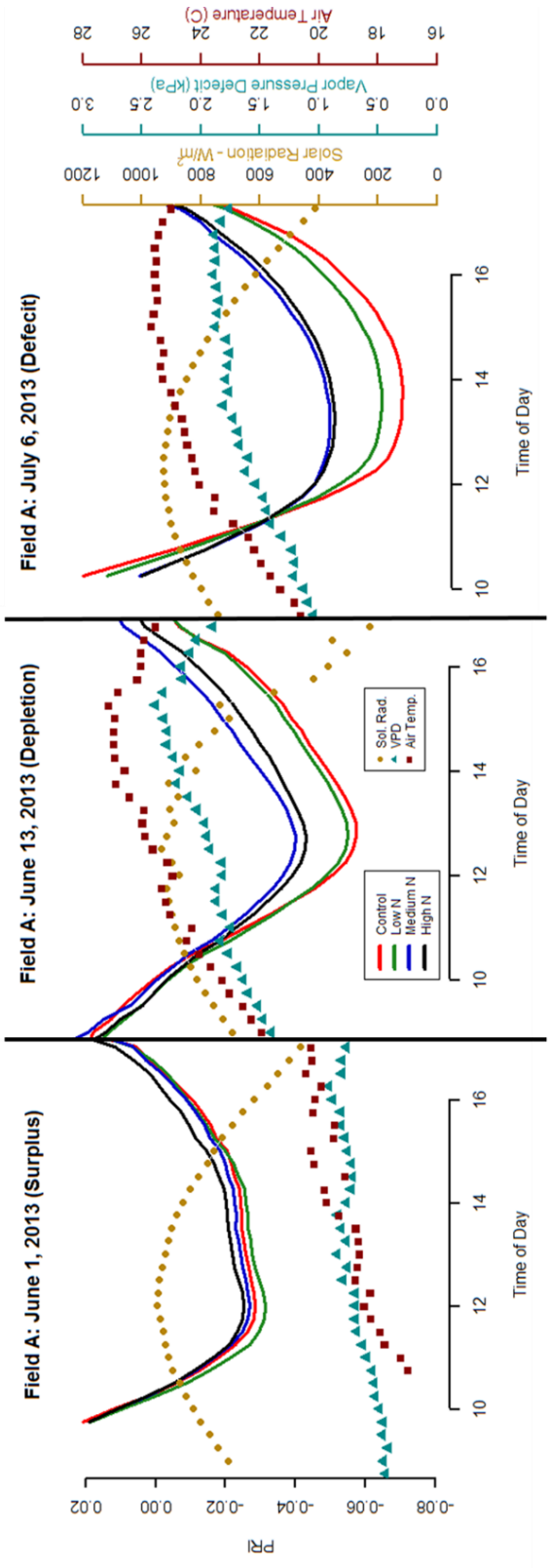

Figure 1.2. Diurnal dynamics of the PRI signal during the early (water surplus), middle (water depletion), and late (water deficit) portions of the 2013 growing season on Field A. These data are compared against diurnal changes in solar radiation (gold dots), VPD (cyan triangles), and Air Temp (crimson squares). The solid lines represent PRI curves that have not been corrected by a dark-state.

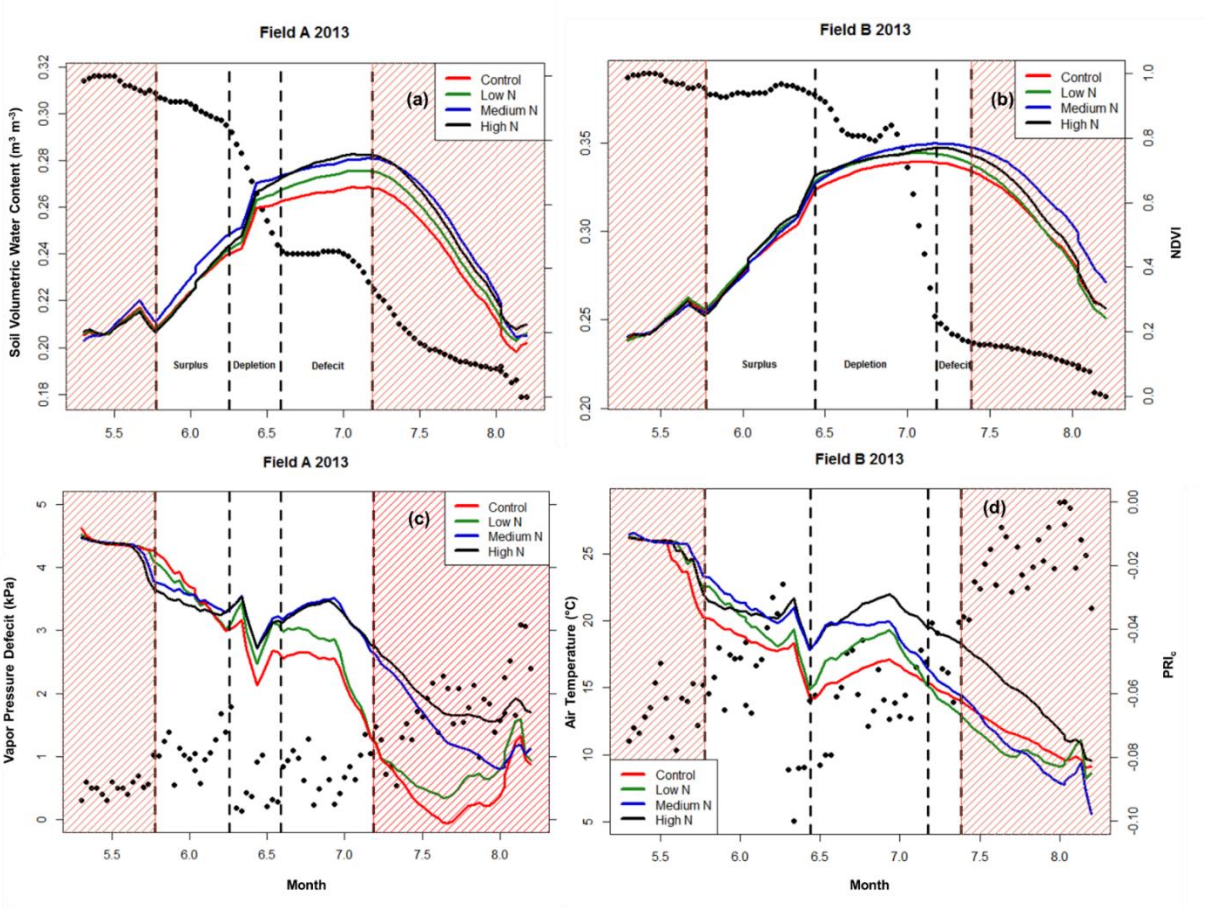

Figure 1.3. (**a**) Seasonal variation in 5 cm depth soil volumetric water content (m^3/m^3, black dots) and midday NDVI over four applied nitrogen rates (control = red, low N = green, medium N = blue, high N = black) on field A (low moisture field position) in 2013. Vertical lines correspond with inflection points in SVWC and NDVI data used to bin the data into three water availability periods: surplus, depletion, and deficit. Diagonal red lines indicate data that was not used in analysis because pre-determined inflection points either prior to crop emergence or after the onset of senescence. (**b**) Same as (a) except at field B (high moisture position). (**c**) Seasonal variation in mean daily VPD (kPa, black dots) and PRI_c over four applied nitrogen rates on field A. (**d**) Same as (c) except at field B and compared to mean daily air temperature. Note: VPD and air temperature were the same for fields A and B, while SVWC was measured at each plot location.

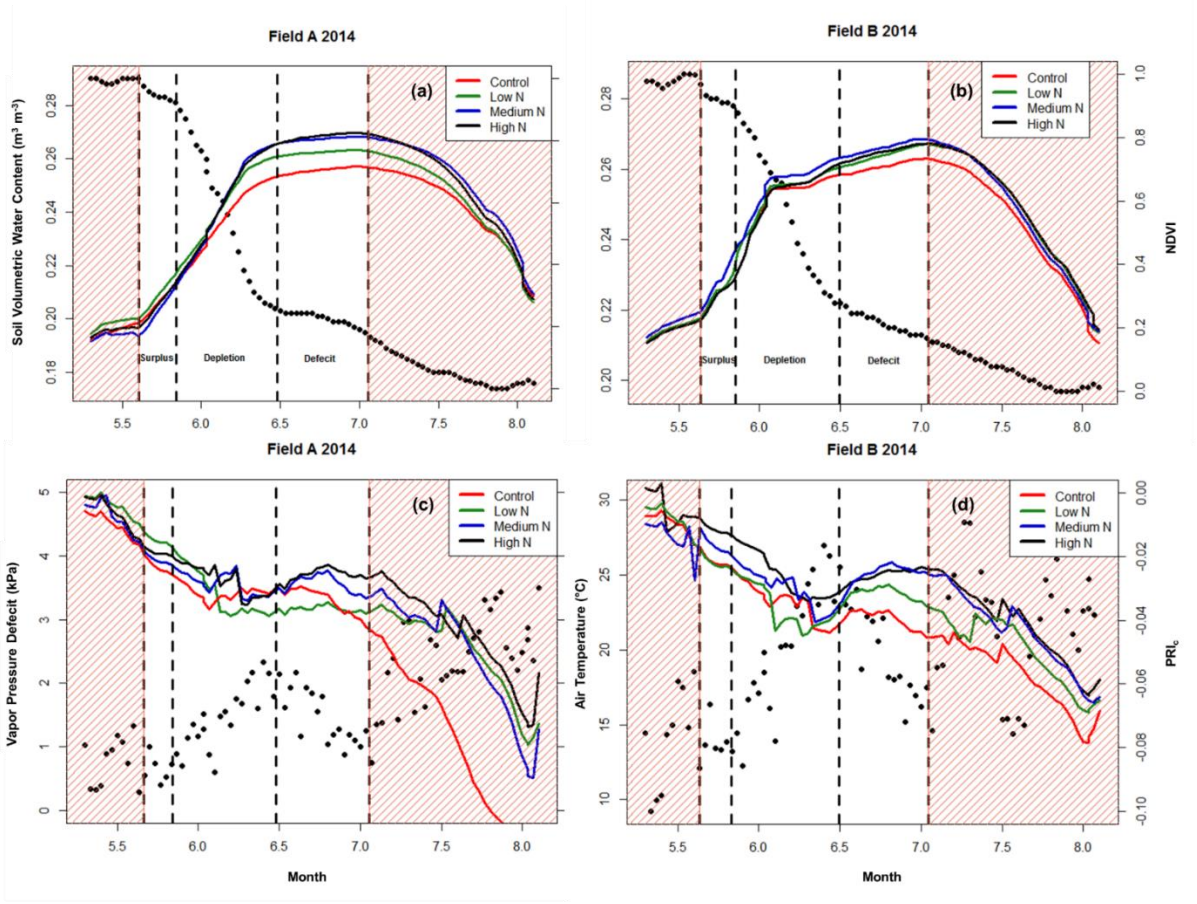

Figure 1.4. (**a**) Seasonal variation in 5 cm depth soil volumetric water content (m^3/m^3, black dots) and midday NDVI over four applied nitrogen rates (control = red, low N = green, medium N = blue, high N = black) on field A (low moisture field position) in 2014. Vertical lines correspond with inflection points in SVWC and NDVI data used to bin the data into three water availability periods: surplus, depletion, and deficit. Diagonal red lines indicate data that was not used in analysis because of pre-determined inflection points either prior to crop emergence or after the onset of senescence. (**b**) Same as (a) except at field B (high moisture position). (**c**) Seasonal variation in mean daily VPD (kPa, black dots) and PRI_c over four applied nitrogen rates on field A. (**d**) Same as (c) except at field B and compared to mean daily air temperature. Note: VPD and air temperature were the same for fields A and B, while SVWC was measured at each plot location.

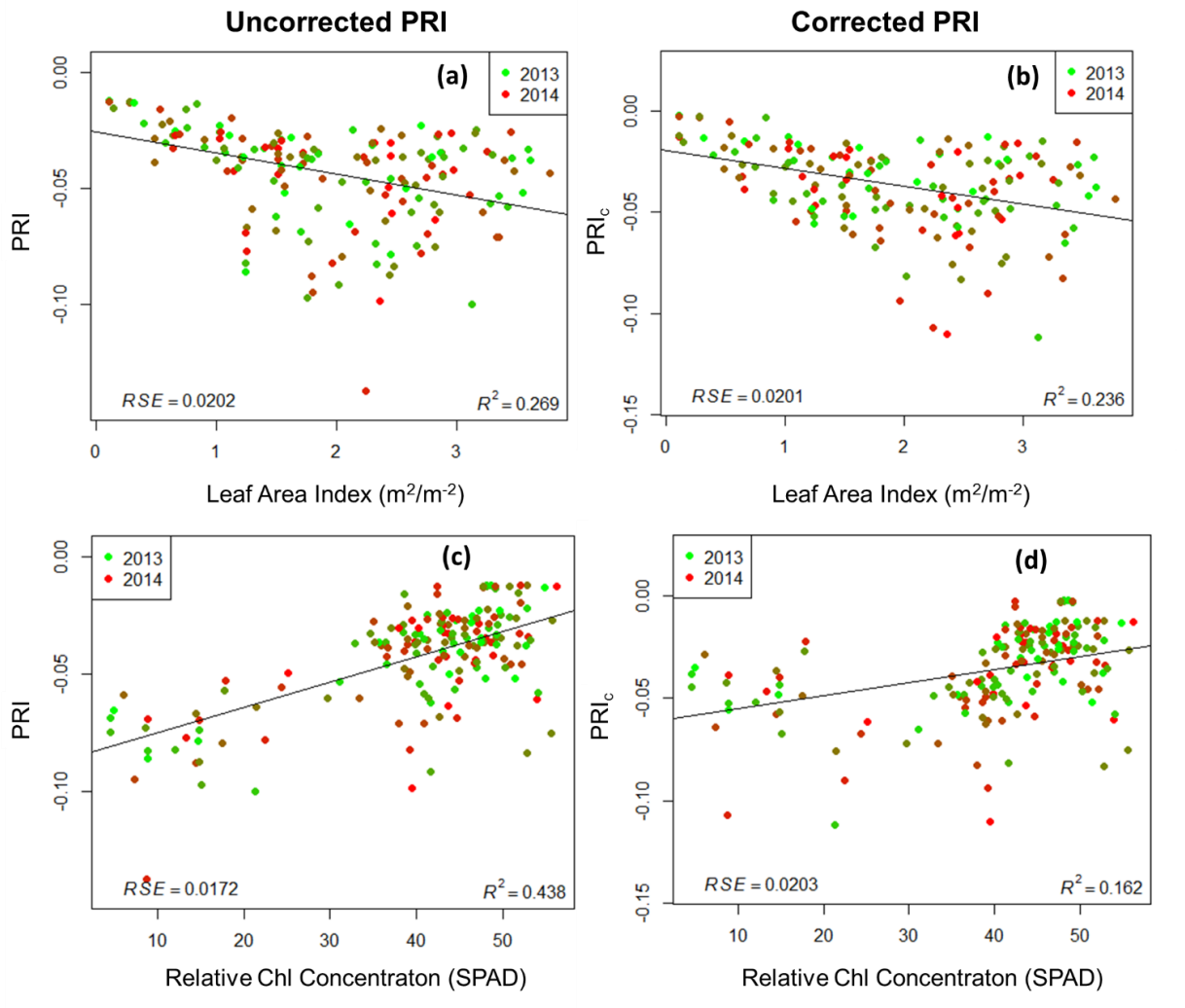

Figure 1.5. (**a**) Seasonal relationship between LAI and PRI over all treatment plots in 2013 (red) and 2014 (green). Shades of red and green represent the different nitrogen treatment plots for each season (n=8). RSE = residual standard error (PRI units (**b**) PRI_c against LAI; $PRI_c = PRI_{daily\ minimum} - PRI_o$); (**c**) Relative chlorophyll concentration (SPAD) vs. uncorrected PRI; **(d)** SPAD vs. corrected PRI_c. Sample size is 176 for Figs. a-d.

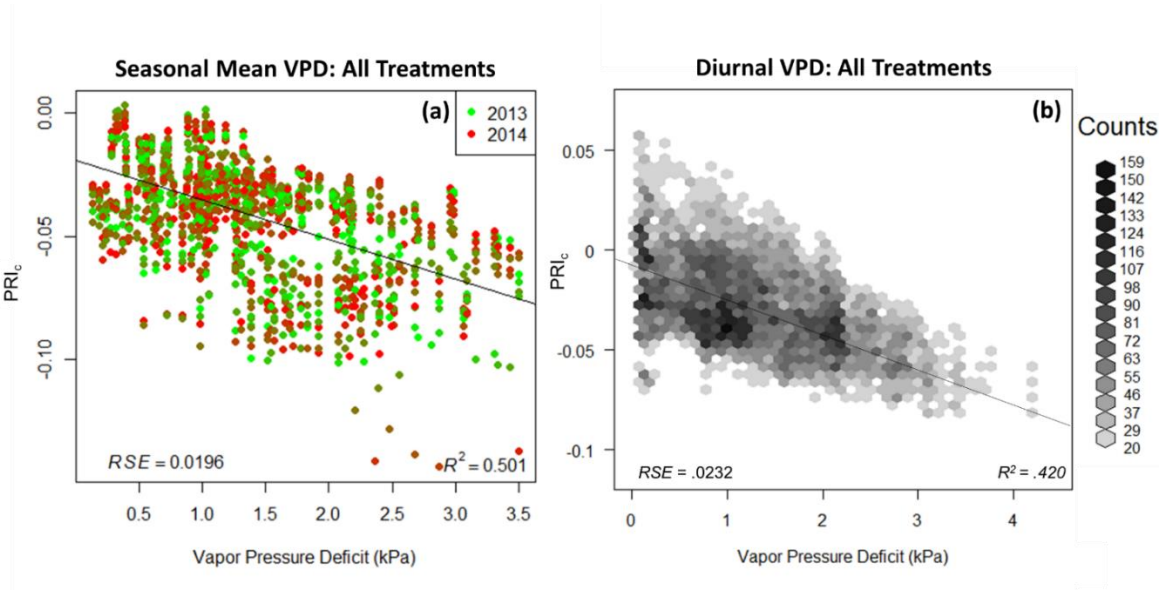

Figure 1.6. (**a**) Seasonal relationship between VPD_d (8:00-18:00) and PRI_c over all treatment plots over both seasons (green = 2013; red = 2014; n= 1416); $PRI_c = PRI_{daily\ minimum} - PRI_o$; RSE = residual standard error (PRI units). Shades of red and green indicate individual treatment plots (**b**) Diurnal PRI_c against VPD for all treatments over both seasons (n = 5,284). Data is binned into hexagonal bins for visualization using count data broken up in groupings of 8-9 (hexbin function, R core team 2014). Bins with counts < 20 were excluded from figure but were included in statistical analysis, and colors were not assigned due to high point density.

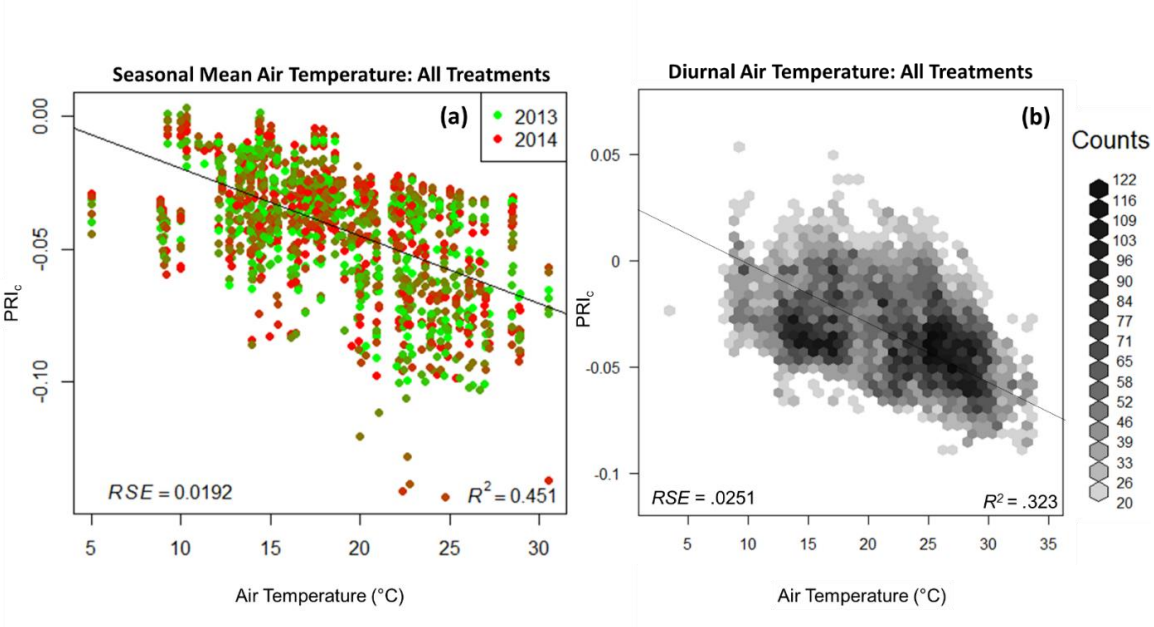

Figure 1.7. (**a**) Seasonal relationship between daily mean air temperature (8:00-18:00) and PRI_c over all treatment plots over both seasons (n= 1416); $PRI_c = PRI_{daily\ minimum} - PRI_o$; RSE = residual standard error (PRI units). (**b**) Diurnal PRI_c against air temperature for all treatments over both seasons (n = 5,284). Data is binned used hexagonal bins for visualization using count data broken up in groupings of 8-9 (hexbin function, R core team). Bins with counts < 20 were excluded from figure but were included in statistical analysis.

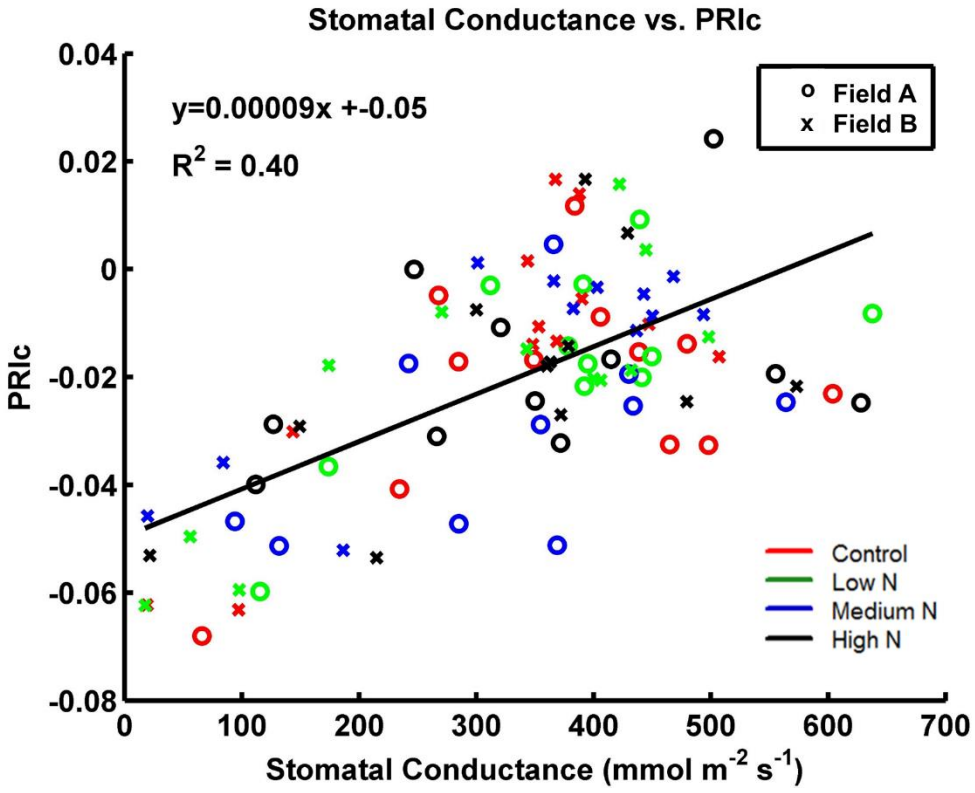

Figure 1.8. Stomatal conductance (g_s, mmol m^{-2} s^{-1}, n = 12 per data point) vs. PRI_c (n=96). g_s measurements taken throughout four days during the 2014 growing season were used as a validation of the PRI_c response to diurnal physiological changes induced by environmental variables.

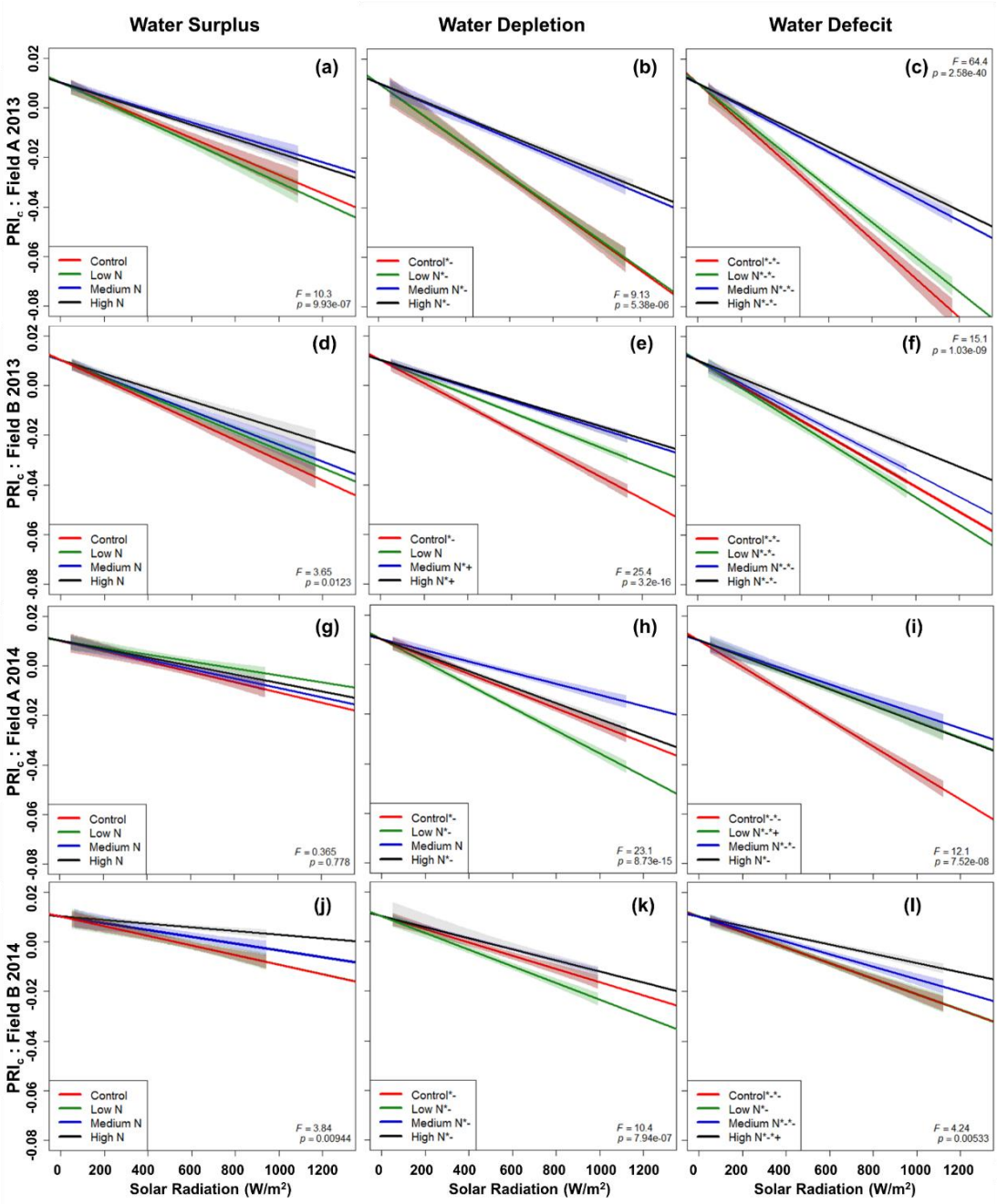

Figure 1.9. (**a**) Field A 2013: Response of PRI_c to solar radiation (W m^{-2}) over all treatment plots (control = red, low = green, medium = blue, high = black) with 95% confidence intervals during water surplus. F and p value from ANCOVA conducted on all four treatment plots. * indicates a significant difference between water availability periods, and a + or - indicates a positive or negative change in slope between (a), (b), and (c) for each treatment plot. (**b**) Same as (a) except during water depletion. (**c**) Same as (a) except during water deficit. (**d-f**) same as a-c except for field B 2013. (**g-i**) same as a-c except for field A 2014. (**j-l**) same as a-c except for field B 2014.

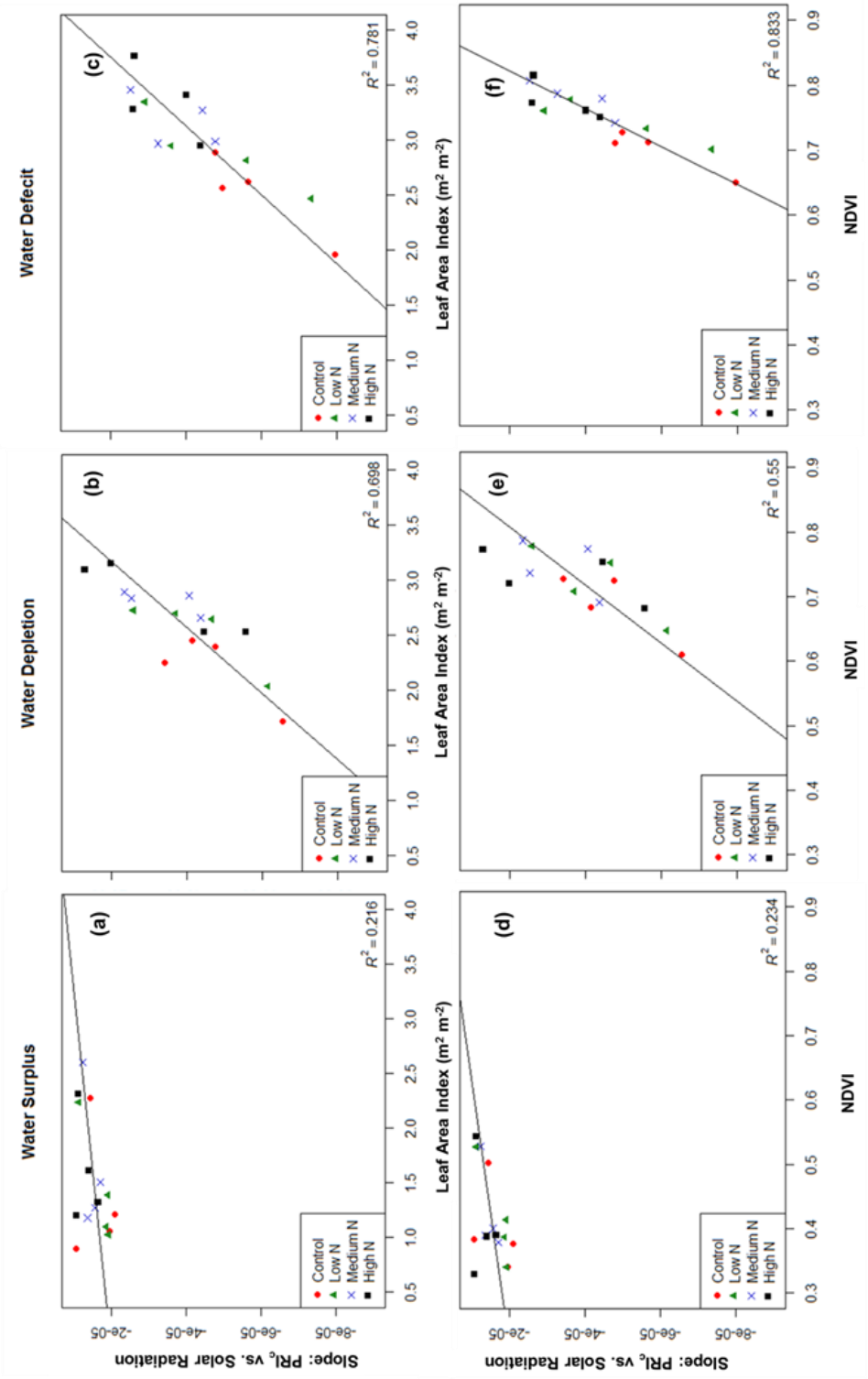

Figure 1.10. (**a**) Slope of PRI_c vs. Irradiance (W m^{-2}) as a predictor of biomass accumulation as measured by LAI (m^2 m^{-2}) at the end of binned water availability period (control = red circle, low = green triangle, medium = blue x, high = black square) (**b**) Same as (a) except during water depletion. (**c**) Same as (a) except during water deficit. (**d**) Slope of PRI_c vs. Irradiance (W m^{-2}) as a predictor of biomass accumulation as measured by NDVI at the end of binned water period. (**e**) Same as (d) except during water depletion. (**f**) Same as (e) except during water deficit.

Chapter 2: Daily NDVI-derived Phenology Metrics Improve In-Season Predictions of Biomass, Grain, Protein, and Nitrogen Accumulation in Spring Wheat

Magney, T.S., Eitel, J.U.H., Huggins, D.R., Vierling, L.A.

to be submitted to Field Crops Research

Abstract: Automated, low-cost and field-deployable remote sensing tools are well suited for continuously monitoring crop growth and providing growers with timely information about crop performance. Because automated sensors provide unprecedented information about crop development and performance across time, we examined the hypothesis that ground-based canopy reflectance data might define crop phenology in new ways over the course of the season that can better forecast crop yield, protein, biomass, and grain nitrogen at harvest. This study examines the utility of high frequency Normalized Difference Vegetation Index (NDVI) data to monitor crop phenology over two complete growing seasons. Spectral reflectance data was collected at a total of sixteen plots under four different applied nitrogen (N) and soil water availability scenarios in rainfed soft white spring wheat (*Triticum aestivum L.)*. Using NDVI at solar noon, four phenological time periods - representative of the onset of 1) tillering, 2), stem extension, 3) heading, and 4) ripening - were derived from the data using a non-parametric regression locally weighted smoothing parameter (loess) to account for day to day variability, and piecewise linear regression to determine inflection points in the seasonal NDVI curve. Phenological metrics (i.e. the change in NDVI per day, and duration (in days) of each phenological period) were compared against daily NDVI values throughout the season to predict harvest metrics including biomass, grain yield, protein concentration, and N accumulation. Daily NDVI data were generally poor predictors of harvest early in the growing season (except for grain N accumulation, $R^2 > 0.60$ during tillering), and reached maximum predictive power at the onset of heading, and the middle of ripening for biomass and yield (R^2 ~0.50 & ~ 0.25 during heading, respectively, and R^2 ~ 0.50 during early ripening). Conversely, using both simple and multiple regression analysis, we found that harvest metrics were better described using the rate and duration of NDVI derived phenological periods. Simple regressions between NDVI derived phenological metrics revealed several physiologically and management relevant correlations including strong

statistically-significant ($p<0.05$) relationships between the rate of tillering & stem extension and total biomass ($R^2 = 0.63$ & 0.54, respectively), the duration of heading and yield ($R^2 = 0.67$), the rate of ripening and grain protein concentration ($R^2 = 0.45$), and the duration of ripening and grain N content ($R^2 = 0.43$), for example. Using multiple regression analysis, 83% of the variance in yield, 67% in protein concentration, 87% in total biomass, and 80% in grain N was explained by two to three NDVI derived phenological metrics. Further, multiple regression analysis using NDVI derived phenological metrics from the early season (tillering and stem extension) periods substantially improved early prediction of yield and biomass as compared to daily NDVI data, whereas protein and grain N were primarily driven by metrics associated with the reproductive development of the crop (heading and ripening). This work has implications for improving in-season management decisions and understanding of the phenological drivers of harvest metrics using daily NDVI data.

2.1. Introduction

Daily information regarding crop development patterns is important for monitoring and predicting grain quantity and quality. Highly resolved, objective, and real-time information about crop phenology and growth can aid in within-season farm management decisions, but also improve the understanding of abiotic and physiological processes controlling plant N uptake, yield, and protein content. The motivation behind tracking key phenological phases in crop development is not new (Hanway et al., 1963; Cleary and Waring, 1969; Zadoks et al., 1974); but its quantification has improved significantly in recent years due to the advent of canopy reflectance data available from spectro-radiometetric platforms (Goodin and Henebry, 1997; Raun et al., 2001; Viña et al., 2004). More recently, several low-cost approaches towards continuous monitoring of plant phenology have been conducted using digital time-lapse cameras (Rundel et al., 2009; Richardson et al., 2007; Sakamoto et al., 2012), filtered photodiodes (Garrity et al., 2010; Magney et al., 2015), light-emitting diodes (Ryu et al., 2010), and autonomously operating terrestrial laser scanners (Eitel et al., 2013). The rapid development of low-cost, easily-interpretable, and field-ready ground based remote sensing systems is the result of a growing interest in tracking temporal and spatial changes in the physiological and phenological status of vegetation (Vierling et al., *in revision*).

Some of the initial development of remotely sensed vegetation indices, such as the normalized difference vegetation index (NDVI) (Tucker, 1979) - a differenced ratio of reflected energy in the red and near-infrared portions of the electromagnetic spectrum - was prompted by the motivation to indirectly predict grain yield using bands available from space using Landsat satellite data (Rouse et al., 1974; Tucker et al., 1980; Pinter et al., 1981; Aase and Siddoway, 1981). Following these early explorations, issues such as sensor view angle, solar angle, atmospheric conditions, radiometric calibration, canopy architecture, and soil background were determined to be important factors confounding crop canopy reflectance (Verhoef, 1984; Huete et al., 1987; Jackson and Huete, 1991; Eitel et al., 2009). Since then, interest has grown quickly around selection of the optimal sensor angles, wavelengths, measurement frequencies, spatial resolution, radiometric resolution, and technical capabilities of instruments used for monitoring and predicting crop growth parameters (see review by Mulla, 2013). For nearly four decades (Tucker et al., 1979), NDVI has remained one of the most consistently measured vegetation indices across a wide variety of sampling platforms, prompting its widespread use in agriculture.

Highly temporally resolved NDVI data has been widely used to track seasonal phenology of green-up and senescence over a wide variety of ecosystems from space using NOAA's advanced high resolution radiometer (AVHRR, e.g., Justice et al., 1985; Myeni et al., 1997; Brown and de Beuers et al., 2008) and NASA's Moderate Resolution Imaging Spectrometer (MODIS, Fisher and Mustard et al., 2007; Soudani et al., 2008). Additionally, more immediately available information has been used at much finer spatial and temporal resolutions using ground-based instruments (Vierling et al., 1997, Huemmrich et al., 1999, Viña et al., 2004; Huete, 2012; Soudani et al., 2012). Accurate interpretation of satellite-based data requires robust, and highly temporally resolved, ground-based reference data (Nguy-Robertson et al., 2013). Furthermore, the inherent complexity, processing time, and difficulties in acquiring and interpreting satellite images at the field scale can make this technology inaccessible for many growers to make within-season management decisions. Ground-based sensors therefore can inform both agricultural management decisions, as well as to track plant phenological variation that can be used by crop scientists seeking a more process-based understanding of dynamics controlling biomass accumulation and grain-fill (e.g., Oscarson, 2000; Farooq et al., 2014).

Because NDVI is an integrated measure of canopy greenness, and ground-based radiometers can repeatedly collect NDVI readings at consistent height and viewing geometry in <1 second, these data can be compared across different field locations, nutrient plots, irrigation regimes, and over cultivars with traits engineered to maximize reproductive growth (e.g., Borrell et al., 2014). The plant breeding community has a keen interest in developing crops that 'stay-green' longer, increasing duration of grain-fill, and decreasing the rate of senescence (Christopher et al., 2014; Gaju et al., 2014). Phenological data has already been used to investigate the physiological and morphological traits necessary to increase grain quality and quantity using visual observations and instruments that quantify at the loss of chlorophyll using a handheld chlorophyll meter (Borrell et al., 2000). Using chlorophyll meters to derive phenological metrics such as the onset and rate of senescence, researchers have found that 'stay-green' phenotypes can retard senescence, promoting a longer grain fill period (Harris et al., 2007). Additionally, phenological dynamics during the post-anthesis period in wheat have been described using logistical models (Pepler et al., 2005). However, hand-held chlorophyll meters are limited in both time and space, with data collections that can suffer from subjective measurement bias, and models require validation over many different growing conditions and cultivars. High temporal automated measurements of NDVI have provided a more robust and objective approach to indirectly estimate crop phenological expression (Lopes et al., 2012).

The overall goal of this study was to investigate the utility of NDVI to derive physiologically and management relevant phenological periods, and investigate their capacity to make within-season predictions of leaf area, biomass, grain yield, N uptake, and grain protein concentration. Our specific objectives were to: 1) Determine how the diurnal variability in NDVI measurements influences the prediction of leaf area throughout the growing season; 2) Investigate the predictive capacity of a daily NDVI value throughout the growing season to model end of season grain yield, biomass, grain N uptake, and protein concentration; and 3) Compare daily NDVI values to the rate and duration of four phenological periods (onset of tillering, stem extension, heading, and ripening) in predicting harvest metrics (biomass, grain yield, N uptake, and grain protein concentration). To accomplish these objectives, we collected and analyzed automated NDVI radiometric data for

two complete growing seasons over four applied nitrogen (N) and four different water availability regimes.

2.2. Methods

2.2.1. Study site

In both 2013 and 2014, soft white spring wheat (*Triticum aestivum* L.) was grown following soft white winter wheat (*Tritivum aestivum* L.) in eight, 100 m^2 (10 m x 10 m) plots with 19 cm row spacing at the Washington State University Cook Agronomy Farm (CAF) near Pullman, Washington, USA (*N* 46.7805, *W* 117.0855). The eight research plots were divided into two fields (hereafter referred to as Field A and Field B) to promote a wide range of soil water availability scenarios (see Table 1). Additionally, four "top-dressed" N application rates were applied at each of the two fields (0, 40, 80, and 120 kg ha^{-1}) using granular urea (46% N) three days post seeding (similar to Eitel et al. 2014). Soil was sampled for inorganic N (NO_3 and NH_4) prior to N application; residual N in the soil did not significantly differ across the plots ($p<0.05$). The study site has silt load soils developed in loess deposits with some ash (fine-silty, mixed, superactive, mesic Pachic Ultic Haploxerolls, Soil Survey Staff, 2014). CAF is a dryland site without any irrigation, and permeability is moderate to high. The average annual precipitation ranges from 260 to 610 mm, and the average available water capacity through the entire soil profile is about 29 cm (Soil Survey Staff, 2013).

2.2.2 Biophysical measurements

We collected both in-season and end-of-season (i.e. harvest) biophysical measurements in the field. The only in-season canopy metric used in this study was plant leaf area index (LAI). LAI has been widely used by ecologists, ecophysiologists, modelers, farmers, and foresters, to investigate the response of plant growth to the surrounding environment (Bréda, et al., 2003). LAI (m^2 leaves per m^2 ground) was measured at all plots (n=8) on a weekly basis using a LI-COR model LAI-2000 plant canopy analyzer (LI-COR, Lincoln, NE). At each plot location, three LAI measurements were collected and averaged for analyses (n=88 (10 weeks, 2013), n=96 (12 weeks, 2014). Soil volumetric water content (SVWC) measurements were collected on the day of planting within close proximity (5 m) of each field location. The SVWC reported here was measured at a soil depth of 5 cm below

ground surface using EC-5 SVWC sensors (Decagon Devices, Pullman, WA, USA). The depth to argillic layer was determined using a soil probe, and determined when a distinct clay layer was found.

End-of-season harvest metrics were determined from a hand harvest, where the crop was removed at <5 cm above the ground surface using a sickle. We bagged, dried at 60º C, and weighed biomass of the three square meters within the field of view of each NDVI radiometer. Samples were threshed using a plot combine to separate the grain from the chaff, and weighed. Aboveground plant and straw biomass were expressed on an area basis. Protein concentration was determined using a NIR analyzer (Infratec^{TM} 1241 Grain Analyzer, Foss, Eden Prarie, MN), and grain N content was determined by dividing protein concentrations by 5.7 and multiplying by the grain yield (Huggins, Pan, & Smith, 2010).

2.2.3 Canopy NDVI spectral reflectance measurements

Canopy reflectance measurements began shortly after planting (prior to emergence) and remained until harvest. NDVI data were collected continuously in a fixed location throughout the sampling period at each of the plots using low cost Spectral Reflectance Sensors (SRS, Decagon Devices, Pullman, WA). SRSs are two-band radiometers that measure incident and reflected radiation in wavelengths appropriate for calculating NDVI (after Garrity et al. 2010). The NDVI wavebands are centered at 630 and 800 nm wavelengths, with 50 and 40 nm full width half maximum band widths, respectively. These wavebands were used in calculating NDVI using Equation 1:

$$NDVI = (\rho 800nm - \rho 630nm) / (\rho 800nm + \rho 630nm) \quad \text{(Eq. 1)}$$

NDVI SRS sensors equipped with Teflon diffusers were placed facing up (view zenith angle of 180º) to make cosine-corrected measurements of incident irradiation. Additional sensors fitted with field-stops (20° field of view) were placed 1.5m above the crop canopy at a 20º view zenith angle to measure upwelling canopy radiance. The upwelling radiation measurement was then divided by the incident irradiation to obtain a true canopy reflectance value (ρ). A test for cross-calibration was done in the field using a 99% reflectance, white Spectralon reference panel (Labsphere Inc., North Sutton, NH); no significant differences between sensors was found (data not shown). Reflectance measurements were logged using Em50 dataloggers (Decagon Devices, Pullman, WA) for each waveband and recorded at five minute intervals throughout the two growing seasons.

2.2.3 Statistical analysis

Initial analysis focused on what time of the day was best suited to relate NDVI to LAI throughout the entire season. For this, we used a simple linear regression and R^2 value for each day that LAI data was collected. We determined that 12:00 noon was the best time of day to use NDVI data, and due to the inherent variability of these values on a day to day basis, smoothing of daily NDVI data was done by using a locally-weighted non-parametric regression with a smoothing parameter (α) of 0.5, Fig. 2.1 (loess, Cleveland, 1979; 1988). The red dots in Fig. 2.1 represent the smoothed NDVI values and 95% confidence intervals to represent the range of daily values (7:00-20:00) at the control plot on field A in 2014.

Tillering, stem extension, heading, and ripening were chosen to represent the onset of significant growing stages (according to Zadoks' 10, 31, 50, 70, respectively; Zadoks, 1974). The onset of each phenological period was determined using piecewise linear regression from the 'segmented' package (Vito & Muggeo, 2003, 2008; similar to Sweet et al., 2014 & Magney et al., 2015) in R (R Core Team, 2014). The outputs from the piecewise linear regression include the x-axis location of the inflection point with a standard error. The three inflection points with the smallest standard errors were used to define and bin the phenological periods. If there was an inflection point between the times when the crop emerged and tillering began, that day was chosen as the onset of tillering. The standard errors were recorded and represented in Figs. 2.5-2.8. The conceptual framework and algorithms used to determine inflection points are described in Vito & Muggeo (2003, 2008). The rate (slope) of each phenological period was calculated using the change in NDVI over the duration (length) of the period.

Step-wise multiple linear regression analysis was done to assess the potential for using one or more predictors for harvest metrics, and to determine the relative importance of phenological time periods (rate and duration) in influencing grain quality and quantity. The 'stepwisefit' package in R used Akaike information criterion (AIC) values to assess the relative quality of multiple regression models by favoring models with fewer explanatory variables. The regression model with the lowest AIC was chosen at different time frames throughout the season to determine that capability of predicting each harvest metric after each phenological period. A variance inflation factor (VIF) with a maximum threshold of 10

(O'Brien, 2007) was used as a test for multi-colinearity within each model - VIF > 10 was discarded from the model.

2.3. Results

2.3.1. Influence of time of day on NDVI vs. LAI relationship

Fig. 2.2 demonstrates the predictive capability of NDVI values at 5 minute intervals throughout the growing season on days when LAI data was collected. Fig. 2.2a suggests that in this system, and with these sensors, data from 12:00 noon provide a tighter fit and better LAI predictive power (Fig. 2.2c). In general, as solar zenith angle increases, NDVI's predictive capacity increases, similar to findings by Sims et al., 2006 and Nguy-Robertson et al., 2013. A primary limitation of NDVI is that it tends to saturate at high LAI values; however, the distribution of points around the best fit line do not suggest saturation at LAI values approaching four (Fig. 2.2c). For these reasons, NDVI at 12:00 was used for all seasonal analyses (similar to Gamon et al., 2006; Ryu et al., 2010; Nguy-Robertson et al., 2013).

2.3.2. Predictions using daily NDVI: Biomass, Yield, Grain N, grain protein

Fig. 2.3 shows how well single, daily NDVI values across all 16 plots can be used to predict end-of-season harvest metrics (i.e. biomass, yield, grain N, and grain protein). Individual daily NDVI values do not perform well in determining early season biomass, yield, or protein concentration. However, greater than 50% of the variance in harvested grain N can be explained during using daily NDVI values during the majority of the stem extension period (17-37 days since emergence), when most N is being taken up by the crop. Yield and biomass prediction are at their peaks when there is the most variation (widest 95% confidence interval bars) in the NDVI data (37-46 days since emergence), at the culmination of vegetative growth and during mid senescence (~75-85 days since emergence). NDVI is a poor predictor of protein throughout the entire growing season, with a small peak towards the end of the season.

2.3.3. Seasonal trends in the rate and duration of phenological periods

Fig. 2.4 shows the seasonal patterns of NDVI-derived phenological periods from 2013 Field A (Fig. 2.4a), 2013 Field B (Fig. 2.4b), 2014 Field A (Fig. 2.4c), and 2014 Field B (Fig. 2.4d). In general, the 2013 crop experienced a slower growth rate at the onset of tillering and stem extension, a shorter duration of heading, and a slower senescence (ripening) rate.

Additionally, the magnitude of the NDVI values is generally lower in 2013. An effect of fertilizer treatment is most apparent in the seasonally dry, south-facing, poorly drained sites (Fields A). The fertilizer treatment response is represented by the control and low plots consistently experiencing slower growth rates, less time during grain-fill (heading), and lower magnitude NDVI values. The onset of most phenological periods is consistent within each field, however, the duration of heading is longer for the medium treatment in Fig. 2.4a-c. There is also a noticeable increase in NDVI values during the heading period in Fig. 2.4 a and c, suggesting that there may have been some additional vegetative growth during this reproductive stage, or larger spikes that could contribute to overall increased reflectance in the NIR and decreased reflectance in the red, similar to the findings by Viña et al., 2004 (see section 2.4.2.3 for discussion).

2.3.4. Predictions using metrics of NDVI over phenological periods: Biomass, Yield, Grain N, grain protein

2.3.4.1. Summary table for all predictor and explanatory variables

Table 2 highlights the coefficient of determination between the rate and duration of each daily NDVI derived phenological period and end of season biomass, grain yield, protein concentration, and grain N uptake.

Our study suggests that the strongest (and all statistically significant at the $p<0.05$ level) predictors of yield are rate of tillering ($R^2 = 0.72$), duration of heading ($R^2 = 0.67$), and duration of ripening ($R^2 = 0.42$). For protein concentration, the rate of heading ($R^2 = 0.64$), rate of ripening ($R^2 = 0.45$), duration of stem extension ($R^2 = 0.35$), duration of tillering through heading ($R^2 = .25$), and the duration of tillering through stem extension ($R^2 = 0.28$) all show significant correlations, with the metrics corresponding to the duration of phenological periods not showing strong correlations. Harvested biomass and grain N are significantly correlated to 7 of the 10 phenological periods: rate of tillering ($R^2 = 0.62, 0.37$, respectively); rate of stem extension ($R^2 = 0.55, 0.53$, respectively); rate of ripening ($R^2 = 0.28, 0.45$, respectively); duration of stem extension ($R^2 = 0.25, 0.35$, respectively); duration of heading ($R^2 = 0.66, 0.36$, respectively); duration of ripening ($R^2 = 0.66, 0.42$, respectively); and duration of tillering through heading ($R^2 = 0.40, 0.46$, respectively). The physiological explanations for these correlations will be elaborated upon in the discussion.

2.3.4.2. Top predictors of biomass

Fig. 2.5 shows the linear regressions between biomass and the top four predictor variables, rate of tillering, rate of stem extension, duration of heading, and duration of ripening.

2.3.4.3. Top predictors of yield Fig. 2.6 shows the linear regressions between grain yield and the top three predictor variables, rate of tillering, duration of heading, and duration of ripening.

2.3.4.4. Top predictors of protein concentration

Fig. 2.7 shows the linear regressions between grain protein concentration (%) and the top two predictor variables, rate of heading and rate of ripening.

2.3.4.5. Top predictors of grain N concentration

Fig. 2.8 demonstrates the top four predictors of end of season grain N concentration, rate of stem extension, rate of ripening, duration of heading, and duration of ripening.

2.3.5. Stepwise regression analysis

Stepwise regression analysis at different times of the season was performed to assess the performance of within-season predictive capacity of NDVI derived phenology, but also to examine how NDVI phenology may explain harvest metrics.

2.3.5.1. Early season prediction of harvest metrics

Table 3 exemplifies the capacity for the rate/duration or a combination of both during tillering to predict end-of-season harvest metrics relevant to crop productivity. The simple regressions previously shown in Table 2 are only improved in the case of biomass prediction, where both the rate and duration of tillering combined marginally improve the R^2 from 0.62 (rate) and 0.55 (duration) to 0.68 with a root mean square error (RMSE) of 82.12 kg/ha. A low VIF between the rate and duration of tillering suggests that a combination of the two does not over-predict biomass due to multi-collinearity. Results suggest that yield and biomass can be predicted during this phenological period, but early information on grain N content and protein concentration is difficult.

2.3.5.2. Early-mid season prediction of harvest metrics

Table 4 shows the results of stepwise multiple linear regression analysis in the prediction of harvest metrics through stem extension. Analysis suggests strong predictive capacity of yield, biomass, and grain N (R^2 = 0.83, 0.87, 0.70; RMSE = 31.44, 82.12, 9.294,

respectively) using phenologically derived metrics - rate of tillering ($p=0.07$), duration of tillering ($p=0.16$), and rate of stem extension for biomass ($p<0.01$); rate of tillering ($p<0.01$), rate of stem extension ($p=0.03$), and duration of stem extension for yield ($p=0.04$); and duration of tillering (0.02) and rate of stem extension ($p<0.01$) for grain N. A lower p-value indicates that the independent variable explains more variance in the final model, and low VIFs (<5) imply lack of multi-collinearity. The ability to predict protein concentration from phenological metrics, and from a daily NDVI value (Fig. 2.3) during the vegetative growth stage (tillering-heading) showed to be weak.

2.3.5.3. Mid-late season prediction of harvest metrics

Table 5 shows the results from the stepwise AIC selection process in the prediction of harvest metrics from tillering through heading (just prior to senescence). These results suggest that using phenological metrics during heading aid only in the prediction of protein concentration ($R^2 = 0.69$ and RMSE = 1.09%, compared to $R^2 = 0.33$ and RMSE = 1.44% through stem extension). The addition of the rate ($p < 0.01$) and duration ($p=0.43$) of heading to the duration of stem extension ($p = 0.18$) suggest that physiological dynamics during the reproductive growth stages are important for determining grain protein concentration. Biomass and grain N prediction did not improve with information during the heading stage, while the duration of heading marginally improved the yield model (RMSE = 29.8 kg/ha from 31.55 kg/ha at the culmination of stem extension). For all models, the VIF is below 3, except for protein where two variables have VIFs of 8.33, and 9.82, which still suggests non multi-collinearity (<10).

2.3.5.4. Late season prediction of harvest metrics

The inclusion of phenological metrics associated with the crop ripening (senescence) time period were used in all AIC selected models; however, the only improved model was in the prediction of grain N ($R^2 = 0.80$ from $R^2 = 0.70$ using data through heading). Protein concentration prediction dropped from $R^2 = 0.69$ to $R^2 = 0.67$, but the model eliminated one independent variable, and as a result has arguably more explanatory power due to increased simplicity. The R^2 did not improve for biomass or grain yield, but the RMSE dropped slightly (82.12 kg/ha to 79.25 kg/ha for biomass; 29.80 kg/ha to 29.63 kg/ha for yield). These results suggest that while phenological information from ripening is useful in understanding biomass, yield, and protein, early and mid-season prediction is equally as strong, except for grain N.

2.4. Discussion

This study highlights the utility of highly temporally resolved reflectance data to derive important phenological periods of crop growth. Using daily NDVI data, a piecewise linear regression approach was employed to determine inflection points in seasonal crop phenology to quantify a rate and duration of phenological time periods relevant to agronomists, plant breeders, plant eco-physiologists, and growers, among others. For sixteen plots of rainfed spring wheat during the 2013 and 2014 growing season, NDVI derived phenological periods improved estimation of harvest metrics. In the following sections, potential explanations for these phenomena will be explored.

2.4.1. Temporal variation in NDVI's predictive capacity

Many researchers have noted the diurnal variability in canopy reflectance resulting from bidirectional reflectance spectra that are confounded by soils, crop residue, solar zenith angles, canopy architecture, and leaf area (Norman et al., 1985; Ranson et al., 1985; Hilker et al., 2009; Nguy-Robertson et al., 2013). Due to these confounding factors, many studies use highly resolved spectral reflectance data from the same time every day when interpreting seasonal data (Gamon et al., 2006; Ryu et al., 2010; Nguy-Robertson et al., 2013). Our results suggest that the time of day NDVI is used does play an important role in estimating LAI (Fig. 2.2). Nguy-Robertson et al., 2013 noted that diurnal reflectance varied little at the end of the corn and soybean growing season between 10:30 and 15:30, when peak solar zenith angles were higher. Similarly, results from this study show that there is a slight variation in canopy reflectance spectra up to and after 12:00, in accordance with decreasing solar zenith angle (Fig. 2.2). It can also be noted that while the slope of the line between the NDVI and LAI relationship remains fairly constant through the day (0.14-0.18), the intercept of the relationship ranges from 0.17 at 7:00 to 0.34 at 20:00, suggesting that this empirical fit will change depending on the time of day. The strongest fit at 12:00 for the NDVI and LAI relationship is likely a result of less bidirectional reflectance contribution confounding the signal during peak sunlight (Norman et al., 1985). The solar zenith angle at 12:00 noon is closest to the viewing angle of the SRS (~20^{o}), thus the observed relationship would likely change depending on both the viewing direction and angle of the sensor.

To assess how time of day selection for the piecewise linear regression would change the rate and duration of phenological time periods changes, a sensitivity analysis was

conducted to determine if inflection points (as shown in Fig. 2.1) drastically change based on time of day (e.g., Fig. 2.9). A qualitative look at the data in Fig. 2.9 suggests that the inflection point does vary depending on time of day NDVI data was used; with the most spread coming from data collected at 8:00, 16:00 and 18:00, and less than ±1 day difference for each inflection point between 10:00-14:00 for this individual plot. While a complete analysis is beyond the scope of this research, we do note a significant effect of time of day over all sixteen plots, where the duration of each phenological period can be up ± 3 days different depending on time of day NDVI is used. Regardless of what time of day is chosen for NDVI, if the sensor and solar geometries are the same at all locations, differences in the rate and duration of phenology can be relatively compared across N or irrigation treatments, cultivars, and different field positions, among others - though future research should investigate this further. Also worth noting is that the magnitude of the NDVI values change depending on time of day, whereby an increase in solar zenith angle generally corresponds with higher NDVI values post senescence (Fig. 2.9, for example). One explanation could be an increase in NIR reflectance coming from the wheat heads themselves (Pimstein et al., 2009; and similar to findings by Veña et al., 2004 for corn), but this non-conclusive hypothesis should be investigated further. Results from both Figs. 2.2 and 2.9 support findings by many researchers that NDVI around 12:00 is the best time of day to use such data.

Using NDVI from 12:00 noon, we investigated the ability of a daily NDVI value to predict harvest metrics throughout the season (Fig. 2.3). Many researchers have used ground based remote sensing tools to predict cereal yield (Mahey et al., 1991; Ruan et al., 2001; Babar et al., 2006), N uptake (Stone et al., 1996; Shanahan et al., 2008; Qualm et al., 2010), protein content (Hansen et al., 2002; Freeman et al., 2003), and biomass (Kleman and Fagerland et al., 1987; Erdle et al., 2011) early in the growing season with mixed results, and often have had more success using more complex vegetation indices (Lindgren et al., 1994; Haboudene et al., 2002; Prasad et al., 2006; Eitel et al., 2008; Panda et al., 2010). In this study, early season predictions were the strongest towards the end of rapid vegetative growth (37-46 days since emergence), and during mid-senescence (75-85 days since emergence, Fig. 2.3, similar to findings by Mahey et al., 1991). Freeman et al., 2003 note that yield prediction using NDVI in wheat can be accurate two months prior to harvest, when yield estimates stabilize; however, in this recognizably different agro-ecosystem, our results suggest that

while yield estimates are strongest just prior to heading (two months before harvest), their predictive capacity drops off during grain-fill, just prior to senescence (Fig. 2.3). The near symmetrical patterns of yield and biomass could be explained by the close correlation between these two parameters in this study (r = .83); however, in the interest of increasing the harvest index (yield/biomass) for crop yield gap analysis (Van den Boogaard et al., 1996; Lobell et al., 2013), harsh conditions (high VPD, high temperature) incurred during the reproductive stage can lower the harvest index, and could be detected by a shortening of the duration of grain fill or increased rate of senescence (Reynolds et al., 2012; this study, Figs. 2.5c,d & 2.6c,d).

The prediction of grain protein has traditionally been based on the premise that the N assimilated in plant tissue components is directly related to grain protein content (Tindal et al., 1995; Wang et al., 2005); however, protein concentration in the grain is a product of not only the amount of N in tissue prior to grain-fill, but the conditions (i.e., abiotic stress) that the crop undergoes during this time period (Masclaux-Daubresse et al., 2010). As a result, individual daily values of canopy NDVI alone is generally a poor predictor of grain protein prior to harvest since it does not consider the abiotic conditions during grain fill (Hansen et al., 2002 and Xue et al., 2007). This study confirms these findings, as R^2 predictive capacity using daily NDVI values never exceeds 0.20 until the final days of the growing season (Fig. 2.9). However, because crop phenology responds to abiotic conditions during grainfill that drive grain protein concentration, this study showed that metrics derived from NDVI-defined phenological stages during ripening can substantially improve protein predictions (Fig. 2.7 and Tables 2-6).

Due to the fact that grain N content in this study is computed using yield and protein concentration, one would expect that its capacity to be predicted using NDVI metrics would fall somewhere between yield and protein concentration. However, the peak predictive power using daily NDVI data occurs 19-30 days after emergence ($R^2 \sim 0.60$), and immediately spikes as soon as rapid vegetative growth (stem extension) is underway. This could be due to the strong relationship between rate of stem extension and N uptake (Miller et al., 1994; and in this study, Fig. 2.8a), as this time period is crucial for establishing baselines for the 50 to 90 percent of N that will ultimately be remobilized from leaf and stem to the grain (Chapin and Wardlaw, 1988). Recognizing that single daily NDVI data might not provide the best

representation of end of season harvest metrics, this study found single daily NDVI derived crop phenological periods showed a > 50% increase in the explained variance of biomass, yield, protein, and N prediction (Fig. 2.3 and Table 2).

2.4.2. Physiological significance of phenological time periods influencing harvest metrics

The results from this analysis suggest that different phenological time periods, derived from daily NDVI data, are indicators of grain quantity and quality; however, there is no direct evidence to explain why or how NDVI derived crop phenology directly influences harvest metrics. As a result, we can only make inferences as to how they *might* be related to end-of-season crop parameters. The goal of this work is to develop a simple method that derives highly resolved phenological data, and supports published observations that note the influence of phenological metrics to harvest data. Explanations of why the rate and duration of tillering (4.2.1), stem extension (4.2.2), heading (4.2.3), and ripening (4.2.4) are discussed in the following sections.

2*.4.2.1. Tillering*

This study found that the rate of tillering is strongly correlated to biomass and yield, and moderately correlated to grain N at harvest in spring wheat (Table 2). N availability produced a small varied response in rate differences within each field according to NDVI data (Fig. 2.4). This observation has been noted under ranges of N availability scenarios; whereby, an increase in weight and number of tillers with increased N availability is often observed (Longnecker et al., 1993; Oscarson et al., 2000). However, at low LAI values (<1), the NDVI signal could have been dominated by soil background reflectance, dampening the overall signal (Huete et al., 1988). The use of a soil adjusted vegetation index during this time period could alleviate this confounding effect, and result in greater observed differences during the NDVI derived tillering period (Qi et al., 1994; Rondeaux et al., 1996; Haboudane et al., 2002; Eitel et al., 2007). To avoid this problem, the first inflection point in the data (when there was a visible increase in rate of growth) was used as the onset of tillering. Further elucidating the discrepancies in tiller response using proximal remote sensing data at this important crop growth stage could aid in early season N management decisions (e.g., Eitel et al., 2014)

At this early growing stage, when soil water content is high, the most limiting contributor to a delayed start date is soil temperature and anaerobic soil conditions - affecting

soil water potential (Lindstrom et al., 1976). These early impediments were experienced in 2013, resulting in delayed crop emergence and a short and slow tillering period, which undoubtedly contributed to lower biomass and yield during this season. As can be seen in Fig. 2.4, the duration of tillering was only one or two days longer in 2014, but the rate of growth (tiller establishment) allowed for greater potential for biomass accumulation and yield. Figs. 2.6a and 2.7a show strong relationships supporting the hypothesis that more tillers result in more spikes and more seeds; however, without the low tiller production observed in Field A in 2013 (resulting in low yield and biomass), the relationship would likely weaken. We suspect that over a wider range of conditions/planting densities and increased sample size this relationship will hold, but it should be noted that not all tillers produce spikes in wheat, and in many cases tillers abort before heading (Gallangher and Biscoe, 1978). In the stepwise multiple regression analysis, rate of tillering proved to be the strongest early season predictor of biomass, yield, and grain N, suggesting that early diagnosis of yield potential could be determined using NDVI derived phenological data during this time period.

2.4.2.2. Stem extension

Results from this study support the observations of much research that has postulated that high growth rate leads to a considerable increase in biomass (Richards, 1987). The rate and duration of stem extension proved to be significant predictors of biomass and grain N at harvest in this experiment (Tables 2 and 4). While strong relationships between biomass at anthesis or during grain fill and yield have been observed, this experiment suggests that the rate of biomass accumulation (rate of stem extension) was not a strong predictor of yield. This could be explained by the wide range in harvest index observed in these trials (0.47-0.65), suggesting that biomass accumulation did not directly translate into yield, making daily NDVI - which is intrinsically sensative to LAI/biomass, and phenological metrics associated with vegetative growth - not necessarily the most useful for predicting yield.

Early work by Van Andel and Jager (1981) and Simane et al., (1993) showed that drought and moisture stress during stem extension result in lower rates of biomass accumulation. In this study, SVWC in both sites in 2013 was higher at planting but increased temperatures during the 2014 season (5°C higher on average during stem extension than in 2013) likely spurred greater growth rates since water is not necessarily limited at the onset of stem extension in this system. As can be observed in Fig. 2.4, the onset and culmination of the

stem extension period falls on or around the same date for fertilizer treatments within the same field position; however, in most cases the rate of change in stem extension is greatest where there is more available N, resulting in a greater NDVI value at the onset of heating. In all four cases, the control plot had the lowest NDVI value after stem extension, and the medium fertilizer plot had the highest NDVI. This could suggest that 80 kg/ha (medium) N is sufficient for achieving maximum nitrogen use efficiencies (NUE).

The multiple regression analysis (Table 4) shows that the rate of stem extension was a strong explanatory variable in the yield, biomass, and grain N predictive models, improving the predictive power of these three harvest metrics to $R^2 = 0.83$ for yield, 0.87 for biomass, and 0.70 for grain N. As previously mentioned, the lack of protein prediction using phenological data up to this point in the growing season is not surprising, as the remobilization of N from leaves and stems to seeds is largely driven by post-anthesis weather conditions. The role of available N in biomass accumulation and grain protein concentration is the result of complex interactions between carbon and nitrogen assimilation that could be further examined with highly resolved information on vegetative growth rate as is shown here (Triboi and Triboi-Blondel, 2002).

2.4.2.3. Heading

The vegetative growth stage (tillering and stem extension) is extremely important to ensure the maximum amount of carbohydrates to be supplied during grain filling (Donmez et al., 2001). Because the Palouse region of the US Pacific Northwest is a rainfed environment, the heading and grain fill time period generally takes place when it is hot and dry - conditions that limit photosynthesis. End-of-season yield greatly depends on the remobilization of assimilates acquired during vegetative growth to the grain (Villegas et al., 2001). Hot and dry conditions will expedite the duration of the grain-fill period, limiting the maximum amount of nutrient translocation to the seed (Bogard et al., 2011). Tables 2 and 5 and Figs. 2.6b and 2.8c support the hypothesis that an extended duration of the heading phenological time period will increase grain yield and translocation of N from vegetative parts to seed. The strength of the relationship between the duration of heading and yield (Fig. 2.6b) shows compelling evidence that the effect of both between and within field location variability has strong predictive power as the points still fall along the relatively same slope (except Field B 2013). Further, if a primary physiological constraint on delayed senescence is the vegetative N reserves, it is

logical that total biomass and grain N are also positively correlated to heading duration (Fig. 2.5c and 2.8c). The simple approach described here could help breeders trying to develop 'stay-green' phenotypes to improve yields under abiotic stress (Borrell et al., 2001; Lopes and Reynolds, 2012).

The relationships between NDVI derived rate of heading and end-of-season harvest metrics are difficult to interpret. Table 2 and Figure 2.7a show a strong relationship between rate of heading and protein concentration. It could be postulated that this is merely a spurious correlation, but we hypothesize that this could be the result of biomass accumulation after the onset of heading. A positive relationship between rate of heading and protein concentration suggests that additional N uptake by the roots occurred after anthesis, and because 5 to 50% of post-anthesis N uptake is translocated to grain N (Van Sanford and MacKown, 1986; de Ruiter and Brooking, 1994; Gaju et al., 2014), the remaining N uptake could have manifested itself in leaf development, ultimately resulting in increasing NDVI values during this time period. This is supported by field trials where high N availability or additional N application at anthesis has shown to increase grain protein concentration (Gooding and Davies, 1992; Bly and Woodward, 2003). Because all proteins consist of amino acids, and N is part of the basic structure of amino acids necessary for protein synthesis, we hypothesize that increased plant vigor (by increased photosynthesis in N rich plants) experienced during the heading phenological period resulted in a greater concentration of protein remobilization, though this is non-conclusive and requires further research. The stepwise multiple regression analysis in Table 5 shows that the predictive capacity of a combination of NDVI derived phenological periods only improves the protein model, where rate and duration of heading play in important role in reducing the model RMSE from 1.44% to 1.09%. Regardless of a true diagnostic interpretation of this relationship, wide bodies of evidence associating rates of senescence to protein concentration support findings in the following section.

2.4.2.4. Ripening

The importance of ripening and crop senescence in determining grain quality has been extensively studied, and confirmed that N remobilization is tied to the rate and duration of senescence (Wang et al., 2005). The rate of leaf senescence is largely controlled by abiotic factors that lead to the gradual deterioration of leaf function due to chlorosis and a decline in photosynthesis (see review by Farooq et al., 2014). An increased rate of senescence has often

been linked to less time for grain-fill, resulting in a lower harvest index (Madani et al., 2010). Our study supports these findings with significant positive relationships observed in Table 2 and Figs. 2.5d, 2.6c, and 2.8d between biomass, yield, and grain N and the duration of ripening. Physiologically, the ripening period is important in the remobilization of nutrients to the grain, implying that a shorter time of senescence results in lower yields and lower grain N content as was observed here (Fig. 2.6c and 2.8d). Drought and heat stress are generally attributed to influencing the rates of senescence, though in different ways. For example, Lopes and Reynolds 2012 used NDVI to monitor wheat phenology and found a positive correlation between yield and senescence rate under heat stress, and a negative correlation between senescence rate and under drought and heat stress. The Palouse region is generally not characterized by high temperatures in mid-summer and thus it is likely that drought stress resulting from soil water depletion in contributing to expedited senescence rates. Also, the NDVI derived duration of ripening shows a strong positive correlation to biomass (Fig. 2.8d), which could likely be explained by the fact that more green leaf area will take longer to senesce.

There is speculation that depletion of soil moisture during ripening (drought related stress) could reduce starch accumulation and thus yields of hard red wheat, while increasing protein concentration (Brown et al., 1999). Soft white winter wheat in this system is not managed to meet minimum protein thresholds, but the dynamics of protein synthesis during ripening are similar, and this study suggests that increased rates of senescence induce greater protein concentration (Fig. 2.7b). As was mentioned previously, protein concentration is likely more closely related to nutrient availability, as a stepwise increase in protein concentration was observed at all four fields according to N availability. Interestingly, the rate of senescence response was both field and N regime specific, suggesting that a combined effect of increased rate of ripening and available N ultimately drove protein concentration and grain N content. At this point, interpretation of relationships between the rate and duration of phenological periods is highly speculative, but is supported by similar findings that relate crop phenology to harvest metrics.

2.5. Conclusion

We evaluated the utility of highly temporally resolved ground based radiometric measurements of NDVI to quantify the rate and duration phenolgical periods during the wheat growing season. NDVI derived phenological metrics were compared to daily NDVI values for their predictive capacity of biomass accumulation, grain yield, protein concentration, and grain N content. Daily NDVI values generally showed poor predictive power of end of season metrics, with peak predictive power occurring at short time intervals throughout the growing season. This finding highlights the importance of when NDVI data should be used (both diurnally and seasonally) as a predictive tool. When a piecewise linear regression was used to determine inflection points in the seasonal NDVI curve, the rate and duration of NDVI derived phenological periods related to the onset of tillering, stem extension, and ripening were determined. These NDVI derived phenological metrics were compared across sixteen plots under varying available N and water scenarios, and strong, notable relationships were observed between 1) rate of tillering and biomass accumulation/yield, 2) rate of stem extension and biomass/yield/grain N content, 3) duration of heading and biomass/yield/grain N content, 4) duration of ripening and yield/ grain N, and 5) rate of ripening and protein concentration. A stepwise multiple regression analysis was also done to assess the viability of combined NDVI derived phenological metrics for early season prediction of harvest data. Using information from tillering and stem extension, strong predictive power was observed for yield, biomass, and grain N; however, mid-season prediction of protein concentration is difficult, as phenological metrics post-anthesis are most relevant to protein synthesis.

Easily interpretable, objective, low-cost, and field-ready ground based remote sensing information could provide growers with information regarding crop growth dynamics prior to mid-season fertilizer or irrigation decisions. Perhaps more immediately, this type of data can be used in a retrospective fashion by agronomists, breeders, and scientists to gain a better understanding of how abiotic conditions influence physiological and phenological patterns throughout the season. Further, this study demonstrated the potential and limitations of daily NDVI data in deriving relevant phenological parameters that could be extrapolated to larger regions using daily satellite imagery available from AVHRR or MODIS, for example. Our primary objective was to provide a simple technique that could be widely used by both growers and scientists to gain a better understanding of crop phenological variability, but

more research is necessary to evaluate the potential of highly resolved radiometric measurements in different systems, under differing conditions, and using alternate wavelengths, with the ultimate goal of providing more diagnostic information on crop status.

References:

Aase, J.K., Siddoway, F.H. (1981). Assessing winter wheat dry matter production via spectral reflectance measurements useful in providing an estimate of residue production for erosion control and as a potential source for feed and energy. *Remote Sensing of Environment, 11,* 267-277.

Babar, M. a., Reynolds, M. P., Van Ginkel, M., Klatt, a. R., Raun, W. R., & Stone, M. L. (2006). Spectral reflectance indices as a potential indirect selection criteria for wheat yield under irrigation. *Crop Science, 46,* 578–588. doi:10.2135/cropsci2005.0059

Bly, A.G., Woodward, H.J. (2003). Foliar nitrogen application timing influence on grain yield and protein concentration of hard red winter and spring wheat. *Agronomy Journal, 95,* 335-338.

Bogard M, Jourdan M, Allard V, et al. (2011). Anthesis date mainly explained correlations between post-anthesis leaf senescence, grain yield, and grain protein concentration in a winter wheat population segregating for flowering time QTLs. *Journal of Experimental Botany, 62,* 3621–3636.

Borrell A.K., Hammer G.L., Henzell G. (2000). Does maintaining green leaf area in sorghum improve yield under drought? 2. Dry matter production and yield. *Crop Science, 40,* 1037–1048. doi:10.2135/cropsci2000. 4041037

Borrell, A. K., van Oosterom, E. J., Mullet, J. E., George-Jaeggli, B., Jordan, D. R., Klein, P. E., & Hammer, G. L. (2014). Stay-green alleles individually enhance grain yield in sorghum under drought by modifying canopy development and water uptake patterns. *New Phytologist*, *203*, 817–830. doi:10.1111/nph.12869

Bréda, N. J. J. (2003). Ground-based measurements of leaf area index: a review of methods, instruments and current controversies. *Journal of Experimental Botany*, *54*(392), 2403–17. doi:10.1093/jxb/erg263

Brown, M. E., & de Beurs, K. M. (2008). Evaluation of multi-sensor semi-arid crop season parameters based on NDVI and rainfall. *Remote Sensing of Environment*, *112*(5), 2261–2271. doi:10.1016/j.rse.2007.10.008

Brown, B., Westcott, M., Christensen, N., Pan, B., & Stark, J. (n.d.). Nitrogen Management for Hard Wheat Protein Enhancement. *PNW Extension Publication*.

Chapin, F.S. III., I.F. Wardlaw. (1988). Effects of phosphorus deficiency on source-sink interactions between the flag leaf and developing grain in barley. *Journal of Experimental Botany, 39,* 165–177.

Christopher, J., Veyradier, M., Borrell, A., Harvey, G., Fletcher, S., & Chenu, K. (2014). Phenotyping novel stay-green traits to capture genetic variation in senescence dynamics. *Functional Plant Biology*, *41*, 1035–1048.

Cleary, B.D., Waring, R.H. (1969). Temperature: Collection of data and its analysis for the interpretation of plant growth and distribution. *Canadian Journal of Botany, 47*, 167–173.

Cleveland, W.S., (1979). Robust locally weighted regression and smoothing scatter- plots. *Journal of the American Statistical Association, 74*, 829–836.

Cleveland, W.S., Devlin, S.J., (1988). Locally weighted regression – an approach to regression analysis by local fitting. *Journal of the American Statistical Association, 86*, 83, 596–610.

de Ruiter, J.M., Brooking, I.R.. (1994). Nitrogen and dry matter partitioning of barley grown in a dryland environment. *New Zealand Journal of Crop Horticultural Sciences. 22*, 45–55.

Donmez E., Sears R.G., Shroyer J.P., Paulsen G.M. (2001). Genetic gain in yield attributes of winter wheat in the great plains. *Crop Science, 41*, 1412–1419.

Eitel, J. U. H., Long, D. S., Gessler, P. E., & Smith, A. M. S. (2007). Using in-situ measurements to evaluate the new RapidEye™ satellite series for prediction of wheat nitrogen status. *International Journal of Remote Sensing*, *28*(18), 4183–4190. doi:10.1080/01431160701422213

Eitel, J. U. H., Long, D. S., Gessler, P. E., & Hunt, E. R. (2008). Combined Spectral Index to Improve Ground-Based Estimates of Nitrogen Status in Dryland Wheat. *Agronomy Journal*. doi:10.2134/agronj2007.0362

Eitel, J. U. H., Long, D. S., Gessler, P. E., Hunt, E. R., & Brown, D. J. (2009). Sensitivity of Ground-Based Remote Sensing Estimates of Wheat Chlorophyll Content to Variation in Soil Reflectance. *Soil Science Society of America Journal*, *73*(5), 1715. doi:10.2136/sssaj2008.0288

Eitel, J.U.H., Vierling, L.A., Magney, T.S. (2013) A lightweight, low cost autonomously operating terrestrial laser scanner for quantifying and monitoring ecosystem structural dynamics. *Agricultural and Forest Meteorology*, *180*, 86–96.

Eitel, J. U. H., Magney, T. S., Vierling, L. A., Brown, T. T., & Huggins, D. R. (2014). LiDAR based biomass and crop nitrogen estimates for rapid , non-destructive assessment of wheat nitrogen status. *Field Crops Research*, *159*, 21–32.

Erdle, K., Mistele, B., & Schmidhalter, U. (2011). Comparison of active and passive spectral sensors in discriminating biomass parameters and nitrogen status in wheat cultivars. *Field Crops Research*, *124*(1), 74–84. doi:10.1016/j.fcr.2011.06.007

Farooq, M., Hussain, M., & Siddique, K. H. M. (2014). Drought Stress in Wheat during Flowering and Grain-filling Periods. *Critical Reviews in Plant Sciences*, *33*(February 2015), 331–349. doi:10.1080/07352689.2014.875291

Fisher, J. I., & Mustard, F. (2007). Cross-scalar satellite phenology from ground, Landsat, and MODIS data. *Remote Sensing of Environment, 109,* 261−273.

Freeman, K. W., Raun, W. R., Johnson, G. V., Mullen, R. W., Stone, M. L., & Solie, J. B. (2003). Late-season Prediction Of Wheat Grain Yield And Grain Protein. *Communications in Soil Science and Plant Analysis*, *34*(13-14), 1837–1852. doi:10.1081/CSS-120023219

Gaju, O., Allard, V., Martre, P., Le Gouis, J., Moreau, D., Bogard, M, Hubbart, S., Foulkes, M. J. (2014). Nitrogen partitioning and remobilization in relation to leaf senescence, grain yield and grain nitrogen concentration in wheat cultivars. *Field Crops Research*, *155*, 213–223. doi:10.1016/j.fcr.2013.09.003

Gallanger, J.N., Biscoe, P.V. (1978). Radiation absorption, growth, and yield of cereals. *Journal of Agricultural Science, 91,* 47-60.

Gamon, J., Cheng, Y., Claudio, H., Mackinney, L., & Sims, D. (2006). A mobile tram system for systematic sampling of ecosystem optical properties. *Remote Sensing of Environment*, *103*(3), 246–254. doi:10.1016/j.rse.2006.04.006

Garrity, S. R., Vierling, L. a., & Bickford, K. (2010). A simple filtered photodiode instrument for continuous measurement of narrowband NDVI and PRI over vegetated canopies. *Agricultural and Forest Meteorology*, *150*(3), 489–496. doi:10.1016/j.agrformet.2010.01.004

Goodin, D.G., and G.M. Henebry. (1997). A technique for monitoring ecological disturbance in tallgrass prairie using seasonal NDVI trajectories and a discriminant function mixture model. *Remote Sensing of Environment, 61,* 270–278.

Gooding, M.J., Davies, W.P. (1992). Foliar urea fertilization of cereals: A review. *Fertilizer Research, 32,* 209-222.

Haboudane, D., Miller, J. R., Tremblay, N., Zarco-Tejada, P. J., & Dextraze, L. (2002). Integrated narrow-band vegetation indices for prediction of crop chlorophyll content for application to precision agriculture. *Remote Sensing of Environment*, *81*(2-3), 416–426. doi:10.1016/S0034-4257(02)00018-4

Hansen, P. M., Jorgenson, J. R., & Thomsen, A. (2002). Predicting grain yield and protein content in winter wheat and spring barley using repeated canopy reflectance measurements and partial. *Journal of Agricultural Science*, *139*, 307–318.

Hanway, J.J. (1963). Growth stages of corn (Zea mays L.). *Agronomy Journal*, *55*, 487–492.

Harris, K., Subudhi, P. K., Borrell, A., Jordan, D., Rosenow, D., Nguyen, H. T., Klein, P., Klein, R., anMullet, J. (2007). Sorghum stay-green QTL individu- ally reduce post-f lowering drought-induced leaf senescence. *Journal of Experimental Botany, 58*, 327–338.

Hilker, T., Coops, N. C., Coggins, S. B., Wulder, M. A., Brown, M., Black, T. Nessic, Z., Lessard, D. (2009). Detection of foliage conditions and disturbance from multi-angular high spectral resolution remote sensing. *Remote Sensing of Environment*, *113*(2), 421–434. doi:10.1016/j.rse.2008.10.003

Huete, A.R. (1987). Soil-dependent spectral response in a developing plant canopy. *Agronomy Journal, 79*, 612-68.

Huete, A. R. (1988). A soil adjusted vegetation index (SAVI). *Remote Sensing of Environment*, *25*, 295–30

Huete, A.R. (2012). Vegetation indices, remote sensing and forest monitoring. *Geography Compass, 6*, 513–532. doi:10.1111/j.1749-8198.2012.00507.x

Huggins, D. R., Pan, W. L., & Smith, J. (2010). Yield , Protein and Nitrogen Use Efficiency of Spring Wheat : Evaluating Field-Scale Performance. *CSANR Research Report 2010-001*, *001*, 1–24.

Huemmrich, K. F., Black, T. A., Jarvis, P. G., McCaughey, J. H., & Hall, F. G. (1999). High temporal resolution NDVI phenology from micrometeorological radiation sensors. *Journal of Geophysical Research*, *104*(D22), 27935–27944. doi:10.1029/1999JD900164

Jackson, R.D., Huete, A.R. (1991). Interpreting vegetation indices. *Preventative Veterinary Medicine, 11*, 185-200.

Justice, C.O., Townsend, J.R.G., Holben, B.N., Tucker, C.J. (1985) Analysis of the phenology of global vegetation using meteorological satellite data. *International Journal of Remote Sensing*, *4*, 369–385.

Kleman, J., Fagerlund, E. (1987). Influence of different nitrogen and irrigation treatments of the spectral reflectance of barley. *Remote Sensing of Environment, 21*, 1–14.

Lindgren, F., Geladi, P., & Wold, S. (1994). Kernal based PLS regression; cross-validation and application to spectral data. *Journal of Chemometrics, 8,* 377e389.

Lindstrom, M.J., R.I. Papendick, and F.E. Koehler. (1976). A model to predict winter wheat emergence as affected by soil temperature, water potential and depth of planting. *Agronomy Journal, 68,* 137–141. doi:10.2134/agronj1976.00021962006800010038x

Lobell, D. B. (2013). The use of satellite data for crop yield gap analysis. *Field Crops Research, 143,* 56–64. doi:10.1016/j.fcr.2012.08.008

Longnecker, N., Kirby, E.J.M, Robson, A., (1993). Leaf emergence, tiller growth, and apical development of nitrogen-deficient spring wheat. *Crop science, 33,* 154-160.

Lopes, M. S., & Reynolds, M. P. (2012). Stay-green in spring wheat can be determined by spectral reflectance measurements (normalized difference vegetation index) independently from phenology. *Journal of Experimental Botany, 63,* 3789–3798. doi:10.1093/jxb/ers071

Madani, A., Rad, A. S., Pazoki, A., Nourmohammadi, G., and Zarghami, R. (2010). Wheat (Triticum aestivum L.) grain filling and dry matter partitioning responses to source:sink modifications under post anthesis water and nitrogen deficiency. *Acta Sci. Agron, 32,* 145–151.

Magney, T.S. (2015). Assessing the spatial and temporal controls on plant function using ground-based remote sensing (Doctoral dissertation, Ch.1).

Mahey, R. K., Singh, R., Sidhu, S. S. and Narang, R. S. (1991). The use of remote sensing to assess the effects of water stress on wheat. *Experimental Agriculture, 27,* 423–429.

Masclaux-Daubresse, C., Daniel-Vedele, F., Dechorgnat, J., Chardon, F., Gaufichon, L., & Suzuki, A. (2010). Nitrogen uptake, assimilation and remobilization in plants: challenges for sustainable and productive agriculture. *Annals of Botany, 105*(7), 1141–57. doi:10.1093/aob/mcq028

Miller, R.O., J.S. Jacobsen and E.O. Skogley. (1994). Aerial accumulation and partitioning of nutrients by hard red spring wheat. *Communications in Soil Science and Plant Analysis, 25,* 891-1911.

Mulla, D. J. (2013). Twenty five years of remote sensing in precision agriculture: Key advances and remaining knowledge gaps. *Biosystems Engineering, 114*(4), 358–371. doi:10.1016/j.biosystemseng.2012.08.009

Myeni, R.B., Keeling, C.D., Tucker, C.J., Asrar, G. & Nemani, R.R. (1997). Increased plant growth in the northern high latitudes from 1981 to 1991. *Nature, 386,* 698–702.

Norman, J.M., Welles, J.M., Walter, E.A. (1985). Contrasts among bidirectional reflectance of leaves, canopies, and soils. *IEEE Transactions on Geoscience and Remote Sensing, 23,* 659-667.

Nguy-Robertson, A., Gitelson, A., Peng, Y., Walter-Shea, E., Leavitt, B., & Arkebauer, T. (2013). Continuous Monitoring of Crop Reflectance, Vegetation Fraction, and Identification of Developmental Stages Using a Four Band Radiometer. *Agronomy Journal, 105*(6), 1769. doi:10.2134/agronj2013.0242

O'Brien, R.M. (2007). A caution regarding rules of thumb for variance inflation factors. *Quality and Quantity, 41,* 673-690.

Oscarson, P. (2000). The strategy of the wheat plant in acclimating growth and grain production to nitrogen availability. *Journal of Experimental Botany, 51*(352), 1921–1929. doi:10.1093/jexbot/51.352.1921

Panda, S. S., Ames, D. P., & Panigrahi, S. (2010). Application of Vegetation Indices for Agricultural Crop Yield Prediction Using Neural Network Techniques. *Remote Sensing, 2*(3), 673–696. doi:10.3390/rs2030673

Prasad, A. K., Chai, L., Singh, R. P., & Kafatos, M. (2006). Crop yield estimation model for Iowa using remote sensing and surface parameters. *International Journal of Applied Earth Observation and Geoinformation, 8*(1), 26–33. doi:10.1016/j.jag.2005.06.002

Pepler S., Gooding M.J., Ford K.E., Ellis R.H. (2005). A temporal limit to the association between flag leaf life extension by fungicides and wheat yields. *European Journal of Agronomy, 22,* 363–373

Pimstein, A., Eitel, J.U.H., Long, D.S., Mufradi, I., Karnieli, A., Bonfil, D.J. (2009). A spectral index to monitor the head emergence of wheat in semi-arid conditions. *Field Crops Research, 111*(3), 218-225.

Pinter, P.J., Jackson, R.D., Idso, S.B., Reginato, R.J. (1981). Multidate spectral reflectance as predictors of yield in water stressed wheat and barley. *International Journal of Remote Sensing, 2,* 43-48.

Qi, J., Chehbouni, Al, Huete, A. R., Kerr, Y. H., & Sorooshian, S. (1994). A modified soil adjusted vegetation index (MSAVI). *Remote Sensing of Environment, 48,* 119−126.

Qualm, a. M., Osborne, S. L., & Gelderman, R. (2010). Utilizing Existing Sensor Technology to Predict Spring Wheat Grain Nitrogen Concentration. *Communications in Soil Science and Plant Analysis, 41*(17), 2086–2099. doi:10.1080/00103624.2010.498538

Rondeaux, G., Steven, M., & Baret, F. (1996). Optimization of soil-adjusted vegetation indices. *Remote Sensing of Environment, 55,*95−107.

Ranson, K.J., C.S.T. Daughtry, L.L. Biehl, and M.E. Bauer. (1985). Sun-view angle effects on reflectance factors of corn canopies. *Remote Sensing of Environment, 18,* 147–161. doi:10.1016/0034-4257(85)90045-8

Raun, W. R., Solie, J. B., Johnson, G. V., Stone, M. L., Lukina, E. V., Thomason, W. E., & Schepers, J. S. (2001). In-Season Prediction of Potential Grain Yield in Winter Wheat Using Canopy Reflectance. *Agronomy Journal*, *93*, 131. doi:10.2134/agronj2001.931131x

Reynolds, M., Foulkes, J., Furbank, R., Griffiths, S., King, J., Murchie, E., … Slafer, G. (2012). Achieving yield gains in wheat. *Plant, Cell & Environment*, *35*(10), 1799–823. doi:10.1111/j.1365-3040.2012.02588.x

Richards, R.A. (1987). Physiology and the breeding of winter-grown cereals for dry area. In: Srivastava J.P., Porceddu, E., Acevedo, E., Varma, S, eds. *Drought tolerance in winter cereals.* Chichester Wiley, 133-150.

Richardson, A. D., Jenkins, J. P., Braswell, B. H., Hollinger, D. Y., Ollinger, S. V, & Smith, M.-L. (2007). Use of digital webcam images to track spring green-up in a deciduous broadleaf forest. *Oecologia*, *152*(2), 323–34. doi:10.1007/s00442-006-0657-z

Rouse, J. W., Haas, R. H., Schell, J. A., Deering, D. W., and Harlan, J. C. (1974). Monitoring the vernal advancement of retrogradation (green wave effect) of natural vegetation. NASA/GSFC, Type III, Final Report, Greenbelt, MD, USA, pp. 1–371.

Rundel, P. W., Graham, E. a, Allen, M. F., Fisher, J. C., & Harmon, T. C. (2009). Environmental sensor networks in ecological research. *The New Phytologist*, *182*(3), 589–607. doi:10.1111/j.1469-8137.2009.02811.x

Ryu, Y., Baldocchi, D. D., Verfaillie, J., Ma, S., Falk, M., Ruiz-Mercado, I., Hehn,T., Sonnentag, O. (2010). Testing the performance of a novel spectral reflectance sensor, built with light emitting diodes (LEDs), to monitor ecosystem metabolism, structure and function. *Agricultural and Forest Meteorology*, *150*(12), 1597–1606. doi:10.1016/j.agrformet.2010.08.009

Sakamoto, T., Gitelson, A. a., Nguy-Robertson, A. L., Arkebauer, T. J., Wardlow, B. D., Suyker, A. E., Verma, S.B., Shibayama, M. (2012). An alternative method using digital cameras for continuous monitoring of crop status. *Agricultural and Forest Meteorology*, *154-155*, 113–126. doi:10.1016/j.agrformet.2011.10.014

Shanahan, J. F., Kitchen, N. R., Raun, W. R., & Schepers, J. S. (2008). Responsive in-season nitrogen management for cereals. *Computers and Electronics in Agriculture*, *61*, 51-62.

Simane, B., Peacock, J.M., Struik, P.C. (1993). Differences in developmental plasticity and growth rate among drought-resistant and susceptible cultivars of durum wheat. *Plant Soil, 157,* 155-166.

Sims, D., Luo, H., Hastings, S., Oechel, W., Rahman, a, & Gamon, J. (2006). Parallel adjustments in vegetation greenness and ecosystem CO2 exchange in response to drought in a Southern California chaparral ecosystem. *Remote Sensing of Environment*, *103*(3), 289–303. doi:10.1016/j.rse.2005.01.020

Soudani, K., le Maire, G., Dufrêne, E., François, C., Delpierre, N., Ulrich, E., & Cecchini, S. (2008). Evaluation of the onset of green-up in temperate deciduous broadleaf forests derived from Moderate Resolution Imaging Spectroradiometer (MODIS) data. *Remote Sensing of Environment*, *112*(5), 2643–2655. doi:10.1016/j.rse.2007.12.004

Soudani, K., Hmimina, G., Delpierre, N., Pontailler, J. Y., Aubinet, M., Bonal, D., … Dufrêne, E. (2012). Ground-based Network of NDVI measurements for tracking temporal dynamics of canopy structure and vegetation phenology in different biomes. *Remote Sensing of Environment*, *123*, 234–245. doi:10.1016/j.rse.2012.03.012

Stone, M. L., Solie, J. B., Raun, W. R., Whitney, R. W., Taylor, S. L., & Ringer, J. D. (1996). Use of spectral radiance for correcting in- season fertilizer nitrogen deficiencies in winter wheat. *Transactions of the ASAE,* 39, 1623e1631.

Sweet, S. K., Griffin, K. L., Steltzer, H., Gough, L., & Boelman, N. T. (2015). Greater deciduous shrub abundance extends tundra peak season and increases modeled net CO 2 uptake. *Global Change Biology*, Early view. doi:10.1111/gcb.12852

Tindall, T.A., Stark, J.C., Brooks, R.H., 1995, Irrigated spring wheat response to topdressed nitrogen as predicted by flag leaf nitrogen concentration. *Journal of Production Agriculture, 8,* 46-52.

Triboi E, Triboi-Blondel AM (2002) Productivity and grain or seed composition: a new approach to an old problem. *European Journal of Agronomy, 16,* 163–186

Tucker, C. J. (1979). Red and photographic infrared linear combinations for monitoring vegetation. *Remote Sensing of Environment,* 8,127–150.

Tucker, C.J., Elgin, J.H., McMurtrey, J.E. (1980). Relationship of spectral data to grain yield variation. *Photogrammetric Engineering & Remote Sensing, 46,* 657-666.

Van Andel J., Jager, J.C. (1981). Analysis of growth and nutrition of six plant species of woodland clearings. *Journal of Ecology, 69,* 871-882.

Van den Boogaard, R., Kostadinova, S., Veneklaas, E., Lambers, H. (1995(. Association of water use efficiency and nitrogen use efficiency with photosynthetic characteristics of two wheat cultivars. *Journal of Experimental Botany, 46,* 1429-1438.

Van Sanford, D.A., MacKown, C.T. (1986). Variation in nitrogen use efficiency among soft red winter wheat genotypes. *Theoretical and Applied Genetics, 72,* 158–163.

Verhoef, W. (1984). Light scattering by leaf layers with application to canopy reflectance modeling: The SAIL model. *Remote Sensing of Environment, 16*,125−141.

Vierling, L.A., Deering, D.W., and Eck, T.F. (1997). Differences in Arctic tundra vegetation type and phenology as seen using bi-directional radiometry in the early growing season. *Remote Sensing of Environment, 60,* 71–82.

Vierling, L.A., Hilker, T., Gamon, J., Coops, N., Baldocchi, D., Magney, T.S.**,** Ryu, T., Papale, D., Sonnentag, O., Garrity, S., Heummrich**,** K.F., Eitel, J.U.H.. (*in revisions).* Tansley Review: Spectral metabolics: Emerging findings, methodologies, and implications of estimating canopy gas exchange using remote sensing. *New Phytologist.*

Villegas, D. (2001). Biomass Accumulation and Main Stem Elongation of Durum Wheat Grown under Mediterranean Conditions. *Annals of Botany*, *88*, 617–627. doi:10.1006/anbo.2001.1512

Viña, A., A.A. Gitelson, D.C. Rundquist, G.P. Keydan, B. Leavitt, & J. Schepers. (2004). Monitoring maize (L.) phenology with remote sensing. *Agronomy Journal*, *96*, 1139–1147.

Vito M. R. Muggeo (2003). Estimating regression models with unknown break-points. *Statistics in Medicine, 22,* 3055-3071.

Vito M. R. Muggeo (2008). segmented: an R Package to Fit Regression Models with Broken-Line Relationships. R News, 8/1, 20-25. URL http://cran.r-project.org/doc/Rnews/.

Wang, Z., Wang, J., Zhao, C., Zhao, M., Huang, W., and Wang, C., 2005, Vertical Distribution of Nitrogen in Different Layers of Leaf and Stem and their Relationship with Quality of Winter Wheat. *Journal of Plant Nutrition, 28,* 73-91.

Xue, L.-H., Cao, W.-X., & Yang, L.-Z. (2007). Predicting Grain Yield and Protein Content in Winter Wheat at Different N Supply Levels Using Canopy. *Pedosphere*, *17*(5), 646–653.

Zadoks J.C., Chang T.T., Zonzak C.F. (1974). A decimal code for the growth stages of cereals. *Weed Research, 14,* 415–421.

Tables:

Table 2.1. Summary of field characteristics for each plot location in study. Each field location included four N addition plots. SVWC = Soil Volumetric Water Content; LAI = Leaf Area Index; DOY = Day of Year.

Year	Field	SVWC at planting (m^3 m^{-3})	Maximum LAI (m^2 m^{-2})	Aspect & Position	Depth to argillic layer (m)	Planting DOY
2013	A	0.319	3.04	South hill-top	1.00	93
	B	0.385	3.61	North draw	>2.50	93
2014	A	0.291	3.71	South toe-slope	>2.50	101
	B	0.292	3.59	South hill-top	1.50	101

.

Table 2.2. R^2 between rate (ΔNDVI/days) and duration (days) of key phenological periods and end-of-season harvest metrics of biomass (kg/ha), yield (kg/ha), protein (%), and grain N (kg/ha). Duration of tillering -> heading represents the length of time for tillering, stem extension, and heading time periods; whereas the duration of tillering -> stem extension represents only the tillering and stem extension time periods. n=16 for all relationships.

Phenological predictor variable	Biomass	Yield	Protein	Grain N
Rate of tillering	0.62*	0.72*	0.01	0.37*
Duration of tillering	0.01	0.12	0.10	0.00
Rate of stem extension	0.55*	0.21	0.24	0.53*
Duration of stem extension	0.25*	0.02	0.35*	0.35*
Duration tillering -> heading	0.40*	0.12	0.25*	0.46*
Rate of heading	0.07	0.03	0.64*	0.22
Duration of heading	0.66*	0.67*	0.00	0.36*
Duration tillering -> stem extension	0.03	0.18	0.28*	0.01
Rate of ripening	0.28*	0.05	0.45*	0.45*
Duration of ripening	0.66*	0.42*	0.03	0.42*

* significant at $p < .05$;

Table 2.3. Results from stepwise multiple linear regression using AIC selection criteria between rate and duration during the earliest phenological time period, tillering.

Independent	Dependent variables	t value	p	R^2	RMSE	AIC	VIF
	rate of tillering	5.23	<0.01				1.21
	duration of tillering	1.51	0.16				1.21
Biomass (kg/ha)	intercept	-1.11	0.29	0.68	82.12	155.07	
	rate of tillering	4.70	<0.01				
Yield (kg/ha)	intercept	6.08	<0.01	0.72	35.17	115.79	N/A
	duration of tillering	0.31	0.25				
Protein (%)	intercept	1.21	0.76	0.09	1.73	19.36	N/A
	rate of tillering	2.66	0.01				
Grain N (kg/ha)	intercept	2.87	0.02	0.37	12.91	83.72	N/A

Table 2.4. Results from stepwise multiple linear regression using AIC selection criteria between rate and duration during the first two phenological time periods: tillering and stem extension.

Independent	Dependent variables	t value	p	R^2	RMSE	AIC	VIF
	rate of tillering	1.96	0.07				2.87
	duration of tillering	-1.55	0.16				2.98
	rate of stem extension	3.79	<0.01				2.99
Biomass (kg/ha)	intercept	1.49	0.16	0.87	82.12	144.46	
	rate of tillering	5.07	<0.01				1.30
	rate of stem extension	2.37	0.03				4.31
	duration of stem extension	2.22	0.04				3.75
Yield (kg/ha)	intercept	-0.97	0.34	0.83	31.44	113.49	
	rate of tillering	6.95	0.25				1.06
	duration of stem extension	-1.19	0.01				1.06
Protein (%)	intercept	-2.99	<0.01	0.33	1.44	14.34	
	duration of tillering	-2.71	0.02				1.26
	rate of stem extension	5.47	<0.01				1.26
Grain N (kg/ha)	intercept	3.25	<0.01	0.70	9.294	74.02	

Table 2.5. Results from stepwise multiple linear regression using AIC selection criteria between rate and duration during the first three phenological time periods: tillering, stem extension, and heading.

Independent	Dependent variables	t value	p	R^2	RMSE	AIC	VIF
	rate of tillering	1.96	0.07				2.87
	duration of tillering	-1.55	0.16				2.98
	rate of stem extension	3.79	<0.01				2.99
Biomass (kg/ha)	intercept	1.49	0.16	0.87	82.12	144.46	
	rate of emergence	2.97	0.01				2.19
	duration of emergence	1.28	0.22				1.19
	duration of heading	2.70	0.02				2.44
Yield (kg/ha)	intercept	-0.31	0.76	0.83	29.8	111.71	
	duration of stem extension	1.43	0.18				9.82
	rate of heading	3.07	0.01				8.33
	duration of heading	0.81	0.43				2.41
Protein (%)	intercept	0.08	0.93	0.69	1.09	2.41	
	duration of tillering	-2.71	0.02				1.26
	rate of stem extension	5.47	<0.01				1.26
Grain N (kg/ha)	intercept	3.25	<0.01	0.70	9.294	74.02	

Table 2.6. Results from stepwise multiple linear regression using AIC selection criteria between rate and duration during all four phenological time periods: tillering, stem extension, heading, and ripening.

Independent	Dependent variables	t value	p	R^2	RMSE	AIC	VIF
	duration of tillering	-3.61	<0.01				1.66
	duration of heading	5.12	<0.01				1.25
	rate of ripening	-4.02	<0.01				1.93
Biomass (kg/ha)	intercept	1.15	0.26	0.87	79.25	143.32	
	duration of tillering	-3.27	<0.01				1.66
	duration of heading	5.69	<0.01				1.25
	rate of ripening	-1.34	<0.01				1.93
Yield (kg/ha)	intercept	3.09	0.19	0.83	29.63	111.84	
	rate of heading	2.92	0.01				1.85
	rate of ripening	-1.08	0.29				1.85
Protein (kg/ha)	intercept	1.71	0.11	0.67	1.09	5.40	
	duration of emergence	-3.56	<0.01				1.94
	duration of heading	1.89	0.08				1.66
	rate of ripening	-5.09	<0.01				1.25
Grain N (kg/ha)	intercept	1.47	0.17	0.80	7.87	69.44	

Figures:

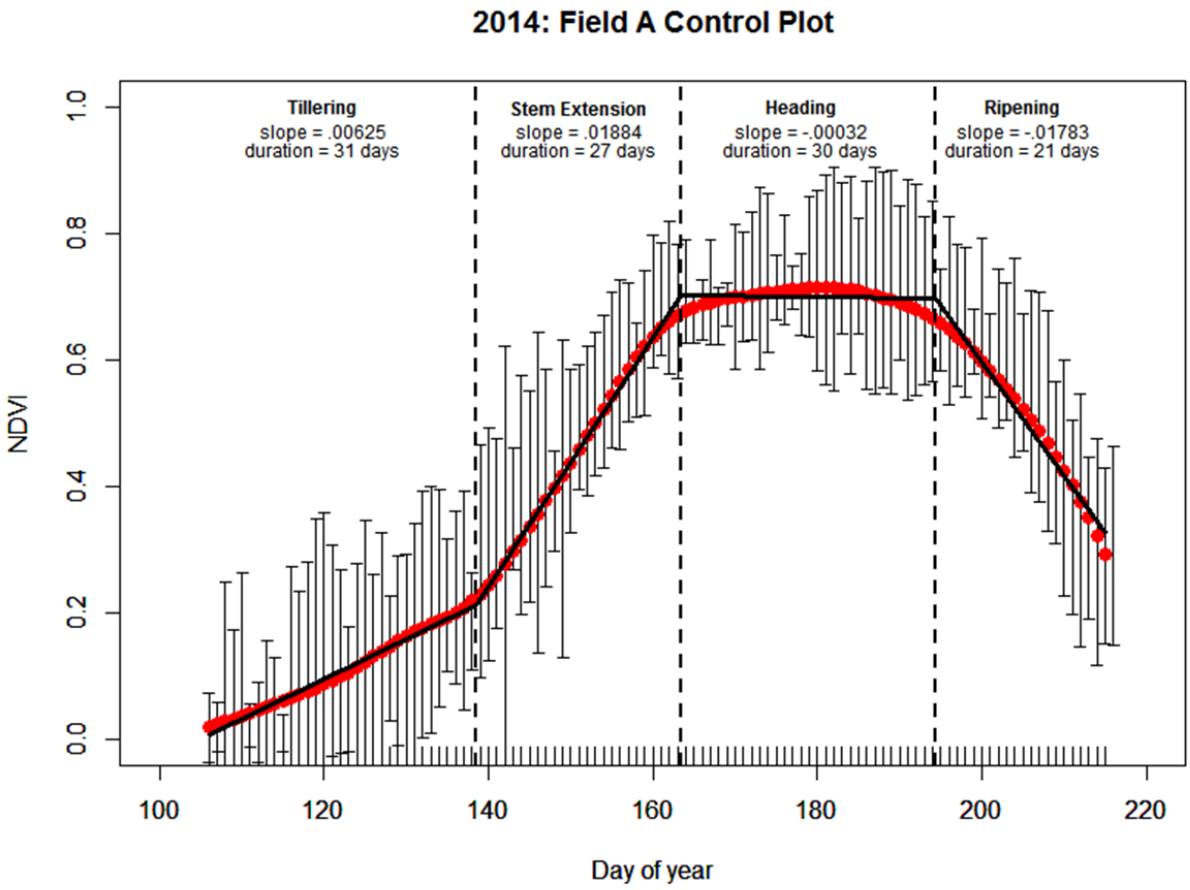

Figure 2.1. Seasonal trends in NDVI data - control plot of Field A in 2014. This figure is used as an example for how inflection points were determined, and to represent the onset of the four phenological stages used in this study. Red points are smoothed daily NDVI values, and error bars represent one standard deviation of the data from 7:00-20:00 each day. The slope of each phenological period is representative of change in NDVI per day.

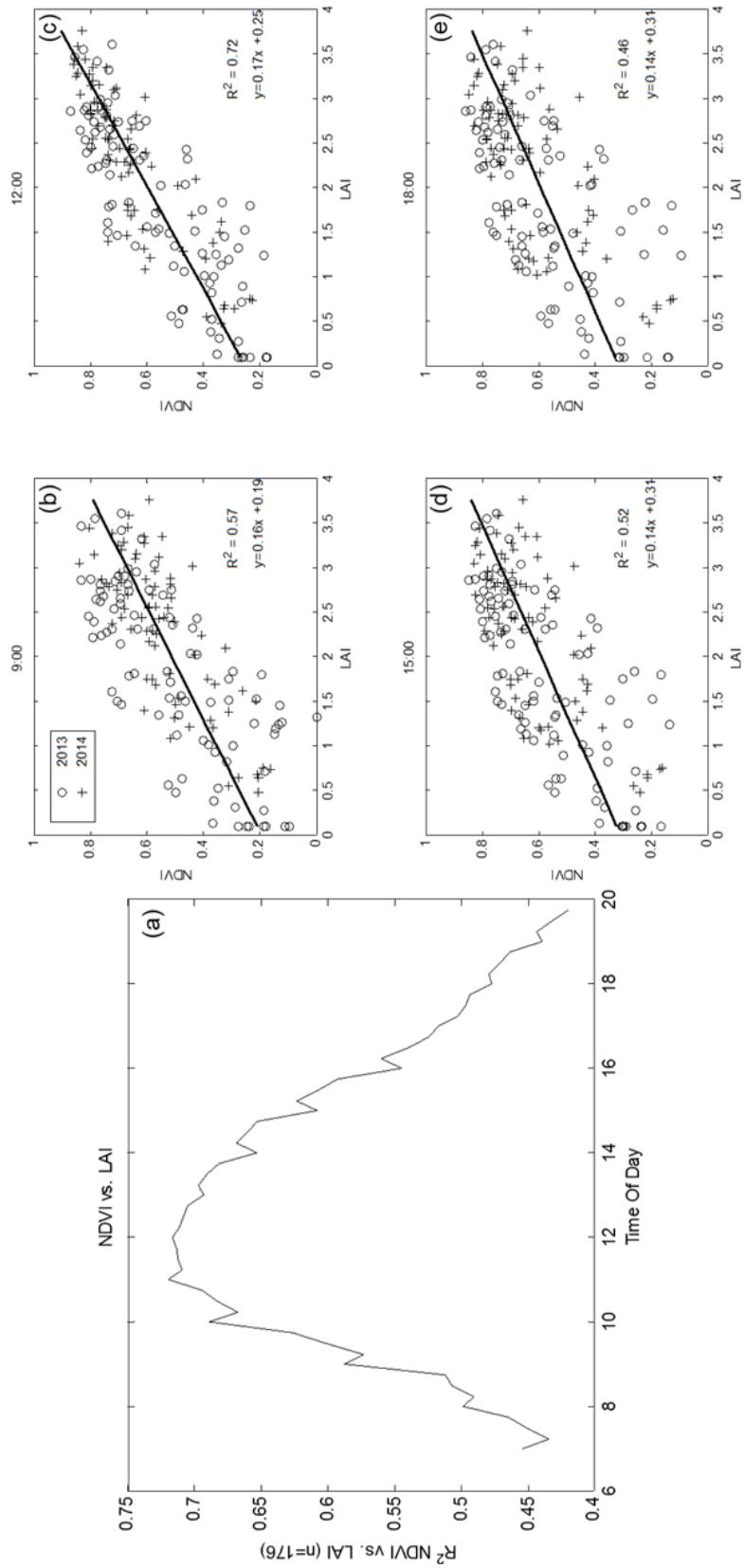

Figure 2.2. Normalized Difference Vegetation Index (NDVI) vs. Leaf Area Index (LAI) at different times of the day. 5 minute resolution NDVI data was used for the same day as LAI was collected (n=176). 2b-e show the relationships between LAI and NDVI at different times throughout the day.

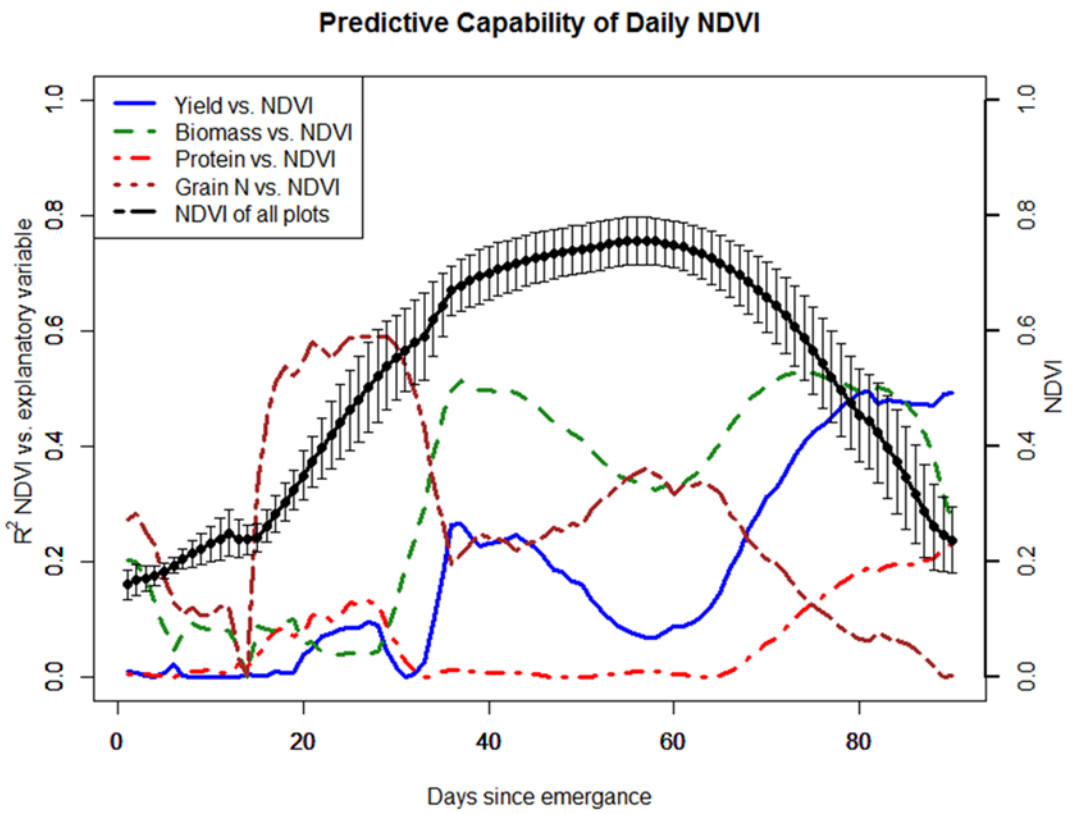

Figure 2.3. Seasonal trend in the daily NDVI data values (black) with error bars representing 95% confidence intervals around daily NDVI data for all plots. All daily NDVI values were normalized to 'days since emergence' since the phenology varied from plot to plot depending on location and season. NDVI vs. yield (blue), biomass (green), protein (red), and grain N (brown) coefficients of determination (R^2) are also plotted throughout the season (each model determined from n=16).

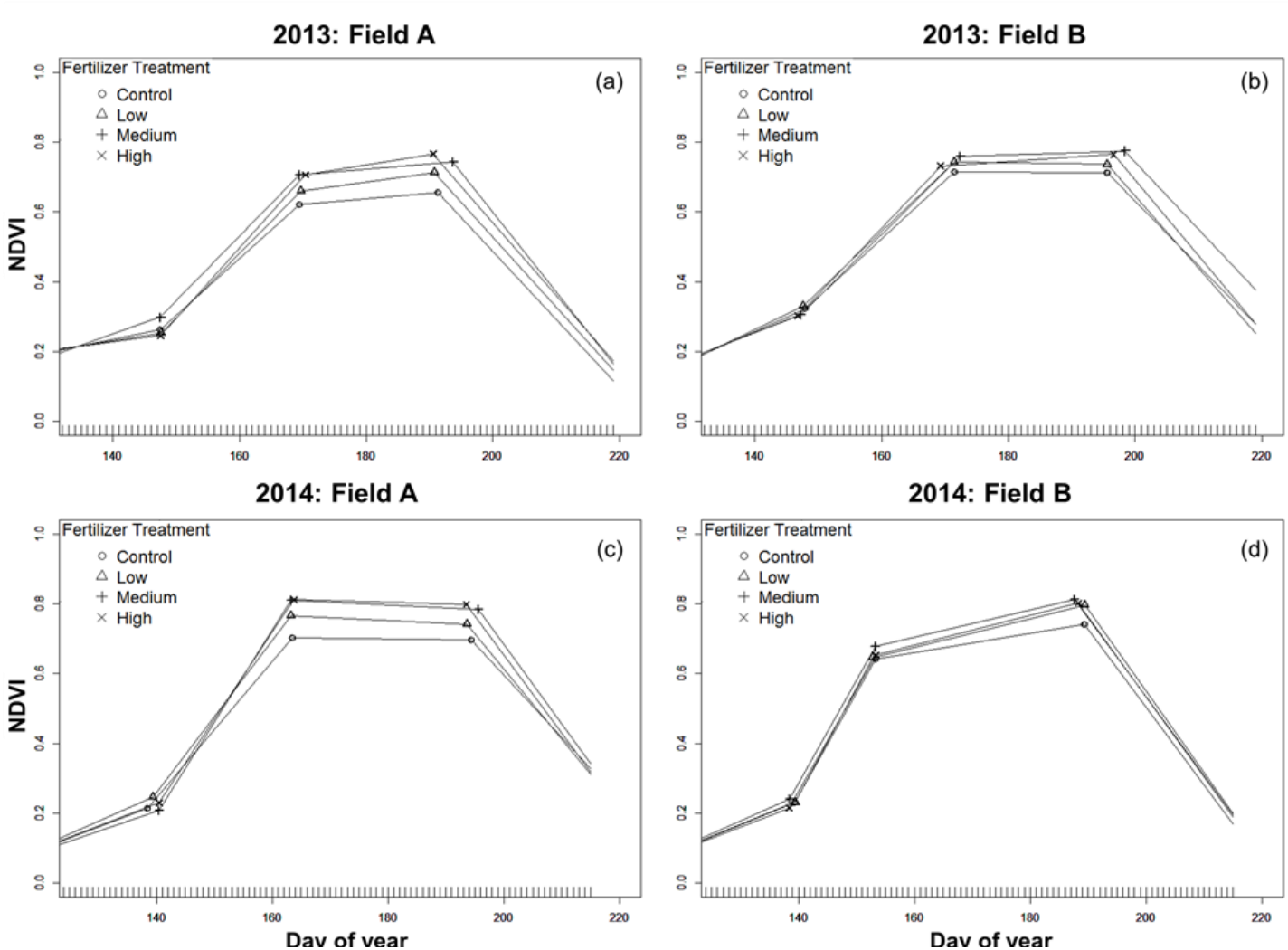

Figure 2.4. Seasonal phenological period patterns across all study plots. First segment = tillering (Zadoks 10-30), second segment = stem extension (Zadoks 31-49) third segment = heading (Zadoks 50-74), fourth segment = ripening (Zadoks 75-100). Symbols at inflection points are representative of treatment plots.

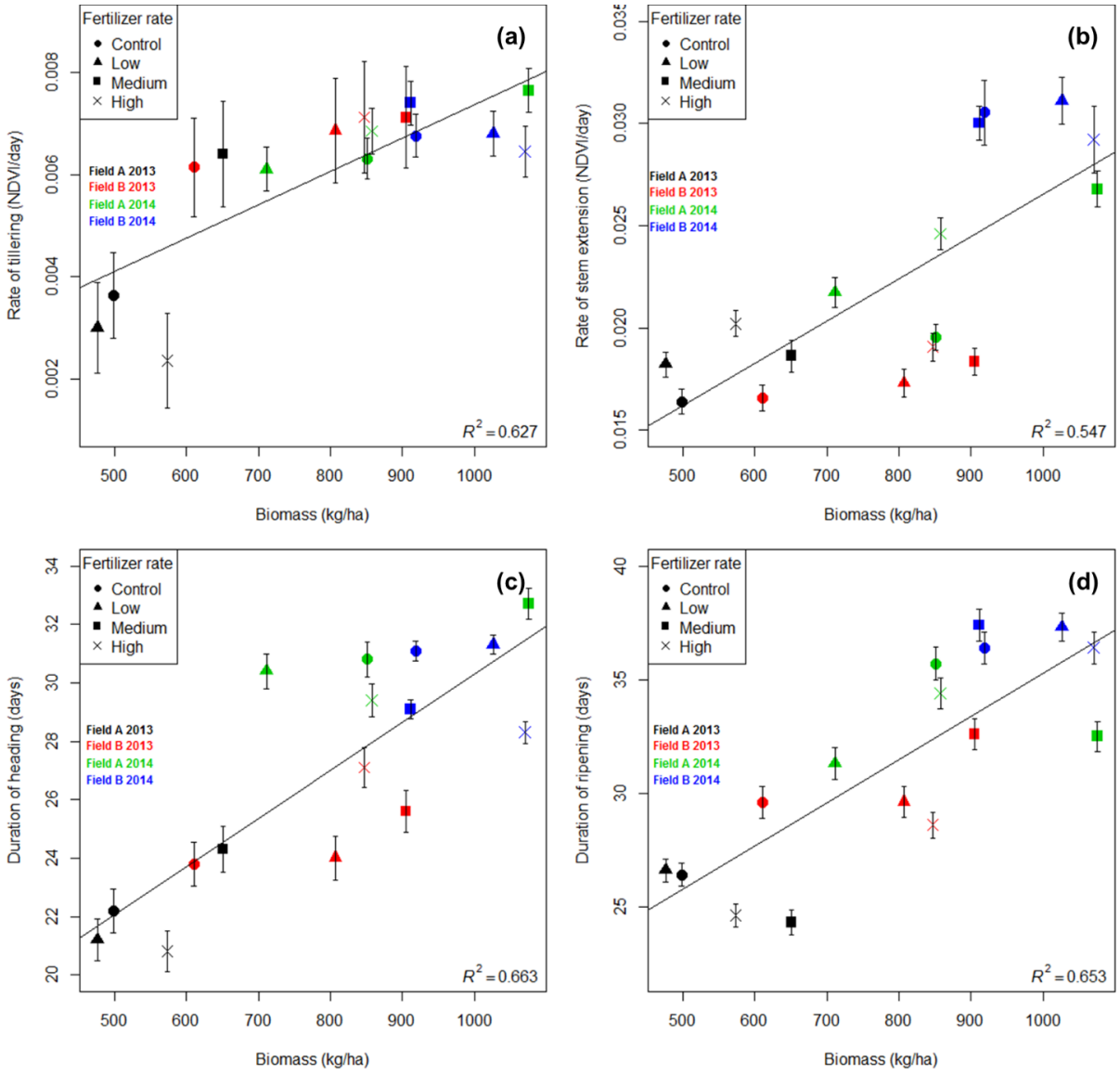

Figure 2.5. Linear regressions between harvested biomass (kg/ha) and (a) rate of tillering (NDVI/day), (b) rate of stem extension (NDVI/day), (c) duration of heading (days), and (d) duration of ripening (days). Symbols represent four different applied N treatments (circle = control, triangle = low, square = medium, and x = high). Colors represent different years and field positions (black = field A 2013, red = field B 2013, green = Field A 2014, and blue = field B 2014). Error bars represent the standard error from the piecewise linear regression in either the location of inflection point (for duration) or slope of the line (for rate).

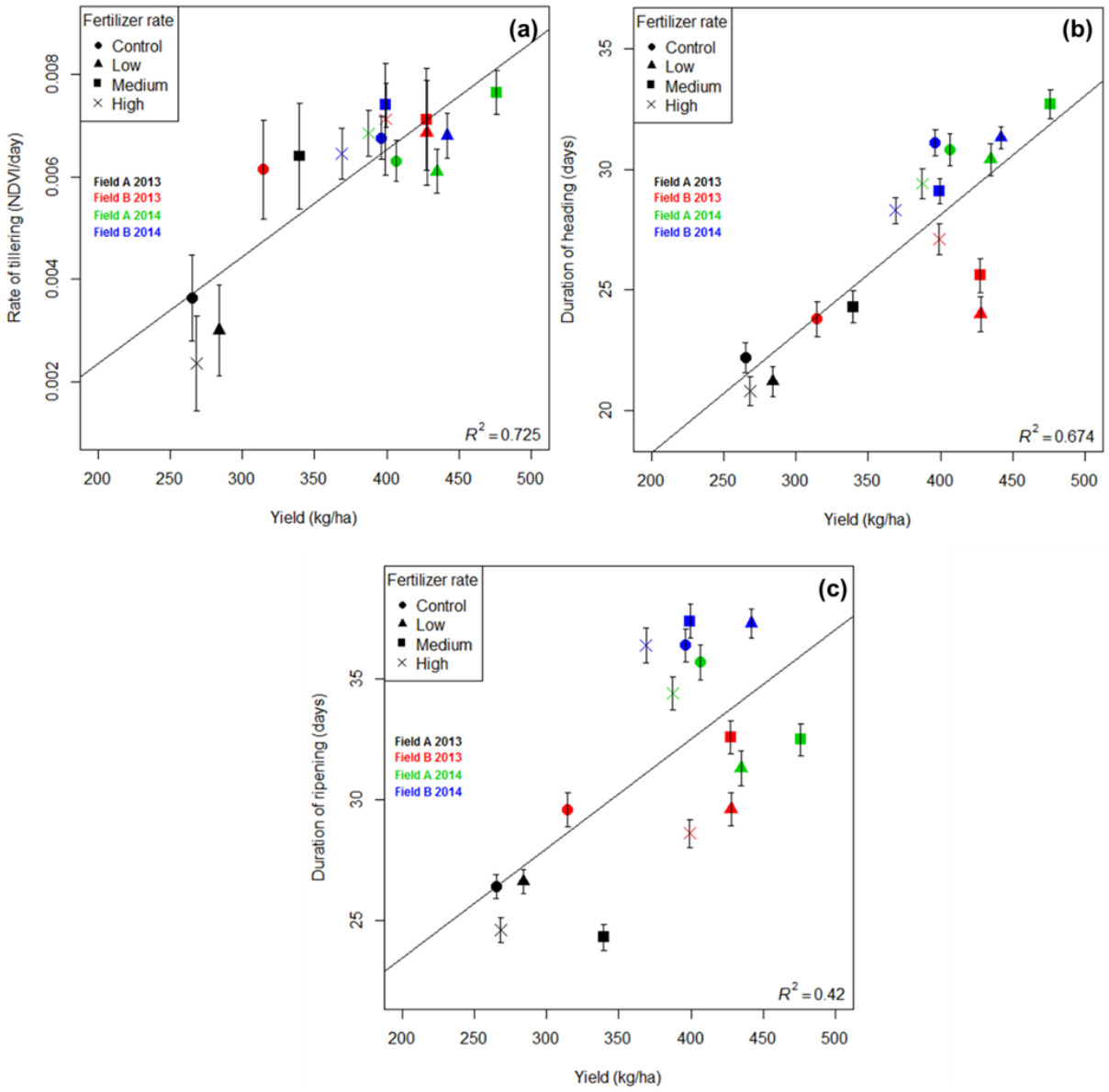

Figure 2.6. Linear regressions between harvested grain yield (kg/ha) and (a) rate of tillering (NDVI/day), (b) duration of heading (days), and (c) duration of ripening (days). Symbols represent four different applied N treatments (circle = control, triangle = low, square = medium, and x = high). Colors represent different years and field positions (black = field A 2013, red = field B 2013, green = Field A 2014, and blue = field B 2014). Error bars represent the standard error from the piecewise linear regression in either the location of inflection point (for duration) or slope of the line (for rate).

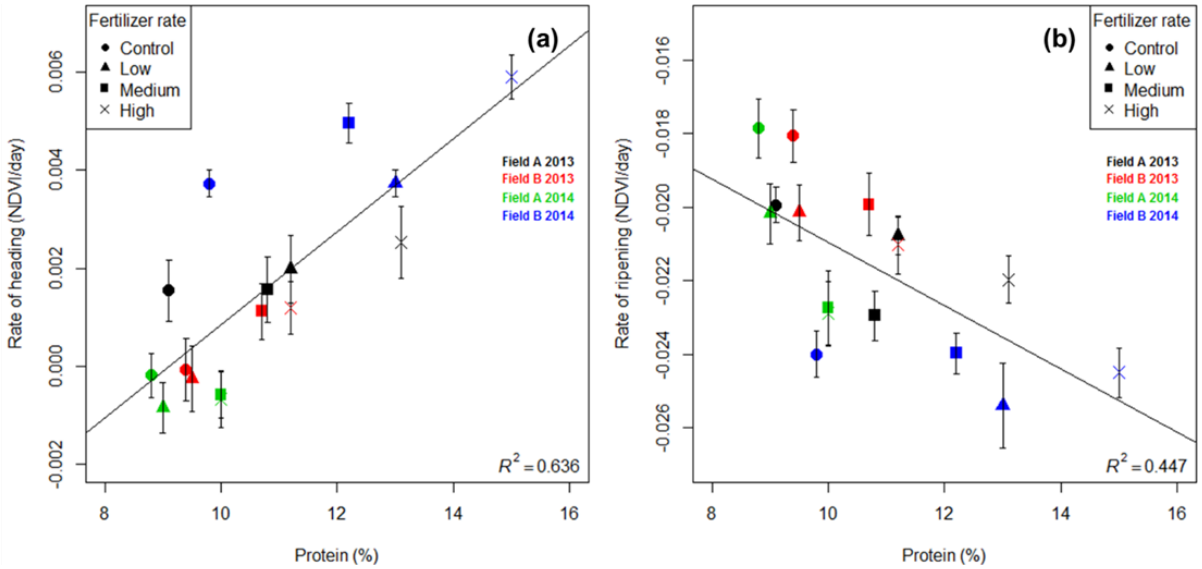

Figure 2.7. Linear regressions between grain protein concentration (%) and (a) rate of heading (NDVI/day), and (b) rate of ripening (NDVI/day). Symbols represent four different applied N treatments (circle = control, triangle = low, square = medium, and x = high). Colors represent different years and field positions (black = field A 2013, red = field B 2013, green = Field A 2014, and blue = field B 2014). Error bars represent the standard error from the piecewise linear regression in either the location of inflection point (for duration) or slope of the line (for rate).

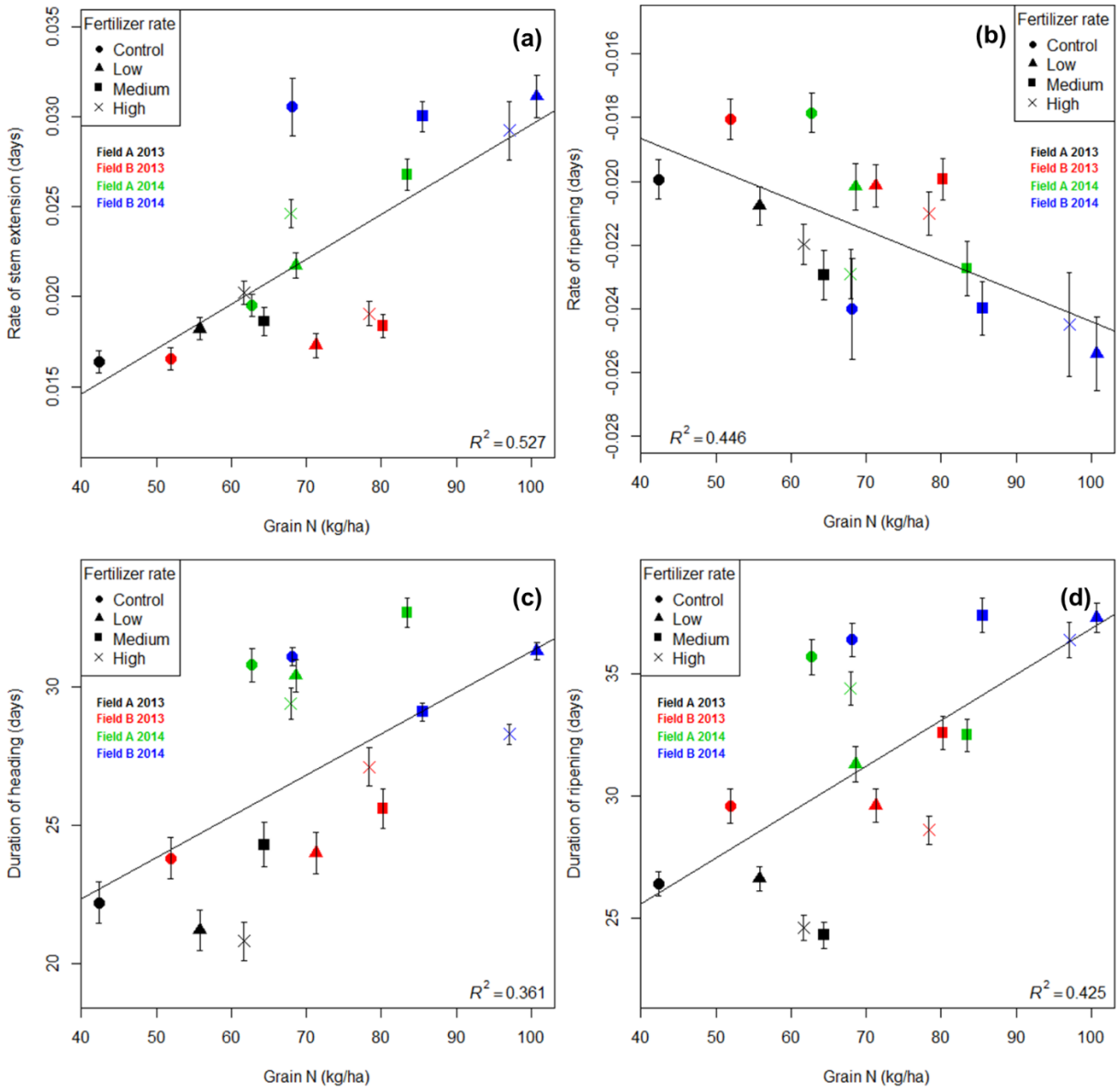

Figure 2.8. Linear regressions between grain N content (kg/ha) and (a) rate stem extension (NDVI/day), (b) rate of ripening (NDVI/day), (c) duration of heading (days), and (d) duration of ripening (days). Symbols represent four different applied N treatments (circle = control, triangle = low, square = medium, and x = high). Colors represent different years and field positions (black = field A 2013, red = field B 2013, green = Field A 2014, and blue = field B 2014). Error bars represent the standard error from the piecewise linear regression in either the location of inflection point (for duration) or slope of the line (for rate).

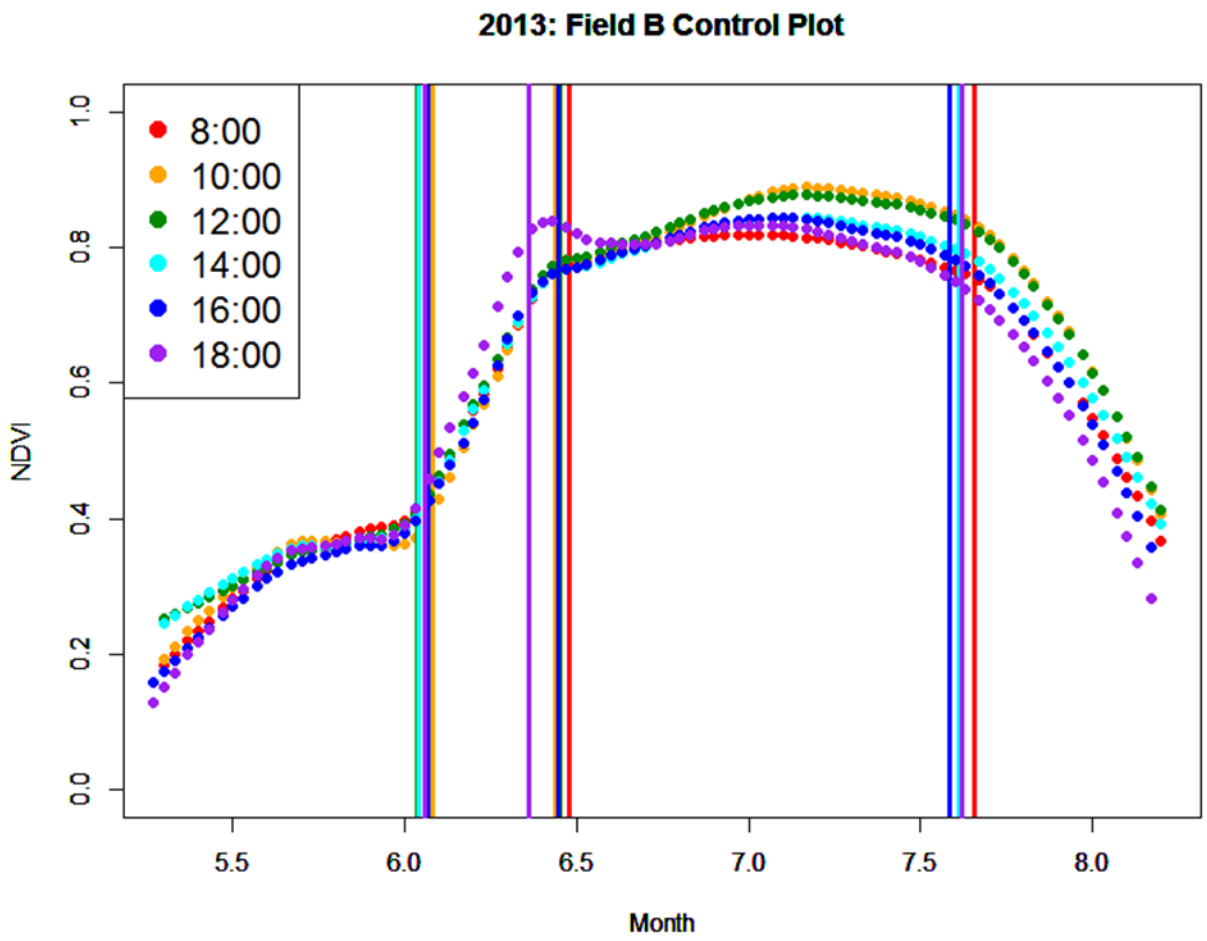

Figure 2.9. Variation in time of day NDVI selection for use in piecewise regression. Vertical lines represent inflection points indicating the onset of tillering, heading, and ripening. All data was recorded similarly to Fig. 2.1.

Chapter 3: LiDAR Canopy Radiation Model Reveals Patterns of Photosynthetic Partitioning in an Arctic Shrub

Magney, T.S., Eitel, J.U.H., Griffin, K.L., Boelman, N.T., Greaves, H., Prager, C.M., Logan, B.A., Zheng, G., Ma, L., Fortin, L., Oliver, R., Vierling, L.A.

to be submitted to Agricultural and Forest Meteorology

Abstract: Characterizing the wide range of light availability and photosynthetic capacity throughout a plant canopy is important for modelling the exchanges of carbon, water, and nutrients between the biosphere and the atmosphere. Such characterization could be especially important in one of the world's most rapidly changing biomes – the arctic tundra. An improved understanding of canopy organization within small arctic shrubs could provide insights into climate feedbacks associated with increasing shrub size, range, and complexity in tundra ecosystems. The multifaceted interactions between 3-D canopy structure, environmental conditions, leaf physiology, and light availability will affect the potentials and limitations of vegetation carbon assimilation and storage. The aim of this study was to elucidate evidence for photosynthetic partitioning according to light availability within a small canopy (< 1 m tall) of *Salix pulchra* exposed to near continuous sunlight at low-solar angles in the arctic tundra. Instantaneous photosynthetic photon flux density (PPFD) and daily integrated quantum flux density (Q_{int}) were modelled from a ray-tracing algorithm for voxels (edge-length .01 m) within the canopy that were assigned a physically based digital gap fraction (DGF) and extinction coefficient (k) to compute an effective leaf area index (LAI_e). Parameters for the ray-tracing model were derived from the x, y, and z locations of high spatial resolution (<1 mm) 3-D maps of shrub canopies from terrestrial LiDAR point clouds. Modelled Q_{int} and a LiDAR derived path-length – determined as the accumulated photon travel distance from the canopy-edge – were compared with traditional light quantification techniques including leaf-area index (LAI), and vertical canopy depth. Weak exponential relationships were observed between the four light quantification techniques ($0.07 < r^2 < 0.28$), suggesting wide variability among these methods. When each of the light environment characterization techniques were compared against leaf-level data on photosynthetic partitioning including percent nitrogen (N %), chlorophyll a to b ratio (Chl *a/b*), and A_{max},

patterns suggesting photosynthetic partitioning only emerged when the LiDAR data derived 3-D locations of the leaf samples were considered (Q_{int} and path length). Statistically significant ($p < 0.05$) trends that follow the theoretical response of leaves to light availability were observed between all three measurements related to photosynthesis and LiDAR data derived Q_{int} ($r = 0.31, 0.46, 0.49$ for N%, Chl *a/b*, and A_{max}, respectively); while 2 of 3 parameters showed a statistically significant response to path length, 1 of 3 to manually measured canopy depth, and 1 of 3 to ceptometer derived LAI. Results from this study suggest that LiDAR based techniques for quantifying the 3-D light environment of small shrubs exposed to low solar angles revealed patterns of photosynthetic partitioning that may otherwise be overlooked using more traditional techniques.

3.1. Introduction

Light availability is the primary factor driving the two- to four fold differences in foliage photosynthetic capacity within a plant canopy (Brunner et al., 1998; Le Roux et al., 2001; Baldocchi et al., 2002; Niinemets et al., 2006; Niinemets, 2007). A better understanding of how light varies throughout vegetation canopies is fundamental to scaling the biophysical processes controlling resource exchange between the biosphere and atmosphere (Baldocchi & Harley et al, 1995, de Pury & Farquer, 1997). The non-linear response of photosynthesis to light has made scaling exercises difficult, requiring a nuanced understanding of vegetation structure and physiology for modeling and predicting carbon sources and sinks at leaf, canopy, and ecosystem scales (e.g., Kirschbaum et al., 1988; Pearcy et al.., 1997; Schurr et al., 2006).

There are several mechanisms by which plants acclimate to the local light environment to maximize photosynthetic potential. In an effort to modify itself for optimal carbon assimilation capacity, plants can alter their anatomy or canopy architecture, change the composition of biomass invested in canopy components (leaves, stems, roots), and partition the relative concentration of biochemical constituents (nitrogen, plant pigments) throughout the canopy (see review by Niinemets et al., 2010). The majority of studies examining the effects of light variability on photosynthetic processes have been conducted on tree canopies often experiencing a five- fold difference in integrated quantum flux density (Q_{int}, Anderson, 1964) – measured as the integral of instantaneous measurements of photosynthetic photon

flux density (PPFD) throughout a day (e.g., Ellsworth & Reich, 1993; Vierling & Wessman, 2000; Kitajima & Hogan, 2003; Niinemets et al., 2004). In general, the theoretical foundation of light attenuation throughout a canopy - the Beer-Lambert law – is observed in field studies, where an exponential decay in radiation occurs coincident with canopy penetration (e.g. Ross, 1981; Brunner et al., 1998). Given the importance of within-canopy photosynthetic partitioning in maximizing whole plant carbon gain, it is important that these processes are investigated across a wide range of species and environmental conditions (Evans & Poorter, 2001).

Traditional field determination of light variability within a plant canopy has been done using a wide range of instruments and techniques: light transmittance determined through leaf area index measurements (LAI, e.g., Hirose & Werger 1987; Pierce & Running, 1988; Ellsworth & Reich, 1993; Bréda, 2003; Weiss et al., 2004), vertical canopy depth (e.g., Bolstad & Gower, 1990; Ellsworth & Reich, 1993; Niinemets, 1996), gap fraction analysis (e.g., Norman & Campbell, 1989; Welles & Cohen, 1996), long-term field placement of photodiodes or quantum sensors (Niinemets et al., 1998, 2004; Vierling & Wessman, 2000), and digital hemispherical photography (Jonckheere et al., 2004; Gonsamo et al., 2010), among others (Jennings et al., 1999; Niinemets, 2010). However, given their often poor spatial and temporal resolution and invasive nature of measurement collection, traditional techniques for quantifying the light environment will be further confounded depending on the solar angle, instrument selection, instrument field of view (FOV), sensor stability and cleanliness, irradiance conditions, spatial heterogeneity within a plant canopy, and user subjectivity in measurement location. As a result, field based techniques for accurately representing the plant light environment can be challenging and highly variable (Bréda, 2003; Jonckheere et al., 2004; Garrigues et al., 2008). To account for the limitations inherent in traditional field-based techniques and to enable the scaling of plant physiological response to light across space and time, there has been increasing interest in linking plant structure and function using three-dimensional (3D) models of ‘virtual plants’ (Whitehead et al., 1990; Hanan, 1997; Sievänen et al., 2000; Godin and Sinoquet, 2005; Pearcy et al., 2005; Vos et al., 2007; Sarlikioti et al., 2011). Models of plant structure in 3D vary widely in their spatial and temporal resolution, and have been used to better understand the link between physiology and structure. By their very nature however, artificial 3D canopy models cannot link empirical measurements made

in the field to actual structural attributes. As a result, there has been increasing interest in mapping 3D plant canopy structure in the field with high-spatial resolution (sub centimeter level) using ground-based light-detection and ranging technology (LiDAR; Lovell et al., 2003; Omasa et al., 2007; Jupp et al., 2009; Eitel et al., 2010, 2013 2014a; Van der Zande et al., 2010, 2011; Beland et al., 2011, 2014; Bittner et al., 2012; van Leeuwen et al., 2013; Vierling et al., 2013; Zheng et al., 2013; Cifuentes et al., 2014; Widlowski et al., 2014; Greaves et al., 2015).

LiDAR is capable of non-invasively providing highly spatially resolved 3D canopy structural information by determining the x, y, and z location of each surveyed laser return based on the angular time-of-flight between laser pulse emission and return. By making use of TLS with low beam divergences and minimizing the distance between the TLS and the survey canopy, high sampling densities can be achieved – allowing for the re-creation of canopy structure at scales < 1mm (e.g., Eitel et al., 2014; Greaves et al., 2015). The high level of canopy structural detail afforded by TLS technology provides the opportunity to model the geometrically explicit canopy internal radiation regime for cubic volume elements, or voxels (Kimes, 1984; Cohen and Fuchs, 1987) throughout plant canopies via ray-tracing (van Leeuwen et al., 2013). Yet, challenges remain that might affect the accuracy of the modeled light regime including viewing obstruction (inability of a laser pulse to reach the inner canopy), movement of canopy elements by wind, determination of the optimum voxel size, leaf clumping and edge laser return values (also known as mixed pixels, ghost returns, or air return values) where the laser is split at the edge of a canopy component and the recorded x, y, and z location does not present a real object but rather the interpolated x, y, and z location between two or more canopy objects (Eitel et al., 2010). Nonetheless, this method has shown great promise to repeatability, objectively, and non-destructively characterize canopy light in 3-D at unprecedented spatial resolutions (Van der Zande et al., 2009; 2010; Bittner et al., 2012; Widlowski et al., 2014). Similar to virtual 3D models describing canopy radiation environment, estimating light transmittance can be done using Beer-Lamberts law by ascribing an extinction coefficient (k, probability that light will not penetrate through a voxel) and a digital gap fraction (DGF, the probability a photon will not reach a canopy element, based on obstructions in a given direction) to each voxel. Combining a TLS derived canopy architectural map with a ray-tracing algorithm could, in theory, offer improvements over

traditionally parameterized (e.g., using virtual 3D canopy models) radiative transfer models that may be limited by overly-simplistic representations of canopy elements.

While it has been speculated that a more representative voxel based light environment could be used to relate to plant physiological measurements, to our knowledge no direct links between LiDAR derived canopy radiation models and empirical physiological data have been published. Utilizing the advantages of LiDAR data driven canopy radiation modeling, this work seeks to make the direct connection between plant physiological measurements and light environment. Three commonly used metrics for assessing photosynthetic acclimation to light environment are the spatial partitioning of leaf nitrogen (N), chlorophyll a to b ratio (Chl *a/b*), and photosynthetic capacity (A_{max}) (Field, 1983; Hirose & Werger, 1987; Ellsworth & Reich, 1993; Niinemets 2007). The close relationship between leaf N and rate of photosynthesis is well understood and based on the premise that Calvin cycle proteins and thylakoids that drive electron transport are primarily N (Evans, 1983, 1989). It is also well established that the Chl *a/b* ratio can be a useful indicator of photosynthetic partitioning within a plant canopy due to its positive correlation with the ratio of photosystem II (PSII) cores to light harvesting chlorophyll-protein complexes, LHCII (Boardman 1977; Martin & Warner, 1984; Hikosaka & Terashima, 1995; Kitajima & Hogan, 2003). Because LHCII contains the bulk of Chl *b*, increases in the relative proportion of Chl *a* to Chl *b* in high light is an adaptive response of chloroplasts maximizing light harvesting capacity (Dale & Causton, 1992). Lastly, the allocation of leaf N and Chl *a/b* along a light gradient implies accumulation of photosynthetic enzymes and the subsequent positive scaling of foliage photosynthetic rates. Gas exchange techniques have been widely used to obtain A_{max} of plants (Farquhar et al., 1980), and further to assess photosynthetic partitioning within plant canopies according to light availability (Niinemets, 2007, 2010). While photosynthetic partitioning has been found using measurements of leaf N, Chl *a/b*, and A_{max} in complex tree canopies, or in relatively homogeneous agricultural environments, there has been limited research on small, sparse, shrub canopies (>1m tall) where resource partitioning may not be hypothesized to exist.

This study investigated photosynthetic partitioning according to light availability within the small, sparse canopy of *Salix pulchra,* which grows among the shrubs *Salix alaxensis, and Betula Nana,* over low-lying mosses, sedges, tussocks, and grammanoids, at high latitudes in the arctic tundra. Several unpublished investigations have shown little or

negligible evidence for photosynthetic partitioning in small arctic shrubs (Heskel et al., 2012, Formica et al., 2013). The significance of partitioning in arctic shrubs is that current models extrapolating carbon exchange in this ecosystem are based on the linear relationship found between LAI and N in arctic plant species (Williams et al., 2001; van Wijk et al., 2005; Shaver et al., 2007; Street et al., 2007). The success of these models is largely due to the assumption that arctic vegetation with LAI values often < 1.0 m m^{-2} are vertically and horizontally homogeneous and that the short growing season, low solar angles, and sparse canopy do not partition resources to maximize photosynthetic optimization (Williams and Rastetter, 1999). However, with the advent of a changing climate, rapid expansion and growth of woody shrubs in the tundra has been observed (see review by Myers-Smith et al., 2011). Over time, as more complex canopies begin to dominate the landscape, more complex models that account for vegetation changes in one of the world's largest biomes will need to be developed to determine the errors associated with modeled and observed canopy photosynthesis. With this motivation, previous work by our group (Heskel et al., 2012, Formica et al., 2013) has attempted to relate measurements of photosynthesis to light environment in tundra shrubs, but have been limited to the quantification of light environment by an LAI-2000 (LICOR, Lincoln, Nebraska), and vertical depth measured by hand. In an attempt to better quantify the light regime of measurements related to photosynthetic partitioning within tundra shrub canopies representative of the future projected arctic ecosystem (e.g., Myers-Smith et al., 2011), our objectives were two-fold:

1) Compare the relative differences in light measurements acquired from traditional (LAI, canopy depth) and TLS/ray-tracing techniques (path length, Q_{int}) made within a *S. pulchra* canopy.
2) Explore how leaf measurements (leaf N, Chl *a/b*, A_{max}) within a *S. pulchra* canopy respond to light availability as quantified by the four techniques in objective one.

To address these objectives, we utilized light information derived from a LiDAR data driven canopy radiation model, LiDAR data derived path length, vertical canopy depth, and LAI measurements, and compared these estimates with leaf level measurements of leaf N, Chl *a/b*, and A_{max} to investigate patterns related to photosynthetic partitioning.

3.2. Methods

3.2.1 Study area

S. pulchra shrubs examined in this experiment were located near the Arctic Long Term Ecological Research Station (LTER) at Toolik Lake (68.63°N, -149.60°W). Twenty-six fully expanded leaves were chosen subjectively to obtain a wide range of potential light conditions within four shrubs, allowing for a total of 104 leaves to be examined for analysis. Large shrubs (height ~ 1 m) representative of what are expected to dominate the tundra ecosystem in the near future include *S. pulchra, S. alaxensis,* and *B.nana* (Myers-Smith et al., 2011). However, *S. alaxensis* are expected to dominate the riparian landscapes, while *B. nana* and *S. pulchra* are expected to increase in size and range in non-riparian tundra. This study only focused on *S. pulchra* primarily due to its larger leaf size compared to *B. nana*. Isolated shrubs were selected for ease of interpretation during canopy radiation simulation and to ensure that obstruction from surrounding vegetation wouldn't occlude the shrub of interest. All shrubs achieved a range in maximum LAI from 2.0 – 2.4 m m^{-2}. *S. pulchra* leaf samples were taken during peak growing season (July 6-16) under diffuse light conditions. *S. pulchra* were growing in the moist acidic tundra complexes (MAT) near Toolik Lake, with the dominant plant community including *Eriophorum vaginatum-Sphagnum, Carex bigelowii-Sphagnum, Salix alaxensis,* and *Betula nana.* The average soil pH in the MAT is < 5.5, mean annual temperature is -8.73 °C and mean annual precipitation is 164.47 mm.

3.2.2. Field data collection and instrumentation

The TLS scans of *S. pulchra* were taken from four opposing directions (in a diamond shape) to avoid directional occlusion effects from one scan angle (Van der Zande et al., 2008). Scans were taken at a consistent range of 2 m with a nominal point spacing of 1 mm and an angular step of 0.5 milliradians (similar to Greaves et al., 2015). A plastic tarp was held in the direction of prevailing winds to minimize moving canopy elements during the scan, after which the effect of wind of leaf movement was negligible. Because an increase in the TLS viewing zenith angle improves estimates of forest canopy gap fraction, the laser scanner head sat atop a tripod approximately 2 m above the ground with approximately a 45º viewing zenith angle to capture all shrub elements from each scanning position (Cifuentes et al., 2014). A discrete return, time-of-flight, Leica Scan Station 2 TLS with a pulsed green (532 nm) laser was used (Leica Geosytems Inc., Heerbrugg, Switzerland). The TLS employs a 4

mm beam diameter, a range of 0-50 m, and a sampling density < 1 mm (as described in Magney et al., 2014 and Eitel et al., 2014a). On the same day TLS scans were acquired, 26 sample locations within each shrub were selected, and marked. Following the initial scans and LAI-2000 measurements, the shrub was trimmed using shears and the x, y, and z sample location were visually identified in the LiDAR point cloud of the trimmed shrub. Four reflective targets with sub-centimeter accurate GPS locations were scanned during each TLS acquisition to permit co-registration of each of the four scans into a local (x, y, and z) and global (Universal Transverse Mercator, UTM) coordinate system. Fig. 3.1 is provided to highlight the spatial variability of samples selected within one of the shrubs. Details on TLS data processing can be found in section 3.2.3.

After the sampling locations were recorded, the nearest four to five leaves attached to the stem were removed and immediately brought back to the laboratory. In the laboratory, gas exchange measurements were taken on each leaf sample (section 3.2.4.1), followed by a leaf punch that was placed in a -80º C freezer within 24 hours of removal from shrub (for pigment analysis, section 2.4.2), and the remaining leaves were dried for leaf N analysis (section 3.2.4.3).

3.2.3. Terrestrial LiDAR processing

At each shrub location, the four scans were co-registered and merged into the local polar (x, y, z) coordinate system, forming a single point cloud using the Cyclone software environment (Version 8.1, Leica Geosystems Inc., Heerbrugg, Switzerland). Following merging into the local coordinate system, the point cloud was then assigned global Cartesian coordinates (UTM, Northing and Easting) that were linked to GPS measurements taken from four geo-referenced targets scanned during each TLS acquisition. The 104 local x, y, z coordinates from sampling locations recorded during the last TLS scan at each shrub were also converted to global coordinates for use in the ray-tracing algorithm described in section 2.5.4. An example of sample locations merged into the single global coordinate point cloud is displayed in Fig. 3.1. Due to the abundance of airborne insects in this study location, each merged shrub point cloud was then manually cleaned to remove "mosquito hits" that would interfere with rays penetrating the canopy (as described in Greaves et al., 2015).
For the final two metrics used to estimate the light environment (path length and Q_{int}), the shrub canopy was divided in voxels with a 0.01 m edge-length (Fig. 3.2).

The 0.01 m voxel edge length is substantially smaller than top performing voxel sizes in other studies (e.g., Van der Zande et al., 2010, 2011; Beland et al., 2014; Cifuentes et al., 2014), but also differs from the aforementioned studies because of the small stature, leaf, and stem size of *S. pulchra*; with the exception of Bittner et al. (2012), who conducted a sensitivity analysis to evaluate a ray-tracing canopy light model using different voxel sizes for beech trees of a similar height to the shrubs used in this study. Bittner and colleagues found that the top performing voxel edge length was 0.031 m, ensuring that voxels where no vegetative component existed were not misrepresented, allowing for more accurate estimates of light transmittance. Similarly, we chose a small voxel size with a 0.01 m edge length for several reasons: 1) The point sampling density was 1 mm to capture the canopy with high resolution, but ultimately resulted in oversampling and the abundance of edge, or 'ghost' points (noise, Eitel et al., 2010), tailing from the canopy elements. This increased the number of points and changed the actual spatial distribution pattern of foliage elements; 2) 0.01 m is close to the characteristic size of the canopy elements, including stem diameters (similar to suggestions provided by Beland et al., 2014). For radiation regime mapping choosing a voxel size based on the characteristic size of canopy elements instead of the sampling space makes intuitive sense with respect to spaces between leaves and branches; 3) The effects of neighboring voxels on radiation environment could be incorporated with a bigger voxel size (i.e., the characteristic size); 4) Since the laser beam is 4 mm, this is the low limit at which the laser can readily resolve a voxel; 5) Lastly, and potentially most importantly, a sensitivity analysis showed that the computed digital gap fraction (DGF, computed as in Zheng et al., 2013 and described in section 3.2.5.4) remained stable beyond 0.01 m (Fig. 3.3). Voxel sizes below this threshold likely overestimated DGF to due to excessive inclusion of noisy canopy elements.

Figs. 2.1 and 2.2 are colored according to height, with no differentiation between non-photosynthetic and photosynthetic canopy components. Unlike some studies that have been able to separate woody from leaf material using the laser return intensity in the near infrared or short-wave infrared wavelengths (Douglas et al., 2012; Beland et al., 2014; Danson et al., 2014), we were not able to reliably separate photosynthetic and non-photosynthetic components based on green (532 nm) laser return intensity. This was primarily due to the small (1 - 10 cm^2) and thin leaves and stems (1-5 cm diameter) within the *S. pulchra* canopy,

which complicated manual visual separation, but also caused wide variability in the intensity return of the green laser, making it difficult to establish thresholds to separate photosynthetic from non-photosynthetic canopy components. Such separation is important for future developments of this work, but because of the low transmittance of energy in the PPFD spectrum (400 – 700 nm) through green leaves (often < 10 %), we determined the difference would be minor.

3.2.4. Physiological measurements

3.2.4.1. Gas exchange measurements

Leaf gas exchange measurements were conducted within a 12-15 hour period after harvest to avoid leaf wilting. In the lab, four prepped and calibrated gas exchange analyzers (IRGA LI-6400XT Portable Photosynthesis System, LI-COR) were used to obtain CO_2 fluxes of photosynthesis and respiration for leaves on each of the branch tips. Leaf selection was determined based on the size (closest to the cuvette size of 6 cm^2) and flatness of the leaf. The gas-exchange method from Heskel et al. (2013) was used to obtain light curves for each sample. Following light-response curve measurements, one-sided leaf area was measured using a leaf area meter (LI-3100, LI-COR Inc., Lincoln, NE, USA). During processing of the gas exchange data, leaf area was corrected for if the leaf did not fill the 6cm^2 cuvette, as rate calculations are based on the leaf area. Maximum light saturated net photosynthetic rate (A_{max}) was estimated by fitting the data to a rectangular hyperbolic function (Excel Solver, Microsoft, Redmond, WA, USA) (Heskel et al., 2013).

3.2.4.2 Pigment analysis

Following gas exchange and leaf area measurements, circular leaf disks were removed from leaf samples using three different size cork borers (0.15, 0.23, 0.24 cm^2) depending on leaf size and to avoid veins. Leaf punches were placed in an aluminum foil envelope and immediately brought to a -80ºC freezer, where they remained until high-performance liquid chromatography (HPLC) analysis (Gilmore & Yamamoto, 1991). Pigments were extracted according to Adams & Demmig-Adams (1992) with one modification: disks were ground using a ball mill (8000D, Specs Cetriprep, Metuchen, NJ, USA) (Magney et al., 2014). The HPLC analysis was done using an Agilent 1100 series HPLC (Agilent Technologies, Palo Alto, CA, USA) with a YMC Carotenoid^{TM} C-30 reverse phase column (YMC Co., Ltd, Kyoto, Japan) at 35º C. Solvent concentrations and gradients according to Magney et al., 2014

were used. Total Chl *a* and *b* (µmol m^{-2}) was quantified using the HPLC peak area (mAU * sec) and the size of the leaf tissue sample, and Chl *b* was divided by Chl *a* to compute the Chl a:b ratio (Logan et al., 1996).

3.2.4.3. Leaf N

Following foliar gas exchange and leaf area measurements, leaves were dried in a drying oven at 50º C for at least 48 hours. After leaf drydown, the leaves were weighed and put into small sample tubes with metal beads to be pulverized using a grinder (Mini Bead Beater, Biospec). This pulverized leaf material was sent to the lab where %N was determined using automated dry combustion on a per mass basis (TruSpec CN, Leco Corporation, St. Joseph, MI).

3.2.5. Quantifying the light regime

3.2.5.1. Leaf Area Index

LAI is a dimensionless measure used to describe the one-sided green leaf area (m^2) per unit ground surface (m^2) in plant canopies. LAI-2000 (LI-COR Inc., Lincoln, NE, USA), which has a 148º FOV fisheye lens, was used to measure relative light transmittance at each leaf sample location within each shrub (for instrument details and assumptions see Jonckheere et al., 2004 & Garrigues et al., 2008). LAI-2000 is an indirect optical method that is commonly used to investigate light transmission through canopies (Jonckheere et al., 2004), and applies the Beer-Lambert law by integrating information at each canopy layer of incident irradiance and canopy structure (Monsi and Saeki, 1953). According to the LAI-2000 manual, one above canopy and four within canopy measurements were taken directly above each sampling location to avoid direct leaf shading. LAI measurements were taken under diffuse illumination for optimal performance (Hyer and Goetz, 2004; Jonckheere et al., 2004). A 270º view cap was placed on top of the lens to eliminate azimuth angles that would be effected by the operator or background (LAI-2000 protocol, Garrigues et al., 2008).

3.2.5.2. Vertical Canopy Depth

Vertical canopy depth has been traditionally used to investigate light gradients in tree canopies at lower latitudes (e.g., Ellsworth & Reich, 1993); but was used here for comparison and to determine if vertical partitioning exists in small shrubs exposed to near continuous, low-solar angles. For more precise determination of vertical depth, the z (elevation) from each sampling location was used and subtracted from the maximum shrub z value in each point

cloud. Canopy depths ranged from 0 cm (top of canopy) to -0.65 cm (near the middle-bottom of the canopy).

3.2.5.3. Terrestrial LiDAR derived path length

Due to the near continuous low-angle sunlight, path length was computed to provide a more accurate 3-D representation of sample location relative to the diurnal course of the sun, whereby a longer path length indicates a sample voxel location deeper in the canopy. A physically based ray tracing (RT) algorithm using the global Cartesian coordinates of shrub voxels was used to model the canopy light environment based on sun angle (θ) and time of day. Similar to Bittner et al., 2012, the RT algorithm simulated the daily course of the sun by using line segments (R_i, in m) with a starting point at outer-edge of the canopy (S_i, in m) and an ending point (E_i, in m) at the sampling location. Over the course of the day, R_i interacted with all voxels between the outer-edge of the canopy (S_i, according to solar zenith angle (θ), and time of day) and the sampling location, E_i, allowing for the angular distance (path length, (*d)* m) between S_i and E_i. to be computed according to equation 1 over the course of the day.

$$Path\ length\ (d) = \sum_{i=1}^{n} (Si - Ei)\ \theta^{-1}\ s^{-1} \quad \text{(Eq. 1)}$$

While the relative light environment according to 3D location within the shrub can be estimated with the path length, it does not count for the varying intensity of irradiance at the top of the canopy (I_o) over the course of the day (section 3.2.5.4).

3.2.5.4 Terrestrial LiDAR derived ray-tracing model

The basic premise underlying the RT model used here was to apply Beer-Lambert's law (Eq. 2) to describe the attenuation of light through each voxel throughout the canopy (Monsi and Seiki, 1953).

$$PPFD\ (voxel) = I_{\circ} * e^{-k*LAIe} \quad \text{(Eq. 2)}$$

In Eq. 2, PPFD (voxel) is the instantaneous irradiance (μmol m^{-2} s^{-1}) at each voxel sample location, which accounts for the top of canopy irradiance, I_o, an extinction coefficient (k), and the effective LAI (LAI_e, m^2 m^{-2}). LAI_e can be defined as the product of LAI (woody and leaf material) and a clumping index (Nilson, 1971, Ryu et al., 2010), which is derived from a computed digital gap fraction (DGF; likelihood for solar beam with fixed direction to penetrate through plant canopy). I_o was recorded at 15 minute intervals throughout the day using a quantum sensor measuring light intensity (μmol m^{-2} s^{-1}) in the 400-700 nm range at the field site during a cloud-free day during the sampling period (LI-191, LI-COR, Lincoln,

Nebraska, USA). To obtain an instantaneous PPFD value for every second during a cloud-free day, I_o was smoothed using a locally weighted non-parametric regression with a smoothing parameter (α) of 0.5 (Cleveland, 1979; Cleveland & Devlin, 1979). Due to the complexity of incorporating diffuse light into the RT model, and this particular studies interest in quantifying the range in relative light environment to investigate patterns of photosynthetic partitioning, only $I_{o,}$ data from one cloud-free day during the sampling period was used. The relatively simplistic nature of this RT model was not able to account for diffuse light or internal canopy scattering, thereby consistently overestimating light incident upon leaves in the upper canopy and underestimating light availability at increasing canopy depths.
With these assumptions, we were able to compute PPFD throughout the day during peak growing season for each sampling location based on LAI_e. The theoretical foundation behind the derivation of LAI_e stems from the development and thorough testing of the digital hemispherical photography (DHF) method to compute LAI (Chen & Black., 1991). Computation of LAI_e requires an estimation of the DGF and the extinction coefficient (*k)* for each solar zenith angle (*θ)* throughout the day according to Zheng et al., 2013 in equation 3.

$$LAI_e\ (\theta) = -\ln DGF(\theta) / k\ (\cos(\theta), \alpha) \quad \text{(Eq. 3)}$$

In eq. 3, DGF and *k* varied for each voxel in the point cloud depending on the time of the day ((*θ)* s^{-1}). DGF and *k* ranged from 0 to 1 depending on the angular specific interaction (*α*) of R_i with foliage elements, with lower *k* values representing voxels with fewer points and stem or leaf angles more parallel to the incident R_i, allowing for more light attenuation through the voxel. A lower DGF was representative of a lower probability that light will reach a given voxel. Details on the computation of DGF, *k*, and *α* from terrestrial LiDAR data can be found in Zheng et al., 2013, who reported a strong correlation between TLS derived LAI_e and DHP, but will be described briefly below.

In summary, for the incident light beams with a fixed θ, *k* for each voxel was obtained by finding the orientation distribution of the "effective foliage elements". Although only a partial surface was sampled due to occlusion resulting from some scan angles, the sampled points represent the effective foliage elements in terms of the penetration of incident rays (R_i) in a specific angular direction. The characterization of the specific foliage element distribution was done using an ellipsoidal model described by Campbell (1986) and following the method developed by Zheng and Moskal (2012). This was done by computing the normal vectors for

every point within the shrub point clouds, whereby the tangential plane was reconstructed based on the six nearest neighbor points around the centroid point and unit vector, and a covariance matrix of the support region (Hoppe et al, 1992; Pierre-Alliez & Guennenbaud, 2010).

To compute DGF, a simulation of incident direct solar beams at all times throughout the day was done using the azimuthal and inclination angles for different solar positions based on the global Cartesian coordinate system during local time according to the "Solar Position Calculator" (http://esrl.noaa.gov/gmd/grad/solcalc/azel.html). By assuming direct solar beams come from the nadir direction, the point cloud data was rotated to each azimuthal and inclination angle throughout the day with an unchanged relative position between solar beams and point cloud data. The point cloud was sliced vertically in the direction of each solar beam upon each rotation throughout the day. The point cloud slicing algorithm used a line quadrat analysis to analyze the number of points in each voxel, rendering a voxel as empty, or composed of canopy elements (non-empty) (Zheng & Moskal 2012). For each slice plane (layer of voxels) within the canopy, the ratio of number of empty voxels over the total number of voxels in the specific slice plane was used to represent the DGF for each vertical plane within the canopy. After computing the DGF for each slice plane and the incident parallel solar beams at each fixed direction, DGF values were summed from the top of the canopy to the sample voxel similarly to eq. 1, according to eq. 4:

$$Accumulated\ DGF = \sum_{i=1}^{n}(DGF(Si) - DGF(Ei))\ \theta^{-1}\ s^{-1} \quad \text{(Eq. 4)}$$

From this, *k* and accumulated DGF allowed for the derivation of LAI_e at each sample voxel according to eq. 3, allowing for the computation of an instantaneous PPFD (eq. 2) value throughout the entire day. Q_{int} was then computed according to equation 5, whereby the integral of instantaneous light (μmol m^{-2} s^{-1}) was summed over an entire day of simulated radiation (mol m^{-2} day $^{-1}$).

$$Qint = \int_{i=0}^{n} PPFD\ \theta^{-1}\ s^{-1} \quad \text{(Eq. 5)}$$

In summary, by ascribing a *k* value associated with an ellipsoidal leaf inclination angle and the direction of incoming solar radiation (Campbell, 1990; Zheng et al., 2013) and a DGF associated with the likelihood for solar beams with fixed direction to penetrate to a given voxel, we were able to compute LAI_e as in input for Beer-Lamberts law (Eq. 2), and compute an integrated Q_{int} over the course of a direct sun day to capture the variability in relative light

environment within the small shrub canopy (Eq. 5). Limitations to this method are discussed in detail in Zheng et al., 2013; and will be elaborated on in section 3.4.

3.2.6. Statistical analysis

To compare the relative differences in light measurements acquired from the LAI-2000, vertical canopy depth, path length, and Q_{int} a histogram of data distribution was used for visual inspection and an exponential best fit curve was fitted between Q_{int} and the remaining three light quantification techniques. To explore how leaf measurements within a *S. pulchra* canopy respond to light availability, two different methods were used to compare the response of photosynthetic parameters, the first are represented by boxplots and the second by linear regression. Boxplots were binned into four categories using the Freedman-Diaconis rule, which defines bin size as $2*\text{IQR}(x)* n^{-1/3}$, where IQR ($x$) represents the interquartile range and n represents the sample size (Freedman & Diaconis, 1981). Sample size varied for measurements of %N, $Chl_{a:b}$, and A_{max}, as a result of instrumentation errors resulting in erroneous values encountered during analysis, but did not alter the chosen bin size according the Freedman-Diaconis rule. Notched boxplots were chosen for visual examination of significant differences ($p < 0.05$) between binned samples, and represent the 95% confidence interval of the mean. To further examine trends in photosynthetic partitioning according to light availability, linear least squares lines were fit to the data and were assigned a correlation coefficient, Pearson's r. In this final step of analysis, Q_{int} and LAI data were log-transformed to account for non-normal exponential distributions.

3.3. Results

3.3.1. Diurnal radiation regime at sampling locations

Fig. 3.4a demonstrates the diurnal radiation regime for all 104 sample locations from all scanned shrubs. Fig. 3.4b-d show a un-voxelized point cloud with 5 example locations that are highlighted by the radiation curves in Fig. 3.4a. A hypothetical rendition of the sun's course at specific of day is provided in 4b. By linking the location of sample 1 on the shrub with the accompanying cyan diurnal radiation (*I (d)*) curve, one notices that this upper canopy location is exposed to near complete radiation, symmetrical with incident PPFD (I_o); whereas, location 4, on the west end of the shrub, was exposed to little light until later in the day,

following the blue *I(d)* curve reaching a maximum of 375 μmol m^{-2} s^{-1} at around 19:00, for example.

3.3.2. Comparisons of light environment estimates

Fig. 3.5 shows histograms of the count distributions of data from each of the four light environment metrics. All x-axes are oriented with more hypothetical light on the left side of the axis. A left exponential distribution was observed in the LAI data (Fig. 3.5a), with nearly 50% of the data measuring LAI values falling below 0.5 m^2 m^{-2}. An opposite observation – exponential right skewed distribution - was observed in the Q_{int} estimates, with more than 50% of the data suggesting sample voxels were exposed to < 5.0 mol m^{-2} day^{-1} of light (Fig. 3.5d). Both measurements related to the relative location within the shrub – not light environment explicitly – were found to have near-normal distributions, with a slight left skew for canopy depth data (Fig. 3.5b) and path length (Fig. 3.5c).

A negative exponential function describes the relationship observed between all response variables and Q_{int} (Fig. 3.6), following the expected response of light attenuation through the canopy according to Beer-Lamberts law in Eqs. 2 & 3. The relationships between Q_{int}, LAI, and vertical canopy depth are not statistically significant ($p > 0.05$), with low coefficients of determination (Q_{int} vs. LAI $r^2 = 0.10$, root mean squared error (RMSE) = 12.20 mol m^{-2} day^{-1}; and Q_{int} vs. canopy depth $r^2 = 0.07$, RMSE = 12.91 mol m^{-2} day^{-1}); while a statistically significant relationship between Q_{int} vs. and path length was observed ($r^2 = 0.28$, RMSE = 11.69 mol m^{-2} day^{-1}).

3.3.3. Boxplots of relationships between light environment and photosynthetic parameters

Fig. 3.7 shows the binned relationships between leaf %N and light environment: LAI (Fig. 3.7a), canopy depth (Fig. 3.7b), path length (Fig. 3.7c), and Q_{int} (Fig. 3.7d). A general trend towards lower leaf %N values is observed in increasingly light limited shrub locations across all light quantification techniques. Binned light regimes are characterized from 1-4, where 1 is the highest light (left side of each plot) and 4 is the lowest light regime (right side of each plot). Statistically significant differences among bins exists for leaf %N and LAI between the 2nd and 3rd light regime (Fig. 3.7a), the 1st and 4th light regime for path length (Fig 3.7c) and between the 1st and both the 3rd and 4th light regime for Q_{int} (Fig. 3.7d). These trends will be discussed in more detail in section 3.3.4.

Fig. 3.8 shows the binned trends between $Chl_{a:b}$ and light variables. A general increasing trend in the means of $Chl_{a:b}$ and LAI, with no significant differences between binned light regimes is observed in Fig. 3.8a. Fig. 3.8b shows no trend between binned canopy depth and *Chl* a:b ratio, while significant differences are observed among binned light regime 4 and regimes 1, 2, and 3 (Fig. 3.8c). The general trend towards decreasing $Chl_{a:b}$ ratio with decreasing light availability is only seen when using path length and Q_{int} as light quantifiers, with significant differences between Q_{int} light regimes 1 and 3 and $Chl_{a:b}$. These trends will be discussed in more detail in section 3.3.4.

The last set of boxplots in Fig. 3.9 only shows a substantial decrease in A_{max} with decreases in $Q_{int,}$ where significant differences exist between light regime 1, and regimes 3 and 4; and between light regime 2, and regimes 3 and 4 (Fig. 3.9d). Significant differences also exist between A_{max} and LAI light regime 4 and regimes 1 and 2. No significant differences are seen among canopy depth and path length light regimes and A_{max}. These trends will be discussed in more detail in section 3.3.4.

3.3.4. Linear trends between light environment and photosynthetic parameters

Fig. 3.10 shows the linear relationships with statistical significance between all light variables and photosynthetic parameters. A negative slope implies photosynthetic partitioning according to light availability, and was only significantly different from zero for the relationship between log transformed LAI and Leaf %N (Leaf % N vs. LAI $r = 0.21$, $p < 0.05$, Fig. 3.10a); $Chl_{a:b}$ vs. log transformed LAI $r = 0.01$, Fig. 3.10e); A_{max} vs. log transformed LAI $r = 0.04$, Fig. 3.10i). Similarly, one significant trend was observed between photosynthetic parameters and canopy depth – leaf %N and canopy depth ($r = 0.26$, $p < 0.05$, Fig. 3.10b), whereas no significant trends were observed between $Chl_{a:b}$ and canopy depth ($r = 0.18$, Fig. 3.10f), or A_{max} and canopy depth ($r = 0.11$, Fig. 3.10j). A statistically significantly different from zero slope was observed between %N and path length ($r = 0.27$, $p < 0.05$, Fig. 3.10c), and between $Chl_{a:b}$ and path length ($r = 0.49$, $p < 0.01$, Fig. 3.10g), but no significant trend was seen between path length and A_{max} ($r = 0.15$, Fig. 3.10k). Strong, significant trends were observed between log transformed Q_{int} and leaf %N ($r = 0.31$, $p < 0.01$, Fig. 3.10d), between $Chl_{a:b}$ and log transformed Q_{int} ($r = 0.46$, $p < 0.01$, Fig. 3.10h), and between log transformed Q_{int} and A_{max} ($r = 0.49$, $p < 0.01$ Fig. 3.10l).

3.4. Discussion

Results from this study suggest that depending on the method used in quantifying the relative light environment within small shrubs, different conclusions regarding photosynthetic partitioning within a *S. pulchra* canopy can be drawn. If a researcher were to use a more traditional method – such as LAI-2000 or vertical depth measurements – they would conclude that there is a weak, slightly significant negative trend towards decreasing %N as light availability decreases, and no statistically significant response of $Chl_{a:b}$ or A_{max} to light availability. However, due to the small, sparse, nature of the *S. pulchra* canopy and the near continuous low-angle sunlight during the arctic growing season, one might want to explore techniques that relate physiological measurements to the actual 3D environment within the shrub (path length), or a simulated Q_{int}. Using this approach, both path length and Q_{int} revealed statistically significant negative trends in leaf %N and $Chl_{a:b}$, from which one would also expect similar trends in A_{max}. However, path length did not reveal patterns of A_{max} partitioning according to light availability, whereas the strongest and most convincing A_{max} trend was exhibited when the radiation regime was quantified using Q_{int}. While several studies have shown the capability of voxel ray tracing to simulate the light distribution throughout a canopy (e.g., Van der Zande et al., 2010, 2011; Bittner et al., 2012), this study is among the first to link TLS derived canopy radiation environment to physiological measurements in the field.

3.4.1. Comparisons between different light environments

A comparison of LAI, vertical canopy depth, and path length with our estimate of Q_{int} suggests that there is substantial variability in light environment quantification techniques. A major limitation to measuring LAI within a *S. pulchra* canopy using an LAI-2000 could be due to the unrepresentative temporal sampling regime, the bias towards high solar zenith angles, and the inability to capture potentially subtle canopy spatial heterogeneity (Weiss et al., 2004). A sensitivity analysis by Garrigues et al. (2008) found that substantial variability exists in LAI-2000 measurements under varying illumination conditions, especially compared to digital hemispherical photography which captures illumination from a wider range of solar zenith angles. While we sought to control for light conditions by sampling LAI under diffuse light, it was difficult to account for inconsistent light intensities throughout the day. While LAI measurements using an LAI-2000 are fast and easily repeatable, the primary success of

this technique has been attributed in larger forested canopies (Breda et al., 2003). LAI-2000 measurements also make the assumption that foliage is an optical black body (absorbing all radiation), having the same leaf geometrical convex projection, and random foliage element distribution throughout the canopy (Jonckheere et al., 2004). In the case of *S. pulchra*, there is substantial variability in leaf size, leaf angular projection, and leaf clumping, making the canopy highly heterogeneous. The heterogeneous nature of *S. pulchra* canopies is thus likely underestimated using LAI-2000 measurements, which was observed here with the abundance of LAI values < 0.5 (Fig. 3.5a, similar to observations by Chason et al., 1992; Dufrene Breda, 1995). Nonetheless, we attempted to account for the impact of external factors such as illumination conditions and background effects (i.e. instrument user, clumping) by taking LAI-2000 measurements using a 270º view cap (Nackaerts and Coppin, 2000).

A negative exponential relationship was also observed between Q_{int} and vertical canopy depth (Fig. 3.6b), albeit with sufficient scatter and a low coefficient of determination. This highlights the expected observation that the low solar zenith angles abundant at high latitudes permit non-vertical distribution of light throughout the canopy. For example, 13 of the sample locations between achieving the top 20% of Q_{int} are at vertical canopy depths between -0.1 and -0.6 m. Some of these points are spatially similar to points 2 & 4 in Fig. 3.2, which are located on the exterior of the shrub, receiving near full sunlight early or late in the day at low solar zenith angles. Also worth noting are the several points at the top of the canopy (near 0) with low reported Q_{int} values ranging from 7 to 20 mol m^{-2} day^{-1}. An explanation for this could be that the shrubs used in this study had relatively flat canopy tops, and that most leaves are located in the upper canopy. These particular leaves could have been located in the center of the canopy, shaded by clumps of leaves during the majority of low light angles experienced throughout the day. The continuous 'shading' by a few voxels may cause underestimation of light by using Beer-Lamberts law under direct sunlight, which leads to an exponential decrease in light through the canopy upon penetrating only a few voxels. Thus if a top-of-canopy leaf was surrounded by two or three voxels on every side, light transmission would decrease on orders of magnitude one to two times that of PPFD at exterior canopy voxels. Due to the lack of vertical photosynthetic partitioning or light distribution in the *S. pulchra* canopy, using a path length term might be more representative of spatial light distribution at a given voxel in 3D.

By not ascribing a DGF, *k*, or LAI_e, to the sample voxels, a path length, representative of the voxels relative 3D location within the shrub was investigated. Due to the normal distribution of data using this method (Fig., 3.5c), it could theoretically be better at capturing the wide range of light availability than the simulated Q_{int} - which shows rapid attenuation of light at voxel locations in the middle or outer-middle part of the shrub (Fig. 3.6c) - particularly under diffuse radiation conditions. The strongest, and only statistically significant negative exponential trend, was observed between path length and Q_{int}; however, there is still substantial scatter in the relationship. This scatter supports the theory that as light penetrates the canopy and interacts with different foliage distributions (affecting *k*) and clumps of canopy elements (affecting DGF) an exponential, yet somewhat unpredictable drop in Q_{int} is observed. This is coincident with suggestions made by Beland et al. (2014) regarding the importance of accounting for leaf clumping from voxelized TLS data, noting that smaller voxel sizes may better eliminate the assumption of random foliage distribution – though data supporting this hypothesis do not exist for this study.

Indeed a more rigorous evaluation and sensitivity analysis of the effectiveness of the RT + TLS model used here would provide us with greater confidence in the model. However, inputs to the model have been validated with ground measurements (Zheng & Moskal, 2012; Zheng et al., 2013; Zheng et al., *in review*), and nonetheless results from this study suggest that wide variability does exist among the four techniques used to quantify relative light regime. As such, caution should be taken when comparing within canopy physiological measurements with light environment measurements in similar canopies. While great strides have been made to improve the quantification of vegetation parameters using TLS data – e.g., biomass (Olsoy et al., 2014; Calders et al., 2014; Eitel et al., 2014a; Greaves et al., 2015) leaf area distribution (Beland et al., 2011; 2014), and leaf area index (Zheng et al., 2012; 2013; Pueschell et al., 2014), there are still several pervading issues associated with the interpretation of high resolution point cloud data on vegetation parameters. These include, but are not limited to, the effect of a species-specific voxel size on determining DGF, occlusion and noise inherent in TLS data, TLS sampling setup, size of canopy elements, the complexity associated with canopy heterogeneity, and the separation of leaf tissue from non-photosynthetic canopy elements.

Firstly, the voxel size was determined based on the sensitivity analysis highlighted in Fig. 3.2, where the average digital gap fraction achieved at each voxel location within the four shrubs reached an asymptote at voxel-edge sizes > 0.01 m. Due to the high sampling density achieved here, we were able to retain a high point density within each voxel, allowing for the computation of DGF and *k* within each voxel. This is coincident with findings by Cifuentes et al., 2014 who reported that smaller voxel sizes in a high density point cloud enhanced the representation of foliage elements within the canopy. Following the diamond sampling design to minimize shadowing (Van der Zande et al., 2008), we were able to increase the amount of data within the small canopy to theoretically account for the short zenith range of the close proximity scan positions (Seidel et al., 2012). However, the high spatial resolution of this point cloud increased the chances of oversampling, potentially leading to the abundance of low Q_{int} estimates (Fig. 3.5d).

Vaccari et al. (2013) attempted to correct for erroneous 'ghost' points and edge hits by examining the canopy perimeter for a bias correction in DGF. In this study, wind, small GPS errors, mosquitos, and the movement of canopy elements among TLS scans undoubtedly produced an excess of 'ghost points' within the point cloud. While some of this noise was removed manually, noise removal using this technique in the inner canopy was limited. This could be another explanation for the rapid light attenuation upon entering the shrub canopy, and abundance of low Q_{int} values at voxel locations. Future studies on small stature vegetation might consider limiting sampling density from each scan angle to account for issues related to oversampling; which is contrary to findings by Van der Zande et al., 2011, who observed an overestimation of TLS+RT derived light penetration, caused by errors in LAD estimation. Rather, our assumed underestimation of Q_{int} was likely due to the high sampling density, abundance of 'ghost points' due to the small leaves and stems of *S. pulchra*, registration errors, and changes in environmental conditions. The quality of the model could be further increased by the separation of woody and vegetative components using the intensity return from a single (Moorthy et al., 2008; Beland et al., 2014) or dual wavelength scanner (Douglas et al., 2012; Gaulton et al.,. 2013; Danson et al., 2014; Eitel et al., 2014b), allowing for a small fraction of transmission through leaves to be accounted for.

One of the primary limitations of this work is the lack of ground validation of radiation environment derived from Q_{int}. While the deployment of quantum sensors that

integrate light throughout the day (as in Bittner et al., 2012) may have been one technique to validate the RT model, it was beyond the scope of this research to robustly validate the model. Rather, it was our goal to use previously published techniques for extracting LAI_e to incorporate into the Beer-Lambert equation to potentially elucidate evidence for photosynthetic partitioning in *S. pulchra*. The use of the RT + TLS model did indeed show greater evidence of photosynthetic partitioning across all three parameters.

3.4.2. Evidence for photosynthetic partitioning in S. alaxensis

Our results suggest that patterns of photosynthetic partitioning within the *S. pulchra* canopy are more noticeable when the 3-D canopy light environment is considered. With an understanding of the limitations discussed above that are inherent in the RT + TLS model used here, modeling results suggest photosynthetic partitioning as has been shown for other vegetation canopies where the light environment is easier to quantify due to less extreme sun angles and denser canopies that make differences in light levels less subtle. This finding is particularly relevant considering the unpublished studies showing negligible evidence for photosynthetic partitioning using %N, A_{max}, and maximum electron transport rate (*J*) in arctic shrubs (Heskel et al., 2012; Formica et al., 2013). Further, this finding challenges the assumption made in current tundra carbon exchange models, whereby LAI, PPFD, and air temperature explain ~80% of the variance in net ecosystem exchange (NEE, Shaver et al., 2007). LAI in the previous study was measured using an exponential model describing the relationship between LAI and NDVI by combining data from van Wijk & Williams 2005, and Williams et al., 2006. The majority of LAI values measured in these two studies are below 1 $m^2\ m^{-2}$, with less than 5% of the measured species having an LAI between 1.5 and 2.0 $m^2\ m^{-2}$. Indeed a strong relationship was observed between total foliar N and LAI in these studies, but as a result of current and ongoing increases in shrub size, abundance, and complexity in the arctic (Thompson et al., 2004; Myers-Smith et al., 2011), we hypothesize that a more dramatic range in light reaching canopy layers will change in the near future.

According to the theory of canopy optimization, increasingly taller individuals will allocate photosynthetically relevant nutrients in a more efficient manner to maximize whole plant carbon gain (Field 1983; Hirose and Werger, 1987). Our results provide some of the first evidence that big leaf models which currently work well in canopies with low LAI and limited self-shading may need to account for small levels of photosynthetic partitioning

within the canopy. While it was not our intention to provide a predictive model describing the relationship between photosynthetic resources and Q_{int}, future work across more species and a wider range of shrub sizes in conjunction with whole plant photosynthesis measurements should be investigated and accounted for in NEE models specific to the arctic ecosystem. This could be exemplified similarly to the arctic soil-plant-atmosphere (SPA) model developed by Williams et al. (2001), which assumes light attenuation throughout shrub canopies according to Beer-Lamberts law. The SPA model, however, attributes a decline in photosynthetic rates vertically throughout the canopy, contradicting results from this study – using shrubs with sizes on the high end of the arctic spectrum – whereby no significant changes in photosynthetic partitioning exists on a vertical profile within the canopy.

The recognizable complexity of relating TLS + RT derived Q_{int} makes the derivation of empirical relationships between light availability and photosynthetic partitioning difficult. As TLS + RT models continue to improve, however, the incorporation of diffuse light could play an important component in the arctic – where it has recently been shown that arctic photosynthetic efficiency is actually enhanced under diffuse light (Williams et al., 2014). This consideration, in addition to accounting for the measurement limitations mentioned earlier could provide a more comprehensive understanding of photosynthetic partitioning in the arctic tundra. Further, the empirical relationships observed between the TLS return intensity and leaf biochemical constituents – chlorophyll (Eitel et al., 2010), nitrogen (Eitel et al., 2011, 2014a, b), water content (Galton et al., 2013) and photoprotective mechanisms (Magney et al., 2014) – could enable the concurrent examination of canopy structure and function in 3D using a single TLS acquisition (see Eitel et al., 2014b and Magney et al. 2014 for further discussion). In order for the 3D mapping of photosynthesis and subsequent understanding of photosynthetic partitioning in 3D using only remotely sensed measurements to become a reality, it is important that TLS + RT models are first related to widely accepted and validated destructive measurements related to photosynthesis such as %N, $Chl_{a:b}$, and A_{max}.

3.5. Conclusion

This study examined four different techniques for estimating light availability at locations where leaf-level measurements related to photosynthesis were made within the small canopy of the arctic shrub, *S. pulchra*. We found that traditional techniques – LAI and vertical

canopy depth – provide limited evidence of photosynthetic partitioning within the shrub canopy. Rather, when the 3D environment derived from TLS was considered (path length) and a RT model was used to describe the light environment, evidence of photosynthetic partitioning according to light availability was observed. This is primarily due to the fact that the low solar zenith angles incident upon arctic vegetation provide a unique light environment which different foliage elements are exposed to throughout the day. By ascribing a Q_{int} value to individual voxels where samples were taken, we discovered – for the first time – evidence of photosynthetic partitioning in small arctic shrubs. This finding suggests that as shrubs in the arctic become increasingly complex due to observed warming from climate change, photosynthetic partitioning to maximize whole plant carbon gain could facilitate further expansion of shrubs in this ecosystem. The observed trends here are not yet strong enough to calibrate arctic ecosystem-level carbon cycling models, but provide a platform for similar investigations to build upon further.

References:

Anderson, M.C. (1964). Studies of the woodland light climate: I. The photographic computation of light conditions. *Journal of Ecology*, 27–41.

Baldocchi, D.D., Harley, P.C. (1995), Scaling carbon dioxide and water vapour exchange from leaf to canopy in a deciduous forest. II. Model testing and application. *Plant, Cell & Environment, 18,* 1157–1173

Baldocchi, D.D.,Wilson, K.B., Gu, L. (2002). How the environment, canopy structure and canopy physiological functioning influence carbon, water and energy fluxes of a temperate broad-leaved deciduous forest – an assessment with the biophysical model CANOAK. *Tree Physiology, 22,* 1065–1077.

Béland, M., Widlowski, J.-L., Fournier, R. a., Côté, J.-F., & Verstraete, M. M. (2011). Estimating leaf area distribution in savanna trees from terrestrial LiDAR measurements. *Agricultural and Forest Meteorology*, *151*(9), 1252–1266. doi:10.1016/j.agrformet.2011.05.004

Béland, M., Baldocchi, D. D., Widlowski, J.-L., Fournier, R. a., & Verstraete, M. M. (2014). On seeing the wood from the leaves and the role of voxel size in determining leaf area distribution of forests with terrestrial LiDAR. *Agricultural and Forest Meteorology*, *184*.

Bittner, S., Gayler, S., Biernath, C., Winkler, J. B., Seifert, S., Pretzsch, H., & Priesack, E. (2012). Evaluation of a ray-tracing canopy light model based on terrestrial laser scans. *Canadian Journal of Remote Sensing*, *38*(5), 619–628. doi:10.5589/m12-050

Boardman, N.K. (1977). Comparative photosynthesis of sun and shade plants. *Annual Review of Plant Physiology,* 355-377

Bolstad, P.V., Gower, S.T. (1990). Estimation of leaf area index in fourteen southern Wisconsin forest stands using a portable radiometer. *Tree Physiology, 7,* 115–124.

Bréda, N. J. J. (2003). Ground-based measurements of leaf area index: a review of methods, instruments and current controversies. *Journal of Experimental Botany*, *54*(392), 2403–17. doi:10.1093/jxb/erg263

Brunner, A. (1998). A light model for spatially explicit forest stand models. *Forest Ecology and Management, 107*, 19-46. doi: 10.1016/ S0378-1127(97)00325-3.

Calders, K., Newnham, G., Burt, A., Murphy, S., Raumonen, P., Herold, M., … Kaasalainen, M. (2015). Nondestructive estimates of above-ground biomass using terrestrial laser scanning. *Methods in Ecology and Evolution*, *6*, 198–208. doi:10.1111/2041-210X.12301.

Campbell, G.S. (1986). Extinction coefficients for radiation in plant canopies calculated using an ellipsoidal inclination angle distribution. *Agricultural and Forest Meteorology, 36,* 317–321.

Campbell, G.S. (1990). Derivation of an angle density-fucntion for canopies with ellipsoidal leaf angle distributions. *Agricultural and Forest Meteorology,* 49, 173-176.

Chason, I.W., Baldocchi, D.D., Huston, M.A. (1991). A comparison of direct and indirect methods for estimating forest canopy leaf area. *Agricultural and Forest Meteorology,* 57, 107–128.

Cifuentes, R., Van der Zande, D., Farifteh, J., Salas, C., & Coppin, P. (2014). Effects of voxel size and sampling setup on the estimation of forest canopy gap fraction from terrestrial laser scanning data. *Agricultural and Forest Meteorology*, *194*, 230–240. doi:10.1016/j.agrformet.2014.04.013

Cleveland, W.S., (1979). Robust locally weighted regression and smoothing scatter- plots. *Journal of the American Statistical Association*, *74*, 829–836.

Cleveland, W.S., Devlin, S.J., (1988). Locally weighted regression – an approach to regression analysis by local fitting. *Journal of the American Statistical Association, 86,* 83, 596–610.

Cohen, S., Fuchs, M. (1987). The distribution of leaf area, radiation, photosynthesis and transpiration in a Shamouti orange hedgerow orchard. Part I. Leaf area and radiation. *Agricultural and Forest Meteorology, 40,* pp. 123-144. doi: 10.1016/0168-1923(87)90002-5.

Dale, M. P., & Causton, D. R. (1992). Use of the chlorophyll a / b ratio as a bioassay for the light environment of a plant. *Functional Ecology*, *6*(2), 190–196.

Danson, F. M., Gaulton, R., Armitage, R. P., Disney, M., Gunawan, O., Lewis, P., … Ramirez, A. F. (2014). Developing a dual-wavelength full-waveform terrestrial laser scanner to characterize forest canopy structure. *Agricultural and Forest Meteorology*, *198-199*, 7–14. doi:10.1016/j.agrformet.2014.07.007

Douglas, E.S., Strahler, A., Martel, J., Cook, T., Mendillo, C., Marshall, R., Chakrabarti, S., Schaaf, C., Woodcock, C., Zhan, L., Xiaoyuan, Y., Culvenor, D., Jupp, D., Newnham, G., Lovell, J., (2012). DWEL: a dual-wavelength echidna LiDAR for ground-based forest scanning. IEEE International Geoscience and Remote Sensing Symposium (IGARSS), pp. 4998–5001.

Dufrêne, E., Bréda, N. (1995). Estimation of deciduous forest leaf area index using direct and indirect methods. *Oecologia, 104*, 156–162.

Eitel, J. U. H., Vierling, L.A.., & Long, D. S. (2010). Simultaneous measurements of plant structure and chlorophyll content in broadleaf saplings with a terrestrial laser scanner. *Remote Sensing of Environment*, *114*(10), 2229–2237. doi:10.1016/j.rse.2010.04.025

Eitel, J.U.H., Vierling, L.A., Magney, T.S., (2013). A lightweight, low cost autonomously operating terrestrial laser scanner for quantifying and monitoring ecosystem structural dynamics. *Agricultural and Forest Meteorology*, *180*, 86–96.

Eitel, J. U. H., Magney, T. S., Vierling, L. A., Brown, T. T., & Huggins, D. R. (2014a). LiDAR based biomass and crop nitrogen estimates for rapid , non-destructive assessment of wheat nitrogen status. *Field Crops Research*, *159*, 21–32.

Eitel, J. U. H., Magney, T. S., Vierling, L. a., & Dittmar, G. (2014b). Assessment of crop foliar nitrogen using a novel dual-wavelength laser system and implications for conducting laser-based plant physiology. *ISPRS Journal of Photogrammetry and Remote Sensing*, *97*, 229–240. doi:10.1016/j.isprsjprs.2014.09.009

Ellsworth, D. S., Reich, P. B. (1993). Canopy structure and vertical patterns of photosynthesis and related leaf traits in a deciduous forest. *Oecologia*, *96*, 169–178.

Evans, J. R. (1983). Nitrogen and Photosynthesis in the Flag Leaf of Wheat (Triticum aestivum L.). *Plant Physiology*, *72*(2), 297–302.

Evans, J. R. (1989). Photosynthesis and nitrogen relationships in leaves of Ca plants. *Oecologia*, *78*, 9–19.

Evans, J. R., & Poorter, H. (2001). Photosynthetic acclimation of plants to growth irradiance : the relative importance of specific leaf area and nitrogen partitioning in maximizing carbon gain. *Plant, Cell and Environment*, (24), 755–767.

Farquhar, G., Caemmerer, S. Von, & Berry, J. A. (1980). A Biochemical Model of Photosynthetic CO2 Assimilation in Leaves of C2 Species. *Planta*, *90*, 78–90.

Field, C. (1983). Allocating leaf nitrogen for the maximization of carbon gain–leaf age as a control on the allocation program. *Oecologia*, *56*, 341–347.

Freedman, D., Diaconis, P. (1981). On the histogram as a density estimator: L_2 theory. *in Probability Theory and Related Fields* (Heidelberg: Springer Berlin) 57 (4): 453–476. ISSN 0178-8051.

Formica, A.F., Griffin, K.L., Boelman, N.B. (2013). Quantifying the physiology of structurally complex arctic vegetation and implications for carbon cycling in a shrubbier tundra. American Geophysical Union Fall Meeting Abstracts, B331-0597.

Garrigues, S., Shabanov, N. V., Swanson, K., Morisette, J. T., Baret, F., & Myneni, R. B. (2008). Intercomparison and sensitivity analysis of Leaf Area Index retrievals from LAI-2000, AccuPAR, and digital hemispherical photography over croplands. *Agricultural and Forest Meteorology*, *148*(8-9), 1193–1209. doi:10.1016/j.agrformet.2008.02.014

Gilmore A.M., Yamamoto H.Y. (1991). Resolution of lutein and zeaxanthin using a non-endcapped, lightly carbon-loaded C-18 high performance liquid chromatographic column. *Journal of Chromatography*, *543*, 137–145.

Godin, C., Sinoquet, H. (2005). Functional–structural plant modelling. *New Phytologist*, *166*, 705–708.

Gonsamo, A., Walter, J.M., Pellikka, P., (2010). Sampling gap fraction and size for estimating leaf area and clumping indices from hemispherical photographs. *Canadian Journal of Forest Research, 40*, 1588–1603.

Greaves, H. E., Vierling, L. a., Eitel, J. U. H., Boelman, N. T., Magney, T. S., Prager, C. M., & Griffin, K. L. (2015). Estimating aboveground biomass and leaf area of low-stature Arctic shrubs with terrestrial LiDAR. *Remote Sensing of Environment*, *164*, 26–35. doi:10.1016/j.rse.2015.02.023

Hanan, J. (1997). Virtual plants: integrating architectural and physiological models. *Environmental Modelling and Software*, *12*, 35–42

Heskel, M., Atkin, O., Turnbull, M., Rastetter, E., Griffin, K.L. (2012). Examining vertical patterns in Arctic tundra shrub canopies: Implication for carbon cycling in a changing environment. American Geophysical Union Fall Meeting Abstracts, 1, 0543.

Heskel, M., Greaves, H., Kornfeld, A., Gough, L., Atkin, O. K., Turnbull, M. H, Shaver, G., Griffin, K. L. (2013). Differential physiological responses to environmental change promote woody shrub expansion. *Ecology and Evolution, 3*(5), 1149–62. doi:10.1002/ece3.525

Hirose, T., & Werger, M. J. A. (1987). Maximizing daily canopy photosynthesis with respect to the leaf nitrogen allocation pattern in the canopy. *Oecologia*, *72*(4), 520–526.

Hikosaka, K., Terashima, I. (1995) A model of the acclimation of photosynthesis in the leaves of C3 plants to sun and shade with respect to nitrogen use. *Plant, Cell & Environment, 18,* 605–618.

Hoppe, H., DeRose, T., Duchamp, T., McDonald, J. (1992). Surface Reconstruction from Unorganized Points. *Computer Graphics -New York Association for Computer Machinery,* 26, 71

Jennings, S. B., Brown, N. D., Sheil, D. (1999). Assessing forest canopies and understorey illumination : canopy closure, canopy cover and other measures. *Forests, 72*(1).

Jonckheere, I., Fleck, S., Nackaerts, K., Muys, B., Coppin, P., Weiss, M., & Baret, F. (2004). Review of methods for in situ leaf area index determination. *Agricultural and Forest Meteorology*, *121*(1-2), 19–35. doi:10.1016/j.agrformet.2003.08.027

Jupp, D., Culvenor, D., Lovell, J., Newnham, G., Strahler, A., and Woodcock, C. (2009). Estimating forest lai profiles and structural parameters using a ground-based laser called 'Echidna (R)'. *Tree Physiology*, *29,* 171 p. doi: 10.1093/treephys/tpn022.

Hyer, E.J., Goetz, S.J., (2004). Comparison and sensitivity analysis of instruments and radiometric methods for LAI estimation: assessments from a boreal forests site. *Agricultural and Forest Meteorology, 122,* 157–174.

Kimes, D. (1984). Modeling the directional reflectance from complete homogeneous vegetation canopies with various leaf-orientation distributions. *Journal of the Optical Society of America A-Optics Image Science and Vision, 1*, pp. 725-737. doi: 10.1364/ JOSAA.1.000725.

Kirschbaum, M.U.F., Pearcy, R.W. (1988). Concurrent measurements of O2 and CO2 exchange during lightflecks in Alocasia macrorrhiza (L.) G. Don. *Planta*, *174*, 527–533. doi:10.1007/BF00634483

Kitajima, K., & Hogan, K. P. (2003). Increases of chlorophyll a/b ratios during acclimation of tropical woody seedlings to nitrogen limitation and high light. *Plant, Cell and Environment*, *26*(6), 857–865. doi:10.1046/j.1365-3040.2003.01017.x

Le Roux, X., Walcroft, A.S., Daudet, F.A., Sinoquet, H., Chaves, M.M., Rodrigues, A., Osorio, L. (2001). Photosynthetic light acclimation in peach leaves: importance of changes in mass: area ratio, nitrogen concentration, and leaf nitrogen partitioning. *Tree Physiology 21,* 377–386.

Logan, B. A., Barker, D. H., Demmig-Adams, B., & Adams, W. W. (1996). Acclimation of leaf carotenoid composition and ascorbate levels to gradients in the light environment within an Australian rainforest. *Plant, Cell and Environment, 19*(9), 1083–1090. doi:10.1111/j.1365-3040.1996.tb00215.x

Lovell, J. L., Jupp, D. L. B., Culvenor, D. S., & Coops, N. C. (2003). Using airborne and ground-based ranging LiDAR to measure canopy structure in Australian forests. *Canadian Journal of Remote Sensing, 29*, 607–622.

Magney, T. S., Eusden, S. A., Eitel, J. U. H., Logan, B. A., Jiang, J., & Vierling, L. A. (2014). Assessing leaf photoprotective mechanisms using terrestrial LiDAR : towards mapping canopy photosynthetic performance in three dimensions. *New Phytologist, 201*, 344–356.

Martin, C.E., Warner, D.A. (1984). The effects of desiccation on concentrations and a/b ratios of chlorophyll in Leucobryum glaucum and Thuidium delicatu- lum. *New Phytologist, 96,* 545-550.

Monsi, M., and Saeki, T. (1953). ber den Lichtfaktor in den Pflanzenge- sellschaften und seine Bedeutung fur die Stoffproduktion. *Japanese Journal of Botany, 15,* 22-52.

Moorthy, I., Miller, J.R., Hu, B., Chen, J., Li, Q., (2008). Retrieving crown leaf area index from an individual tree using ground-based lidar data. *Canadian Journal of Remote Sensing, 34* (3), 320–332.

Myers-Smith, I. H., Forbes, B. C., Wilmking, M., Hallinger, M., Lantz, T., Blok, D, et al. (2011). Shrub expansion in tundra ecosystems: dynamics, impacts and research priorities. *Environmental Research Letters, 6*(4), 045509. doi:10.1088/1748-9326/6/4/045509

Naekaerts, K., Coppin, P., Muys, B., Hermy, M. (2000). Sampling methodology for LAI measurements with LAI-2000 in small forest stands. *Agricultural and Forest Meteorology, 101,* 247-250.

Niinemets Ü. (1996). Changes in foliage distribution with tree size and relative irradiance: differences between the saplings of Acer platanoides and Quercus robur. *Ecological Research, 11,* 269–281

Niinemets, U., Bilger, W., Kull, O., & Tenhunen, J. D. (1998). Acclimation to high irradiance in temperate deciduous trees in the field: changes in xanthophyll cycle pool size and in photosynthetic capacity along a canopy light gradient. *Plant, Cell and Environment, 21*(12), 1205–1218. doi:10.1046/j.1365-3040.1998.00364.x

Niinemets, Ü., Kull, O., & Tenhunen, J. D. (2004). Within-canopy variation in the rate of development of photosynthetic capacity is proportional to integrated. *Plant, Cell and Environment, 27,* 293–313.

Niinemets, Ü., Cescatti, A., Rodeghiero, M., Tosens, T. (2006). Complex adjustments of photosynthetic capacity and internal mesophyll conductance to current and previous light availabilities and leaf age in Mediterranean evergreen species Quercus ilex. *Plant, Cell & Environment, 29,* 1159–1178.

Niinemets, U. (2007). Photosynthesis and resource distribution through plant canopies. *Plant, Cell & Environment*, *30*(9), 1052–71. doi:10.1111/j.1365-3040.2007.01683.x

Niinemets, Ü. (2010). A review of light interception in plant stands from leaf to canopy in different plant functional types and in species with varying shade tolerance. *Ecological Research*, *25*(4), 693–714. doi:10.1007/s11284-010-0712-4

Norman, J. M., & Campbell, G. S. (1989). Canopy structure. In R. W. Pearcy, L. Ehleringer, H. A. Mooney & P. W. Rundel (Eds.), Plant Physiological Ecology: Field Methods and Instrumentation (pp. 301−325). New York: Chapman and Hall.

Olsoy, P. J., Glenn, N. F., Clark, P. E., & Derryberry, D. R. (2014). Aboveground total and green biomass of dryland shrub derived from terrestrial laser scanning. *ISPRS Journal of Photogrammetry and Remote Sensing*, *88*, 166–173. doi:10.1016/j.isprsjprs.2013.12.006

Omasa, K., Hosoi, F., & Konishi, A. (2007). 3D lidar imaging for detecting and understanding plant responses and canopy structure. *Journal of Experimental Botany*, *58*(4), 881–98. doi:10.1093/jxb/erl142

Pearcy, R.W., Gross, L.J., He, D. (1997). An improved dynamic model of photosynthesis for estimation of carbon gain in sunfleck light regimes. *Plant, Cell & Environment, 20,* 411–424. doi:10.1046/j.1365-3040.1997. d01-88.x

Pearcy, R. W., Muraoka, H., & Valladares, F. (2005). Crown architecture in sun and shade environments: assessing function and trade-offs with a three-dimensional simulation model. *New Phytologist*, *166*(3), 791–800. doi:10.1111/j.1469-8137.2005.01328.x

Pierce, L.L., Running, S.W. (1988). Rapid estimation of coniferous forest leaf area index using a portable integrating radiometer. *Ecology, 69,* 1762–1767.

Pierre Alliez, L.S., Guennebaud, G. (2010). Surface reconstruction from point sets. *CGAL User and Reference Manual,* vol. CGAL Editorial Board.

Pueschel, P., Newnham, G., & Hill, J. (2014). Retrieval of Gap Fraction and Effective Plant Area Index from Phase-Shift Terrestrial Laser Scans. *Remote Sensing*, *6*(3), 2601–2627. doi:10.3390/rs6032601

de Pury, D.G.G., Farquhar, G.D. (1997), Simple scaling of photosynthesis from leaves to canopies without the errors of big-leaf models. *Plant, Cell & Environment, 20*, 537–557.

Ross, J. (Ed.) (1981), The Radiation Regime and Architecture of Plant Stands, Dr. W. Junk, Boston, Mass.

Sarlikioti, V., de Visser, P. H. B., & Marcelis, L. F. M. (2011). Exploring the spatial distribution of light interception and photosynthesis of canopies by means of a functional-structural plant model. *Annals of Botany*, *107*(5), 875–83. doi:10.1093/aob/mcr006

Schurr, U., Walter, A., & Rascher, U. (2006). Functional dynamics of plant growth and photosynthesis - from steady-state to dynamics - from homogeneity to heterogeneity. *Plant, Cell and Environment*, *29*(3), 340–352. doi:10.1111/j.1365-3040.2005.01490.x

Seidel, D., Fleck, S., Leuschner, C., (2012). Analyzing forest canopies with ground- based laser scanning: a comparison with hemispherical photography. *Agricultural and Forest Meteorology, 154,* 1-8.

Shaver, G. R., Street, L. E., Rastetter, E. B., Van Wijk, M. T., & Williams, M. (2007). Functional convergence in regulation of net CO 2 flux in heterogeneous tundra landscapes in Alaska and Sweden. *Journal of Ecology*, *95*(4), 802–817. doi:10.1111/j.1365-2745.2007.01259.x

Street, L.E., Shaver, G.R., Williams, M., Van Wijk, M.T. (2007). What is the relationship between changes in canopy leaf area and changes in photosynthetic CO2 flux in arctic ecosystems? *Journal of Ecology*, *95*, 139–150.

Thompson, C., J. Beringer, F. S. Chapin, III, and A. D. McGuire. (2004). Structural complexity and land-surface energy exchange along a gradient from arctic tundra to boreal forest. *Journal of Vegetation Science,* 15, 397–406.

Van der Zande, D., Jonckheere, I., Stuckens, J., Verstraeten, W.W., Coppin, P., (2008). Sampling design of ground-based LiDAR measurements and its effect on shad- owing. *Canadian Journal of Remote Sensing,* 34 (6), 526–538.

Van der Zande, D., Mereu, S., Nadezhdina, N., Cermak, J., Muys, B., Coppin, P., Manes, F., (2009). 3D upscaling of transpiration from leaf to tree using ground based LiDAR: application on a mediterranean holm oak (Quercus Ilex L.) tree. *Agricultural and Forest Meteorology, 149,* 1573–1583.

Van der Zande, D., Stuckens, J., Verstraeten, W. W., Muys, B., & Coppin, P. (2010). Assessment of Light Environment Variability in Broadleaved Forest Canopies Using Terrestrial Laser Scanning. *Remote Sensing*, *2*(6), 1564–1574. doi:10.3390/rs2061564

Van der Zande, D., Stuckens, J., Verstraeten, W. W., Mereu, S., Muys, B., & Coppin, P. (2011). 3D modeling of light interception in heterogeneous forest canopies using ground-based LiDAR data. *International Journal of Applied Earth Observation and Geoinformation*, *13*(5), 792–800. doi:10.1016/j.jag.2011.05.005

Van Leeuwen, M., Coops, N. C., Hilker, T., Wulder, M. a., Newnham, G. J., & Culvenor, D. S. (2013). Automated reconstruction of tree and canopy structure for modeling the internal canopy radiation regime. *Remote Sensing of Environment*, *136*, 286–300. doi:10.1016/j.rse.2013.04.019

Van Wijk, M. T., Williams, M., & Shaver, G. R. (2005). Tight coupling between leaf area index and foliage N content in arctic plant communities. *Oecologia*, *142*(3), 421–7. doi:10.1007/s00442-004-1733-x

Vierling, L.A., & Wessman, C.A. (2000). Photosynthetically active radiation heterogeneity within a monodominant Congolese rain forest canopy. *Agricultural and Forest Meteorology*, *103*(3), 265–278. doi:10.1016/S0168-1923(00)00129-5

Vierling, L., Xu, Y., Eitel, J., & Oldow, J. (2013). Shrub characterization using terrestrial laser scanning and implications for airborne LiDAR assessment. *Canadian Journal of Remote Sensing*, *38*(6), 709–722. Retrieved from http://pubs.casi.ca/doi/abs/10.5589/m12-057

Vos, J., Evers, J.B., Buck-Sorlin, G.H., Andrieu, B., Chelle, M., de Visser, P.H.B. (2010). Functional–structural plant modelling: a new versatile tool in crop science. *Journal of Experimental Botany, 61*, 2101–2115.

Weiss, M., Baret, F., Smith, G. J., Jonckheere, I., Coppin, P. (2004). Review of methods for in situ leaf area index (LAI) determination: Part II. Estimation of LAI, errors and sampling. *Agricultural and Forest Meteorology, 121*, 37−53

Welles, J.M., Cohen, S. (1996). Canopy structure measurement by gap fraction analysis using commercial instrumentation. *Journal of Experimental Botany,* 302, 1335–1342.

Whitehead, D., Grace, J.C., Godfrey, M.J.S., (1990). Architectural distribution of foliage in individual pinus-radiata d don crowns and the effects of clumping on radiation interception. *Tree Physiology, 7,* (1-4), 135-155.

Widlowski, J.-L., Côté, J.-F., & Béland, M. (2014). Abstract tree crowns in 3D radiative transfer models: Impact on simulated open-canopy reflectances. *Remote Sensing of Environment*, *142*, 155–175. doi:10.1016/j.rse.2013.11.016

Williams, M., & Rastetter, E. B. (1999). Vegetation characteristics and primary productivity along an arctic transect: implications for scaling-up. *Journal of Ecology*, *87*(5), 885–898. doi:10.1046/j.1365-2745.1999.00404.x

Williams, M., Rastetter, E. B., Shaver, G. R., Hobbie, J. E., Carpino, E., & Kwiatkowski, B. (2001). Primary production of an arctic watershed: an uncertainty analysis. *Ecological Applications*, *11*(6), 1800–1816.

Williams, M., Street, L., Wijk, M.T.V., Shaver, G.R. (2006). Identifying differences in carbon exchange among arctic ecosystem types. *Ecosystems*, *9*, 288–304.

Zheng, G., & Moskal, L. M. (2012). Spatial variability of terrestrial laser scanning based leaf area index. *International Journal of Applied Earth Observation and Geoinformation*, *19*, 226–237. doi:10.1016/j.jag.2012.05.002

Zheng, G., Moskal, L. M., & Kim, S.-H. (2013). Retrieval of Effective Leaf Area Index in Heterogeneous Forests With Terrestrial Laser Scanning. *IEEE Transactions on Geoscience and Remote Sensing*, *51*(2), 777–786. doi:10.1109/TGRS.2012.2205003

Figures:

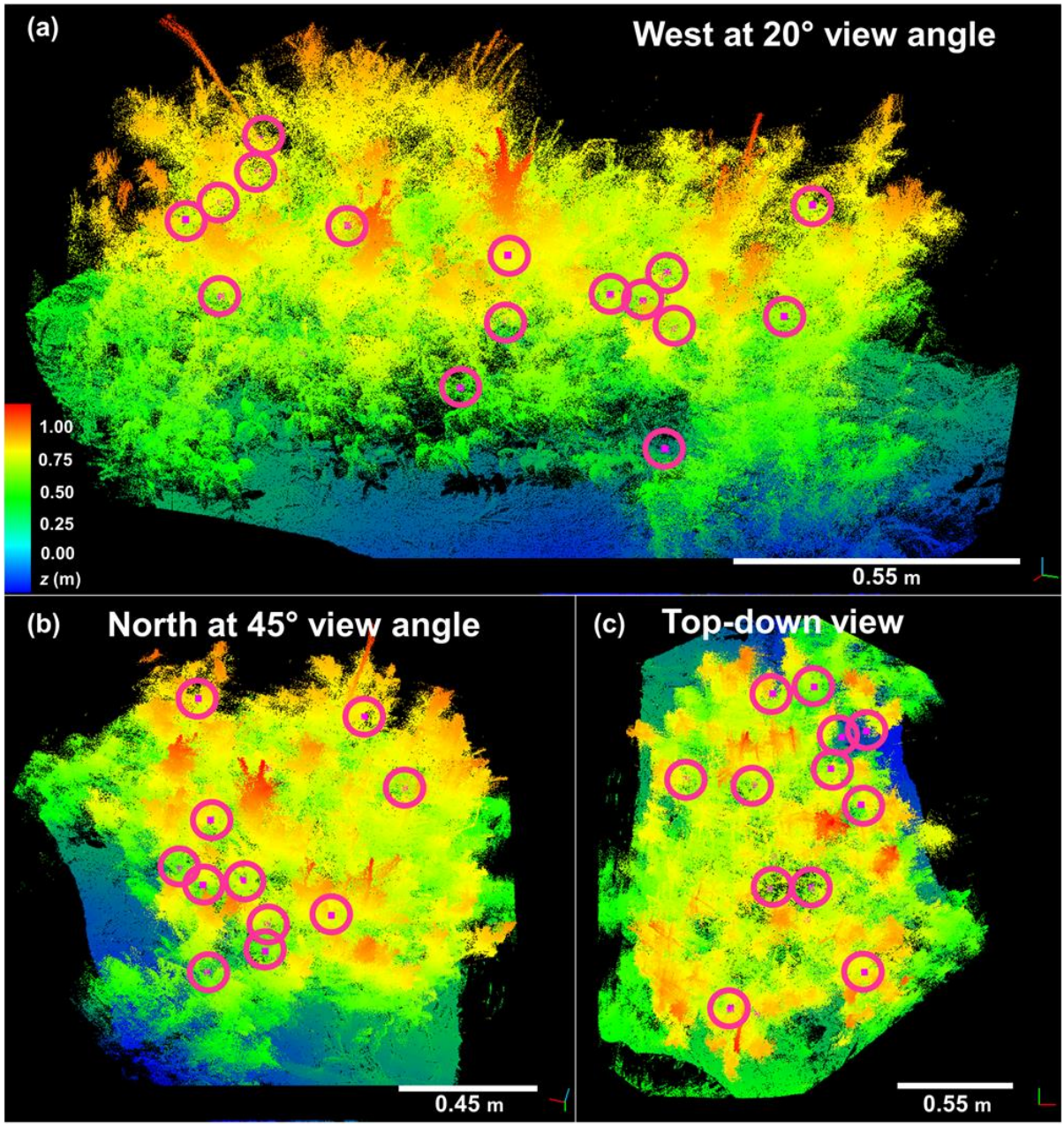

Figure 3.1. Example of sampling locations within one shrub point cloud. Sampled leaves are denoted by pink squares, and emphasized using a surrounding pink circle. A total of 26 locations within this shrub were chosen, through some are not visible due to occlusion effects.

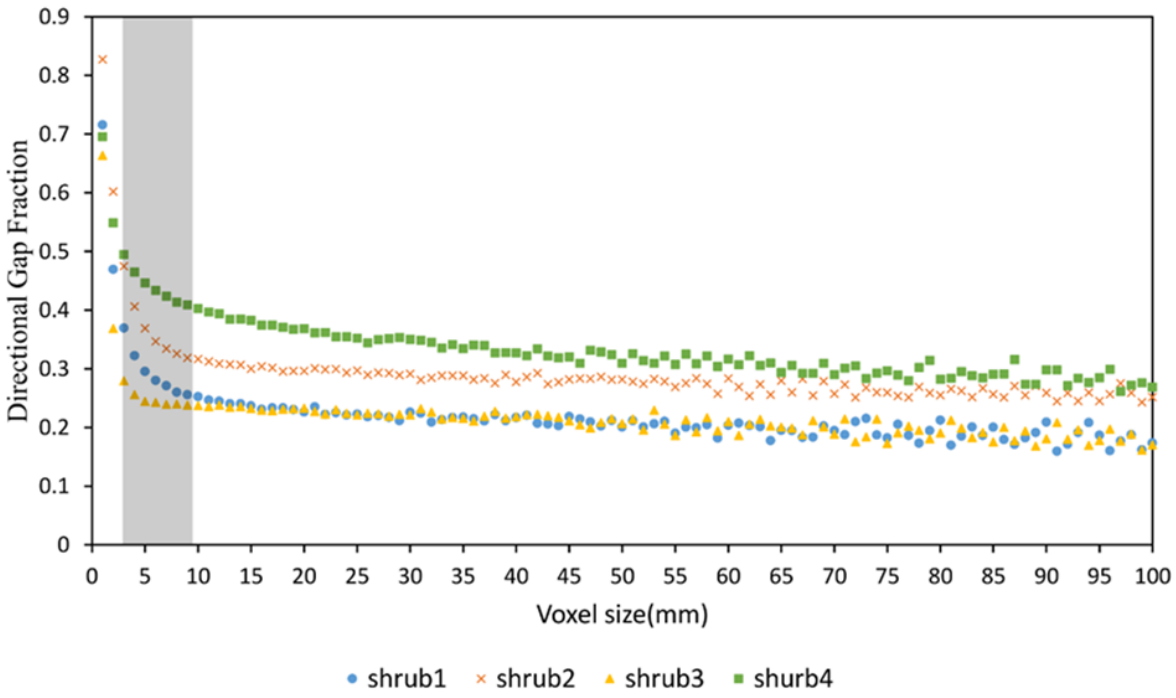

Figure 3.2. Sensitivity analysis showing the variability of the estimated average digital gap fraction (DGF) of all of the sampled voxels for each of the four shrubs (n=26 per shrub). The grey bar denotes the points prior to a DGF vs. voxel size asymptote.

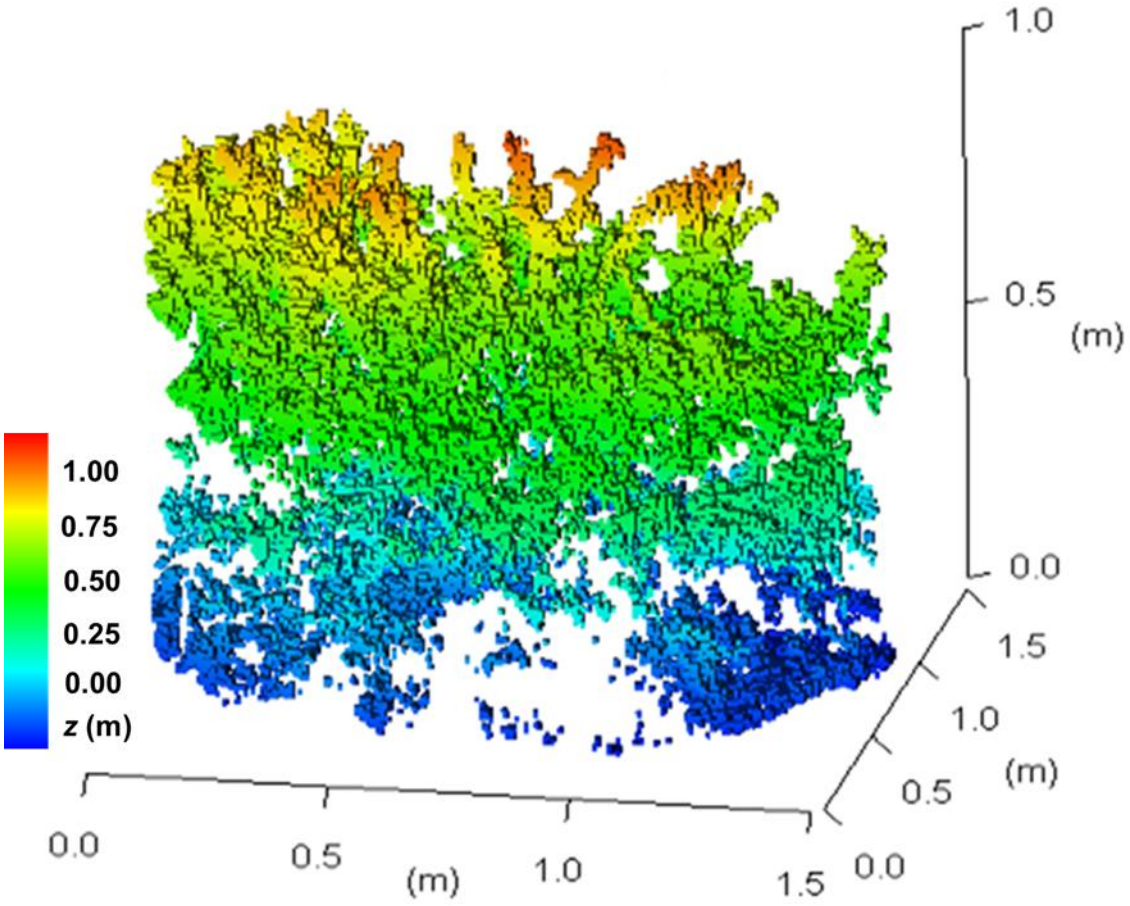

Figure 3.3. Example voxelized point cloud showing 0.01 m^3 voxels. A colorized height ramp was applied for visualization purposes.

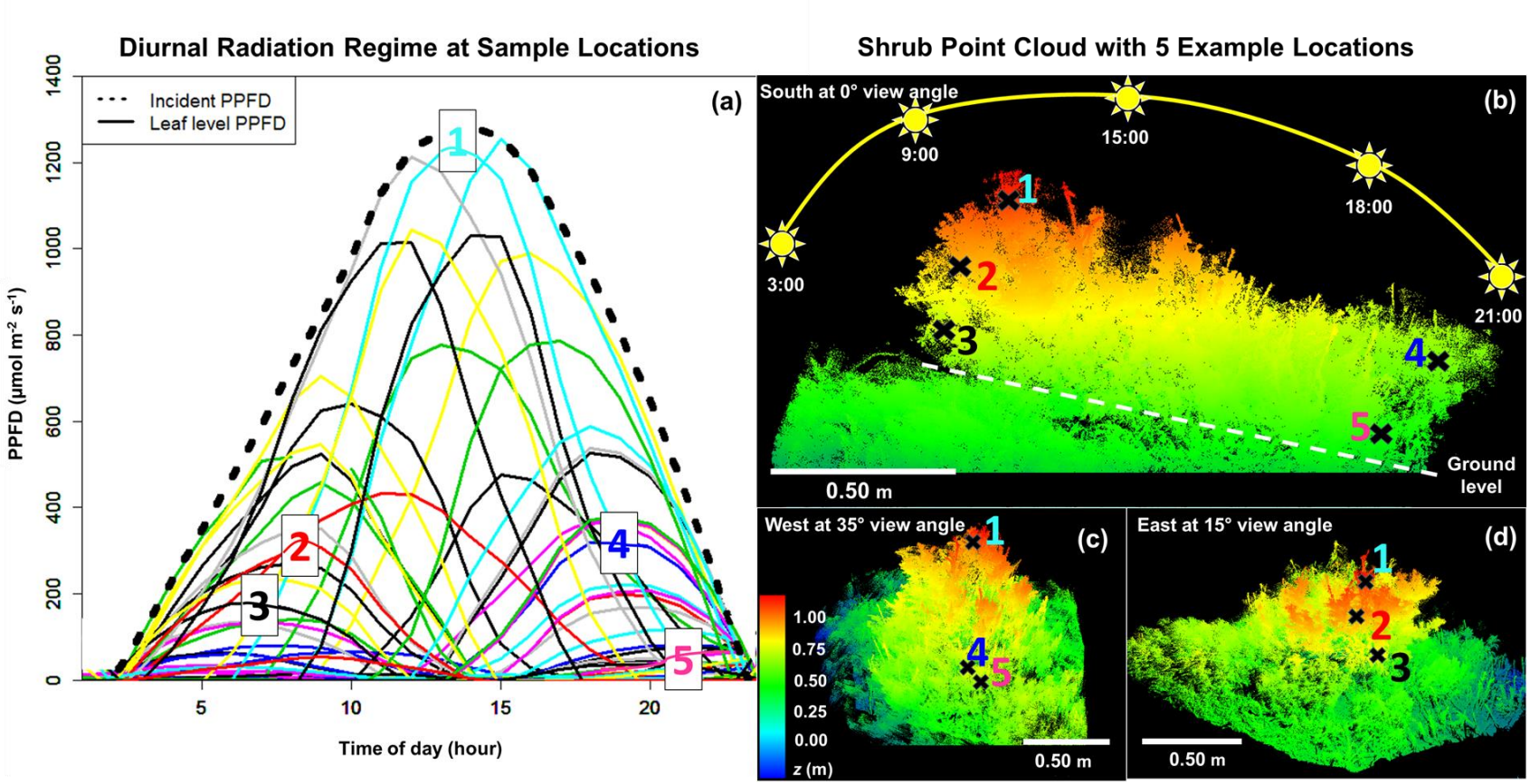

Figure 3.4. (a) Temporal variability in instantaneous PPFD (colored lines) of sample locations (n = 104) compared to incident PPFD at the top of the canopy (dashed line). The numbers overlaying 5 of the curves correspond with the shrub locations in 4b, c & d. (b) Example shrub showing corresponding diurnal radiation pattern in (a). Diurnal course of the sun added for visualization (not drawn to scale). (c) Same shrub from west viewing angle, showing example points 1, 4 & 5. (d) Same shrub showing example locations 1, 2, & 3 from east viewing angle.

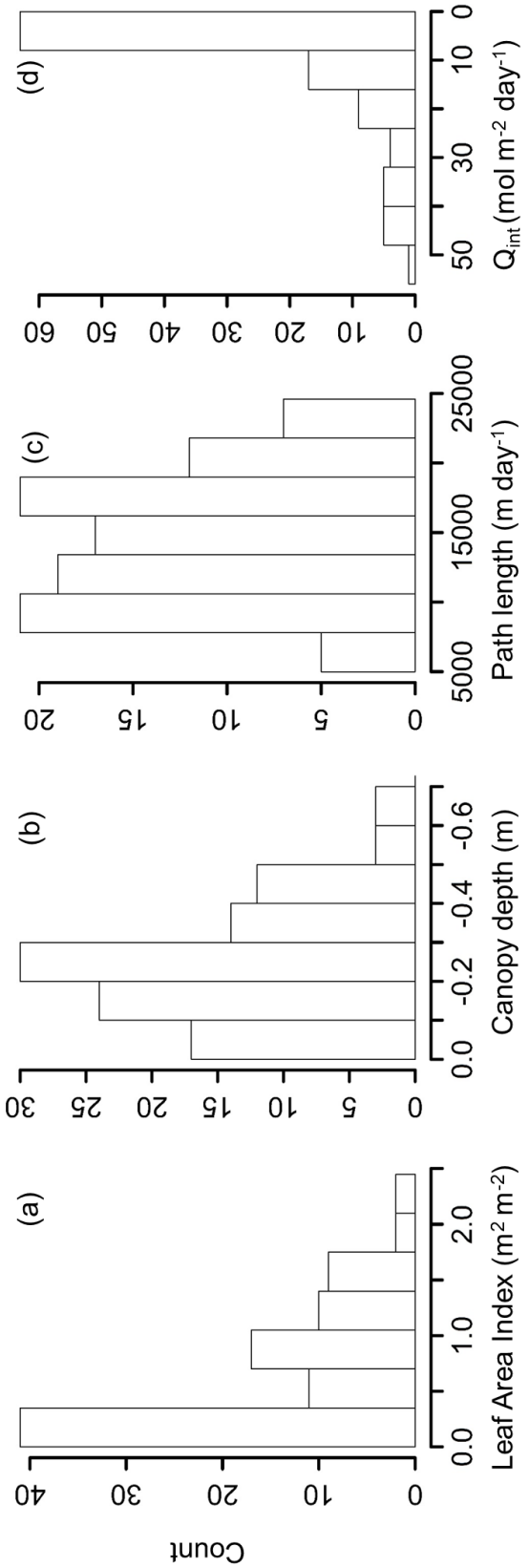

Figure 3.5. Histograms of count distributions for (a) leaf area index (LAI), (b) vertical canopy depth, (c) path length, and (d) integrated quantum flux density (Q_{int}) computed from TLS derived radiation model. All x-axes are oriented with more hypothetical light on the left side of the axis.

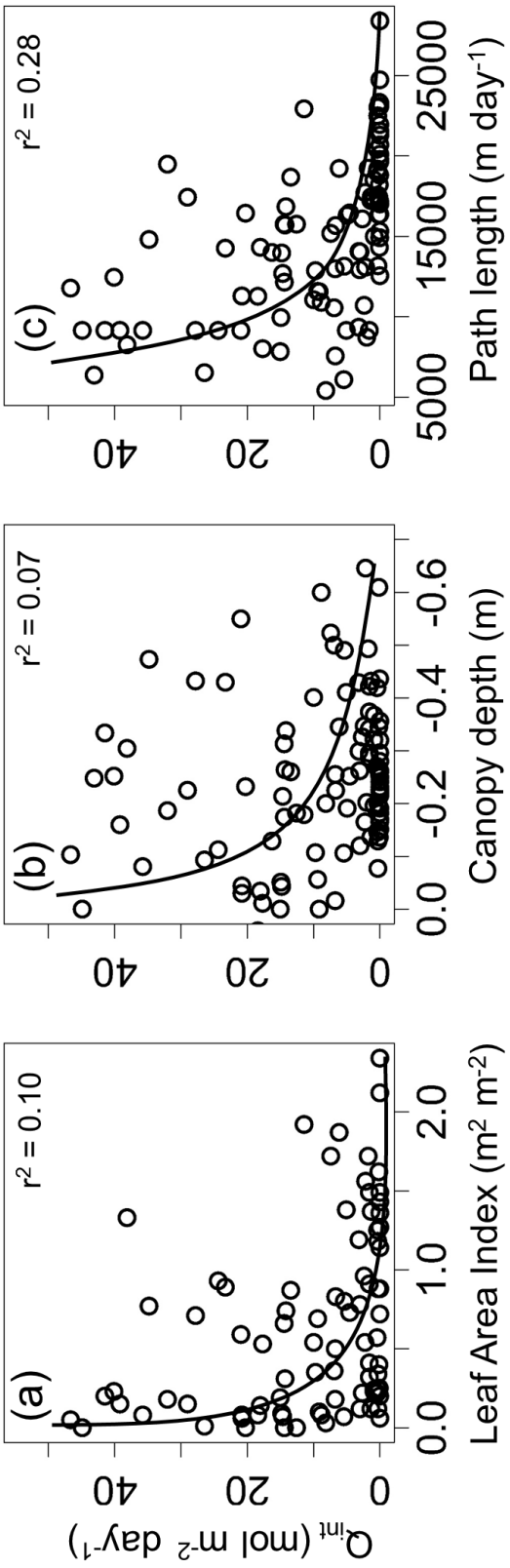

Figure 3.6. Relationships between integrated quantum flux density (Q_{int}) and (a) leaf area index (LAI), (b) vertical canopy depth, and (c) path length.

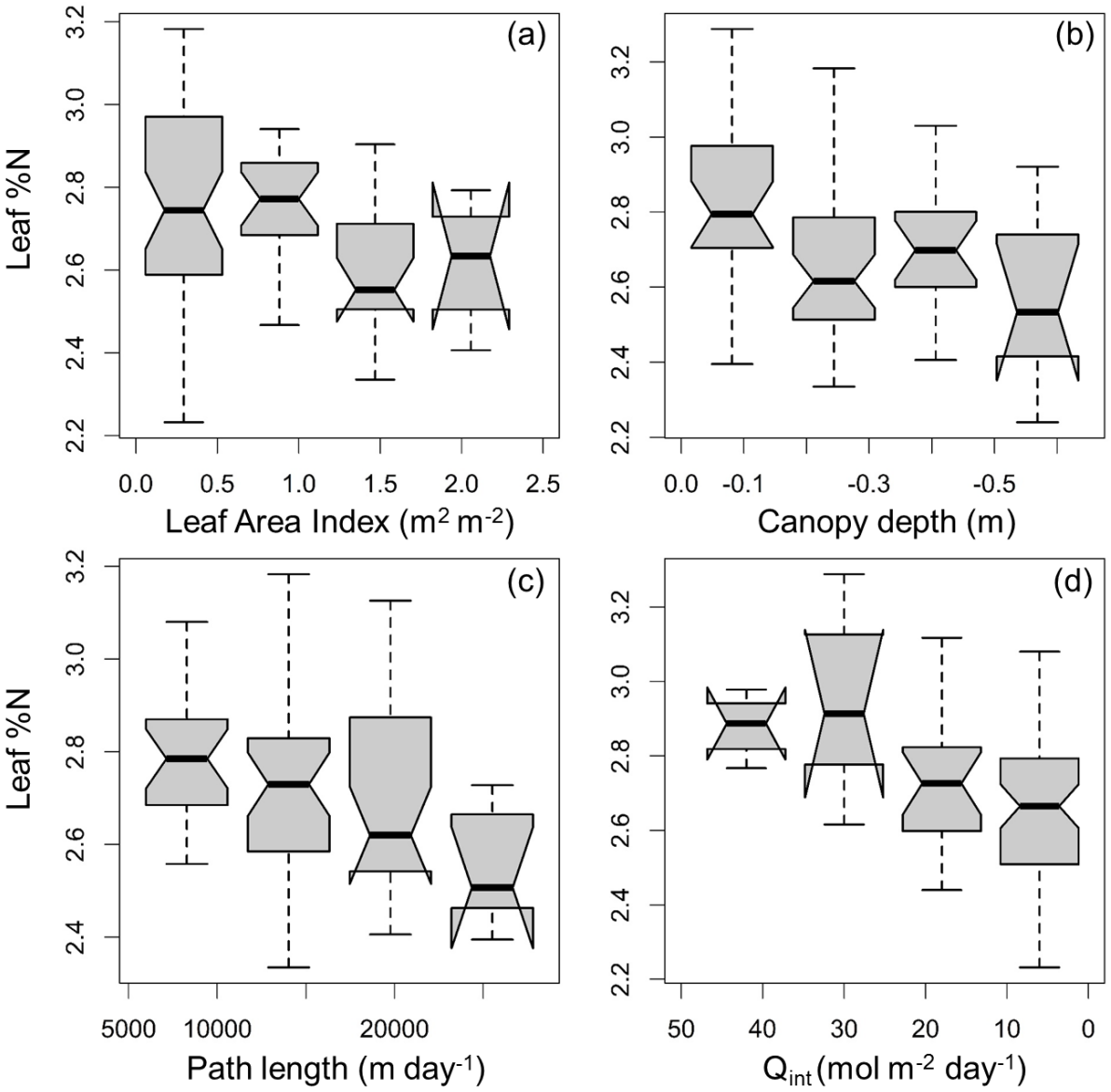

Figure 3.7. Relationships between leaf %N and (a) leaf area index (LAI), (b) vertical canopy depth, (c) path length, and (d) integrated quantum flux density (Q_{int}) derived from TLS radiation model. Data are binned into four boxplots for visualization and statistical comparisons between binned light regimes. Notches represent the 95% confidence interval of the mean.

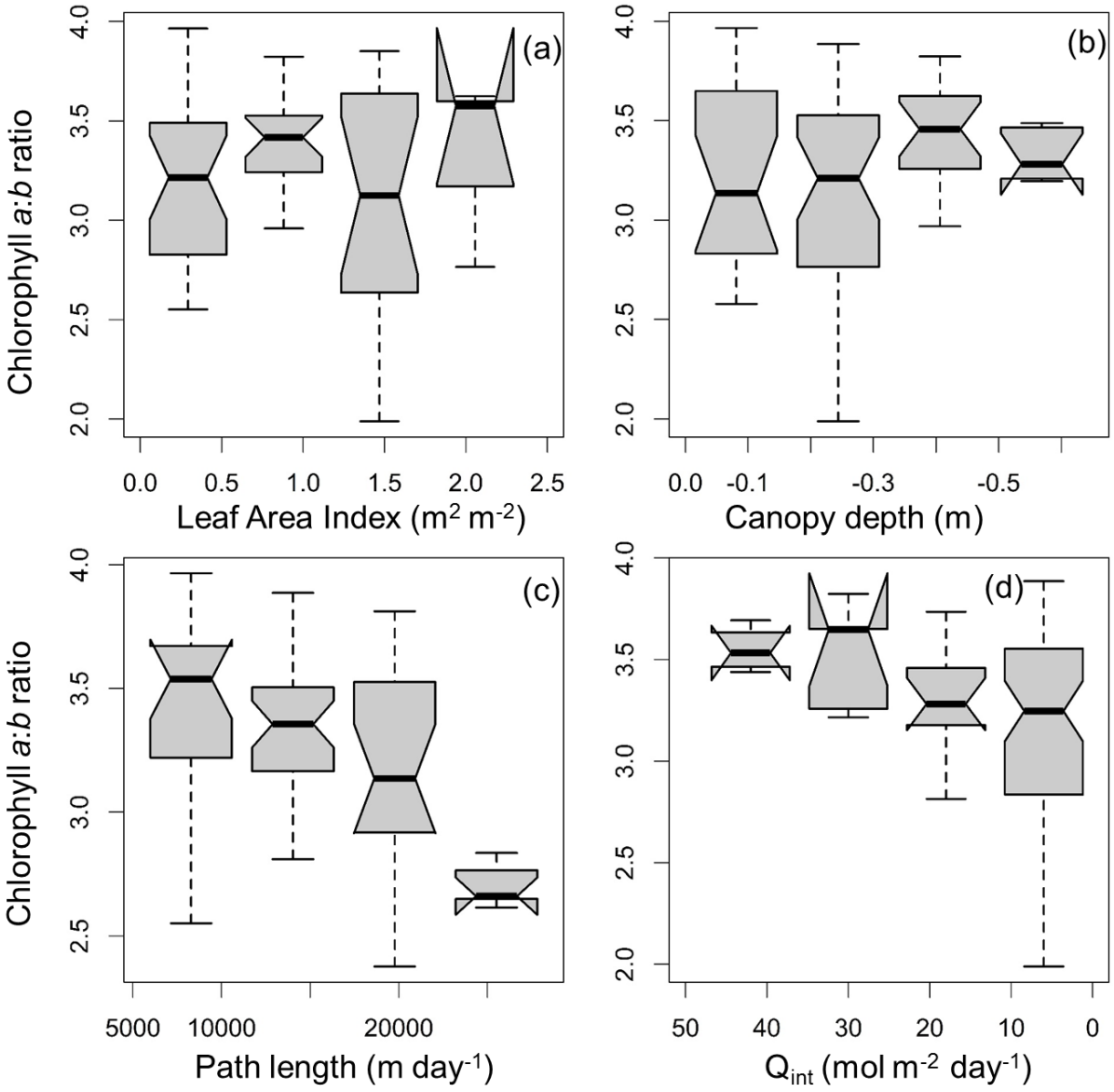

Figure 3.8. Relationships between *chlorophyll* a:b ratio and (a) leaf area index (LAI), (b) vertical canopy depth, (c) path length, and (d) integrated quantum flux density (Q_{int}) derived from TLS radiation model. Data are binned into four boxplots for visualization and statistical comparisons between binned light regimes. Notches represent the 95% confidence interval of the mean.

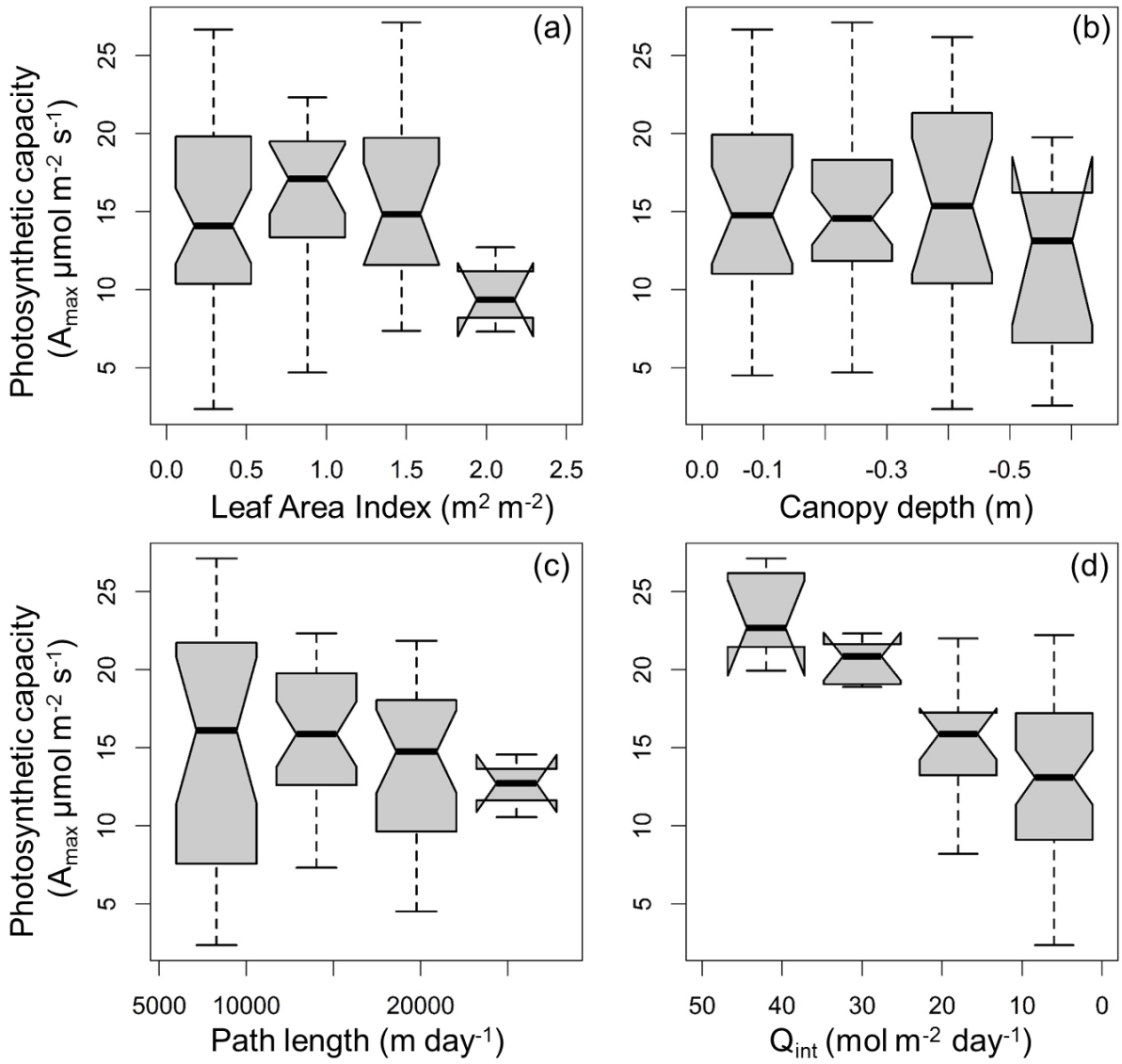

Figure 3.9. Relationships between photosynthetic capacity (A_{max}) and (a) leaf area index (LAI), (b) vertical canopy depth, (c) path length, and (d) integrated quantum flux density (Q_{int}) derived from TLS radiation model. Data are binned into four boxplots for visualization and statistical comparisons between binned light regimes. Notches represent the 95% confidence interval of the mean.

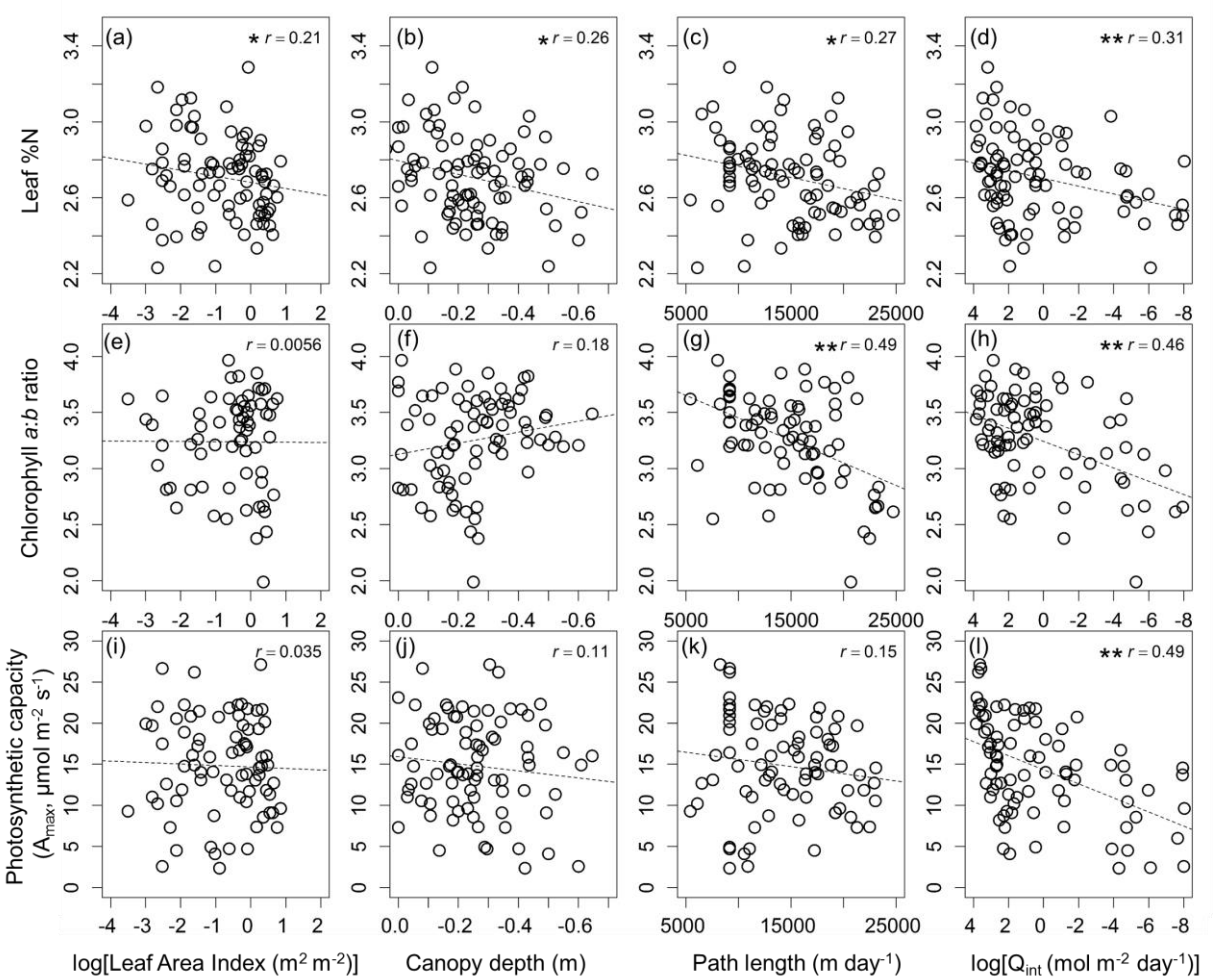

Figure 3.10. Relationships between leaf % N and (a) leaf area index (LAI), (b) vertical canopy depth, (c) path length, and (d) integrated quantum flux density (Q_{int}); *chlorophyll* a:b ratio and (e) LAI, (f) vertical canopy depth, (g) path length, and (h) Q_{int}; photosynthetic capacity (A_{max}) and (i) LAI, (j) vertical canopy depth, (k) path length, and (l) Q_{int}. Dashed lines represent the linear least squares best fit line for the entire dataset. * indicates the slope is significantly different from zero at the p>0.05 level and ** p>0.01.

Chapter 4: Enhanced xanthophyll cycle activity in arctic willow contrasted with a meta-analysis of higher plant species

Magney, T.S, Logan, B.A., Griffin, K.L., Eitel, J.U.H, Boelman, N.T., Abatzoglou, J.T., Greaves, H., Prager, C.M., Logan, B.A., Fortin, L., Oliver, R., Eusden, S., Vierling, L.A.

to be submitted to Plant, Cell, and Environment

Abstract: When the capacity for photosynthesis is inhibited by unfavorable growing conditions, excess light is dissipated as thermal energy via the interconversion of xanthophyll cycle pigments – a photoprotective mechanism ubiquitous among higher plants. The relatively low irradiance conditions of the arctic (low direct/diffuse ratio) yet highly stressful environment (short growing season, frozen soil, low nutrient availability) suggest contrasting hypotheses regarding the necessity for plant investment in photoprotective mechanisms. Xanthophyll cycle pigment pool sizes and interconversion rates were investigated in arctic willow, *Salix pulchra*. Our data suggest that bulk xanthophyll pigment pools from upper canopy *S. pulchra* leaves are remarkably high as compared to other higher plant species (168 ± 34 mol V+A+Z mmol Chl a + b $^{-1}$). Further, we observed high zeaxanthin retention in dark-acclimated leaves and high rates of xanthophyll cycle inter-conversion – saturating at low irradiances, compared to greenhouse grown annual crops grown under favorable conditions (unstressed). In an effort to explain the potential drivers of the high xanthophyll cycle pools sizes found here, a meta-analysis was conducted using pigment data from 155 vascular plant species across 9 biomes. The meta-analysis provides concrete evidence of elevated xanthophyll pools in environments exposed to increasingly stressful conditions, i.e. the arctic tundra. Building on this, an analysis using climate metrics (derived from annual temperature, precipitation, and evapotranspiration data) from globally distributed field locations was performed, and supported the hypothesis that during peak photosynthesis, plant photoprotective pigments are more abundant in environments prone to extreme temperatures and water deficits.

4.1. Introduction

The photosynthetic process, whereby chemical energy is produced from a variable stream of solar photons, ultimately provides energy for most life on earth. During instances when a majority of the incoming solar energy is converted into chemical energy by plants, the chances for problems to occur are minimal. However, this is often not the case during periods when high levels of irradiance are incident upon a leaf surface, during which 50-90% of the sun's energy is not utilized by the plant (Björkman and Demmig-Adams, 1994; Demmig-Adams et al., 1995). It is well understood that the proportion of incoming solar photons not used for photosynthetic electron transport increases with exposure to plant stress (Demmig-Adams & Adams, 2006). Plant stress here is defined as environmental conditions that adversely affect plant growth, causing a decline in plant physiological function (Chapin, 1991, Niinemets, 2010). When the capacity of a plant to perform photosynthesis is restricted, excess light energy can result in the formation of reactive oxygen species (ROS), ultimately leading to leaf damage and death (Ledford & Niyogi 2005). To avoid the consequences of ROS formation, plants employ a host of photoprotective mechanisms to safely dissipate excess energy away from photosystem II (PSII, Demmig-Adams & Adams, 1996; Kanervo et al., 2005; Niyogi et al., 2005). One of the most ubiquitous mechanisms utilized by plants to modulate the efficiency of solar energy into chemical energy is through the xanthophyll cycle (Demmig et al, 1987, 1988).

Over the last several decades, a wide body of research has emerged, highlighting the seemingly complex role of the xanthophyll cycle in thermal energy dissipation (Demmig-Adams & Adams 2006, Demmig-Adams et al., 2012; Jahns & Holzwarth, 2012). Much of the foundational work has been done by manipulating irradiance and/or nutrients in a greenhouse environment to examine the role of the xanthophyll cycle in the photoprotection of plants under stressful conditions (e.g., Verhoeven et al., 1997; Logan et al., 1999). These studies have found that plants under increasing stress employ a greater rate of xanthophyll-cycle interconversion, whereby violaxanthin (V) is converted to antheraxanthin (A), and zeaxanthin (Z) via successive, enzyme-catalyzed de-epoxidations (Yamamoto, 1979). In concert with the strong empirical evidence supporting increased thermal energy dissipation via the interconversion of xanthophyll cycle pigments (e.g., Demmig Adams & Adams, 1994; Demmig-Adams, 1998), field studies have examined both xanthophyll de-epoxidation

throughout the course of the day (e.g., Adams et al., 1999; Barker et al., 2002) and the fluctuation of xanthophyll cycle pool size throughout the season (e.g., Adams et al., 1995; Logan et al., 1998a; Verhoeven et al., 1998; Adams et al., 2002; Porcar-Castell et al., 2008), and under varying light environments (e.g., Logan et al., 1998b; Matsubara et al., 2009). The majority of field based studies have been conducted in temperate, semi-arid, and Mediterranean climates, with limited xanthophyll investigations conducted in the endmembers of our global climate system, such as the tropical rainforest (Königer et al., 1995, Matsubara et al., 2009; Thiele et al., 2000, Krause et al., 2012); desert (Barker et al., 1997, 2002); boreal forest (Esminger et al., 2004; Porcar-Castell et al., 2008, 2012); or tundra (*this study*).

If xanthophyll cycle variability is indeed an indicator of environmental stress, we can hypothesize that high xanthophyll cycle pool sizes would exist across an increasingly stressful environmental gradient. For this reason, our attention is brought to the arctic tundra, where long, persistent winters, cold temperatures, and low annual precipitation, invoke deep frozen soils, a short growing season, and therefore limited opportunity for plant nutrient uptake contributing to the creation of carbohydrates from photosynthesis. Compounding these stresses is the near complete 24 hours of sunlight during the growing season at high latitudes, where one would hypothesize that the availability of excess light energy exceeds photosynthetic capacity, and the necessity for photoprotection high. However, the fraction of diffuse to direct sunlight is very high, with over 80% of days during a typical summer in Northern Alaska (68.63°N, -149.60°W, same as in this study) exceeding a diffuse/direct fraction of .8 (Williams et al., 2014). On a global scale, the diffuse fraction of sunlight in the arctic is on the high end of the spectrum, with relatively low average summer midday photosynthetic photon flux density (PPFD) of 1032 μmol m^{-2} s^{-1} above vegetation canopies under sunlit conditions and 351 μmol m^{-2} s^{-1} during diffuse conditions (Williams et al., 2014). From this, opposing hypotheses could suggest 1) high xanthophyll cycle pool size resulting from long days in a stressful environment, or 2) low xanthophyll cycle pool size due to the high fraction of diffuse sunlight and relative low overall irradiance conditions. These dueling hypotheses provided the motivation for this research - to investigate the role of the xanthophyll cycle as a potential physiological indicator of environmental stress in the arctic, as compared to higher plant species over a wide range of growing conditions.

There has recently been a growing interest in examining the convergence or divergence of plant traits across environmental gradients spanning the globe (Wright et al., 2004; Atkin et al., 2015). A limitation to these studies is the relative lack of information coming from one of the world's largest biomes, the arctic tundra. While neither of the aforementioned meta-analyses focus on plant pigments directly, there are rapidly accumulating published datasets on plant pigments from ecosystems around the world. Further, because changes in visible (400-700 nm) spectral reflectance on the leaf surface are driven by plant pigments, the remote sensing community has taken a keen interest in observing and interpreting changes in plant pigments over space and time (Ollinger, 2010; Ustin & Gamon, 2010). In particular, there has been an exponentially increasing number of publications relating spectral indices to plant function due to, for example, the strong link between rates of photosynthesis/CO_2 uptake/light-use efficiency (LUE) and the xanthophyll cycle (Gamon et al., 1992; Peñuelas et al., 1995). For this reason, it is important that the theory used in the extrapolation of remotely sensed vegetation indices without direct validation from leaf level pigment data is well established (Garbulsky et al., 2011). A step forward would be to gain a better understanding of how xanthophyll cycle components vary across space and time (Gamon & Berry, 2012) in response to environmental conditions, yet a compilation of published investigations related to these important plant pigments is lacking. For this reason, our goals were threefold:

1) Investigate the effect of xanthophyll pool constituents (bulk xanthophyll cycle pool size, and xanthophyll interconversion rates) on photosynthetic capacity and non-photochemical quenching in arctic willow, as compared to two greenhouse grown crops.
2) Compare xanthophyll pool sizes in the arctic with similarly collected (sun exposed leaves in the field during peak photosynthesis, previously published) pigment data spanning a wide range of environmental gradients.
3) Investigate the climatic drivers of bulk xanthophyll cycle pool size broadly using geographical climate metrics: mean annual temperature (MAT), standard deviation of MAT, actual evapotranspiration (AET), mean annual precipitation (MAP), absolute latitude, and the aridity index (AI).

4.2. Methods

4.2.1. Study area

This study took place in the Northern Alaska tundra during peak growing season (July 6-16) at the Arctic Long Term Ecological Research Station (LTER) at Toolik Lake (68.63°N, -149.60°W). Leaves from *Salix pulchra* were examined, as this is one of the primary shrubs attributed to shrub expansion in the arctic associated with climate change (Myers-Smith et al, 2011). All sampled leaves were fully expanded and were chosen subjectively to ensure that sun, shade, and a mix of sun/shade leaves were chosen. Sun/shade conditions were quantified using a using a LI-COR model LAI-2000 (Lincoln, NE, USA), and data was collected during diffuse sky conditions to reduce sun/sensor geometry effects (Bréda et al., 2003). To encompass the top, middle and lower third of the measured LAI data, LAI values < 0.5 were determined to be sun leaves, 1.5 > LAI > 0.5 were considered mixed, and LAI values > 1.5 were determined shade leaves. The mean shrub height was ~ 1 meter tall, and samples were taken from a total of eight shrubs in the moist acidic tundra complexes near the Toolik Lake LTER site. This ecosystem is dominated by shrubs (*S. pulchra, S. alaxensis, Betula nana)* and graminoids, with the dominant plant communities including *Eriophorum vaginatum-Sphagnum* and *Carex bigelowii-Sphagnum*, and average soil pH < 5.5). MAT for this region is -8.73° C and MAP is 164.47 mm.

4.2.2. Experiment protocol

In the analysis of bulk xanthophyll cycle pool size, expressed on a total chlorophyll basis (mmol V + A +Z, mmol Chl a + b $^{-1}$), a total of 94 leaf samples encompassing 33 sun-exposed leaves, 39 mixed sun/shade leaves, and 22 shade leaves were analyzed. Of these samples, a total of 40 leaves were taken back to the laboratory for dark-acclimation and eventual exposure to full sunlight to induce xanthophyll cycle interconversion. Different sampling protocols were used for pigment extraction in the field and laboratory experiment. In the field, leaves were removed during mid-day and brought back to the laboratory for foliar gas exchange analysis (section 4.2.3). Following gas exchange work, a 0.25 cm^2 disk of leaf tissue was removed using a cork borer and brought to a -80°C freezer. For this initial part of the experiment protocol, we were only interested in quantifying bulk xanthophyll cycle pool size and therefore kept time between leaf removal and freezer placement < 24 hrs. On the contrary, for the leaf samples used in the laboratory experiment, leaf punches were

immediately frozen between blocks of dry ice for determination of xanthophyll pigment composition and rates of interconversion. While only single leaves were removed for the bulk xanthophyll/photosynthesis analysis, laboratory analysis leaves remained on the stem with 5-10 leaves remaining and facing all angles. Experiment protocol in the laboratory was similar to Magney et al., 2014; whereby leaves were dark acclimated in ample water for > 2hrs to allow for the relaxation of thermal energy dissipation consequent with the epoxidation of the xanthophyll cycle carotenoids. Following dark acclimation, the initial pigment and Chl fluorescence emission collection, the stem was then placed under a bank of lights (high-intensity discharge metal halide lamps) facing directly towards the leaves to induce xanthophyll pigment interconversion. Leaf level irradiance ranged from 200 μmol m^{-2} s^{-1} to 1200 μmol m^{-2} s^{-1}. The range in light exposure was the result of varying leaf angles on the stem, and was quantified as photosynthetically photon flux density (PPFD) measured by the quantum sensor on the fluorimeter (described in section 4.2.5). After exposure to light for greater than three minutes, it was assumed that xanthophyll de-epoxidation occurred - at this time, a leaf pigment sample was collected and placed immediately between the blocks of dry ice, followed by PPFD and chlorophyll fluorescence emission measurements on the same leaf the pigment sample was taken on. During analysis, light intensities were binned into low (<300 μmol m^{-2} s^{-1}), medium (800> PPFD > 300 μmol m^{-2} s^{-1}), and high light (PPFD > 800 μmol m^{-2} s^{-1}).

A similar protocol was taken for the greenhouse grown species, following Magney et al., 2014. The species used for comparison were *Triticum aestivum L*. (n=19) and *Helianthus annuus L*. (n=18). Both of these annual crops were grown in a greenhouse with ample water and nutrients. Half of the *T. aestivum* and *H. annuus* plants were placed under a 50% shade cloth three weeks prior to conducting the experiment. The light environment in the greenhouse peaked at around ~1500 μmol m^{-2} s^{-1} above the canopy of "sun" exposed canopies, while leaves under the shade cloth peaked around ~ 500 μmol m^{-2} s^{-1}, which are similar to the observed light conditionsfor *S. pulchra* sun and shade leaves during the peak growing season and hence suitable for cross-comparison.

4.2.3. Pigment analysis

Leaf disks were stored at -80°C until extraction in acetone according to Adams & Demmig-Adams (1992). Pigment separation and quantification were achieved by high-

performance liquid chromatography (HPLC), as described in Gilmore & Yamamoto (1991), using an Agilent 1100 series HPLC (Agilent Technologies, Palo Alto, CA, USA) equipped with a YMC Carotenoid C-30 reverse phase column (YMC Co., Ltd, Kyoto, Japan) at 35°C with the following modification to the solvent gradient: 0–4 min (72 : 8 : 3, acetonitrile : methanol : 0.1MTris-HCl (pH 8.0)) followed by a linear gradient to 80% (4 : 1, methanol : hexanes) from 4 to 40 min, and the completion of the quantification with the latter mobile phase. The level of de-epoxidation of the xanthophyll cycle was expressed as the conversion state as a fraction of the total xanthophyll cycle pool (Z + A)/(V + A + Z), because of the involvement of Z and A in the energy dissipation process (Gilmore &Yamamoto, 1993). Bulk xanthophyll cycle pool size (mmol (V + A +Z) mmol Chl a + b $^{-1}$) were expressed on a per chlorophyll basis to allow for cross-comparison to other studies as total xanthophyll cycle pool size could vary depending on HPLC procedure used. Further, differences in leaf thickness across species would add variability to xanthophyll cycle pool size expressed on a leaf area basis.

4.2.4. Foliar gas exchange

Foliar gas exchange data was only conducted on the 68 leaves that were used in the field extraction experiment described above. Mature, fully expanded leaves were brought back to the laboratory and were immediately sampled. Leaf gas exchange measurements were conducted within a 12-15 hour period after harvest to avoid leaf wilting. In the lab, four prepped and calibrated gas exchange analyzers (IRGA LI-6400XT Portable Photosynthesis System, LiCOR) were used to obtain CO_2 fluxes of photosynthesis and respiration for leaves on each of the branch tips. Leaf selection was determined based on the size (closest to the cuvette size of 6 cm^2) and flatness of the leaf. The gas-exchange method from Heskel et al. (2013) was used to obtain light curves for each sample. Following light-response curve measurements, leaf area was measured using a leaf area meter (LI-3100, LI-COR Inc., Lincoln, NE, USA). During processing of the gas exchange data, leaf area was corrected for if the leaf did not fill the 6 cm^2 cuvette, as rate calculations are based on the leaf area. Maximum light saturated net photosynthetic rate (A_{max}) was estimated by fitting the data to a rectangular hyperbolic function (Excel Solver, Microsoft, Redmond, WA, USA) (Heskel et al., 2013).

4.2.5. Chlorophyll fluorescence emission

Chlorophyll fluorescence measurements were only conducted on the 40 leaves that were brought back to the laboratory for the dark light transition experiment to quantify thermal energy dissipation via non-photochemical quenching (NPQ), bearing in mind pigment analysis was only done on 26 of these leaves. An FMS2 fluorimeter (Hansatech Instruments, Kings Lynn, Norfolk, UK) was used to quantify parameters associated with Chl fluorescence emission. Measurement of the maximal fluorescence emission (F_m) during exposure to a 0.8-s saturating pulse of light (> 3000 μmol m^{-2} s^{-1}) generated by the instrument was collected immediately after dark adaption. After a period of acclimation sufficient to allow fluorescence during illumination (i.e. F_s) to achieve steady state (c.2–5 min), the maximal fluorescence (F_m') during exposure to a saturating pulse of light was recorded. NPQ of chlorophyll fluorescence was calculated as $[(F_m/F_m') - 1]$ according to Bilger & Björkman (1990). Variable over maximal fluorescence emission (F_v/F_m) was used to indicate conditions of dark-adapted leaves. F_v/F_m in this context is used to represent the degree of stress incurred by the plant (Maxwell & Johnson, 2000).

4.2.6. Meta-analysis

A meta-analysis with a consistent selection procedure was conducted to compare bulk xanthophyll cycle pool size (mmol (V + A +Z) mmol Chl a + b $^{-1}$) globally to those collected from *S. pulchra*. Due to the variation in sampling time and analysis protocol, expressing VAZ on a Chl_{ab} basis provides a consistent ratio for cross-comparison, and is the most widely used way to express bulk xanthophyll. Similar to the arctic dataset, we only used data from studies that were sampled close to the particular ecosystems peak photosynthetic period. For this reason, studies including overwintering evergreens (e.g., Adams & Demmig-Adams, 1995), for example – though also experiencing stress induced increases in xanthophylls – were not used in this study. For each species at each site, the mean value for VAZ/Chl_{ab} pool was used. It is well known that shade leaves have lower xanthophyll cycle pool size than sun leaves, so to avoid biasing towards low xanthophyll cycle pool size in other ecosystems, we only chose to use reported values from sun exposed leaves. Similarly, in order to avoid complications due to experimentally-imposed nutrient, water, temperature, or otherwise stress, only control (non-manipulated) data from recently matured leaves in the natural field environment were used (except for data from the "urban" and "agricultural" biome). All

agricultural and urban sites fall under the shrubland/woodland biome (Fig. 4.2), but due to the manipulated and highly impacted environment caution should be taken when cross comparing with data from natural field conditions. Published rates of xanthophyll interconversion and Z+A retention are difficult to interpret because dark to light transition experiments and the exact conditions the leaves were exposed to is difficult to compare across studies, and were left out of the analysis.

Fig. 4.1 shows a map of the latitude and longitude of bulk xanthophyll pool (mmol (V + A +Z) mmol Chl a + b $^{-1}$) data used in the meta-analysis. The distribution of points highly favors Northern hemisphere temperate climates. In some cases, studies were conducted at the same field location and therefore the points on the map do not add up to the complete list of the 39 studies seen in Table 1. Biome designations were assigned to each location according to Wright et al., 2004 and Whittaker et al., 1996 and can be seen in Fig. 4.2. Figs. 4.1 & 4.2 show the lack of published xanthophyll pool data in more extreme ecosystems such as the desert, tundra, boreal forest, and tropical/tropical seasonal rainforests. Because the biome distribution of studies here highly favors temperate and shrubland/woodland biomes, climate data was used in a continuous fashion to examine the effect of broad ecosystem climate characteristics on xanthophyll accumulation.

4.2.7. Climate data

Monthly temperature, precipitation and potential evapotranspiration (PET) data from 1981-2010 were acquired from the Climatic Research Unit (CRU) TS3.22 dataset (Harris et al., 2013). These data cover global land surfaces at a 0.5-degree spatial resolution as derived from long-term high-quality observations. We applied a modified Thornthwaite Water Balance Runoff model (e.g., Willmott et al., 1985) using a pre-defined 150-mm soil available water holding capacity to derive monthly actual evapotranspiration (AET), aridity index (MAP/PET), and climatic water deficit (PET-AET). Climate summaries were compiled from annual mean temperature, cumulative precipitation, climatic water deficit, AET and PET co-located at each of the site locations. We considered both 30-year climate normals, as well as the standard deviation over the 1981-2010 time period. After Wright et al., 2004 (MAT, MAP) and Atkin et al., 2015 (AI, absolute Latitude), only annual climate metrics were used to quantify the growing environment. Climate information used to compute metrics used here, as

well as the location, number of species, and total xanthophyll cycle pool size are reported in Table 1.

4.2.8. Statistical Analysis

Data were compared using *t*-tests to search for statistically significant differences ($p < 0.05$) between xanthophyll cycle constituents, NPQ, and A_{max}, among light environments, species, and biomes. As this study primarily focuses on the interconversion rates of xanthophylls in arctic willow, an analysis of variance (ANOVA) was only conducted between annual crop species and *S. pulchra*. Simple linear regression analysis using a Pearson's correlation coefficient (r) was done to examine the response of xanthophyll cycle pool size to generalizable climate conditions. A multiple linear regression analysis was conducted to highlight the complimentary effects of extreme temperatures, aridity, and xanthophyll accumulation. To meet the assumptions required to perform multiple regression analysis, tests for collinearity, normality of residuals, homogeneity of error variances, and independence of error terms were tested.

4.3. Results

4.3.1. Xanthophylls, photosynthetic capacity, and F_v/F_m of sun/shade S.pulchra leaves

Fig 4.3a shows differences in bulk xanthophyll per chlorophyll content of shade (n=22), mixed sun/shade (n=39), and sun leaves (n=33) in *S. pulchra.* A stepwise increase in VAZ/Chl_{ab} according to sun exposure shows a clear pattern of the increasing need for investment in photoprotective pigments in arctic willow. Means and standard deviations of pigment pools are 86.7 ± 14.5, 107.76 ± 17.8, and 168.4 ± 24.3 for shade, mixed, and sun leaves, respectively. A statistically significant ($p < 0.05$) difference in xanthophylls on a chlorophyll basis between all light environments was observed. Differences in the photosynthetic capacity (A_{max}) of these same leaves, with a slight increase in A_{max} in the outer parts of the canopy were observed, though not statistically significantly different (Fig. 4.3b). Means and standard deviations of photosynthetic capacities are 12.4 ± 1.88, 15.1 ± 3.09, and 15.2 ± 2.89 for shade, mixed, and sun leaves, respectively. Fig 4.3c shows the dark adapted F_v/F_m values from leaves used in the laboratory experiment (sun n = 20, shade n = 20). There is a statistically significant difference in F_v/F_m with means and standard deviations of 0.84 ±0 .01, and 0.80 ± 0.01, for shade and sun leaves, respectively (Fig. 4.3c).

4.3.2. Xanthophyll cycle interconversion and non-photochemical quenching

Levels of xanthophyll cycle interconversion (Z+A/V+A+Z) and non-photochemical quenching under varying light intensities are shown in Fig. 4.4. There is an evident increase in Z and A concentration when the shade grown *T. aestivum* and *H. annuus* were exposed to low and medium light; and a significant increase at only the lowest light level for arctic willow (Fig. 4.4a). A similar pattern can be found, albeit at a greater magnitude in the sun grown plants, where a general stepwise increase in Z + A interconversion occurs under increasing light, with statistically significant within species jumps at low light for wheat; low, medium, and high light for sunflower, and low light for arctic willow (Fig. 4.4b). There was a statistically significant difference between sun and shade plants in each species at all light levels except for wheat, where no statistically significant change between sun and shade plants exist.

There was a statistically significant difference at all light levels between the arctic willow and the annual crops, with high levels of Z & A in the dark acclimated willow. Saturation of Z + A concentration at low light intensities occurs at low light levels for *S. pulchra*, with no apparent saturation in the annual crop species (*T. aestivum* and *H. annuus*).

NPQ show a similar stepwise increase under increasing light intensities across all species coincident with xanthophyll interconversion; however, saturation under low and medium light for arctic willow does not persist, with a statistically significant NPQ jump under high light intensities (Fig. 4.4c,d). For both shade and sun leaves, a statistically significant within species NPQ increase occurred at all light levels for all species except under low light in shade *T. aestivum*, medium light under sun *T. aestivum*, and medium light in both sun and shade *S. pulchra* leaves. NPQ is statistically significantly higher in *S. pulchra* than both *T. aestivum* and *H. annuus* at low light for both shade and sun leaves, and medium light for sun leaves. Further, low, medium, and high light NPQ data is significantly higher in sun than shade leaves for *S. pulchra.*

4.3.3. Comparing arctic xanthophyll cycle pool size across biomes with a meta-analysis

Biome delineation in the bar chart in Fig. 4.5 was taken from Fig. 4.2. Fig. 4.5 reiterates the lack of species and studies conducted in environments prone to more extreme temperatures and water deficits. The diversity of species used in this meta-analysis tends to be

representative of the relative species diversity in each biome, but it is worth noting that several studies which assessed a wide range of species carotenoid pools in the tropical rainforest are heavily influencing the diversity of values used here (Königer et al., 1995, Matsubara et al., 2009). No statistically significant difference existed between xanthophyll cycle pool sizes among the tundra, desert, and boreal forest biome; however, statistically significant differences exist between these three biomes and all other biomes (not including agricultural and urban).

4.3.4. Climate metrics driving xanthophyll pigment pools globally

Fig. 4.6 shows the simple linear regressions between mean site xanthophyll pool (with SD error bars) and trends in MAT (6a, r = -0.49; root mean square error (RMSE) = 35.3 VAZ/Chl_{ab}); standard deviation of MAT (6b, r = 0.48; RMSE = 35.5 VAZ/Chl_{ab}); AET (6c, r = -0.49; RMSE = 35.2 VAZ/Chl_{ab}); MAP (6d, r = -0.45; RMSE = 36.2 VAZ/Chl_{ab}); absolute latitude (6e, r = 0.45; RMSE = 36.3 VAZ/Chl_{ab}); and AI (6f, r = -0.38; RMSE = 37.5 VAZ/Chl_{ab}).

All assumptions for the multiple regression analysis performed in Fig. 4.7 were met and both of the predictor variables (MAT and MAP) were significant predictors. The slope of the best fit plane is highly significant ($p=1.93e^{-11}$), with a coefficient of determination (R^2) of 0.28, and a RMSE of 36.52 VAZ/Chl_{ab}. The multiple regression did improve predictive capacity of xanthophyll pigment pools substantially, but predictive model construction was beyond the scope of this research; rather, we are interested in the general relationship between xanthophyll cycle pool size and generalizable climate conditions. Unlike Fig. 4.6, standard deviations of the species means were not placed on the 3D-scatter plot; rather, a line was drawn through points coming from a similar study to highlight the range of inter-species pools from the same study.

4.4. Discussion

This study presents new insights regarding the accumulation of bulk xanthophyll cycle constituents during peak photosynthesis across environmental gradients, with special attention to an abundant arctic species, *S. pulchra*. Increasingly high levels of xanthophyll pigments were found in sun/shade and sun exposed leaves of the small (<1.5 m tall) and relatively sparse *S. pulchra* canopy. High xanthophyll interconversion rates and zeaxathin retention

following dark adaption suggest that these high xanthophyll cycle pool size undergo near complete inter-conversion at low light. Despite the high capacity for the employment of photoprotective mechanisms in this arctic willow species, *S. pulchra* leaves show modestly higher photosynthetic capacities (A_{max}) and higher PSII efficiencies (F_v/F_m) than have been observed in previous studies with similarly high xanthophyll cycle pool size (see section 4.4.1.. for further discussion).

The initial focus on quantifying the capacity for thermal energy dissipation in the arctic spurred a meta-analysis of higher plant species pigment pools from 39 published studies of 155 species, and results suggest that the bulk xanthophyll pool sizes found in sun leaves in an arctic willow are statistically significantly higher than those reported from plants in other biomes, with a trend towards higher xanthophyll cycle pool size in ecosystems prone to more extreme temperatures and water availabilities. Recognizing that the meta-analysis was limited by species and field locations in ecosystems that are characterized by more stressful growth conditions such as the arctic, we highlight the need for further research to build upon these values as baseline data in the context of global change (see section 4.4.2 for further discussion). Further, regardless of limited biome specific data points in the desert, boreal forest, and tundra, this study utilized continuous climate metrics used to quantify generalizable growing conditions at each field location, and showed significantly negative relationships between bulk xanthophylls and MAT, MAP, ET, and AI; and significantly positive relationships between xanthophyll cycle pool size and abosolute latitude and standard deviation of MAT (see section 4.4.3 for further discussion).

4.4.1. High xanthophyll content and interconversion rates in the arctic

Though the role of the xanthophyll cycle in thermal energy dissipation is remarkably complex, it is well understood that plants exposed to increasing environmental stress rely on photoprotective mechanisms to dissipate excess light away from PSII (Demmig-Adams & Adams, 2006). Contrary to findings from this study, an increase in xanthophyll cycle constituents generally corresponds decreasing photosynthetic capacities (Demmig-Adams & Adams, 1996). In the introduction of this paper we presented two opposing hypotheses regarding our expectations for high or low capacity for photoprotection in the arctic. The former resulting from increased environmental stress at high latitudes, and the latter resulting from diffuse skies and relatively low light intensity.

Arctic vegetation is nutrient limited, primarily by nitrogen and phosphorus, though it is projected that increasing air temperatures in the arctic will increase soil temperatures, microbial activity, and nutrient availability (Shaver et al., 1998; Hobbie et al., 2002). This nutrient limitation hypothesis, whereby slow nitrogen mineralization constrains plant growth and ecosystem carbon storage, has been extensively studied in experimental fertilization plots across the arctic (e.g., Mack et al., 2004). The high xanthophyll cycle pool size found in the arctic could be explained by several environmental conditions that are all inter-related; whereby climate conditions control thaw layer depth and therefore limit nutrient availability. Nutrient limitation has been widely attributed to substantial increases in xanthophyll cycle pool size for crops grown in the greenhouse (Verhoeven et al., 1997) and in the field (Khamis et al., 1990; Tóth et al., 2002); additionally, N-limited plants have shown elevated levels of antioxidant enzymes such as superoxide dismutase, ascorbate peroxidase, and glutathione reductase (Logan et al., 1999), which are all involved in the detoxification of ROS (Anderson et al., 1992; Grace and Logan 1996). Given this dataset we cannot quantify the exact stressor or biochemical mechanism contributing to photoprotection, but the bulk xanthophyll cycle pool size shown here could serve as a baseline to improve interpretation of plant responses to environmental conditions – whereby, remote sensing techniques to quantify bulk xanthophyll pools (using a 'dark-state' photochemical reflectance index, PRI_o, Gamon & Berry, 2012; Magney et al., *in review*), for example, could be used as a rapid indicator of plant adaptation to the environment.

It becomes difficult quickly to compare xanthophyll cycle pools under extreme conditions with those found during the "least stressful" time in the arctic, which is why our meta-analysis tried to mimic this by only using data that was similarly sampled during some of the "least-stressful" times of the season. Nonetheless, if we compare our results to data from overwintering species in winter, when cold temperatures inhibit plant physiological function, xanthophyll cycle pool size during peak summer in *S. alexensis* would be considered low. For example, Adams et al., 2002 showed that sun leaves of *Vinca minor*, have V+A+Z pools (in mmol mol^{-1} Chl) that reach up to 156 ± 1 in October, 480 ± 78 in January, and 203 ± 33 in May, before settling back around 127 ± 11 during the summer. In the same study, the seasonal fluctuation of xanthophyll per Chl pools in sun exposed *Pseudotsuga menziesii* and *Pinus ponderosa* needles range from ~100 mmol mol^{-1} Chl in the spring when photosynthesis

is the highest, to ~150 mmol mol^{-1} Chl in the summer when photosynthesis declined, and up to ~225 mmol mol^{-1} Chl in the winter when photosynthesis is at a minimum. Similarly, Verhoeven et al., 1999 found that bulk xanthophyll pool size increased by 33%, up to 101 ± 8 mmol mol^{-1} Chl, in *Pinus ponderosa* during the relatively mild winters experienced on the University of Colorado campus. Future studies should consider the seasonal dynamics of xanthophyll activity in arctic species, as bulk xanthophyll cycle pool size are likely to be even higher during the shoulder seasons.

The aforementioned studies also quantified (Z+A) retention rates throughout the season, and found that as plants transitioned into winter there was in increasing presence of (Z+A) relative to the bulk xanthophyll pool (V +A +Z), often reaching retention rates > 0.8. In these studies, while both the bulk xanthophyll and (Z+A) retention rates are strikingly high in the winter, they are accompanied by a substantial decline in photosynthesis. Meanwhile, the summer (Z+A) retention rates shown in *S. pulchra* are among the highest we have observed during the period of peak photosynthesis. It is worth noting that the high photoprotective capacity (Fig. 4.3a), and the saturation of Z + A interconversion at low light intensities (Fig. 4.4) of *S. pulchra* does not appear to have a substantial effect on decreases in photosynthesis (Fig. 4.3b). An explanation for this could be that high xanthophyll cycle pool size persist in the arctic because of the exposure to continuous sunlight, albeit at low relative intensities.

We can further postulate then that *S. pulchra* maintains modest levels of photosynthesis because it is adapted to maximize efficiency under the prevailing diffuse light conditions that dominate the arctic ecosystem. Fig. 4.3b suggests that there is no significant difference between shade, sun, and mixed shade/sun leaves photosynthetic rates, implying that leaves most exposed to direct solar irradiation invest more energy into photoprotective mechanisms, while maintaining the same levels of photosynthesis as leaves located inside the canopy. This finding is supported by Williams et al., 2014 who showed that photosynthetic efficiency is enhanced under diffuse light at this same field site (Arctic LTER at Toolik Lake) in arctic shrub canopies. This potentially suggests that the small, sparse canopies of *S. pulchra* are allocating resources (photoprotective xanthophylls) according to light availability to achieve maximal rates of photosynthesis throughout the canopy. We hypothesize that local stress conditions place constraints on photosynthetic capacity equally throughout the small

canopy, and investment in photoprotective mechanisms vary throughout the canopy to account for this. However, it is extremely difficult to quantify the light regime for every leaf sampled, and therefore we conservatively only binned the data into three light categories based on LAI values collected at each leaf sample location.

Complimentary to the notion that high xanthophyll cycle pool size are necessary in shade and sunlit portions of the canopy, high rates (Z+A) retention in dark acclimated leaves were observed (>0.23). This is likely due to the necessity for sustained thermal dissipation under near continuous sunlight at high latitudes. The lack of full Z+A relaxation upon darkening of leaves and high NPQ values under low intensity light in arctic willow suggest that *S. pulchra* likely maintains an actual trans-thylakoid pH gradient (ΔpH), allowing sustained thermal energy dissipation to occur independent of rapidly occurring flexible energy dissipation (Gilmore and Björkman, 1994a,b; Gilmore 1997).

The findings mentioned previously by Williams et al., 2014 are supported by data from the laboratory experiment here, where (Z+A) inter-conversion (Fig. 4.4a,b) saturates at low light intensities. This may suggest that the maximum efficiency for photosynthesis is achieved at low light, and therefore any light above ~300 μmol m^{-2} s^{-1} may be safely dissipated as heat through NPQ. Because photosynthesis is enhanced under low light in this system, the need for regulating photosynthesis via xanthophyll mediated photoprotection in this ecosystem could decrease in the near future as predicted climatic warming will increase nutrient availability (Post et al., 2009) and result in increased cloudiness in the arctic (Vavrus et al., 2009).

Contrary to (Z+A)/(V+A+Z) saturation at low light, results from our laboratory experiment suggest that NPQ is potentially being controlled at high light by something other than the xanthophyll cycle (Fig. 4.6 c,d). While NPQ in wheat and sunflower increases with increasing light coincident with a stepwise increase in (Z+A)/(V+A+Z) inter-conversion, NPQ in *S. pulchra* saturates at medium light (similar to (Z+A)/(V+A+Z)) but increases to the same magnitude as NPQ observed in annual crops in high light (while (Z+A)/(V+A+Z)) remains saturated). This could highlight the role of non-zeaxanthin induced NPQ, which could potentially be driven by Lutein, which has been proposed to act as a quencher of excited $^{1}Chl^{+}$ in the ΔpH-regulated mechanism of NPQ, but this remains unclear (Jahns & Holzwarth, 2012). Further, the relative magnitude of NPQ is an intriguing comparison between these

species, whereby higher NPQ values in *S. pulchra* are found in low and medium light as compared with the annual crops, but are not significantly different from sunflower and wheat in high light (Fig. 4.4c,d). Although our study was limited from achieving high light scenarios (>1500 μmol $^{m-2}$ s^{-1}) necessary for expressing full NPQ or xanthophyll interconversion, the saturation of (Z+A)/(V+A+Z) at low light levels suggests this may not have been necessary in this study. On the contrary, the continually increasing NPQ values might be explained by other important photoprotective mechanisms such as antioxidations or tocopherols that might account for a lack of xanthophylls in NPQ (Müller et al., 2001, Robinson et al., 2005).

4.4.2. Functional converge of xanthophyll pigments according to growing conditions

Recognizing that the motivation behind conducting a meta-analysis of xanthophyll pigment pools was to develop means of comparison to the arctic willow dataset presented here, our meta-analysis is placed very much in the shadows of two large global plant trait datasets (e.g., Wright et al., 2004; Atkin et al., 2015). The limited datasets and lack of consistencies in sampling protocol reduced our meta-analysis from over 100 published papers on the xanthophyll cycle in higher plants to 39 studies. The relative scarcity of xanthophyll pigment data is due to the comparatively new nature of xanthophyll related research, not gaining traction until the early-mid 1990s. Additionally, the expensive, time-consuming, and difficult nature of HPLC methods for quantifying xanthophylls has hampered the widespread adoption of types of analyses. For this reason, we established a protocol that enabled patterns to be examined across biomes and climate conditions. Unfortunately, this limited our dataset to two studies in the desert biome, three in the tropical rainforest, and three in the boreal forest. Nonetheless, there is a convincingly statistically significant trend towards increasing xanthophyll cycle pool size across a gradient from the cold, dry arctic to the warm, moist tropics.

Comparative ecophysiological research has highlighted both the divergent and convergent properties of plant traits to their environment but is complicated by the scale at which measurements are being made (Ehleringer and Field 1993; Meinzer 2003). A similar complication arises with this dataset, whereby micrometeorological and abiotic conditions present during each sample used in this meta-analysis are likely to vary widely regardless of our attempt to only use xanthophyll cycle pool size sizes collected under similar conditions. Somewhat surprisingly, there is much consistency in the range (determined by standard

deviations bars seen in each biome (Fig. 4.5)) of values experienced over the wide diversity of species in some biomes. Our interpretation is thus that there may be some degree of functional convergence in the accumulation of xanthophyll pigments according to environmental conditions in which these species are found. This pattern is also found in studies that do not report xanthophylls according to our protocol. For example, high levels of sustained thermal energy dissipation or high concentrations of Z+A have been observed in evergreen conifers adapted to extreme environments (i.e., Ottander er al., 1995; Zarter et al., 2006a,b,c). As more research relating bulk xanthophyll cycle pool size to total chlorophyll content emerges, we suspect that the trend across biomes shown here will remain consistent.

There is little debate that fluctuations in xanthophyll cycle components are good indicators of photoprotection, canopy light-use efficiency, and plant stress. A global compilation of baseline xanthophyll cycle pool size over a wide range of biomes could provide researchers with new techniques to monitor environmental change. With the advent of the increasingly popular remotely sensed vegetation index, the photochemical reflectance index (PRI) (Gamon et al., 1992; Garbulsky et al., 2011) - which is sensitive to changes xanthophyll pigment components - it is important that the plant research community gains a better understanding of the dynamics and controls on xanthophyll accumulation and modulation from seconds and seasons before we can be confident that satellite data may explain variability in photosynthetic light-use efficiency across large scales in space and time (i.e., Hilker et al., 2012; Hall et al., 2012). Further, because satellite data cannot collect continuous data over one location, it is especially important that the constitutive component (bulk xanthophyll pool) of the PRI inferred xanthophyll status is recognized (Gamon and Berry, 2012). Because xanthophyll cycle components are known to vary widely depending on light environment, time of year, and climate conditions (Demmig-Adams 2012), and if there is indeed functional convergence of xanthophyll pigment pools, baseline PRI measurements should, in theory, reveal the same patterns - which could promote the eventual global mapping of baseline "xanthophyll status" to more accurately interpret light-use efficiency data. Eventually, satellite data on photosynthetic light efficiency – inferred from the physical relationship between spectral reflectance and the xanthophyll cycle - could be incorporated into global terrestrial biosphere models that currently use plant functional types and climate

variability to represent carbon exchange between the plants and the atmosphere (Sitch et al., 2007).

4.4.3. Cold, dry, and more extreme climates promote greater xanthophyll accumulation

To further support the hypothesis that environmental conditions characteristic of global biomes seen in Fig. 4.5, we used the best available climate data to characterize in a more continuous fashion the growing conditions experienced at each one of the field locations used in the meta-analysis. The addition of data from a common species found in the arctic tundra rounds out this analysis by providing an endmember (cold, arid) on the global spectrum of climate conditions. In Figs. 4.6 and 4.7, data from the tundra xanthophyll cycle pool size falls on the low end of the spectrum for MAT, AET, and MAP, and on the high end of the spectrum for absolute latitude, standard deviation of MAT, and the AI. Similarly, data from the tropical rainforest, desert, and boreal biomes fall out as endmembers on this spectrum. Data in the middle of these relationships come from the highest density of reported values in temperate and semi-arid ecosystems and yet, still show relatively consistent trends across climate metrics, further strengthening the highly significant positive relationship between MAT, MAP, ET, AI and xanthophyll abundance reported here.

It could be argued that annual climate data does not accurately represent the growing conditions present at the time of sampling; however, seasonal metrics, such as temperature of the warmest quarter (as used in the global meta-analysis of leaf respiration in Atkin et al., 2015), might not be representative of universal plant responses to environmental conditions. We instead conducted a broad analysis that attributes common abiotic stressors, such as the range of temperatures experienced at each field location (std. dev. of MAT), water availability (AI), and water use (AET), to the relate the accumulation of xanthophyll constitutes as photoprotective mechanisms in extreme environments. Nonetheless, a substantial component of the response variance (RMSE ~ 35 VAZ/Chl_{ab} across all metrics) of bulk xanthophyll cycle pool size is not accounted for by annual climate metrics, further supporting the notion that other characteristics, such as soil characteristics, biotic stressors, and nutrient availability (Demmig-Adams & Adams, 2006) are influencing bulk xanthophyll cycle pool size across broad environmental gradients.

4.5. Conclusion

This paper provides the first published record of xanthophyll pigment data related to thermal energy dissipation in an arctic tundra shrub species. In *S. pulchra* we found that leaves at the top of the canopy have greater pools of xanthophyll cycle carotenoid pigments responsible for regulating photosynthesis, achieving similar photosynthetic capacity as those in inner canopy leaves. This finding resonates with previous research that shows that photosynthetic efficiency is enhanced under diffuse light in the arctic, with full inter-conversion of the xanthophyll cycle at low light. We build on previous research highlighting the role of photoprotective mechanisms in the regulation of photosynthesis by noting the equally modest capacity for carbon assimilation throughout this small, sparse canopy. The high pools of xanthophyll constituents expressed on a chlorophyll basis found in this arctic willow prompted a meta-analysis, where we showed - with datasets collected similarly to the tundra dataset - that there is evidence of a relationship between biome and bulk xanthophyll cycle pool size. A highly significant positive relationship between MAT, MAP, AET, AI, and bulk xanthophyll cycle pool size imply that ecosystems prone to more stressful conditions promote xanthophyll accumulation, with an emphasis on species in cold, arid environments. This work could have implications for understanding the ecological significance of photoprotective mechanisms as a response to excess light, and may help to explain large scale fluctuations in photosynthetic capacity due to environmental stress.

References:

Adams, W. W., & Barker, D. H. (1998). Seasonal changes in xanthophyll cycle-dependent energy dissipation in Yucca glauca Nuttall. *Plant, Cell and Environment, 21*, 501–511. doi:10.1046/j.1365-3040.1998.00283.x

Adams W.W. III & Demmig-Adams B. (1992) Operation of the xanthophyll cycle in higher plants in response to diurnal changes in incident sunlight. *Planta, 186*, 390-398.

Adams, W. W., & Demmig-Adams, B. (1995). The xanthophyll cycle and sustained thermal-energy dissipation activity in Vinca minor and Euonymus kiaufschovicus in winter. *Plant Cell and Environment, 18*(2), 117–127.

Adams, W. W., Demmig-Adams, B., Logan, B. a., Barker, D. H., & Osmond, C. B. (1999). Rapid changes in xanthophyll cycle-dependent energy dissipation and photosystem II efficiency in two vines, Stephania japonica and Smilax australis, growing in the

understory of an open Eucalyptus forest. *Plant, Cell and Environment*, *22*, 125–136. doi:10.1046/j.1365-3040.1999.00369.x

Adams III, W. W., Demmig-Adams, B., Rosenstiel, T. N., Brightwell, a. K., & Ebbert, V. (2002). Photosynthesis and Photoprotection in Overwintering Plants. *Plant Biology*, *4*(5), 545–557. doi:10.1055/s-2002-35434.

Anderson, J.V., Chevone, B.I., Hess, J.L. (1992). Seasonal variation in the antioxidant system of eastern white pine needles: evidence for thermal dependence. *Plant Physiology, 98,* 501–508.

Atkin, O. K., Bloomfield, K. J., Reich, P. B., Tjoelker, M. G., Asner, G. P., Bonal, D., et al. (2015). Global variability in leaf respiration in relation to climate , plant functional types and leaf traits. *New Phytologist*.

Balaguer, L., Martinex-Ferri, E., Valladares, F., Perez-Corona, M., Baquedano, F., Castillo, F., & Manrique, E. (2001). Population divergence in the plasticity of the response of Quercus coccifera to the light environment. *Functional Ecology*, *65*, 43–59.

Barker, D. H., & Adams, W. W. (1997). The xanthophyll cycle and energy dissipation in differently oriented faces of the cactus Opuntia macrorhiza. *Oecologia*, *109*, 353–361. doi:10.1007/s004420050093

Barker, D. H., Logan, B. a., Iii, W. W. A., & Demmig-Adams, B. (1998). Photochemistry and xanthophyll cycle-dependent energy dissipation in differently oriented cladodes of Opuntia stricta during the winter. *Australian Journal of Plant Physiology*, *25*, 95. doi:10.1071/PP97106

Barker, D. H., Adams, W. W., Demmig-Adams, B., Logan, B. a., Verhoeven, A. S., & Smith, S. D. (2002). Nocturnally retained zeaxanthin does not remain engaged in a state primed for energy dissipation during the summer in two Yucca species growing in the Mojave Desert. *Plant, Cell and Environment*, *25*, 95–103. doi:10.1046/j.0016-8025.2001.00803.x

Bréda, N. J. J. (2003). Ground-based measurements of leaf area index: a review of methods, instruments and current controversies. *Journal of Experimental Botany*, *54*(392), 2403–17. doi:10.1093/jxb/erg263

Bilger W, Björkman O. (1990). Role of the xanthophylls cycle in photoprotection elucidated by measurements of light-induced absorbance changes, fluorescence and photosynthesis in leaves of Hedera canariensis. *Photosynthesis Research, 25,* 173–186.

Björkman, O., Demmig-Adams, B. (1994). Regulation of photosynthetic light energy capture, conversion, and dissipation in leaves of higher plants. In 'Ecophysiology of Photosynthesis'. (Eds E.-D. Schulze and M. M. Caldwell.) pp. 17-47. Springer-Verlag: Berlin.

Burkle, L. A., & Logan, B. A. (2003). Seasonal Acclimation of Photosynthesis in Eastern Hemlock and Partridgeberry In Different Light Environments. *Northeastern Naturalist*, *10*(1), 1–16.

Chapin, F.S.. (1991). Integrated responses of plants to stress. *BioScience*, *41*, 29–36.

Cheng, L. (2003). Xanthophyll cycle pool size and composition in relation to the nitrogen content of apple leaves. *Journal of Experimental Botany*, *54*(381), 385–393. doi:10.1093/jxb/erg011

Cheng, L. (2003). Xanthophyll cycle pool size and composition in relation to the nitrogen content of apple leaves. *Journal of Experimental Botany*, *54*(381), 385–393. doi:10.1093/jxb/erg011

Corcuera, L., Morales, F., Abadía, a, & Gil-Pelegrín, E. (2005). Seasonal changes in photosynthesis and photoprotection in a Quercus ilex subsp. ballota woodland located in its upper altitudinal extreme in the Iberian Peninsula. *Tree Physiology*, *25*, 599–608. doi:10.1093/treephys/25.5.599

Demmig, B., Winter, K., Kruger, A., Czygan, F.C. (1987). Photoinhibition and zeaxanthin formation in intact leaves. A possible role of the xanthophyll cycle in the dissipation of excess light. *Plant Physiology*, *84*, 218–224.

Demmig, B., Winter, K., Krüger, A., & Czygan, F. C. (1988). Zeaxanthin and the Heat Dissipation of Excess Light Energy in Nerium oleander Exposed to a Combination of High Light and Water Stress. *Plant Physiology*, *87*, 17–24. doi:10.1104/pp.87.1.17

Demmig-Adams, B., & Adams III, W. W. (1994). Capacity for Energy Dissipation in the Pigment Bed in Leaves with Different Xanthophyll Cycle Pools *. *Australian Journal of Plant Physiology*, *21*, 575–88.

Demmig-Adams B., Adams W.W. III, Logan B.A., Verhoeven A.S. (1995). Xanthophyll cycle-dependent energy dissipation and flexible PSII efficiency in plants acclimated to light stress. *Australian Journal of Plant Physiology*, *22*, 261-276

Demmig-Adams, B., Adams, W. W. (1996). Xanthophyll cycle and light stress in nature: uniform response to excess direct sunlight among higher plant species. *Planta*, *198*(3), 460–470. doi:10.1007/BF00620064

Demmig-Adams, B. (1998). Survey of Thermal Energy Dissipation and Pigment Composition in Sun and Shade Leaves. *Plant and Cell Physiology*, *39*(5), 474–482. doi:10.1093/oxfordjournals.pcp.a029394

Demmig-Adams, B., Cohu, C. M., Muller, O., & Adams, W. W. (2012). Modulation of photosynthetic energy conversion efficiency in nature: from seconds to seasons. *Photosynthesis Research*, *113*(1-3), 75–88. doi:10.1007/s11120-012-9761-6.

Ehlringer, J.R., Field, C.B. (1993). Scaling Physiological Processes: Leaf to Globe. Academic Press, New York, pp. 41–76.

Ensminger, I., Sveshnikov, D., Campbell, D. a., Funk, C., Jansson, S., Lloyd, J., et al. (2004). Intermittent low temperatures constrain spring recovery of photosynthesis in boreal Scots pine forests. *Global Change Biology*, *10*, 995–1008. doi:10.1111/j.1365-2486.2004.00781.x

Fernàndez-Martínez, J., Zacchini, M., Elena, G., Fernández-Marín, B., & Fleck, I. (2013). Effect of environmental stress factors on ecophysiological traits and susceptibility to pathogens of five Populus clones throughout the growing season. *Tree Physiology*, *33*(Blake 1983), 618–627. doi:10.1093/treephys/tpt039

Gamon, J. A., Penuelas, J., & Field, C. B. (1992). A Narrow-Waveband Spectral Index That Tracks Diurnal Changes in Photosynthetic Efficiency. *Remote Sensing of Environment*, *41*, 35–44.

Gamon, J. a., & Berry, J. a. (2012). Facultative and constitutive pigment effects on the Photochemical Reflectance Index (PRI) in sun and shade conifer needles. *Israel Journal of Plant Sciences*, *60*(1), 85–95. doi:10.1560/IJPS.60.1-2.85

Garbulsky, M. F., Peñuelas, J., Gamon, J., Inoue, Y., & Filella, I. (2011). The photochemical reflectance index (PRI) and the remote sensing of leaf, canopy and ecosystem radiation use efficienciesA review and meta-analysis. *Remote Sensing of Environment*, *115*(2), 281–297. doi:10.1016/j.rse.2010.08.023

Garcoa-Plazaola, J. I., Faria, T., Abadia, J., Abadia, A., Chaves, M. M., & Pereira, J. S. (1997). Seasonal changes in xanthophyll composition and photosynthesis of cork oak (Quercus suber L .) leaves under mediterranean climate. *Journal of Experimental Botany*, *48*(314), 1667–1674.

Gilmore A.M., Yamamoto H.Y. (1991). Resolution of lutein and zeaxanthin using a non-endcapped, lightly carbon-loaded C-18 high performance liquid chromatographic column. *Journal of Chromatography*, *543*, 137–145.

Gilmore A.M., Yamamoto H.Y. (1993). Linear models relating xanthophylls and lumen acidity to non-photochemical fluorescence quenching. Evidence that antheraxanthin explains zeaxanthin-independent quenching. *Photosynthesis Research*, *35*, 67–78.

Gilmore A.M., Bjorkman 0. (1994a) Adenine nucleotides and the xanthophyll cycle in leaves. I. Effects of CO2 and temperature- limited photosynthesis on adenylate energy charge and violax- anthin de-epoxidation. *Planta*, *192*, 526-536

Gilmore A.M., Bjorkman 0. (1994b) Adenine nucleotides and the xanthophyll cycle in leaves. II. Comparison of the effects of CO2 and temperature-limited photosynthesis on photosystem II flu- orescence quenching, the adenylate energy charge and violax- anthin de-epoxidation in cotton. *Planta, 192,* 537-544

Gilmore A.M. (1997). Mechanistic aspects of xanthophyll cycle-dependant photoprotection in higher plant chloroplast and leaves. *Physiologica Planetarium,*99:197–209.

Grace, S.G., Logan, B.A. (1996). Acclimation of foliar antioxidant systems to growth irradiance in three broad-leaved evergreen species. *Plant Physiology, 112,* 1631–1640

Hall, F. G., Hilker, T., & Coops, N. C. (2012). Data assimilation of photosynthetic light-use efficiency using multi-angular satellite data: I. Model formulation. *Remote Sensing of Environment*, *121*, 301–308. doi:10.1016/j.rse.2012.02.007

Han, Q., Katahata, S., Kakubari, Y., & Mukai, Y. (2004). Seasonal changes in the xanthophyll cycle and antioxidants in sun-exposed and shaded parts of the crown of Cryptomeria japonica in relation to rhodoxanthin accumulation during cold acclimation. *Tree Physiology*, *24*, 609–616.

Harris, I., Jones, P.D., Osborn, T.J. and Lister, D.H. (2014). Updated high-resolution grids of monthly climatic observations - the CRU TS3.10 Dataset. *International Journal of Climatology*, *34*, 623-642. doi: 10.1002/joc.3711

Heskel, M., Greaves, H., Kornfeld, A., Gough, L., Atkin, O. K., Turnbull, M. H., Shaver, G., Griffin, K. L. (2013). Differential physiological responses to environmental change promote woody shrub expansion. *Ecology and Evolution*, *3*(5), 1149–62. doi:10.1002/ece3.525

Hilker, T., Hall, F. G., Tucker, C. J., Coops, N. C., Black, T. A., Nichol, C. J., … Munger, J. W. (2012). Data assimilation of photosynthetic light-use efficiency using multi-angular satellite data: II Model implementation and validation. *Remote Sensing of Environment*, *121*, 287–300. doi:10.1016/j.rse.2012.02.008

Hobbie, S. E., Nadelhoffer, K.J., Hogberg, P. (2002). A synthesis: the role of nutrients as constraints on carbon balances in boreal and arctic regions. *Plant and Soil, 242,* 163–170.

Hughes, N. M., Burkey, K. O., Cavender-Bares, J., & Smith, W. K. (2012). Xanthophyll cycle pigment and antioxidant profiles of winter-red (anthocyanic) and winter-green (acyanic) angiosperm evergreen species. *Journal of Experimental Botany*, *63*(5), 1895–905. doi:10.1093/jxb/err362

Jahns, P., & Holzwarth, A. R. (2012). The role of the xanthophyll cycle and of lutein in photoprotection of photosystem II. *Biochimica et Biophysica Acta*, *1817*(1), 182–93. doi:10.1016/j.bbabio.2011.04.012

Jiang, C. D., Li, P. M., Gao, H. Y., Zou, Q., Jiang, G. M., & Li, L. H. (2005). Enhanced photoprotection at the early stages of leaf expansion in field-grown soybean plants. *Plant Science*, *168*, 911–919. doi:10.1016/j.plantsci.2004.11.004

Kanervo, E., Suorsa, E., Aro, E.M. (2005). Functional flexibility and acclimation of the thylakoid membrane. *Photochemical Photobiological Science*, 4, 072–1080.

Khamis, S., Lamaze, T., Lemoine, Y., Foyer, C. (1990). Adaptation of the photosynthetic apparatus in maize leaves as a result of nitrogen limitation. *Plant Physiology, 94,* 1436–1443.

Königer, M., Harris, G. C., Virgo, A., Winter, K., Winter, K., & Harris, C. (1995). Xanthophyll-Cycle Pigments and Photosynthetic Capacity in Tropical Forest Species: A Comparative Field Study on Canopy , Gap and Understory Plants. *Oecologia*, *104*(3), 280–290.

Krause, G. H., Winter, K., Matsubara, S., Krause, B., Jahns, P., Virgo, A., … García, M. (2012). Photosynthesis, photoprotection, and growth of shade-tolerant tropical tree seedlings under full sunlight. *Photosynthesis Research*, *113*, 273–285. doi:10.1007/s11120-012-9731-z

Krause, G. H., Winter, K., Matsubara, S., Krause, B., Jahns, P., Virgo, A., Aranda, J., García, M. (2012). Photosynthesis, photoprotection, and growth of shade-tolerant tropical tree seedlings under full sunlight. *Photosynthesis Research*, *113*, 273–285. doi:10.1007/s11120-012-9731-z

Kyparissis, A., P, D., & Manetas, Y. (2000). Seasonal fluctuations in photoprotective (xanthophyll cycle) and photoselective (chlorophylls) capacity in eight Mediterranean plant species belonging to two different growth forms. *Australian Journal of Plant Physiology*, *27*, 645. doi:10.1071/PP97167

Ledford, H.K., Niyogi, K.K. (2005). Singlet oxygen and photo-oxidative stress management in plants and algae. *Plant, Cell & Environment, 28,* 1037–1045.

Logan, B. a., Barker, D. H., Demmig-Adams, B., & Adams, W. W. (1996). Acclimation of leaf carotenoid composition and ascorbate levels to gradients in the light environment within an Australian rainforest. *Plant, Cell and Environment*, *19*(9), 1083–1090. doi:10.1111/j.1365-3040.1996.tb00215.x

Logan, B. A., Grace, S. C., Adams III, W. W., & Demmig-Adams, B. (1998a). Seasonal differences in xanthophyll cycle characteristics in Mahonia and antioxidants repens growing in different light environments. *Oecologia*, *116*(1/2), 9–17.

Logan, B. A., Demmig-Adams, B., Adams III, W. W., & Grace, S. C. (1998b). Antioxidants and xanthophyll cycle-dependent energy dissipation in Cucurbita pepo L . and Vinca major L . acclimated to four growth PPFDs in the field. *Journal of Experimental Botany*, *49*(328), 1869–1879.

Logan, B., Demmig-Adams, B., Rosenstiel, T., & Adams, W. (1999). Effect of nitrogen limitation on foliar antioxidants in relationship to other metabolic characteristics. *Planta*, *209*(2), 213–220.

Lovelock, C. E., & Clough, B. F. (1992). Influence of Solar Radiation and Leaf Angle on Leaf Xanthophyll Concentrations in Mangroves. *Oecologia*, *91*(4), 518–525.

Mack, M. C., Schuur, E. a G., Bret-Harte, M. S., Shaver, G. R., & Chapin, F. S. (2004). Ecosystem carbon storage in arctic tundra reduced by long-term nutrient fertilization. *Nature*, *431*(7007), 440–3. doi:10.1038/nature02887

Magney, T. S., Eusden, S. A., Eitel, J. U. H., Logan, B. A., Jiang, J., & Vierling, L. A. (2014). Assessing leaf photoprotective mechanisms using terrestrial LiDAR : towards mapping canopy photosynthetic performance in three dimensions. *New Phytologist*, *201*, 344–356.

Matsubara, S., Krause, G. H., Aranda, J., Virgo, A., Beisel, K. G., Jahns, P., & Winter, K. (2009). Sun-shade patterns of leaf carotenoid composition in 86 species of neotropical forest plants. *Functional Plant Biology*, *36*(1), 20. doi:10.1071/FP08214

Maxwell, K., & Johnson, G. N. (2000). Chlorophyll fluorescence--a practical guide. *Journal of Experimental Botany*, *51*(345), 659–68.

Meinzer, F. C. (2003). Functional convergence in plant responses to the environment. *Oecologia*, 1–11. doi:10.1007/s00442-002-1088-0

Muller, P., Li, X., & Niyogi, K. K. (2001). Update on Photosynthesis Non-Photochemical Quenching . A Response to Excess Light Energy. *Plant Physiology*, *125*(April), 1558–1566.

Myers-Smith, I. H., Forbes, B. C., Wilmking, M., Hallinger, M., Lantz, T., Blok, D, et al. (2011). Shrub expansion in tundra ecosystems: dynamics, impacts and research priorities. *Environmental Research Letters*, *6*(4), 045509. doi:10.1088/1748-9326/6/4/045509

Nakaji, T., Oguma, H., & Fujinuma, Y. (2006). Seasonal changes in the relationship between photochemical reflectance index and photosynthetic light use efficiency of Japanese larch needles. *International Journal of Remote Sensing*, *27*(3), 493–509.

Niinemets, U., Bilger, W., Kull, O., & Tenhunen, J. D. (1998). Acclimation to high irradiance in temperate deciduous trees in the field: changes in xanthophyll cycle pool size and in photosynthetic capacity along a canopy light gradient. *Plant, Cell and Environment*, *21*(12), 1205–1218. doi:10.1046/j.1365-3040.1998.00364.x

Niinemets, U., Bilger, W., Kull, O., & Tenhunen, J. D. (1999). Responses of foliar photosynthetic electron transport, pigment stoichiometry, and stomatal conductance to interacting environmental factors in a mixed species forest canopy. *Tree Physiology*, *19*(13), 839–852. doi:10.1093/treephys/19.13.839

Niinemets, Ü. (2010). A review of light interception in plant stands from leaf to canopy in different plant functional types and in species with varying shade tolerance. *Ecological Research*, *25*(4), 693–714. doi:10.1007/s11284-010-0712-4

Niyogi, K.K., Li, X.P., Rosenberg, V., Jung, H.S. (2005). Is PsbS the site of non-photochemical quenching in photosynthesis? *Journal of Experimental Botany, 56,* 375–382.

Oh, S., Iii, W. W. A., Demmig-adams, B., & Koh, S. C. (2013). Seasonal Photoprotective Responses in Needles of Korean Fir (Abies koreana) over an Altitudinal Gradient on Mount Halla , Jeju Island , Korea. *Arctic, Antarctic, and Alpine Research*, *45*(2), 238–248.

Ollinger, S. V. (2010). Sources of variability in canopy reflectance and the convergent properties of plants. *New Phytologist*, 375–394. doi:10.1111/j.1469-8137.2010.03536.x

Ottander, C., Campbell, D., Oquist, G. (1995). Seasonal changes in photosystem II organization and pigment composition in Pinus sylvestris. *Planta*, 197, 176-183

Peguero-Pina, J. J., Gil-Pelegrín, E., & Morales, F. (2013). Three pools of zeaxanthin in Quercus coccifera leaves during light transitions with different roles in rapidly reversible photoprotective energy dissipation and photoprotection. *Journal of Experimental Botany*. doi:10.1093/jxb/ert024

Peñuelas, J., Filella, I., & Gamon, J. A. (1995). Assessment of photosynthetic radiation-use efficiency with spectral reflectance. *New Phytologist*, *131*(3), 291–296. doi:10.1111/j.1469-8137.1995.tb03064.x

Porcar-Castell, A., Juurola, E., Ensminger, I., Berninger, F., Hari, P., & Nikinmaa, E. (2008). Seasonal acclimation of photosystem II in Pinus sylvestris. II. Using the rate constants of sustained thermal energy dissipation and photochemistry to study the effect of the light environment. *Tree Physiology*, *28*, 1483–1491. doi:10.1093/treephys/28.10.1483

Porcar-Castell, A., Garcia-Plazaola, J. I., Nichol, C. J., Kolari, P., Olascoaga, B., & Kuus. (2012). Physiology of the seasonal relationship between the photochemical reflectance index and photosynthetic light use efficiency. *Oecologia*, *170*, 313–323. doi:10.1007/s00442-012-2317-9

Post, E., Forchhammer, M. C., Bret-Harte, M. S., Callaghan, T. V, Christensen, T. R., Elberling, B., et al. (2009). Ecological dynamics across the Arctic associated with recent climate change. *Science (New York, N.Y.)*, *325*(5946), 1355–8. doi:10.1126/science.1173113

Robinson, S. a., Turnbull, J. D., & Lovelock, C. E. (2005). Impact of changes in natural ultraviolet radiation on pigment composition, physiological and morphological characteristics of the Antarctic moss, Grimmia antarctici. *Global Change Biology*, *11*, 476–489. doi:10.1111/j.1365-2486.2005.00911.x

Shaver GR, Johnson LC, Cades DH, Murray G, Laundre JA, Rastetter EB, Nadelhoffer KJ, Giblin AE (1998) Biomass and CO2 flux in wet sedge tundras: response to nutrients, temperature, and light. *Ecological Monographs, 68*, 75–97

Sitch, S., McGuire, a D., Kimball, J., Gedney, N., Gamon, J., Engstrom, R., et al.. (2007). Assessing the carbon balance of circumpolar Arctic tundra using remote sensing and process modeling. *Ecological Applications : A Publication of the Ecological Society of America*, *17*(1), 213–34.

Thiele, A., Krause, G., & Winter, K. (2000). In situ study of photoinhibition of photosynthesis and xanthophyll cycle activity in plants growing in natural gaps of the tropical forest. *Australian Journal of Plant Physiology*, *27*, 645. doi:10.1071/PP97167

Tóth, V. R., Mészáros, I., Veres, S., & Nagy, J. (2002). Effects of the available nitrogen on the photosynthetic activity and xanthophyll cycle pool of maize in field. *Journal of Plant Physiology*, *634*.

Ustin, S. L., & Gamon, J. a. (2010). Remote sensing of plant functional types. *New Phytologist*, *186*(4), 795–816. doi:10.1111/j.1469-8137.2010.03284.x

Vavrus, S., Waliser, D., Schweiger, A., Francis, J. (2009). Simulations of 20th and 21st century Arctic cloud amount in the global climate models assessed in the IPCC AR4. *Climate Dynamics, 33*, 1099–1115.

Verhoeven, a. S., Demmig-Adams, B., & Adams III, W. W. (1997). Enhanced Employment of the Xanthophyll Cycle and Thermal Energy Dissipation in Spinach Exposed to High Light and N Stress. *Plant Physiology*, *113*(3), 817–824.

Verhoeven, a. S., Adams, W. W., & Demmig-Adams, B. (1998). Two forms of sustained xanthophyll cycle-dependent energy dissipation in overwintering Euonymus kiautschovicus. *Plant, Cell and Environment*, *21*, 893–903. doi:10.1046/j.1365-3040.1998.00338.x

Verhoeven, a. S., Adams, W. W., & Demmig-Adams, B. (1999). The xanthophyll cycle and acclimation of Pinus ponderosa and Malva neglecta to winter stress. *Oecologia*, *118*(3), 277–287. doi:10.1007/s004420050728

Williams, M., Rastetter, E. B., Van der Pol, L., & Shaver, G. R. (2014). Arctic canopy photosynthetic efficiency enhanced under diffuse light, linked to a reduction in the fraction of the canopy in deep shade. *The New Phytologist*, *202*(4), 1267–76. doi:10.1111/nph.12750

Willmott, C. J., C. M. Rowe, Mintz, Y.. (1985). Climatology of the Terrestrial Seasonal Water Cycle. *Journal of Climatology*, 5, 589-606.

Whittaker, R. *Communities and Ecosystems* 2nd edn, 167 (MacMillan, New York, 1975).

Wright, I.J., Reich, P.B., Westoby, M., Ackerly, D.D., Baruch, Z., Bongers, F., Cavender-Bares, J., Chapin, F.S., Cornelissen, J.H.C., Diemer, M., Flexas, J., Garnier, E., Groom, P.K., Gulias, J., Hikosaka, K., Lamont, B.B., Lee, T., Lee, W., Lusk, C., Midgley, J.J., Navas, M-L., Niinemets, U., Oleksyn, J., Osada, N., Poorter, H., Poot, P., Prior, L., Pyankov, V.I., Roumet, C., Thomas, S.C., Tjoelker, M.G., Veneklaas, E. & Villar, R. (2004). The worldwide leaf economics spectrum. *Nature*, *428*(6985), 821–7. doi:10.1038/nature02403.

Yamamoto, H.Y. (1979). Biochemistry of the violaxanthin cycle in higher plants. *Pure Applied Chemistry, 51,* 639–648.

Zarter, C.R., Adams, W.W. III, Ebbert, V., Cuthbertson, D., Adamska, I., Demmig-Adams, B. (2006a). Winter downregulation of intrinsic photosynthetic capacity coupled with upregulation of Elip-like proteins and persistent energy dissipation in a subalpine forest. *New Phytologist,192,* 272–282.

Zarter, C.R., Adams, W.W. III, Ebbert, V., Adamska, I., Jansson, S., Demmig-Adams, B. (2006b). Winter acclimation of PsbS and related proteins in the evergreen Arctostaphylos uva-ursi as influenced by altitude and light environment. *Plant, Cell, & Environment, 29,* 869–878.

Zarter, C.R., Demmig-Adams, B., Ebbert, V., Adamska, I., Adams, W.W.III .(2006c). Photosynthetic capacity and light harvesting efficiency during the winter-to-spring transition in subalpine conifers. *New Phytologist, 172* ,283–292.

Tables:

Table 4.1. Summary of studies used in meta-analysis, with location, biome, annual climate metrics, number of species, and mean + SD of mol (V+A+Z) mmol Chl a + b $^{-1}$.

Study	lat	long	Biome	MAT (C)	SD MAT	MAP (mm)	AET (mm)	PET (mm)	No. sp.	VAZ/Chlab	SD VAZ/Chlab
Adams & Barker, 1998	40.22	-105.38	shrubland/woodland	7.68	0.58	463.97	463.97	1176.20	1	85.25	24.92
Adams & Demmig-Adams, 1995	40.03	-105.25	urban	7.68	0.58	463.97	463.97	1176.20	2	121.25	48.11
Adams et al., 2002 - site 1	40.01	-105.28	shrubland/woodland	7.68	0.58	463.97	463.97	1176.20	3	98.51	30.48
Adams et al., 2002 - site 2	40.00	-105.29	shrubland/woodland	6.80	0.57	456.13	456.13	1140.10	3	121.53	53.01
Adams et al.,1999	-30.83	153.00	tropical seasonal forest	19.26	0.35	1497.00	1165.30	1203.70	2	138.25	7.82
Balaguer et al., 2001	40.50	-3.48	shrubland/woodland	13.61	0.51	444.69	444.69	1114.10	1	141.33	4.50
Barker et al., 1997	40.22	-105.38	desert	7.68	0.58	463.97	463.97	1176.20	1	141.00	40.93
Barker et al., 1998	-31.42	149.00	shrubland/woodland	16.10	0.69	712.67	712.67	1145.80	1	101.00	22.83
Barker et al., 2002	36.12	-115.25	desert	18.14	0.77	166.75	166.75	2125.50	1	133.88	7.43
Burkle & Logan	43.91	-69.99	temperate forest	9.03	0.64	1273.60	811.76	817.54	2	51.50	13.50
Chen & Cheng, 2003	42.43	-76.48	agricultural	8.47	0.69	956.64	801.70	822.07	1	138.00	0.00
Chytyk et al., 2011	52.13	-106.63	agricultural	2.59	1.14	354.44	354.44	779.78	1	70.20	7.26
Corcuera et al., 2005	41.12	-1.65	shrubland/woodland	11.15	0.53	530.26	530.26	1133.00	1	84.42	27.71
Demmig-Adams & Adams 1996	40.03	-105.25	urban	7.68	0.58	463.97	463.97	1176.20	7	134.81	29.86
Demmig-Adams 1998	40.03	-105.25	urban	7.68	0.58	463.97	463.97	1176.20	17	107.65	21.80
Ensminger et al., 2004	60.75	89.38	boreal forest	-2.29	1.20	562.17	444.63	468.97	1	153.33	0.00
Fernandex-Martinez et al., 2013	42.68	12.10	temperate forest	14.07	0.46	732.31	682.52	938.46	3	35.20	5.19
Garcia-Plazaola et al., 1997	38.56	7.90	shrubland/woodland	17.52	0.39	645.68	624.37	1126.80	1	39.85	48.11
Han et al., 2004	34.98	138.45	temperate forest	16.29	0.57	2091.20	1000.50	1000.50	1	58.14	48.11
Hughes et al., 2012	36.13	-80.22	temperate forest	14.54	0.63	1116.80	1036.80	1077.10	7	58.10	13.69
Jiang et al., 2005	36.10	117.01	agricultural	13.01	0.53	683.99	683.99	1115.30	1	132.40	32.73
Koniger et al., 1995	9.01	-79.50	tropical rainforest	25.51	0.28	2848.20	1158.40	1257.40	12	89.55	16.64
Krause et al., 2012	9.00	-79.00	tropical rainforest	26.03	0.28	2424.20	1146.00	1283.70	5	111.20	20.66
Kyparissis et al., 2000	38.25	21.73	urban	15.76	0.52	682.92	534.82	1023.70	8	121.25	0.97
Logan et al., 1996	-30.34	152.82	temperate forest	16.60	0.28	1398.10	1069.70	1082.20	5	136.69	21.80
Logan et al., 1998	39.97	-105.27	shrubland/woodland	6.80	0.57	456.13	456.13	1140.10	1	96.00	11.00
Lovelock & Clough et al., 1992	-16.28	145.44	tropical seasonal forest	22.55	0.33	1829.90	1206.70	1427.10	3	31.43	4.23
Magney et al., *this study*	68.63	-149.60	tundra	-8.73	1.05	164.47	164.47	375.99	1	168.61	34.95
Matsubara et al., 2009	9.00	-79.50	tropical rainforest	25.51	0.28	2848.20	1158.40	1257.40	39	50.22	15.43
Nakaji et al., 2006	42.73	141.52	temperate forest	7.32	0.60	1176.40	630.09	630.24	1	65.79	0.00
Niinemets et al., 1998	58.37	27.33	shrubland/woodland	5.75	0.90	665.05	537.94	567.72	4	87.33	34.21
Niinemets et al., 1999	58.37	27.33	shrubland/woodland	5.75	0.90	665.05	537.94	567.72	2	90.00	30.00
Oh et al., 2013	33.35	126.55	temperate forest	14.98	0.55	1856.00	963.78	963.78	1	71.00	8.64
Peguero-Pina et al., 2013	41.65	-0.88	urban	14.60	0.58	474.28	474.28	1240.80	1	32.00	0.00
Porcar Castell et al., 2008	61.85	24.28	boreal forest	3.77	0.94	579.87	453.45	477.92	1	141.88	29.04
Porcar-Castell et al., 2012	61.85	24.30	boreal forest	3.77	0.94	579.87	453.45	477.92	1	145.00	30.00
Thiele et al., 2000	9.15	-79.85	tropical rainforest	26.32	0.30	3035.90	1121.70	1309.30	8	57.00	11.00
Toth et al., 2002	47.00	18.00	agricultural	10.60	0.72	571.06	571.06	779.11	1	44.93	4.33
Verhoeven et al., 1998	40.03	-105.25	urban	7.68	0.58	463.97	463.97	1176.20	1	119.00	13.00
Verhoeven et al., 1999	40.03	-105.25	urban	7.68	0.58	463.97	463.97	1176.20	2	115.50	44.50

Figures:

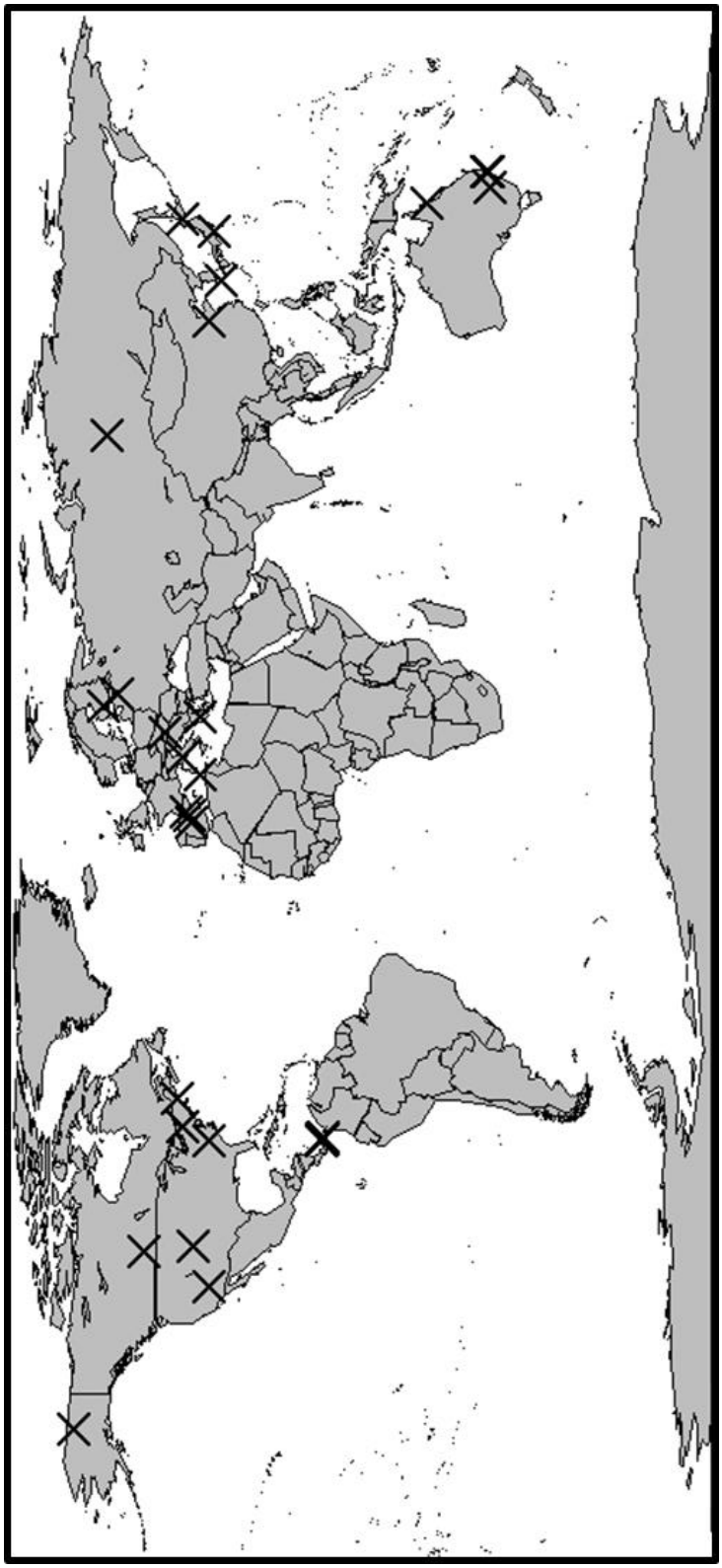

Figure 4.1. Map of locations from 39 studies used in meta-analysis. In some instances, several studies are represented by one point on the map.

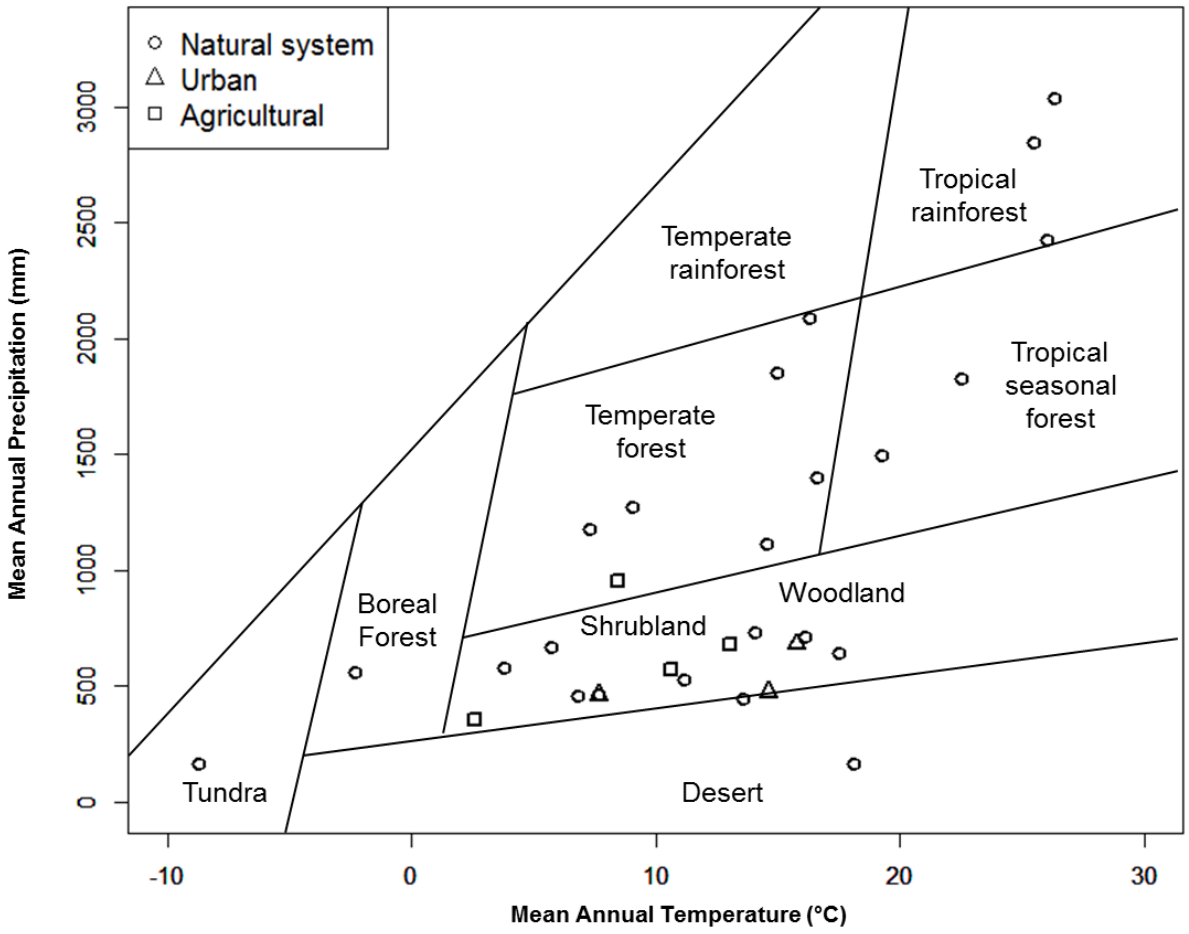

Figure 4.2. Delineation of biomes represented by data used in this study by MAT and MAP.

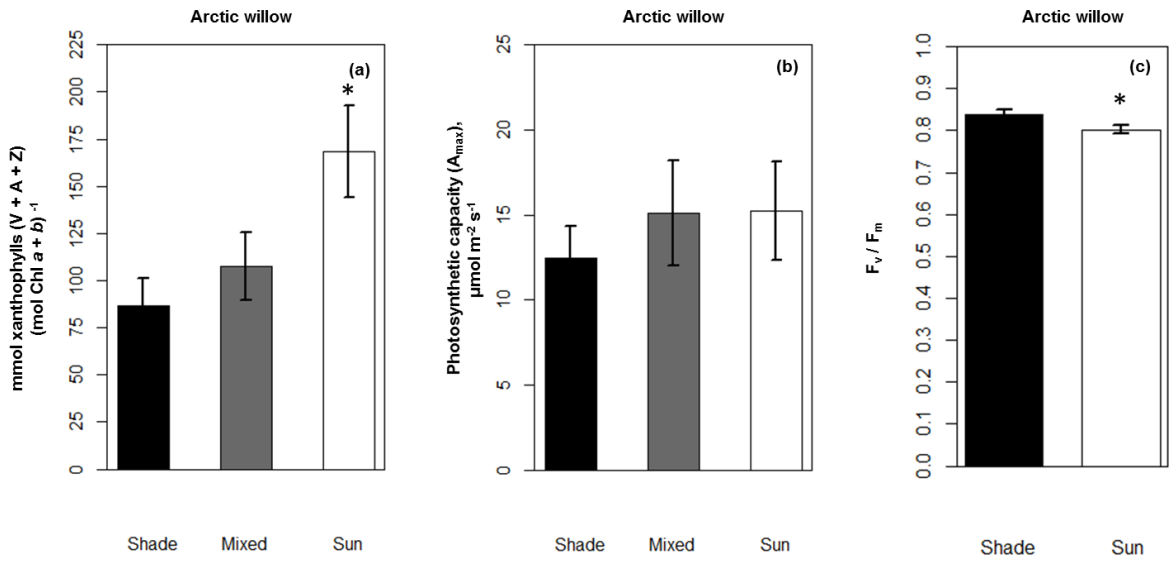

Figure 4.3. Bulk xanthophyll cycle pool size in shade (LAI < .5), mixed (1.5 > LAI > .5) sun (LAI>1.5) locations on *Salix alexensis* (a). Photosynthetic capacity of *Salix alexensis* in shade, mixed, and sun locations. (c) Fv/ Fm for shade and sun species. Asteric indicates a significant difference using ANCOVA between populations.

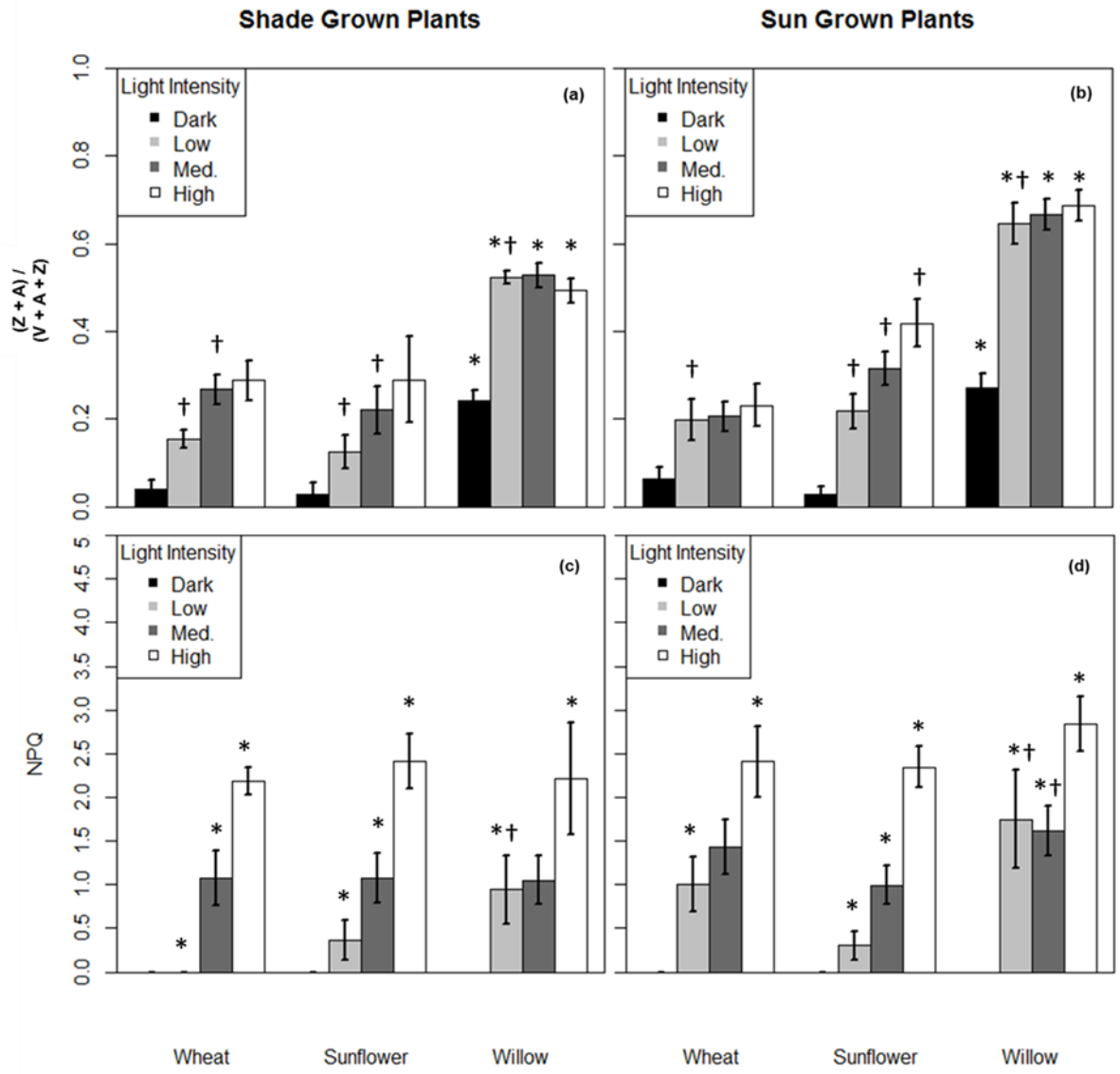

Figure 4.4. Xanthophyll interconversion rates (a,b) and non-photochemical quenching (c,d) of greenhouse grown wheat and sunflower plants compared to arctic willow in the field under increasing light intensities in the laboratory. Plants were dark adapted for > 2hrs and then placed under increasing light intensities ranging for low (photosynthetic photon flux density (PPFD) <300 μmol m^{-2} s^{-1}), medium (800> PPFD > 300 μmol m^{-2} s^{-1}), and high light (PPFD > 800 μmol m^{-2} s^{-1}). Laboratory conditions were consistant across experiments. Wheat and sunflower were placed under a 50% shade cloth for the duration of the growing period, and arctic will were from the deepest part of the canopy (LAI > 1.5) (a,c). In (b) wheat and sunflower were exposed to high irradiance conditions (daily PPFD reaching 2,000 μmol m^{-2} s^{-1}) in the greenhouse, and arctic willow leaves were taken from exposed top of canopy leaves (LAI < 0.5) (b,d). Asteric indicates a significant difference using ANCOVA between willow and other species and † indicates significant differences within species from prior light regime.

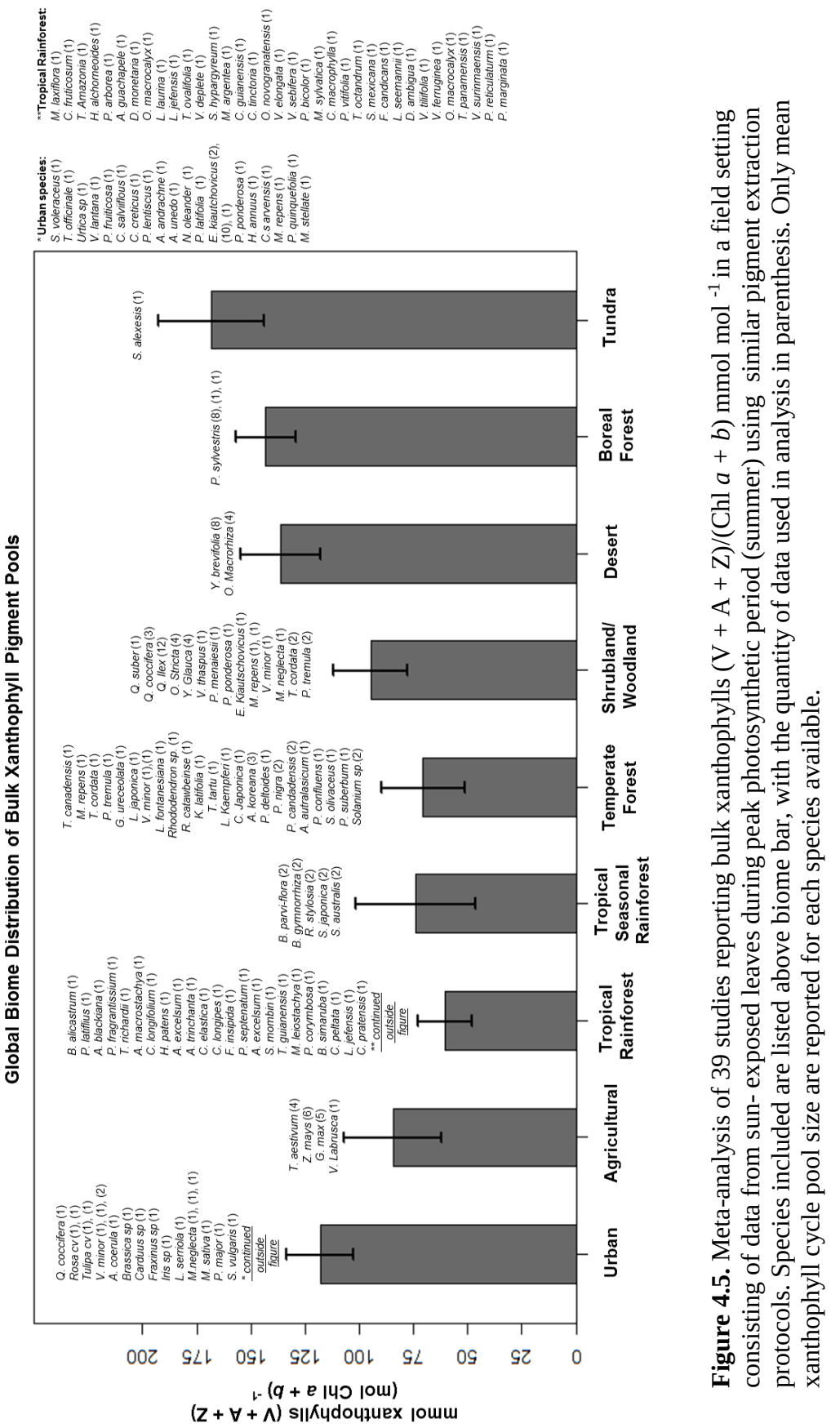

Figure 4.5. Meta-analysis of 39 studies reporting bulk xanthophylls (V + A + Z)/(Chl *a* + *b*) mmol mol $^{-1}$ in a field setting consisting of data from sun- exposed leaves during peak photosynthetic period (summer) using similar pigment extraction protocols. Species included are listed above biome bar, with the quantity of data used in analysis in parenthesis. Only mean xanthophyll cycle pool size are reported for each species available.

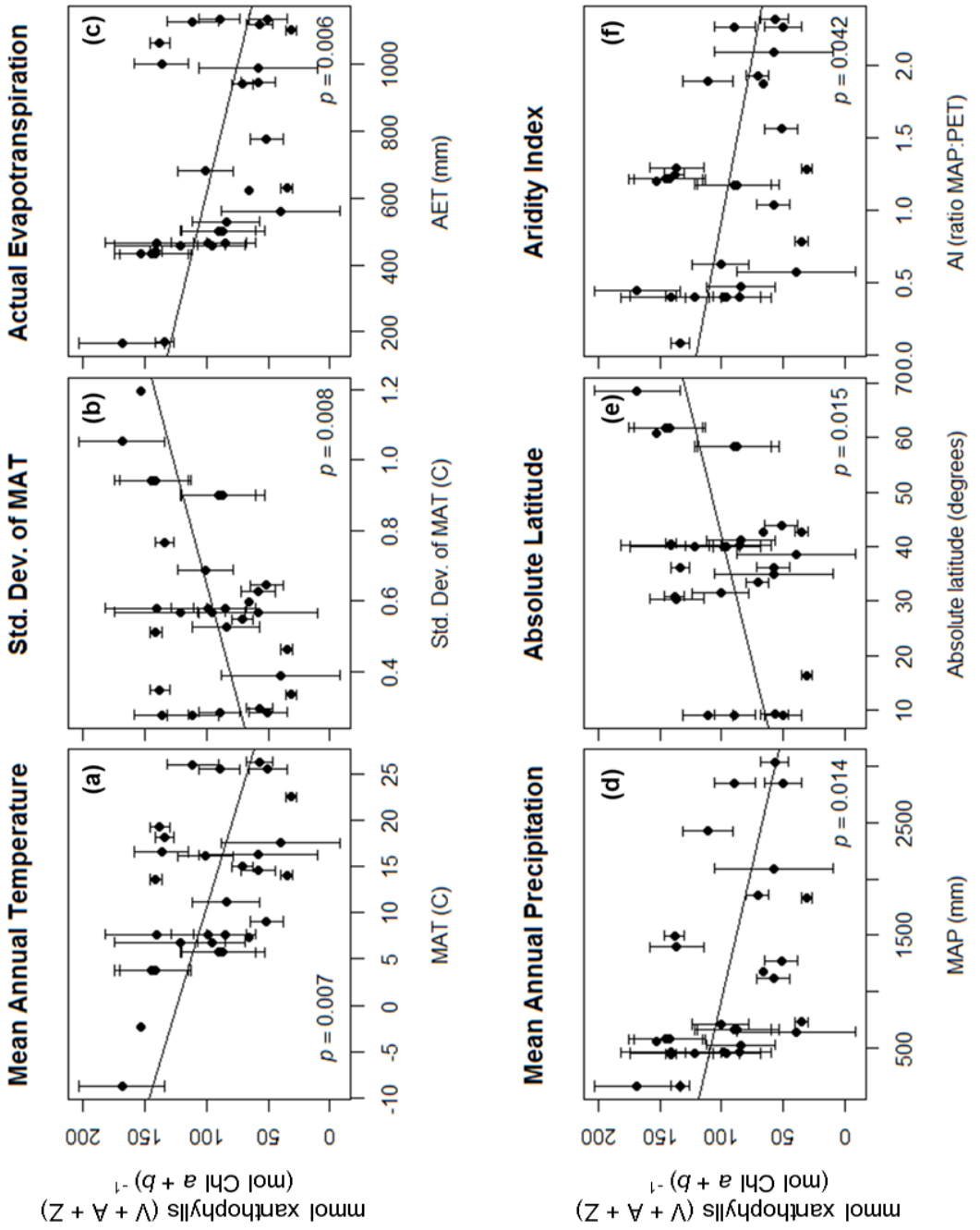

Figure 4.6. Relationships between bulk xanthophyll cycle pool size and climate metrics.

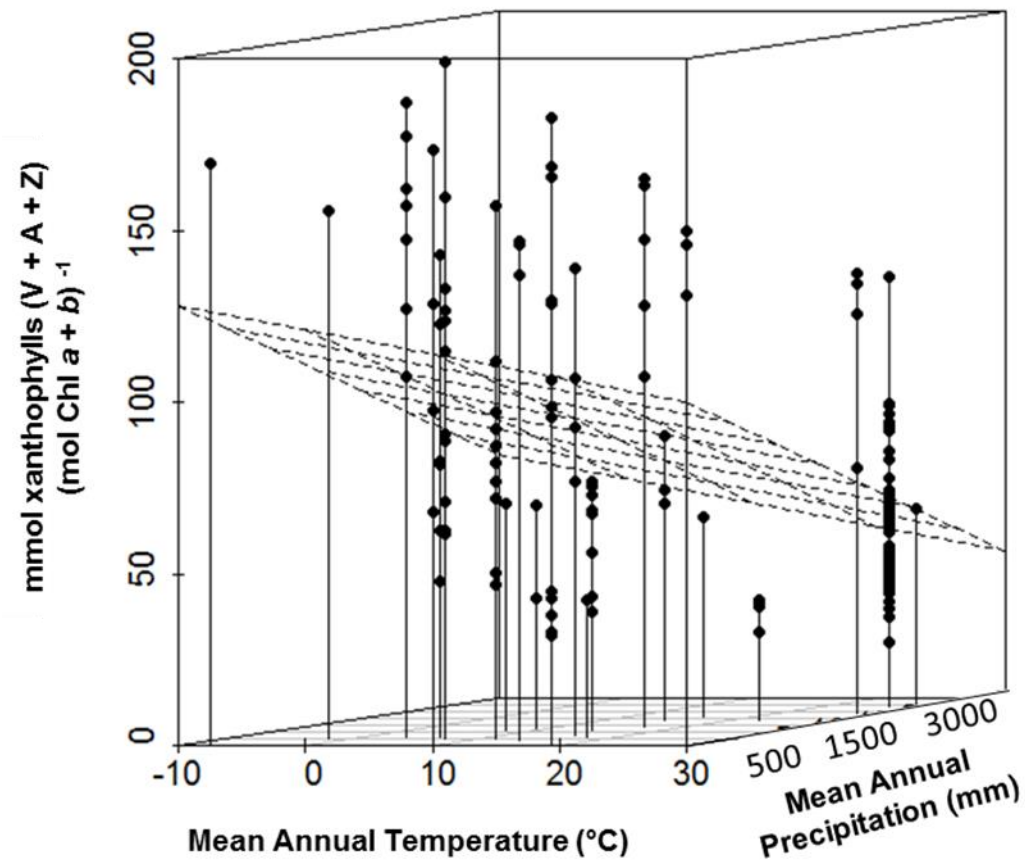

Figure 4.7. Multiple linear regression between xanthophyll cycle pool size and mean annual precipitation (MAP) and mean annual temperature (MAT) of field locations where data from meta-analysis was used. The best fit linear plane is show by the dashed lines.

Conclusions and Future Work

Photosynthesis drives the global carbon cycle, and ultimately provides energy for life on Earth. Due to a changing climate and increased anthropogenic pressures on our planet's ecosystems, it is critical that we improve our capability to make highly resolved measurements related to photosynthesis and ecosystem health. The research bound within this dissertation has developed new – and validated current – remote sensing approaches that are responsive to physiological and structural vegetation changes in increasingly sensitive ecosystems - primarily dryland agriculture of the Pacific Northwest and the Arctic tundra. Development of such tools enables better understanding of how controls on vegetation-atmosphere carbon exchange vary across time and space. Remote sensing driven investigations were conducted using terrestrial LiDAR and ground-based spectral reflectance. As an empiricist, I sought to validate remotely sensed data with information on plant leaf pigments, photosynthetic performance, environmental conditions, and vegetation structure. As a process-driven scientist, I coupled remotely sensed data with biophysical, radiative transfer, and meteorological data, to gain a more mechanistic understanding of the controls on plant function. Fig. 5.1 provides a conceptual framework and visual interpretation of this dissertation that encompasses the key research objectives.

This dissertation sought to improve interpretations of highly resolved (in space and time) remote sensing measurements related indirectly to photosynthesis through: 1) the spectral tracking of seasonal and diurnal plant photoprotection via the PRI ; 2) the prediction of harvest metrics using the rate and duration of phenological periods derived from daily NDVI data; 3) an assessment of photosynthetic partitioning in an Arctic shrub via the coupling of a 3-D LiDAR canopy and a ray-tracing model; and 4) highlighting the variability in bulk xanthophyll cycle pool pigments across nine biomes as a response to environmental conditions. In chapter 1, we developed a 'corrected PRI' (PRI_c), which was able to deconvolve confounding seasonal and diurnal pigment effects on the PRI signal in spring wheat. On both a diurnal and seasonal time-step, PRI_c showed a strong response to VPD, air temperature, g_s, water, and N availability. Because PRI did indeed respond to increasing VPD and air temperature – thereby limiting g_s – and decreasing N and water availability, we assumed that the theoretical underpinnings behind the development of PRI held true – suggesting increased xanthophyll cycle interconversion as a response to increasingly stressful

conditions. As a result, strong relationships were observed between the magnitude of the PRI signal and plant productivity. Lastly, the seasonal time-series of NDVI and PRI_c suggests that PRI could be used as an indicator of 'physiological phenology,' whereby a dramatic decline in PRI occurred nearly 15 days prior to senescence (observed via a decline in NDVI) signal in some cases. This work could have implications for scientists and growers seeking to gain a better understanding of physiological crop response to environmental conditions – in particular, to nutrient and water availability – for potential applications towards developing tools for precision agriculture.

In chapter 2, ground-based spectral reflectance sensors were used to derive physiologically relevant phenological periods from NDVI data in spring wheat. We devised a method to smooth and break up daily NDVI data using piecewise linear regression which enabled the quantification of a rate and duration of four key wheat phenological periods: tillering, stem extension, heading, and ripening. Using the rate and duration of these phenological periods, we were able to predict end of season grain yield, biomass, nitrogen uptake, and protein concretion, showing a significant improvement from using a single, daily NDVI value. These results have implications for growers, plant breeders, and agronomists seeking to develop 'stay-green' phenotypes to lengthen the duration of heading; for the early prediction of harvest metrics; and for understanding the drivers of wheat phenology.

Chapter 3 highlighted the wide variability in measurements used to quantify the light environment of small shrubs exposed to low solar angles, from which each technique showed different trends when relating photosynthetic parameters (A_{max}, %N, and Chl a:b) to light availability. A high resolution model of 3-D shrub structure was used in conjunction with a ray-tracing model to estimate Q_{int} and path length at different locations within the shrub. These techniques were compared with more traditional measurements using an LAI-2000 and vertical canopy depth. Evidence of photosynthetic partitioning within small arctic shrubs using all three parameters was only revealed using light estimates of Q_{int}. This work shows that depending on the technique used to quantify the light environment, different conclusions could be drawn regarding the physiological organization of canopy components in small shrubs. We discussed implications for Arctic carbon cycle models, which currently assume a linear relationship between photosynthesis and LAI in shrubs. As Arctic shrubs increase in size, abundance, and range as a result of climate change, an improved understanding of

photosynthetic partitioning within these increasingly complex canopies could provide evidence for the ability of these plants to optimize themselves to achieve maximal carbon gain and facilitate further expansion.

The final chapter of this dissertation did not use any remote sensing measurements; rather, it examined the variability in xanthophyll cycle pigments on a global scale in response to growing environment. Xanthophyll pigments are of wide interest to the remote sensing community because of their direct link to thermal energy dissipation, which is modulated by the efficiency of the photosynthetic apparatus in the conversion of light energy to carbohydrates. This work highlighted the high concentrations of xanthophylls in an Arctic shrub, and compared it with xanthophyll pigments from 155 species across 9 biomes. Climate metrics were derived from the location of each pigment sample, and significant trends were seen in the response of xanthophyll cycle pool accumulation to extreme temperatures and water deficits. Building on chapter 1, where PRI was corrected by a 'dark-state' PRI – theoretically sensitive to bulk xanthophyll cycle pigments – this chapter noted the variability in pigment pools across a wide range of environmental conditions. Future work should investigate the utility of spectral reflectance to estimate bulk xanthophyll cycle pool size as a technique to rapidly evaluate the physiological status of leaves, canopies, and ecosystems.

A primary goal of this dissertation was to emphasize the value of ground-based remote sensing, particularly with the advent of new satellites designed to monitor plant function directly. It is increasingly important that a rigorous evaluation of the spatial and temporal controls on canopy radiative transfer, and its direct link to plant function, are more extensively investigated to enable accurate interpretation of space-based measurements related the photosynthesis. Tactful scaling – from the ground, to the air, and to space - and more robust radiative transfer models will help build confidence in satellite measurements. Finally, as is true of all science, this dissertation has raised more questions than answers: For example, can measurements related to plant function from space really be representative of what is happening at the leaf and canopy scales? And if so, to what extent can we exploit these measurements? What spatial, temporal, and spectral resolutions are necessary to use remote sensing data for advancing global mapping of GPP? It is under the guise of these questions that I seek to take my future work.

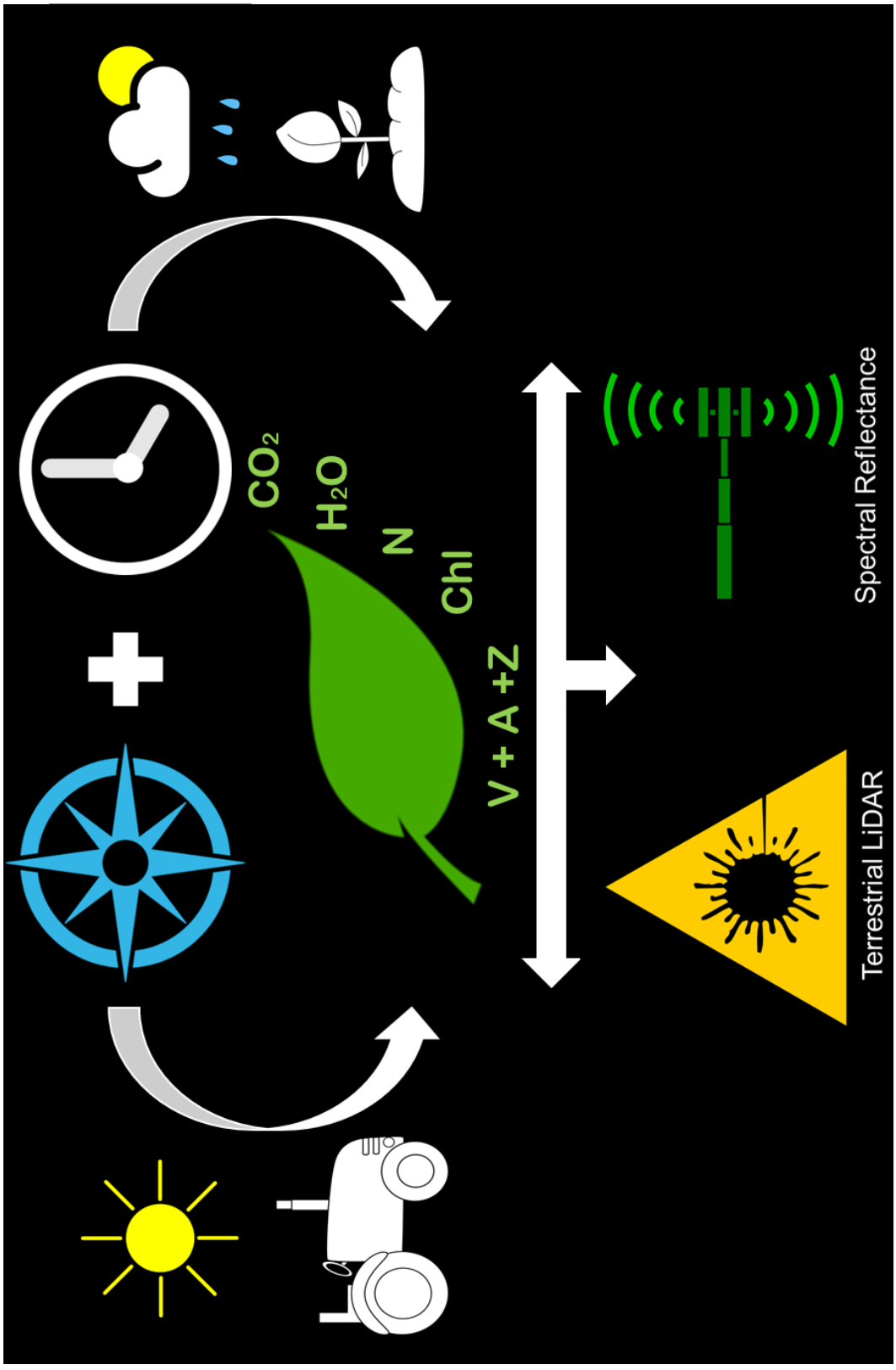

Figure 5.1. Conceptual diagram of dissertation.